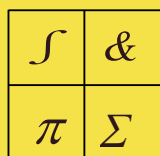


**GEORGIAN ACADEMY OF SCIENCES**

*Proceedings*

**Institute of Cybernetics**

**Vol.1, N 1-2, 2000**



**Institute of Cybernetics**

Georgian Academy of Sciences

Sandro Euli 5, Georgia 86, Tbilisi

E-mail: [cyber@hepi.edu.ge](mailto:cyber@hepi.edu.ge)

<http://cyber.hepi.edu.ge/proceedings>

**GEORGIAN ACADEMY OF SCIENCES**

*Proceedings*

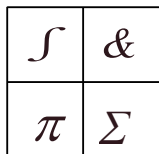
**Institute of Cybernetics**

**Vol.1, N 1-2, 2000**

---

*The collection of works is dedicated  
to the 40-th anniversary of foundation the  
Institute of Cybernetics*

---



**Institute of Cybernetics**  
Georgian Academy of Sciences  
Sandro Euli 5, Tbilisi 86, Georgia  
E-mail: [cyber@hepi.edu.ge](mailto:cyber@hepi.edu.ge)  
<http://cyber.hepi.edu.ge/proceedings>

$\int$	$\&$
$\pi$	$\Sigma$

**Institute of Cybernetics**

Georgian Academy of Sciences

Sandro Euli 5, Tbilisi 86, Georgia

E-mail: [cyber@hepi.edu.ge](mailto:cyber@hepi.edu.ge)

<http://cyber.hepi.edu.ge/proceedings>

---

**Chairman of the Editorial Board:** Kharatishvili Guram, Academician

**Managing Editor:** Bezhanishvili Guram, Dr.

**Editorial Board:** Giorgadze Gia, Dr.

Japaridze Kolchta, Academician

Kakichashvili Shenmazan, Prof.

Tsintsadze Givi, Prof.

---

*Proceedings of the Institute of cybernetics – 2000*  
*Vol.1, N 1-2*

---

**Contents**

---

**Vol.1, N 1.**

<i>Mathematical Modeling and Optimal Control of Multistructural Control Systems with Delays</i> <b>G. Kharatishvili, T. Tadumadze</b>	<b>1</b>
<i>Subalgebras of the Free Cyclic Heyting Algebra</i> <b>G. Bezhanisvili, R. Grigolia</b>	<b>9</b>
<i>The Gauge Quantum Computation</i> <b>G. Giorgadze</b>	<b>18</b>
<i>A Representation of Gaussian Random Processes in the Form of Stochastic Series and its Application for Modeling</i> <b>Z. Piranashvili</b>	<b>31</b>
<i>Optoelectronic Processor for Artificial Problems</i> <b>G. Lezhava</b>	<b>38</b>
<i>Theoretical Principles of the Systems of Pattern Recognition and some Expert-systems</i> <b>N. Tkemaladze</b>	<b>45</b>
<i>Dynamic Adaptive Learning Networks</i> <b>A. Kvitashvili</b>	<b>56</b>
<i>Decision Making: Superiority Degree</i> <b>V. Zhukovin, Z. Alimbarashvili</b>	<b>67</b>
<i>Decision Making on the Example of Informational System Projecting</i> <b>I. Bokuchava, N. Chkhikvadze, Z. Alimbarasvili</b>	<b>77</b>
<i>Control of Pacemaker Mechanisms and Synchronization Processes</i> <b>D. Danelia, N. Beckauri, E. Gonashvili</b>	<b>84</b>
 <b>Short reports</b>	
<i>General Solution of Gauss Nonhomogeneous Hypergeometric Equations of Partical Class</i> <b>G. Kharatishvili</b>	<b>91</b>

<i>On Some Relations Between One-particle Density and Energy Characteristics in the System of One-dimensional Fermions</i> <b>R. Bakuradze</b>	<b>93</b>
<i>Numerical Method of Establishing Dependence Parameters Between Two Variables</i> <b>A. Toronjadze, L. Revishvili</b>	<b>96</b>
<i>Heterogeneous Biological Systems</i> <b>L. Andriadze</b>	<b>98</b>
<i>Selection of Artificial Parameters for Unsupervised Objects Classification</i> <b>M.Kuridze, V. Jikhvashvili</b>	<b>101</b>
<i>Expert System of Class Formation</i> <b>M. Menabde, M. Khanjalashvili, E. Buchukury</b>	<b>103</b>
<i>The Mechanism and Function of Pacemaker Potential</i> <b>B. Partsvania</b>	<b>105</b>
 <b>Vol.1, N 2.</b>	
<i>Photo- and Thermo-sensitive System</i> <b>K. Japaridze, Z. Elashvili, J. Maisuradze, L. Devadze, N. Sepashvili</b>	<b>107</b>
<i>Optical and Electrooptical Characteristics of Chiral Liquid Crystals</i> <b>G. Chilaya</b>	<b>118</b>
<i>The Percolation Conductivity, Josephson Effect and Magnetic Properties of the IITSC Systems</i> <b>J. Sanikidze, S. Odenov, R. Kokhraidze</b>	<b>140</b>
<i>Spectroscopic Properties and Luminescence Dynamics from <math>^1D_2</math>, <math>^1I_6</math> and <math>^3P_{0,1,2}</math> levels of <math>Tm^{3+}</math> Doped <math>YLiF_4</math> Crystals</i> <b>T. Medoidze, Z. Melikishvili, A. Papashvili, G. Tsintsadze</b>	<b>150</b>
<i>Quantum Dynamics of Qubit with Polarization Switch</i> <b>T. Medoidze, Z. Melikishvili, G. Tsintsadze</b>	<b>160</b>
<i>Properties of <math>CuI</math> Nanocrystallites Embedded in a Glass Matrix: from. Quantum. Confinement to Bulk Band Parameters</i> <b>O. Gogolin, G. Mshvelidze, E. Tsitsishvili, M. Schmidt, A. Hepting, C. Klingshirn, A. Kamilli, W. Send, D. Gerthsen</b>	<b>164</b>
<i>Fine Structure of Exiton Levels in Strained Quantum Dots</i> <b>E. Tsitsishvili</b>	<b>171</b>

<i>An a posteriori Experiment in Polarization Holography</i> <b>Sh. Kakichashvili, A. Purtseladze</b>	<b>182</b>
<i>Synthesis of Polarized Hologram by Micro Half-wave Phase Plates</i> <b>T. Ebralidze</b>	<b>188</b>
<i>Bioferromagnetic Liquid (BFML) as a Tool for Investigation Biophysico-Chemical Activity of Cell</i> <b>M.Akhalaya, V. Beria</b>	<b>193</b>

## Short reports

<i>Pseudoforn-an Optical Element Forming a Pseudoscopic Image</i> <b>Sh. Kakichashvili</b>	<b>198</b>
<i>Polarization Holographic Memory of Superhigh Capacity</i> <b>Sh.Kakichashvili, B. Kilosanidze</b>	<b>201</b>
<i>Dispersion of the Rotation of the Axis of Photoinduced Anisotropy in Polarization-sensitive Media</i> <b>Sh. Kakichashvili, S. Petrova</b>	<b>205</b>
<i>Electrochemically Deposited Shottky Barrier Height</i> <b>T. Laperashvili, I. Imerlishvili</b>	<b>208</b>
<i>Ellipsometrical Methods of the Measurements of the Magneto-Optical Parameter</i> <b>O.Bakradze</b>	<b>212</b>
<i>Relationship of Porous Media Tortuosity on Porosity Coefficient</i> <b>T. Karchava</b>	<b>215</b>
<i>IR — Spectra and Electrone Structure of Indolinospirochromenes</i> <b>M.Gugava, I. Pavlenishvili</b>	<b>218</b>
<i>High-Temperature Superconductivity in the Lu-Ca-Ba-Cu-O System</i> <b>G. Tsintsadze, N. Margiani, V. Jgamadze, I. Mzhavanadze, N.Sabashvili, G. Shurgaia</b>	<b>220</b>
<i>Fiber Optics in Optoelectronics</i> <b>Kh. Gaprindashvili</b>	<b>224</b>

ISSN 1512-1372

**GEORGIAN ACADEMY OF SCIENCES**

*Proceedings*

**Institute of Cybernetics**

**Vol.1, N 1-2, 2000**



**Institute of Cybernetics**  
Georgian Academy of Sciences  
Sandro 86, Georgia Euli 5, Tbilisi  
E-mail: cyber@hepi.edu.ge  
<http://cyber.hepi.edu.ge/proceedings>

# GEORGIAN ACADEMY OF SCIENCES

Institute of Cybernetics  
Georgian Academy of Sciences  
Sandro Euli 5, Tbilisi 86, Georgia  
E-Mail: cyber@hepi.edu.ge  
<http://cyber.hepi.edu.ge/proceedings>



*Proceedings*

## Institute of Cybernetics

Vol.1, N 1-2, 2000

---

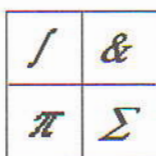
*The collection of works is dedicated  
to the 40-th anniversary of foundation the  
Institute of Cybernetics*

---

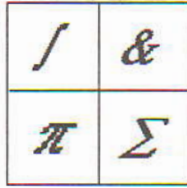
---

Chairman of the Editorial Board: Kakachashvili Guram, Academician  
Managing Editor: Bekhanshvilivi Guram, Dr.  
Editorial Board: Giorgadze Gia, Dr.  
Iaparidze Kokhta, Academician  
Kakichashvili Shermazan, Prof.  
Tsinitsadze Givi, Prof.

---



Institute of Cybernetics  
Georgian Academy of Sciences  
Sandro Euli 5, Tbilisi 86, Georgia  
E-mail: [cyber@hepi.edu.ge](mailto:cyber@hepi.edu.ge)  
<http://cyber.hepi.edu.ge/proceedings>



**Institute of Cybernetics**  
Georgian Academy of Sciences  
Sandro Euli 5, Tbilisi 86, Georgia  
E-Mail: [cyber@hepi.edu.ge](mailto:cyber@hepi.edu.ge)  
<http://cyber.hepi.edu.ge/proceedings>

Proceedings  
Institute of Cybernetics  
Vol.1, N 1-2, 2000

The collection of works is dedicated  
to the 40-th anniversary of foundation the  
Institute of Cybernetics

---

**Chairman of the Editorial Board:** Kharatishvili Guram, Academician  
**Managing Editor:** Bezhanishvili Guram, Dr.  
**Editorial Board:** Giorgadze Gia, Dr.  
Japaridze Kokhta, Academician  
Kakichashvili Shermazan, Prof.  
Tsintsadze Givi, Prof.

---



# Proceedings of the Institute of Cybernetics – 2000

## Vol.1, N 1-2

---

### Contents

---

#### Vol.1, N 1.

<i>Mathematical Modeling and Optimal Control of Multistructural Control Systems with Delays</i> <b>G. Kharatishvili, T. Tadumadze</b>	1
<i>Subalgebras of the Free Cyclic Heyting Algebra</i> <b>G. Bezhanisvili, R. Grigolia</b>	9
<i>The Gauge Quantum Computation</i> <b>G. Giorgadze</b>	18
<i>A Representation of Gaussian Random Processes in the Form of Stochastic Series and its Application for Modeling</i> <b>Z. Piranashvili</b>	31
<i>Optoelectronic Processor for Artificial Problems</i> <b>G. Lezhava</b>	38
<i>Theoretical Principles of the Systems of Pattern Recognition and some Expert-systems</i> <b>N. Tkemaladze</b>	45
<i>Dynamic Adaptive Learning Networks</i> <b>A. Kvitashvili</b>	56
<i>Decision Making: Superiority Degree</i> <b>V. Zhukovin, Z. Alimbarashvili</b>	67
<i>Decision Making on the Example of Informational System Projecting</i> <b>I. Bokuchava, N. Chkhikvadze, Z. Alimbarashvili</b>	77
<i>Control of Pacemaker Mechanisms and Synchronization Processes</i> <b>D. Danelia, N. Beckauri, E. Gonashvili</b>	84
<b>Short reports</b>	
<i>General Solution of Gauss Nonhomogeneous Hypergeometric Equations of Partical Class</i> <b>G. Kharatishvili</b>	91

<i>On Some Relations Between One-particle Density and Energy Characteristics in the System of One-dimensional Fermions</i> <b>R. Bakuradze</b>	93
<i>Numerical Method of Establishing Dependence Parameters Between Two Variables</i> <b>A. Toronjadze, L. Revishvili</b>	96
<i>Heterogeneous Biological Systems</i> <b>L. Andriadze</b>	98
<i>Selection of Artificial Parameters for Unsupervised Objects Classification</i> <b>M. Kuridze, V. Jikhvashvili</b>	101
<i>Expert System of Class Formation</i> <b>M. Menabde, M. Khanjalashvili, E. Buchukury</b>	103
<i>The Mechanism and Function of Pacemaker Potential</i> <b>B. Partsvania</b>	105
 <b>Vol.1, N 2.</b>	
<i>Photo- and Thermo-sensitive System</i> <b>K. Japaridze, Z. Elashvili, J. Maisuradze, L. Devadze, N. Sepashvili</b>	107
<i>Optical and Electrooptical Characteristics of Chiral Liquid Crystals</i> <b>G. Chilaya</b>	118
<i>The Percolation Conductivity, Josephson Effect and Magnetic Properties of the HTSC Systems</i> <b>J. Sanikidze, S. Odenov, R. Kokhreidze</b>	140
<i>Spectroscopic Properties and Luminescence Dynamics from <math>^1D_2</math>, <math>^1I_6</math> and <math>^3P_{0,1,2}</math> levels of <math>Tm^{3+}</math> Doped <math>YLiF_4</math> Crystals</i> <b>T. Medoidze, Z. Melikishvili, A. Papashvili, G. Tsintsadze</b>	150
<i>Quantum Dynamics of Qubit with Polarization Switch</i> <b>T. Medoidze, Z. Melikishvili, G. Tsintsadze</b>	160
<i>Properties of <math>CuI</math> Nanocrystallites Embedded in a Glass Matrix: from Quantum Confinement to Bulk Band Parameters</i> <b>O. Gogolin, G. Mshvelidze, E. Tsitsishvili, M. Schmidt, A. Hepting, C. Klingshirn, A. Kamilli, W. Send, D. Gerthsen</b>	164
<i>Fine Structure of Exciton Levels in Strained Quantum Dots</i> <b>E. Tsitsishvili</b>	171

<i>An a posteriori Experiment in Polarization Holography</i> <b>Sh. Kakichashvili, A. Purtseladze</b>	<b>182</b>
<i>Synthesis of Polarized Hologram by Micro Half-wave Phase Plates</i> <b>T. Ebralidze</b>	<b>188</b>
<i>Bioferromagnetic Liquid (BFML) as a Tool for Investigation Biophysico-Chemical Activity of Cell</i> <b>M. Akhalaya, V. Beria</b>	<b>193</b>
 <b>Short reports</b>	
<i>Pseudoform-an Optical Element Forming a Pseudoscopic Image</i> <b>Sh. Kakichashvili</b>	<b>198</b>
<i>Polarization Holographic Memory of Superhigh Capacity</i> <b>Sh. Kakichashvili, B. Kilosanidze</b>	<b>201</b>
<i>Dispersion of the Rotation of the Axis of Photoinduced Anisotropy in Polarization-sensitive Media</i> <b>Sh. Kakichashvili, S. Petrova</b>	<b>205</b>
<i>Electrochemically Deposited Shottky Barrier Height</i> <b>T. Laperashvili, I. Imerlishvili</b>	<b>208</b>
<i>Ellipsometrical Methods of the Measurements of the Magneto-Optical Parameter</i> <b>O. Bakradze</b>	<b>212</b>
<i>Relationship of Porous Media Tortuosity on Porosity Coefficient</i> <b>T. Karchava</b>	<b>215</b>
<i>IR – Spectra and Electrone Structure of Indolinospirochromenes</i> <b>M. Gugava, I. Pavlenishvili</b>	<b>218</b>
<i>High-Temperature Superconductivity in the Lu-Ca-Ba-Cu-O System</i> <b>G. Tsintsadze, N. Margiani, V. Jgamadze, I. Mzhavanadze, N. Sabashvili, G. Shurgaia</b>	<b>220</b>
<i>Fiber Optics in Optoelectronics</i> <b>Kh. Gaprindashvili</b>	<b>224</b>



## Mathematical Modeling and Optimal control of Multistructural Control Systems with Delays

**Guram Kharatishvili, Tamaz Tadumadze**

*Institute of Cybernetics & Tbilisi State University*

### Abstract

There has been posed and studied a problem of optimal control for a general controlled systems with delays and non-fixed initial moment of time, including, in particular, the optimal problem for multistructure controlled system having important applied value.

**Keywords:** mathematical model, maximum principle, admissible control.

### 1. Multistructural Control system.

Let, one control system is controlling by control influence at the time  $t_0 \leq t \leq t_1$  interval, which is worked out by another control system at the same time interval, with this, before the control influence infects on the first control system, it goes distinct time  $\tau > 0$ .

Above examined, as the form of mathematical model, is possible to describe in the following way

$$\begin{cases} L(p)X(t) = Y(t - \tau), \\ M(p)Y(t) = U(t), a < t_0 \leq t \leq t_1 < b, \end{cases}$$

here,  $L(p)$  and  $M(p)$  are given linear differential operators with continuous coefficients at the  $a < t < b$  interval, the orders of which are  $\mu$  and  $\nu$ , respectively;  $U(t)$ ,  $t_0 \leq t \leq t_1$  is control influence.

There are described many real (physical, economical etc.) control objects by such mathematical model. For example a rocket, which is controlling at the process of flight  $U(t)$ ,  $t_0 \leq t \leq t_1$ , by radio signal.

It is clear, that such weak influence as radio signal is, cannot impact directly the rocket; it is necessary transformation-intensification of radio signal, which needs distinct time  $\tau > 0$ .

Let imagine now, that we have distinct totality of such type of controlling objects, which have common purpose function (for ex. rocket complex).

For this case, initial mathematical model will be generalized in following way:

$$\begin{cases} L_i(p)x_i(t) = y_i(t - \tau_i), \\ M_i(p)y_i(t) = u_i(t), i = \overline{1, k}, a < t_0 \leq t \leq t_1 < b, \end{cases} \quad (1)$$

where  $L_i(p)$ ,  $M_i(p)$  are given linear differential operators with continuous coefficients at  $a < t < b$  interval, the orders of which are  $\mu_i$ ,  $\nu_i$ ,  $i = \overline{1, k}$  respectively;  $u_i(t)$ ,  $t_0 \leq t \leq t_1$ ,  $i = \overline{1, k}$  are control influences;  $\tau_k > \dots > \tau_1 > 0$  are delays.

For realizing the simply suitable controlling system, control by controlling influence  $u_i(t)$ ,  $t_0 \leq t \leq t_1$ ,  $\forall i = \overline{1, k}$  at the time interval  $t_0 \leq t \leq t_1$ , it is necessary to be given the initial conditions:

$$\begin{cases} x_i^{(j)}(t_0) = x_{i_0}^j, y_i^{(l)}(t_0) = x_{i_0}^{\mu_i+l}, j = \overline{0, \mu_i - 1}, l = \overline{0, \nu_i - 1}, \\ y_i(t) = \varphi_i(t), t_0 - \tau_k \leq t < t_0, i = \overline{1, k}, \end{cases} \quad (2)$$

where  $x_i^{(j)}(t) = \frac{d^j x_i(t)}{dt^j}$ ,  $y_i^{(l)}(t) = \frac{d^l y_i(t)}{dt^l}$ ;  $x_{i_0}^j$ ,  $j = \overline{0, \mu_i + \nu_i - 1}$ ,  $i = \overline{1, k}$  are given initial values;  $\varphi_i(t)$ ,  $t_0 - \tau \leq t < t_0$ ,  $i = \overline{1, k}$  are given continuous initial functions. The case, when  $y_i(t_0) \neq \varphi_i(t_0)$ ,  $i \in K$ ,  $K \subseteq \{1, \dots, k\}$  is permissible.

The initial  $t_0$  moment is not given, but its selection occurs optimally. For ex.  $t_0$  moment of the rocket complex setting in motion is possible to be belonged to preliminary given time interval  $t' \leq t_0 < t''$  and definition of  $t_0$  moment occurred optimally as it follows from the purpose function.

For every fixed value  $i = \overline{1, k}$  system (1) is equivalent to the  $n_i = \mu_i + \nu_i$  order linear normal control system

$$\begin{cases} \frac{dx_i^1(t)}{dt} = x_i^2(t), \\ \dots \\ \frac{dx_i^{\mu_i-1}(t)}{dt} = x_i^{\mu_i}(t), \\ \frac{dx_i^{\mu_i}(t)}{dt} = a_i^1(t)x_i^1(t) + \dots + a_i^{\mu_i}(t)x_i^{\mu_i}(t) + x_i^{\mu_i+1}(t - \tau_i), \\ \frac{dx_i^{\mu_i+1}(t)}{dt} = x_i^{\mu_i+2}(t), \\ \dots \\ \frac{dx_i^{n_i-1}(t)}{dt} = x_i^{n_i}(t), \\ \frac{dx_i^{n_i}(t)}{dt} = a_i^{\mu_i+1}(t)x_i^{\mu_i+1}(t) + \dots + a_i^{n_i}(t)x_i^{n_i}(t) + u_i(t), \\ a < t_0 \leq t \leq t_1 < b, i = \overline{1, k}, \end{cases}$$

which will be written by the form of following vector matrix

$$\frac{dz_i(t)}{dt} = A_i(t)z_i(t) + B_i z_i(t - \tau_i) + C_i u_i(t), a < t_0 \leq t \leq t_1 < b, i = \overline{1, k}, \quad (3)$$

here  $z_i(t) = \begin{pmatrix} x_i^1(t) \\ \dots \\ x_i^{n_i}(t) \end{pmatrix}$ ;  $u(t) = \begin{pmatrix} u_1(t) \\ \dots \\ u_k(t) \end{pmatrix}$ .

$C_i - n_i \times k$  is the matrix every element of which is equal to zero, but the element standing at the intersection of  $n_i$  row and  $i$  column which is equal to 1;

$B_i - n_i \times n_i$  is the matrix, every element of which is zero but the element standing on the intersection of  $\mu_i$  row and  $\mu_i + 1$  column which is equal to 1;

$$A_i(t) = \begin{pmatrix} A_i'(t) & 0 \\ 0 & A_i''(t) \end{pmatrix}$$

is the matrix where

$$A_i'[t] = \begin{pmatrix} 0 & 1 & 0 & \dots & 0 \\ & & \dots & & \\ 0 & 0 & \dots & 0 & 1 \\ a_i^1(t) & & & & a_i^{\mu_i}(t) \end{pmatrix}, A_i''[t] = \begin{pmatrix} 0 & 1 & 0 & \dots & 0 \\ & & \dots & & \\ 0 & 0 & \dots & 0 & 1 \\ a_i^{\mu_i+1}(t) & & & & a_i^{n_i}(t) \end{pmatrix}$$

If introduce

$$x(t) = \begin{pmatrix} z_1(t) \\ \dots \\ z_k(t) \end{pmatrix}, A(t) = \begin{pmatrix} A_1(t) & & 0 \\ & \dots & \\ 0 & & A_k(t) \end{pmatrix},$$

$$D_1 = \begin{pmatrix} B_1 & & 0 \\ & 0 & \\ & & \ddots \\ 0 & & 0 \end{pmatrix}, \dots, D_k = \begin{pmatrix} 0 & & 0 \\ & 0 & \\ & & \ddots \\ 0 & & 0 \end{pmatrix}, C = \begin{pmatrix} C_1 \\ \dots \\ C_k \end{pmatrix},$$

then the system (3) will obtain following form

$$\frac{dx(t)}{dt} = A(t)x(t) + \sum_{i=1}^k D_i x(t - \tau_i) + Cu(t), \quad a < t_0 \leq t \leq t_1 < b, \quad (4)$$

and initial condition (2) will be written

$$\begin{cases} x(t_0) = x_0 \\ x(t) = \varphi(t, i), t_0 - \tau_k \leq t < t_0, i = \overline{1, k} \end{cases} \quad (5)$$

where  $x_0$  is  $n = n_1 + \dots + n_k$  dimension vector having coordinates with initial values  $x_{10}^0, \dots, x_{10}^{n_1-1}, \dots, x_{k0}^0, \dots, x_{k0}^{n_k-1}$ , and  $\varphi(t, i)$  is  $n$  dimensioned initial vector-function, the coordinate  $\mu_i + 1$  of which is  $\varphi_i(t)$ ,  $i = \overline{1, k}$ , remainder coordinates are equal to zero.

The boundary condition has the following form at the final moment  $t_1$

$$q^\alpha(t_1, x(t_1)) = 0, \alpha = \overline{1, m}, \quad (6)$$

where  $q^\alpha(t_1, y) = 0, \alpha = \overline{1, m}$ , are continuous and continuously differentiable functions to their arguments.

The purpose function is expressed with the integral functional

$$I(z) = \int_{t_0}^{t_1} f^0(t, x(t), x(t - \tau_1), \dots, x(t - \tau_k), u(t)) dt, \quad (7)$$

where  $z = (t_0, t_1, x(\cdot), u(\cdot))$ ,  $f^0(t, y_0, \dots, y_k, u)$  is continuous function to their arguments and continuously differentiable with respect  $y_i, i = \overline{0, k}$ .

Any piecewise continuous function  $u(t)$  which is defined at its  $t_0 \leq t \leq t_1$  interval has finite number of discontinuity points at this interval and obtains values from closed, bounded  $U_0$  set of  $k$  dimension vector space, is considered as admissible control.

For above examined case, optimal control problem will be formulated in following way.

It is necessary to find such admissible control  $u(t)$ , moments  $t_0, t_1$ , the suitable (4) system trajectory of which will satisfy boundary conditions (2), (6) and confers the minimal value to  $I(z)$  functional. (In section 2, necessary conditions of optimality for the optimal problem (4)-(7) are given (see 4), 5); 6), 7)).

Formulated optimal problem is private case of below examined general optimal problem.

## 2. General optimal control problem with delayed arguments.

### Necessary conditions of optimality.

Consider the problem

$$\frac{dx(t)}{dt} = f(t, x(\tau_0(t)), \dots, x(\tau_s(t)), u(\theta_0(t)), \dots, u(\theta_v(t))),$$

$$t \in [t_0, t_1] \subset J = [a, b], u(\cdot) \in \Omega, \quad (8)$$

$$x(t) = \varphi(t), t \in [\tau(t_0), t_0], x(t_0) = x_0, \varphi(\cdot) \in \Delta, x_0 \in O, \quad (9)$$

$$q^i(t_0, t_1, x_0, x(t_1)) = 0, i = \overline{1, m} \quad (10)$$

$$I(z) = q(t_0, t_1, x_0, x(t_1)) + \int_{t_0}^{t_1} f^0(t, x(\tau_0(t)), \dots, x(\tau_s(t)), u(\theta_0(t)), \dots, u(\theta_v(t))) dt \rightarrow \min,$$

$$z = (t_0, t_1, x_0, \varphi(\cdot), u(\cdot)) \in A = J^2 \times O \times \Delta \times \Omega.$$

Here  $f = (f^1, \dots, f^n)$ ;  $f^i(t, y_0, \dots, y_s, u_0, \dots, u_v)$ ,  $i = \overline{0, n}$  are continuous functions on  $J \times G^{1+s} \times V^{1+r}$  and continuously differentiable with respect to  $y_i \in G$ ,  $i = \overline{0, s}$ ;  $G \in R^n$ ,  $O \in G$ ,  $V \in R^r$  are open sets;  $\tau_i(t)$ ,  $t \in R$ ,  $i = \overline{1, s}$  are absolutely continuous functions satisfying the conditions:  $\tau_0(t) \equiv t$ ,  $\tau_i(t) \leq t$ ,  $\dot{\tau}_i(t) > 0$ ; the functions  $\theta_i(t)$ ,  $i = \overline{0, v}$ , satisfy the conditions:  $\theta_0(t) \equiv t$ ,  $\theta_i(t) \leq \theta^{k_i}(t)$ ,  $i = \overline{1, v}$ ,  $k_v > \dots > k_1$  are natural numbers,  $\theta^i(t) = \theta(\theta^{i-1}(t))$ ,  $\theta^0(t) = t$ ,  $\theta(t)$  is the absolutely continuous functions satisfying the conditions:  $\theta(t) < t$ ,  $\dot{\theta}(t) > 0$ ;  $\Omega$  is the set of measurable functions  $u: [\theta_v(a), b] \rightarrow U$  is such that  $cl\{u(t): t \in [\theta_v(a), b]\}$  is a compact lying in  $V$ ,  $U \subset V$  is an arbitrary set;  $\Delta$  is the set of piecewise continuous functions  $\varphi: [\tau(a), b] \rightarrow N$  with a finite number of discontinuity points,  $\tau(t) = \min\{\tau_1(t), \dots, \tau_s(t)\}$ ,  $N \subset G$  is the convex bounded set;  $q^i(t_0, t_1, y_0, y_1)$ ,  $i = \overline{0, m}$  are functions continuously differentiable on  $J^2 \times G^2$ .

**Definition 1.** The function  $x(t) = x(t, z) \in G$ ,  $t \in [\tau(t_0), t_1]$ ,  $t_0 \in [a, t_1)$  is said to be solution of system (8), corresponding to the element  $z = (t_0, t_1, x_0, \varphi(\cdot), u(\cdot)) \in A$  if on  $[\tau(t_0), t_0]$  it satisfies the conditions (9), while on the interval  $[t_0, t_1]$  is absolutely continuous and the pair  $(x(\cdot), u(\cdot))$  satisfies the equation (8) almost everywhere (a. e.) on  $[t_0, t_1]$ .

**Definition 2.** The element  $z \in A$  is said to be admissible if the corresponding solution  $x(t)$  satisfies the condition (10).

The set of admissible elements will denote by  $A_0$ .

**Definition 3.** The element  $\tilde{z} = (\tilde{t}_0, \tilde{t}_1, \tilde{x}_0, \tilde{\varphi}(\cdot), \tilde{u}(\cdot)) \in A_0$  is said to be optimal if for an arbitrary element  $z \in A_0$  the inequality  $I(\tilde{z}) \leq I(z)$  holds.

The problem of optimal control consists in finding a optimal element.

Introduce the following notations:

$$F = (f^0, f); R_{\tilde{t}_0}^- = (-\infty, \tilde{t}_0], R_{\tilde{t}_0}^+ = [\tilde{t}_0, \infty); \gamma_i(t) \text{ is the function inverse to } \tau_i(t),$$

$$\gamma_i = \gamma_i(t_0);$$

$$\begin{cases} F(t, y_0, \dots, y_s) = F(t, y_0, \dots, y_s, \tilde{u}(\theta_0(t)), \dots, \tilde{u}(\theta_v(t))), \\ F[t] = F(t, \tilde{x}(\tau_0(t)), \dots, \tilde{x}(\tau_s(t))); \end{cases} \quad (11)$$

$$\begin{cases} \omega_i^- = (\gamma_i, \tilde{x}(\tau_0(\gamma_i)), \dots, \tilde{x}(\tau_{i-1}(\gamma_i)), \tilde{x}_0, \tilde{\varphi}(\tau_i(\gamma_i -)), \dots, \tilde{\varphi}(\tau_s(\gamma_i -))), & i = \overline{0, s}, \\ \dot{\omega}_i^- = (\gamma_i, \tilde{x}(\tau_0(\gamma_i)), \dots, \tilde{x}(\tau_{i-1}(\gamma_i)), \tilde{\varphi}(\tilde{t}_0 -), \tilde{\varphi}(\tau_i(\gamma_i -)), \dots, \tilde{\varphi}(\tau_s(\gamma_i -))), & i = \overline{1, s}, \\ \omega_{s+1}^- = (t_1, \tilde{x}(\tau_0(\tilde{t}_1 -)), \dots, \tilde{x}(\tau_0(\tilde{t}_1 -))) \end{cases} \quad (12)$$

further  $\varpi = (t, y_0, \dots, y_s)$ ,  $F(\varpi) = F(\omega, \tilde{u}(\theta_0(t)), \dots, \tilde{u}(\theta_v(t)))$ ;

$$\begin{cases} \lim_{t \rightarrow \varpi_0^-} F(\omega) = F_0^-, & \omega \in R_{t_0}^- \times G^{1+s}; \\ \lim_{(\omega_1, \omega_2) \rightarrow (\omega_i^-, \dot{\omega}_i^-)} [F(\omega_1) - F(\omega_2)] = F_i^-, & \omega_1, \omega_2 \in R_{\gamma_i}^- \times G^{1+s}, \quad i = \overline{1, s}; \\ \lim_{t \rightarrow \varpi_{s+1}^-} F(\omega) = F_{s+1}^-, & \omega \in R_{t_0}^- \times G^{1+s}; \\ \lim_{t \rightarrow \tilde{t}_0^-} \dot{\gamma}_i(t) = \dot{\gamma}_i^-, & t \in R_{t_0}^-, \quad i = \overline{1, s}; \end{cases} \quad (13)$$

**Theorem 1.**  $\tilde{z} \in A_0$  be a optimal element,  $\tilde{t}_0 \in (a, b)$ ,  $\tilde{t}_1 \in (a, b]$ ,  $\tilde{t}_0 < \gamma_1 < \dots < \gamma_s < \tilde{t}_1$ ; let now, there exist the finite limits  $F_i^-$ ,  $i = \overline{0, s+1}$ ,  $\dot{\gamma}_i^-$ ,  $i = \overline{1, s}$ . Then there exists a non-zero vector  $\pi = (\pi_0, \dots, \pi_m)$ ,  $\pi_0 \leq 0$  and solution  $\psi(t)$  of the equation

$$\begin{cases} \dot{\psi}(t) = - \sum_{i=0}^s \Phi(\gamma_i(t)) F_{y_i}[\gamma_i(t)] \dot{\gamma}_i(t), & t \in [t_0, t_1], \\ \Phi(t) = (\psi_0(t), \psi(t)), \psi_0(t) = \pi_0, & t \in [t_0, t_1]; \\ \Phi(t) = 0, & t \notin [t_0, t_1]. \end{cases} \quad (14)$$

such that the following conditions are fulfilled:

1) the maximum principle for the initial function

$$\left[ \sum_{i=1}^s \Phi(\gamma_i(t)) F_{y_i}[\gamma_i(t)] \dot{\gamma}_i(t) \right] \tilde{\varphi}(t) = \max_{\varphi \in N} \left[ \sum_{i=1}^s \Phi(\gamma_i(t)) F_{y_i}[\gamma_i(t)] \dot{\gamma}_i(t) \right] \varphi(t)$$

a.e. on  $[\tau(\tilde{t}_0), \tilde{t}_0]$ ;

2) the maximum principle for the control

$$\sum_{i=1}^v \Phi(\rho_i(t)) F[\rho_i(t)] \dot{\rho}_i(t) = \max_{u \in U} \Phi(\rho_i(t)) F(\rho_i(t), \tilde{x}(\tau_0(\rho_i(t))), \dots, \tilde{x}(\tau_0(\rho_i(t))), \tilde{u}(\theta_0(\rho_i(t))), \dots, \tilde{u}(\theta_{i-1}(\rho_i(t))), u, \tilde{u}(\theta_{i+1}(\rho_i(t))), \dots, \tilde{u}(\theta_v(\rho_i(t))))$$

a.e. on  $[\theta_v(\tilde{t}_0), \tilde{t}_0]$ ;

3) the conditions of transversally

$$\pi \tilde{Q}_{y_0} = -\psi(\tilde{t}_0), \pi \tilde{Q}_{y_1} = -\psi(\tilde{t}_1) \quad (15)$$

$$\pi \tilde{Q}_{t_0} \geq \Phi(\tilde{t}_0) F_0^- + \sum_{i=1}^s \Phi(\gamma_i) F_i^- \dot{\gamma}_i^-, \quad \pi \tilde{Q}_{t_1} \geq -\Phi(\tilde{t}_1) F_{s+1}^-.$$

Here  $\tilde{Q}_{y_0} = \frac{\partial \tilde{Q}}{\partial y_0}$ , the tilde over  $Q = (q^0, \dots, q^m)$  means that there corresponding gradient is

calculated at the point  $(\tilde{t}_0, \tilde{t}_1, \tilde{x}_0, \tilde{x}_1)$ ,  $\tilde{x}_1 = \tilde{x}(t_1)$ . If  $\text{rank}(\tilde{Q}_{y_0}, \tilde{Q}_{y_1}) = 1+m$ , then in the theorem 1  $\Phi(t) \neq 0$ .

It is obvious, that if there exist the finite limits

$$\tilde{u}(\tilde{t}_0 -), \tilde{u}(\tilde{t}_1 -), \tilde{u}(\theta_i(\gamma_j -)), \quad i = \overline{0, v}, \quad j = \overline{1, s}, \text{ then}$$

$$F_0^- = F[\tilde{t}_0 -];$$

$$F_i^- = F(\gamma_i^-, \tilde{x}(\tau_0(\gamma_i)), \dots, \tilde{x}(\tau_{i-1}(\gamma_i)), \tilde{x}_0, \tilde{\varphi}(\tau_{i+1}(\gamma_i^-)), \dots, \tilde{\varphi}(\tau_s(\gamma_i^-))) - \\ F(\gamma_i^-, \tilde{x}(\tau_0(\gamma_i)), \dots, \tilde{x}(\tau_{i-1}(\gamma_i)), \tilde{\varphi}(\tilde{t}_0^-), \tilde{\varphi}(\tau_i(\gamma_i^-)), \dots, \tilde{\varphi}(\tau_s(\gamma_i^-))); \\ F_{s+1}^- = F[\tilde{t}_1^-]. \text{ (see(11)).}$$

If  $\tilde{\varphi}(\tilde{t}_0^-) = \tilde{x}_0$ , then  $F_i^- = 0$ ,  $i = \overline{1, s}$ .

**Theorem 2.** Let  $\tilde{z} \in A_0$  be a optimal element,  $\tilde{t}_0 \in (a, b)$ ,  $\tilde{t}_1 \in (a, b]$ ,  $\tilde{t}_0 < \gamma_1 < \dots < \gamma_s < \tilde{t}_1$ ; let now, there exist the finite limits  $F_i^+$ ,  $i = \overline{0, s+1}$ ,  $\dot{\gamma}_i^+$ ,  $i = \overline{1, s}$ . (see(12), (13)). Then there exists a non-zero vector  $\pi = (\pi_0, \dots, \pi_m)$ ,  $\pi_0 \leq 0$  and solution  $\psi(t)$  of the equation (14) such that the conditions 1), 2), (15) hold. Moreover

$$\pi \tilde{Q}_{t_0} \leq \Phi(\tilde{t}_0) F_0^+ + \sum_{i=1}^s \Phi(\gamma_i) F_i^+ \dot{\gamma}_i^+, \quad \pi \tilde{Q}_{t_1} \leq -\Phi(\tilde{t}_1) F_{s+1}^+.$$

If  $\tilde{\varphi}(\tilde{t}_0^+) = \tilde{x}_0$ , then  $F_i^+ = 0$ ,  $i = \overline{1, s}$ .

**Theorem 3.** Let  $\tilde{z} \in A_0$  be a optimal element,  $\tilde{t}_i \in (a, b)$ ,  $i = \overline{0, 1}$ ,  $\tilde{t}_0 < \gamma_1 < \dots < \gamma_s < \tilde{t}_1$ ; let now, there exist the finite limits  $F_i^-$ ,  $F_i^+$ ,  $i = \overline{0, s+1}$ ,  $\dot{\gamma}_i^-$ ,  $\dot{\gamma}_i^+$   $i = \overline{1, s}$ . Besides

$$F_0^- = F_0^+ = F_0, \quad F_i^- \dot{\gamma}_i^- = F_i^+ \dot{\gamma}_i^+ = F_i, \quad i = \overline{1, s}, \quad F_{s+1}^- = F_{s+1}^+.$$

Then there exists a non-zero vector  $\pi = (\pi_0, \dots, \pi_m)$ ,  $\pi_0 \leq 0$  and solution  $\psi(t)$  of the equation (14) such that the conditions 1), 2), (15) hold.

Moreover

$$\pi \tilde{Q}_{t_0} = \Phi(\tilde{t}_0) F_0 + \sum_{i=1}^s \Phi(\gamma_i) F_i, \quad \pi \tilde{Q}_{t_1} = -\Phi(\tilde{t}_1) F_{s+1}.$$

If  $\text{rank}(\tilde{Q}_{t_0}, \tilde{Q}_{t_1}, \tilde{Q}_{y_0}, \tilde{Q}_{y_1}) = 1 + m$ , then in the theorem 3  $\Phi(t) \neq 0$ . If  $\tilde{\varphi}(\tilde{t}_0^-) = \tilde{\varphi}(\tilde{t}_0^+) = \tilde{x}_0$ , then  $F_i = 0$ ,  $i = \overline{1, s}$ .

**Remark 1.** Assume that the function  $\tilde{\varphi}(t)$  is continuous at the points  $\tilde{t}_0$ ,  $\tau_j(\gamma_j(\tilde{t}_0))$ ,  $j = \overline{1, s-1}$ ,  $i = \overline{j+1, s}$ ; the function  $\tilde{u}(\theta_i(t))$ ,  $i = \overline{0, \nu}$  are continuous at points  $\tilde{t}_0$ ,  $\tilde{t}_1$ ,  $\gamma_j$ ,  $j = \overline{1, s}$ ; the function  $\gamma_i(\tilde{t})$  is continuous at point  $\tilde{t}_0$ . Then

$$F_0 = F[\tilde{t}_0]; \\ F_i = [F(\gamma_i, \tilde{x}(\tau_0(\gamma_i)), \dots, \tilde{x}(\tau_{i-1}(\gamma_i)), \tilde{x}_0, \tilde{\varphi}(\tau_i(\gamma_i)), \dots, \tilde{\varphi}(\tau_s(\gamma_i))) - \\ F(\gamma_i, \tilde{x}(\tau_0(\gamma_i)), \dots, \tilde{x}(\tau_{i-1}(\gamma_i)), \tilde{\varphi}(\tilde{t}_0^-), \tilde{\varphi}(\tau_i(\gamma_i)), \dots, \tilde{\varphi}(\tau_s(\gamma_i)))] \dot{\gamma}_i(\tilde{t}_0), \quad i = \overline{1, s} \\ F_{s+1} = F[\tilde{t}_1].$$

If  $\tilde{\varphi}(\tilde{t}_0) = \tilde{x}_0$ , then  $F_i = 0$ ,  $i = \overline{1, s}$ .

In conclusion, we will formulate the necessary conditions of optimality for the optimal problem (4)-(7).

**Theorem 4.** Let  $\tilde{z} = (\tilde{t}_0, \tilde{t}_1, \tilde{x}(\cdot), u(\cdot))$  be a optimal element for problem (4)-(7) (see def.3);  $\tilde{t}_i \in (a, b)$ ,  $i = \overline{0, 1}$ ,  $\tilde{t}_0 + \tau_k < \tilde{t}_1$ , let now, the function  $u(t)$  is continuous at the points  $\tilde{t}_0$ ,  $\tilde{t}_1$ ,  $\tilde{t}_0 + \tau_i$ ,  $i = \overline{1, k}$ . Then there exists a non-zero vector  $\pi = (\pi_0, \dots, \pi_m)$ ,  $\pi_0 \leq 0$  and solution  $\psi(t) = (\psi_1(t), \dots, \psi_n(t))$  of the equation

$$\dot{\psi}(t) = -\psi(t)A(t) - \sum_{i=1}^k \psi(t + \tau_i) D_i - \sum_{i=1}^k \psi_0(t + \tau_i) f_{y_i}^0[t + \tau_i], \quad t \in [\tilde{t}_0, \tilde{t}_1],$$

$$\psi_0(t) = \pi_0, \quad t \in [\tilde{t}_0, \tilde{t}_1], \quad \psi_0(t) = 0, \quad \psi(t) = 0, \quad t > \tilde{t}_1, \quad \tau_0 = 0,$$

such that the following conditions are fulfilled:

4)

$$\psi_0(t)f^0[t] + \psi(t)Cu(t) = \max_{u \in U_0} [\psi_0(t)f^0(t, \tilde{x}(t - \tau_0), \dots, \tilde{x}(t - \tau_k), u) + \psi(t)Cu]$$

$$t \in [\tilde{t}_0, \tilde{t}_1]$$

where

$$f^0[t] = f^0(t, \tilde{x}(t - \tau_0), \dots, \tilde{x}(t - \tau_s), \tilde{u}(t));$$

5)

$$\sum_{\alpha=1}^m \pi_\alpha q_{y_i}^\alpha(\tilde{t}_1, \tilde{x}(\tilde{t}_1)) = \psi_i(\tilde{t}_1), \quad i = 1, \dots, n;$$

$$\psi_0(\tilde{t}_0)f^0[\tilde{t}_0] + \psi(\tilde{t}_0) \left[ A(\tilde{t}_0)\tilde{x}(\tilde{t}_0) + \sum_{i=1}^k D_i \tilde{x}(\tilde{t}_0 - \tau_i) + C\tilde{u}(\tilde{t}_0) \right] + \sum_{i=1}^k \psi_0(\tilde{t}_0 + \tau_i) \left[ f^0(\tilde{t}_0 + \tau_i, \tilde{x}(\tilde{t}_0 + \tau_i - \tau_0), \dots, \tilde{x}(\tilde{t}_0 + \tau_i - \tau_{i-1}), x_0, \varphi(\tilde{t}_0 + \tau_i - \tau_{i+1}), \dots, \varphi(\tilde{t}_0 + \tau_i - \tau_k), \tilde{u}(\tilde{t}_0 + \tau_i)) - f^0(\tilde{t}_0 + \tau_i, \tilde{x}(\tilde{t}_0 + \tau_i - \tau_0), \dots, \tilde{x}(\tilde{t}_0 + \tau_i - \tau_{i-1}), \varphi(\tilde{t}_0), \varphi(\tilde{t}_0 + \tau_i - \tau_{i+1}), \dots, \varphi(\tilde{t}_0 + \tau_i - \tau_k), \tilde{u}(\tilde{t}_0 + \tau_i)) \right] + \sum_{i=1}^k \psi(\tilde{t}_0 + \tau_i) D_i [x_0 - \varphi(\tilde{t}_0)] = 0;$$

$$\sum_{\alpha=1}^m \pi_\alpha q_{t_i}^\alpha(\tilde{t}_1, \tilde{x}(\tilde{t}_1)) = \psi_0(\tilde{t}_1)f^0(\tilde{t}_1) + \psi(\tilde{t}_1) \left[ A(\tilde{t}_1)\tilde{x}(\tilde{t}_1) + \sum_{i=1}^k D_i \tilde{x}(\tilde{t}_1 - \tau_i) + C\tilde{u}(\tilde{t}_1) \right].$$

It is not difficult to see, that this theorem is a corollary of the Theorem 3.

**Theorem 5.** Let  $\tilde{z} = (\tilde{t}_0, \tilde{t}_1, \tilde{x}(\cdot), u(\cdot))$  be an optimal element for problem (4)-(7) and  $\tilde{t}_i \in (a, b)$ ,  $i = 0, 1$ ,  $\hat{t}_0 + \tau_i \neq \tilde{t}_1$  besides

$$q^i(t_1, x(t_1)) = x^i(t_1) - x_1^i, \quad i = \overline{1, n},$$

where  $x_1^i$ ,  $i = \overline{1, n}$  are the fixed numbers;

$$f^0(t, y_0, \dots, y_n, u) = \sum_{i=0}^k a_i(t)y_i + b(t)u(t);$$

$$U_0 = \left\{ u = \begin{pmatrix} u_1 \\ \vdots \\ u_k \end{pmatrix} \in R^k : |u_i| \leq 1 \right\}$$

Then there exists a non-zero vector  $\pi = (\pi_0, \dots, \pi_n)$ ,  $\pi_n \leq 0$  and solution  $\psi(t)$  of the equation

$$\dot{\psi}(t) = -\psi(t)A(t) - \sum_{i=1}^k \psi(t + \tau_i)D_i - \sum_{i=0}^k \psi_0(t + \tau_i)a_i[t + \tau_i], \quad t \in [\tilde{t}_0, \tilde{t}_1]$$

$$(\psi_0(\tilde{t}_1), \psi(\tilde{t}_1)) = \pi, \quad \psi_0(t) = \pi_0, \quad t \in [\tilde{t}_0, \tilde{t}_1], \quad \psi_0(t) = 0, \quad \psi(t) = 0, \quad t > \tilde{t}_1,$$

such that the following conditions are fulfilled:

6) if  $\sigma_i(t) \neq 0$  then  $\tilde{u}_i(t) = \text{sign}(\sigma_i(t))$ , where  $\sigma_i(t)$  is  $i$ -th coordinate of the vector function  $\psi_0(t)b(t) + \psi(t)C$ ;

7)

$$\psi_0(\tilde{t}_0) \left[ \sum_{i=0}^k a_i(\tilde{t}_0)\tilde{x}(\tilde{t}_0 - \tau_i) + b(\tilde{t}_0)\tilde{u}(\tilde{t}_0) \right] + \psi(\tilde{t}_0) \left[ A(\tilde{t}_0)\tilde{x}(\tilde{t}_0) + \sum_{i=1}^k D_i \tilde{x}(\tilde{t}_0 - \tau_i) + C\tilde{u}(\tilde{t}_0) \right] + \left[ \sum_{i=1}^k \psi_0(\tilde{t}_0 + \tau_i)a_i(\tilde{t}_0 + \tau_i) + \psi(\tilde{t}_0 + \tau_i)D_i \right] [x_0 - \varphi(t_0)] = 0;$$

$$\psi_0(\tilde{t}_1) \left[ \sum_{i=0}^k a_i(\tilde{t}_1)\tilde{x}(\tilde{t}_1 - \tau_i) + b(\tilde{t}_1)\tilde{u}(\tilde{t}_1) \right] + \psi(\tilde{t}_1) \left[ A(\tilde{t}_1)\tilde{x}(\tilde{t}_1) + \sum_{i=1}^k D_i \tilde{x}(\tilde{t}_1 - \tau_i) + C\tilde{u}(\tilde{t}_1) \right] = 0.$$

### References

- [1]. L. S. Pontryagin, V. G. Boltianskii, R. V. Gamkrelidze, E. F. Mishchenko, The mathematical theory of optimal processes (Russian), Nauka, Moscow, 1961.
- [2]. R. E. Belman, Dynamic programming (Russian), , Moscow, 1960.
- [3]. G. L. Kharatishvili, Optimal processes with delays, (Russian), Metsniereba, Tbilisi, 1966.
- [4]. G. L. Kharatishvili, Z.A. Machaidze, N.I. Markorashvili and T.A.Tadumadze, Abstract variational theory and its application to the optimal problems with delays (Russian), Metsniereba, Tbilisi, 1973.
- [5]. M. N. Oguztoreli, Time lag control systems, Academic Press, New York, London, 1966.
- [6]. A. Manitius, Optimal control of hereditary systems, in: Control theory and topics in functional analysis, v.2, Intern. Atomic Energy, Ag. Vienna, 1976, p.45-178.
- [7]. R. T. Ianushevskii, Control of the objects with delays, Nauka, Moscow, 1978.



## SUBALGEBRAS OF THE FREE CYCLIC HEYTING ALGEBRAS

**Guram Bezhanisvili and Revaz Grigolia**  
*Institute of Cybernetics*

### Abstract

We characterize all subalgebras of the free cyclic Heyting algebra  $F(1)$ . In particular, we prove that every subalgebra of  $F(1)$  is projective, and that a finite Heyting algebra is a subalgebra of  $F(1)$  iff it is projective.

### 1 Introduction

Heyting algebra  $(H, \vee, \wedge, \rightarrow, 0, 1)$  is a bounded distributive lattice  $(H, \vee, \wedge, 0, 1)$  with an additional binary operation  $\rightarrow : H \times H \rightarrow H$  such that for any  $a, b \in H$

$$x \leq a \rightarrow b \Leftrightarrow a \wedge x \leq b.$$

(Here  $x \leq y$  iff  $x \wedge y = x$  iff  $x \vee y = y$ .)

It is well-known that the class of all Heyting algebras forms a variety, which will be subsequently denoted by **HA**. Heyting algebras play an important role in different branches of mathematics: opens of a topological space, the lattice of congruences of a lattice, the object classifier of a topos, as well as algebraic models of Intuitionistic Logic all form Heyting algebras. These (and other) important features boosted a thorough investigation of Heyting algebras. A lot of results have been obtained. We will list only some of them: representation of Heyting algebras by means of Esakia spaces, which are "good" Priestley spaces [5]; description of finitely generated free Heyting algebras [14], Grigolia [8], Bellissima [2], Ghilardi [7], Butz [3].

§3 characterizes all subalgebras of the free cyclic Heyting algebra  $F(1)$  -- the so-called Rieger-Nishimura ladder. It is shown that every subalgebra of  $F(1)$  is projective, and that a finite Heyting algebra is a subalgebra of  $F(1)$  iff it is projective. Atoms and co-atoms of the lattice  $S(F(1))$  of all subalgebras of  $F(1)$  together with the Frattini subalgebra of  $F(1)$  are also described.

### 2 Preliminaries

Recall that a topological space  $(X, \Omega)$  is called a *Stone space* if it is 0-dimensional, compact and Hausdorff.  $A \subset X$  is said to be *clopen* if  $A$  is simultaneously closed and open. For these and other elementary notions from general topology the reader is referred to Engelking [4]. We denote the set of all clopen subsets of  $X$  by  $CP(X)$ .

Let  $(X, R)$  be a partially ordered set. For any  $x \in X$  and  $A \subseteq X$ , let  $R(x) = \{y \in X : xRy\}$ ,  $R(A) = \bigcup_{x \in A} R(x)$ ,  $R^{-1}(x) = \{y \in X : yRx\}$  and  $R^{-1}(A) = \bigcup_{x \in A} R^{-1}(x)$ .

$A$  is said to be a *R-cone* of  $X$  if  $R(A) = A$  ( $-R^{-1} - A = A$ ). We call  $A$  a *down R-cone* if  $R^{-1}(A) = A$ ,  $-R - A = A$ .

Suppose a triple  $(X, \Omega, R)$  is given, where  $(X, \Omega)$  is a Stone space and  $R$  -- a partial order on  $X$ .  $R$  is said to be *point-closed* if the set  $R(x)$  is closed for every  $x \in X$ .  $R$  is said to be an *Esakia relation* if  $R$  is point-closed and the following condition is satisfied:

$$(*) \quad A \in CP(X) \Rightarrow R^{-1}(A) \in CP(X).$$

We denote by  $CON_R(X)$  the set of all clopen  $R$ -cones of  $X$ . Recall that every Esakia relation satisfies the following Priestley separation property:

(\*\*) For any  $x, y \in X$ , if  $x$  is not  $R$ -related to  $y$ , then there exists  $U \in \text{CON}_R(X)$  such that  $x \in U$  and  $y \notin U$ .

Hence every Esakia space is a Priestley space, but the converse is not true in general. An easy counterexample is the space shown in Fig.1 below.

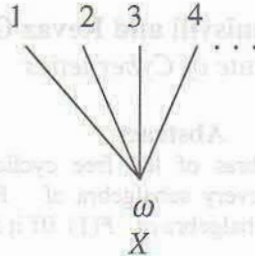


Fig. 1

Here  $X$  is the Alexandroff compactification of the set of all natural numbers (with the discrete topology), and the order is defined by putting  $nRm$  iff  $n=m$ ,  $\omega Rn$  for any natural  $n$ , and  $\omega R\omega$ . Then it is obvious that  $\{n\}$  is clopen for every natural  $n$ , while  $R^{-1}\{n\} = \{n, \omega\}$  is closed, but not open. Hence  $X$  is not an Esakia space. On the other hand, it is easy to check that  $X$  is indeed a Priestley space.

Now in the same way as Priestley spaces serve as duals of distributive lattices (Priestley [11]), Esakia spaces serve as duals of Heyting algebras (Esakia [5]). In fact, we have that every Heyting algebra is represented as the algebra of all clopen  $R$ -cones of the corresponding Esakia space.

Here we recall that the dual space  $(X, \Omega, R)$  of a Heyting algebra  $H$  is constructed in the following way:  $X$  is the set of all prime filters of  $H$ ,  $R$  is the set-theoretical inclusion,  $\varphi(a)$  denotes the set  $\{x \in X : a \in x\}$  for every  $a \in H$ ,  $\varphi(H)$  denotes the set  $\{\varphi(a)\}_{a \in H}$  and  $\Omega$  is defined on  $X$  by announcing the Boolean closure  $B(\varphi(H))$  of the set  $\varphi(H)$  as a base for the topology.

Also recall that  $(\varphi(H), \cup, \cap, \rightarrow, \emptyset)$ , where  $A \rightarrow B = -R^{-1}(A - B) = \{x \in X : \forall y(xRy \ \& \ y \in A \Rightarrow y \in B)\}$  for every  $A, B \in \varphi(H)$ , constitutes a Heyting algebra which is isomorphic to the initial  $H$ , and that  $\varphi(H) = \text{CON}_R(X)$ . Hence every Heyting algebra is represented as the algebra of all clopen  $R$ -cones of the corresponding Esakia space.

This correspondence between Heyting algebras and Esakia spaces can be extended to the dual equivalence of the appropriate categories. For given two partial orders  $(X_1, R_1)$  and  $(X_2, R_2)$ , call a function  $f : X_1 \rightarrow X_2$  *monotone* if  $xR_1y$  implies  $f(x)R_2f(y)$ , for any  $x, y \in X_1$ . Call  $f$  *strongly monotone* if in addition  $f(x)R_2y$  implies  $(\exists z \in X_1)(xR_1z \ \& \ f(z) = y)$ , for any  $x \in X_1$  and  $y \in X_2$ .

Now  $f$  is said to be an *Esakia morphism* if  $f$  is continuous and strongly monotone. Hence Esakia morphisms are stronger than Priestley morphisms, since Priestley morphisms are only continuous and monotone. An easy example of a monotone map, which is not strongly monotone, is shown in Fig.2 below.

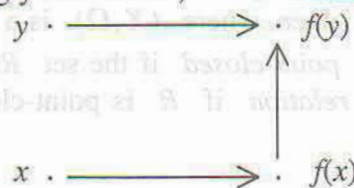


Fig.2

Now we have that the category of Heyting algebras and Heyting homomorphisms is dual (dually equivalent) to the category of Esakia spaces and Esakia morphisms (Esakia [5]).

Exploring this duality, many important algebraic results can be simply proved using the dual category of HA. For instance, homomorphic images of a Heyting algebra  $H$  correspond to closed  $R$ -cones, while subalgebras of  $H$  correspond to images under Esakia morphisms of its dual  $X_H$ . For further results in this direction we refer to Esakia [6].

### 3 Subalgebras of the Rieger-Nishimura ladder

This section is devoted to subalgebras of  $F(1)$ . In order to characterize them, we define the  $\omega$ -sum of Heyting algebras, which generalizes the ordinary sum  $H_1 \oplus H_2$  of two Heyting algebras  $H_1$  and  $H_2$  constructed in the following way.  $H_1 \oplus H_2 = \overline{H}_1 \cup \overline{H}_2$ , where  $\overline{H}_1$  and  $\overline{H}_2$  are such isomorphic copies of  $H_1$  and  $H_2$  respectively that  $\overline{H}_1 \cap \overline{H}_2 = \{1_{H_1}\} = \{0_{H_2}\}$ ; further, for any  $a, b \in H_1 \oplus H_2$  put  $a \leq_{H_1 \oplus H_2} b$  if either  $a \leq_{H_1} b$ ,  $a \leq_{H_2} b$  or  $a \in H_1$  and  $b \in H_2$  ( $a$  and  $b$  are taken from  $H_1 \oplus H_2$  up to isomorphism). Figuratively speaking, we put  $H_2$  over  $H_1$ . It is easy to prove that  $\leq_{H_1 \oplus H_2}$  is a lattice order on  $H_1 \oplus H_2$ , and that  $H_1 \oplus H_2$  forms a Heyting algebra with respect to  $\leq_{H_1 \oplus H_2}$ .

Let  $\{H_n\}_{n \in \omega}$  be a countable family of Heyting algebras. Define  $\bigoplus_{n \in \omega} H_n$  by putting  $\bigoplus_{n \in \omega} H_n = \bigcup_{n \in \omega} \overline{H}_n \cup \{T\}$ , where  $\overline{H}_n$  are such isomorphic copies of  $H_n$  that  $\overline{H}_n \cap \overline{H}_{n+1} = \{1_{H_n}\} = \{0_{H_{n+1}}\}$ , and  $T \notin \overline{H}_n$  for any  $n$ ; further, for any  $a, b \in \bigoplus_{n \in \omega} H_n$  put  $a \leq_{\bigoplus_{n \in \omega} H_n} b$  if either there is  $n \in \omega$  such that  $a \leq_{H_n} b$  or  $a \in H_m$ ,  $b \in H_k$  and  $m \leq k$ ; and  $a \leq T$  for any  $a \in \bigoplus_{n \in \omega} H_n$ . It is easy to prove that  $\leq_{\bigoplus_{n \in \omega} H_n}$  is a lattice order on  $\bigoplus_{n \in \omega} H_n$ , and that  $\bigoplus_{n \in \omega} H_n$  forms a Heyting algebra with respect to  $\leq_{\bigoplus_{n \in \omega} H_n}$ . If each  $H_n$  is equal to  $H$ , then we simply write  $\bigoplus_{\omega} H$ .

Subsequently we will be interested in  $\bigoplus_{n \in \omega} B_n$ , where each  $B_n$  is either the two-element or four element Boolean algebra, which we denote by  $\mathbf{2}$  and  $\mathbf{2}^2$ . The dual spaces of  $\bigoplus_{\omega} \mathbf{2}$  and  $\bigoplus_{\omega} \mathbf{2}^2$  are shown in Fig.3 below.

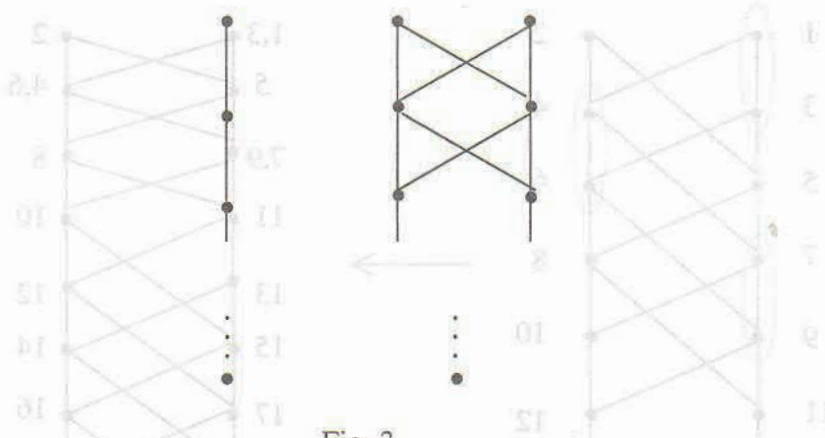


Fig. 3

**Lemma 1.** Every  $\bigoplus_{n \in \omega} B_n$  is a subalgebra of  $F(1)$ .

**Proof.** First let us show that  $\bigoplus_{\omega} \mathbf{2}^2$  is a subalgebra of  $F(1)$ . Consider the map  $f : X_{F(1)} \rightarrow X_{\bigoplus_{\omega} \mathbf{2}^2}$

which identifies the points in the circles shown in Fig.4 below. Then it is an easy exercise to check that  $f$  is an onto Esakia morphism. Hence  $\oplus_{\omega} 2^2$  is a subalgebra of  $F(1)$ . Now since every  $\oplus_{n \in \omega} B_n$  is a subalgebra of  $\oplus_{\omega} 2^2$ , every  $\oplus_{n \in \omega} B_n$  is a subalgebra of  $F(1)$  either.  $\square$

**Corollary 2.** Every  $(\oplus_{n=1}^k B_n) \oplus 2$  is a subalgebra of  $F(1)$ .

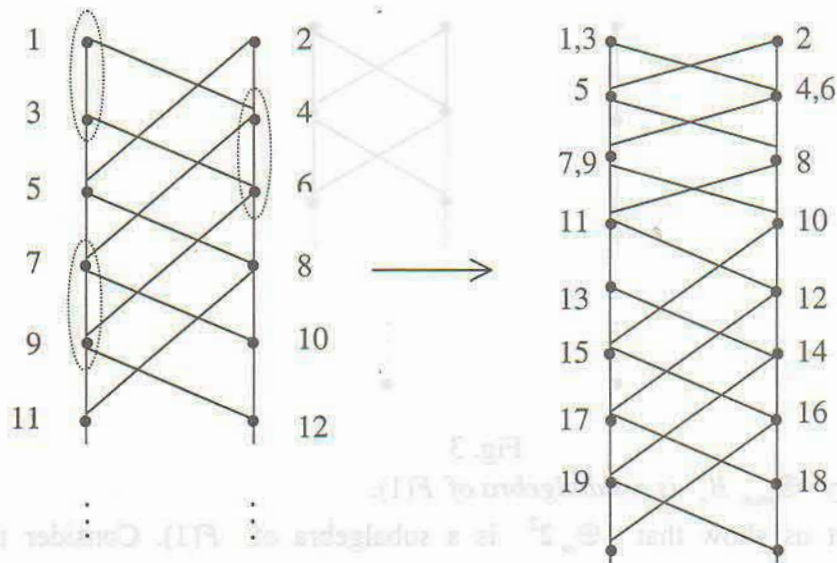
**Proof.** First note that for every  $k$ ,  $(\oplus_k 2^2) \oplus 2$  is a subalgebra of  $\oplus_{\omega} 2^2$ . The corresponding Esakia morphism is constructed by identifying all the points of  $X_{\oplus_{\omega} 2^2}$  of the depth greater or equal to  $k$ . Now since every  $(\oplus_{n=1}^k B_n) \oplus 2$  is a subalgebra of  $(\oplus_k 2^2) \oplus 2$ , every  $(\oplus_{n=1}^k B_n) \oplus 2$  is a subalgebra of  $\oplus_{\omega} 2^2$  either. Hence every  $(\oplus_{n=1}^k B_n) \oplus 2$  is a subalgebra of  $F(1)$ .  $\square$



Fig. 4

**Lemma 3.** Every  $(\oplus_{n=1}^k B_n) \oplus F(1)$  is a subalgebra of  $F(1)$ .

**Proof.** First let us show that for every  $k$ ,  $(\oplus_{n=1}^k B_n) \oplus F(1)$  is a subalgebra of  $F(1)$ . Indeed, for every  $k$ , consider the map  $g_k : X_{F(1)} \rightarrow X_{\oplus_{\omega} 2^2 \oplus F(1)}$ , which is analogous to  $f$  from Lemma 1, but stops identifying points starting from the depth  $k+2$  (see Fig. 5 below).



•  
ω

•  
ω

Fig. 5

Then it is easy to check that  $g_k$  is an onto Esakia morphism. Hence  $(\bigoplus_k 2^2) \oplus F(1)$  is a subalgebra of  $F(1)$ . Now since every  $\bigoplus_{n=1}^k B_n$  is a subalgebra of  $\bigoplus_k 2^2$ , every  $(\bigoplus_{n=1}^k B_n) \oplus F(1)$  is a subalgebra of  $(\bigoplus_k 2^2) \oplus F(1)$ , and hence is a subalgebra of  $F(1)$  as well.  $\square$

**Theorem 4.** *A Heyting algebra  $H$  is a subalgebra of  $F(1)$  iff either  $H = \bigoplus_{n \in \omega} B_n$ ,  $H = \bigoplus_{n=1}^k B_n$  or  $H = (\bigoplus_{n=1}^k B_n) \oplus F(1)$ .*

**Proof.** As follows from Lemmas 1 and 3 and Corollary 2,  $\bigoplus_{n \in \omega} B_n$ ,  $\bigoplus_{n=1}^k B_n$  and  $(\bigoplus_{n=1}^k B_n) \oplus F(1)$  are all subalgebras of  $F(1)$ .

In order to prove the converse, we need some preparation. First let us recall that a partition  $E$  of an Esakia space  $X$  is said to be *correct* if the following two conditions are satisfied:

- 1) For all  $x, y, z \in X$ , if  $xEy$  and  $yRz$ , then there exists  $w \in X$  such that  $xRw$  and  $wEz$ ;
- 2) For all  $x, y \in X$ , if it is not the case that  $xEy$ , then there exists an  $E$ -saturated clopen  $A$  (that is  $E(A)=A$ , where  $E(A) = \bigcup_{w \in A} E(w)$  and  $E(w) = \{v \in X : wEv\}$ ) such that  $x \in A$  and  $y \notin A$ .

(Note that 2) implies that every equivalence class of  $E$  is closed.)

It is well-known that there exists a one-to-one correspondence between correct partitions of  $X$  and images of  $X$  under Esakia morphisms. Hence there is a one-to-one correspondence (actually dual isomorphism) between subalgebras of a Heyting algebra  $H$  and correct partitions of the dual  $X_H$  of  $H$ .

**Claim 5.** *For any correct partition  $E$  of  $X_{F(1)}$ , every equivalence class  $C$  of  $E$  is convex, that is from  $x, y \in C$  and  $xRzRy$  it follows that  $z \in C$ .*

**Proof.** Indeed, suppose  $x, y \in C$  and  $xRzRy$ . Since  $yEx$  and  $xRz$ , then 1) implies that there exists  $w$  such that  $yRw$  and  $zEw$ .  $wEz$  and  $zRy$  imply that there exists  $v$  such that  $wRv$  and  $vEy$ . Continuing this process, we obtain an increasing chain of points of  $X_{F(1)}$ . Since  $X_{F(1)}$  is dually well-founded, this process will end up at a maximal point, say  $u$ . Now since  $u$  is maximal, 1) implies that  $u$  is  $E$ -equivalent to both  $x$  and  $z$ . Hence  $z \in C$ .  $\square$

Now let us get back to our proof of Theorem 18. Suppose  $H$  is a subalgebra of  $F(1)$ . Let  $E$  be the corresponding correct partition of  $X_{F(1)}$ . Then either every equivalence class of  $E$  is finite (hence  $H$  is infinite), or there are only finitely many equivalence classes of  $E$  (hence  $H$  is finite), and all but one of them is finite. Indeed, since every equivalence class of  $E$  is closed, if a class contains infinitely many points, it also should contain  $\omega$ . Hence there can not be two infinite equivalence classes of  $E$ .

In either case  $(X_{F(1)}/E, R)$  is dually well-ordered, where  $R$  is defined on  $X_{F(1)}$  componentwise.  $v$  is said to *cover*  $w$  if  $wRv$  and whenever  $wRuRv$ , either  $w=u$  or  $u=v$ . Call a point  $w$  of  $X_{F(1)}/E$  *degenerate* if there exist two non- $R_E$ -comparable points  $w_1, w_2 \in X_{F(1)}/E$  such that  $w_1$  is the only cover of  $w$  and it is not the case that  $wR_Ew_2$ . (Note that in  $X_{F(1)}$  there is just one degenerate point denoted by 3 in Fig.5.)

**Claim 6.** *If there is no degenerate point in  $X_{F(1)}/E$ , then  $X_{F(1)}/E$  is isomorphic to the dual of either  $\bigoplus_{n \in \omega} B_n$  or  $(\bigoplus_{n=1}^k B_n) \oplus 2$ .*

**Proof.** Since the width (that is the cardinality of a maximal anti-chain of points) of  $X_{F(1)}$  is 2, the width of  $X_{F(1)}/E$  is no more than 2. Further,  $X_{F(1)}/E$  is dually well-ordered and contains the least element  $E(\omega)$ . (Note that either  $E(\omega) = \omega$  or  $E(\omega)$  contains the whole lower part of  $X_{F(1)}$ .) Furthermore, for any  $w \in X_{F(1)}/E$ , if  $wRu$  and  $u$  and  $v$  are of the same  $R$ -depth, then  $wRv$  as well. Hence  $X_{F(1)}/E$  is the sum of 1- and 2- element sets, and hence is isomorphic to the dual of either  $\bigoplus_{n \in \omega} B_n$  or  $(\bigoplus_{n=1}^k B_n) \oplus 2$ .

□

**Claim 7.** *There may exist only one degenerate point in  $X_{F(1)}/E$ , say  $x_E$ . Moreover, the equivalence class  $x_E$  consists of just one point, and so do all other equivalence classes which are  $R$ -related to  $x_E$ .*

**Proof.** Suppose  $x_E$  is a degenerate point of  $X_{F(1)}/E$ . Then there exist  $w_1, w_2 \in X_{F(1)}/E$  such that  $w_1$  is the only cover of  $x_E$  and it is not the case that  $x_E R w_2$ . Suppose  $x_E$  consists of at least two points. From the structure of  $X_{F(1)}$  it directly follows that one of those points is  $R$ -related to a point from  $w_2$ , and hence  $x_E R w_2$ , a contradiction. Hence  $x_E$  consists of just one point  $x$ .

Now suppose  $x$  is of the depth  $n$ , and show that the equivalence class containing another point of depth  $n$  also consists only of that point. Indeed, denote another point of depth  $n$  by  $y$ . Suppose  $yEz$  and  $z \neq y$ . Then Claim 5 implies that  $zRx$ . Hence there should exist  $u$  such that  $yRu$  and  $uEx$ , which is impossible. Thus the equivalence class containing  $y$  consists only of  $y$ . Now consider a point  $z$  of depth  $n+1$  which is not related to  $y$  and show that the equivalence class containing  $z$  also consists only of  $z$ . Suppose  $zEu$  and  $u \neq z$ . Then Claim 5 implies that  $uRy$ , and from  $zEu$  and  $uRy$  it follows that there exists  $v$  such that  $zRv$  and  $vEy$ , which is again a contradiction, hence the equivalence class containing  $z$  also consists only of  $z$ . In the same way one can show that the equivalence class containing another point of depth  $n+1$  also consists only of that point. Continuing this process we get that every equivalence class  $R$ -related to  $x_E$  consists of just one point.

It follows that there may exist only one degenerate point in  $X_{F(1)}/E$ . Indeed, since  $X_{F(1)}/E$  is dually well-founded, there exists the first degenerate point  $x_E = \{x\}$ . Now all the equivalence classes  $R$ -related to  $x_E$  contain only a single point, and  $X_{F(1)}/E$  repeats the lower part of  $X_{F(1)}$  starting from  $x$ . Hence there is just one degenerate point in  $X_{F(1)}/E$ . □

It directly follows from Claim 7 that if  $X_{F(1)}/E$  contains a degenerate point, then the upper part of  $X_{F(1)}/E$  is the sum of either 1- or 2- element sets, and the lower part of  $X_{F(1)}/E$  is isomorphic to  $X_{F(1)}$ . Hence  $X_{F(1)}/E$  is isomorphic to the dual of  $H = (\bigoplus_{n=1}^k B_n) \oplus F(1)$ . Thus, if  $H$  is a subalgebra of  $F(1)$ , then either  $H = \bigoplus_{n \in \omega} B_n$ ,  $H = \bigoplus_{n=1}^k B_n \oplus 2$  or  $H = (\bigoplus_{n=1}^k B_n) \oplus F(1)$ . □

Let us note that A.I. Zitkin in [15] has shown that finite subdirectly irreducible Heyting algebra  $H$  is a subalgebra of countably many generated free Heyting algebra  $F(\omega)$  if and only if  $H = \bigoplus_{n=1}^k B_n \oplus 2$ .

It follows that the lattice  $S(F(1))$  of all subalgebras of  $F(1)$  contains countably many atoms, which are all isomorphic to the three element Heyting algebra  $\mathbf{3}$ , but are incomparable inside  $F(1)$ , and two coatoms  $F_1$  and  $F_2$ , whose duals are shown in Fig.6 below.

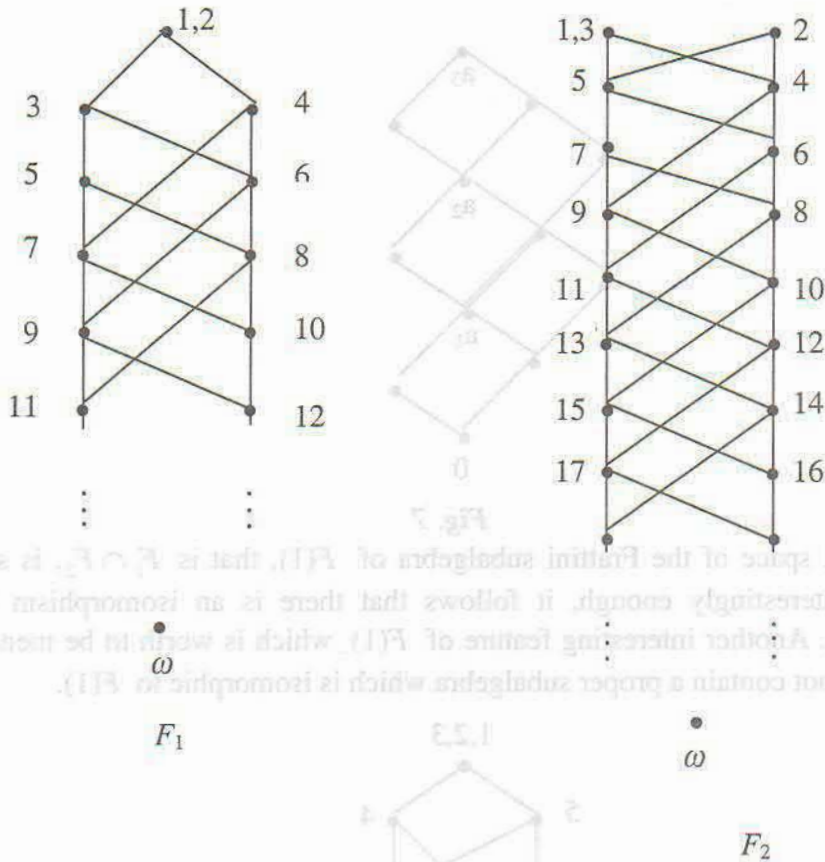


Fig. 6

Indeed, it is obvious that  $\mathbf{2}$  and  $F(1)$  are a least and a greatest elements of  $S(F(1))$  respectively.

Further, for any natural  $n$  define a partition  $E_n$  which consists of two classes, in one we have all the points of  $X_{F(1)}$  of the depth  $\leq n$ , and in another -- all the points of  $X_{F(1)}$  of the depth  $> n$ . Then it is obvious that every  $E_n$  is a correct partition of  $X_{F(1)}$ , that  $E_n$  is incomparable with  $E_m$ , if  $n \neq m$ , that  $X_{F(1)} / E_n$  is isomorphic to  $X_3$  for every  $n$ , and that for any other correct partition  $E$  of  $X_{F(1)}$ , there is  $n$  such that  $E \subseteq E_n$ . Hence there exist countably many atoms of  $S(F(1))$ , they are the algebras  $\{0, a_n, 1\}$ ,  $n \in \omega$  (see Fig.7 below).

Furthermore, suppose  $H$  is a proper subalgebra of  $F(1)$ . Let  $E$  be the corresponding partition of  $X_{F(1)}$ . Then there are at least two  $E$ -equivalent points in  $X_{F(1)}$ . This means that at least two back-to-back points are  $E$ -equivalent, which in turn means that either 1,2 or 1,3 are  $E$ -equivalent as well. In the former case consider a subpartition of  $E$  which only identifies 1,2, and in the latter case the one which only identifies 1,3. Then we obtain that either  $H$  is a subalgebra of  $F_1$ , or  $H$  is a subalgebra of  $F_2$ . Hence  $F_1$  and  $F_2$  are the only coatoms of  $F(1)$ .

(It should be noted that  $F_1$  is isomorphic to a subalgebra of  $F_2$ , but as subalgebras of  $F(1)$  they are incomparable.)

It follows that the lattice  $\mathcal{S}(F(1))$  of all subalgebras of  $F(1)$  contains countably many atoms, which are all isomorphic to the three element Heyting algebra  $\mathcal{H}$ , but are incompatible inside  $F(1)$  and two atoms  $F_1$  and  $F_2$ , whose duals are shown in Fig. 6 below.

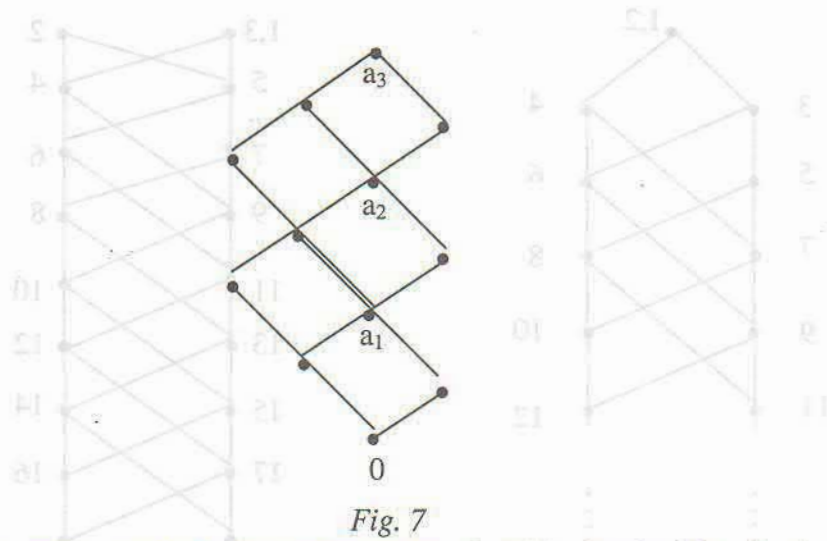


Fig. 7

The dual space of the Frattini subalgebra of  $F(1)$ , that is  $F_1 \cap F_2$ , is shown in Fig.8 below. Interestingly enough, it follows that there is an isomorphism between  $F_1 \cap F_2$  and  $F_1$ . Another interesting feature of  $F(1)$  which is worth to be mentioned is that  $F(1)$  does not contain a proper subalgebra which is isomorphic to  $F(1)$ .

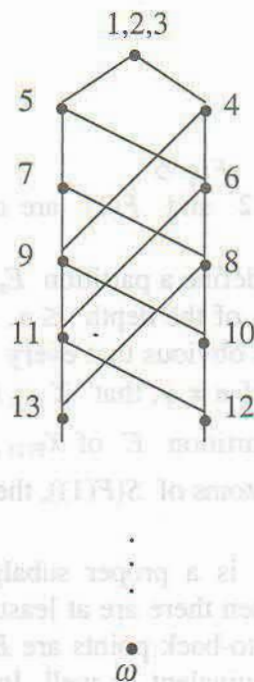


Fig. 8

Let us finish the paper by showing that every subalgebra of  $F(1)$  is projective. Recall that an algebra  $A$  from a variety  $\mathbf{V}$  is said to be *projective* if it is a retract of a free  $\mathbf{V}$ -algebra.

**Corollary 8.** 1) A finite Heyting algebra is a subalgebra of  $F(1)$  iff  $H = \bigoplus_{n=1}^k B_n \oplus \mathbf{2}$ .

2) A finite Heyting algebra is a subalgebra of  $F(1)$  iff  $H$  is projective.

**Proof.** 1) directly follows from Theorem 4.

2) As follows from Balbes and Horn [1], a finite Heyting algebra  $H$  is projective iff  $H = \bigoplus_{n=1}^k B_n \oplus 2$ . Now apply 1).  $\square$

**Corollary 9.** If  $H$  is a subalgebra of  $F(1)$ , then  $H$  is projective.

**Proof.** If  $H = \bigoplus_{n=1}^k B_n \oplus 2$ , then as follows from Corollary 8,  $H$  is projective. Further, it is shown in Grigolia [9] that if either  $H = \bigoplus_{n \in \omega} B_n$  or  $H = (\bigoplus_{n=1}^k B_n) \oplus F(1)$ , then  $H$  is a retract of  $F(\omega)$  -- the free countably generated Heyting algebra. Hence  $H$  is projective. (Though  $H = \bigoplus_{n \in \omega} B_n$  and  $H = (\bigoplus_{n=1}^k B_n) \oplus F(1)$  are not retracts of  $F(1)$ ).  $\square$

## References

- [1] R. Balbes and A. Horn, *Injective and projective Heyting algebra*, Trans. Amer. Math. Soc. 148(1970), pp. 549-559.
- [2] F. Bellissima, *Finitely generated free Heyting algebras*, Journal of Symbolic Logic 51(1986), pp. 152-165.
- [3] C. Butz, *Finitely presented Heyting algebras*, 1998, preprint.
- [4] R. Engelking, *General Topology*, Warszawa, 1977.
- [5] L. Esakia, *Topological Kripke models* [in Russian], Dokl. Akad. Nauk SSSR 214(1974), pp. 298-301.
- [6] L. Esakia, *Heyting Algebras I, Duality Theory* [in Russian], Metsniereba Press, Tbilisi, 1985.
- [7] S. Ghilardi, *Free Heyting algebras as bi-Heyting algebras*, C. R. Math. Rep. Acad. Sci. Canada 14(1992), pp. 240-244.
- [8] R. Grigolia, *Free Algebras of Non-Classical Logics* [in Russian], Metsniereba Press, Tbilisi, 1987.
- [9] R. Grigolia, *Projective Heyting algebras*, preprint, 2000.
- [10] I. Nishimura, *On formulas of one variable in intuitionistic propositional calculus*, Journal of Symbolic Logic 25(1960), pp. 327-331.
- [11] H. Priestley, *Ordered topological spaces and the representation of distributive lattices*, Proceedings of the London Mathematical Society 24(1972), pp. 507-530.
- [12] L. Rieger, *A note on the so-called closure algebras* [in Russian], Czechoslovak Math. J. 7(1957), pp. 16-20.
- [13] A. Troelstra, *On intermediate propositional logics*, Indagationes Mathematicae 27(1965), pp. 141-152.
- [14] A. Urquhart, *Free Heyting algebras*, Algebra Universalis 3(1973), pp. 94-97.
- [15] A. I. Zitkin, *On permissible roots of intuitionistic logic* [in Russian], Math. Sb., 102(144)(1977), N. 2, pp. 314-323.

$\int$	$\&$
$\pi$	$\Sigma$

Institute of Cybernetics  
 Georgian Academy of Sciences  
 E-mail: [cyber@hepi.edu.ge](mailto:cyber@hepi.edu.ge)  
<http://cyber.hepi.edu.ge/proceedings>

*Proceedings*  
**Institute of Cybernetics**  
 Vol.1, N1, 2000

## THE GAUGE QUANTUM COMPUTATION

Gia Giorgadze

*Institute of Cybernetics*

### Abstract

A model of quantum computation is presented, based on gauge field theory. In our opinion, it generalizes holonomic quantum computation introduced in [1],[2]. In addition to the construction given in [3] which we reproduce in the third section, a vector bundle on the parameter space  $M$  is constructed also when an ODE on  $M$  is given [4]. This is done in the second section. This will give a simulation of gauge field theory on quantum computers similarly to [5].

### 1. Quantum model of the computation

After the celebrated work [6] of P.Shor, model of quantum computation were considered by many authors. For introducing necessary notions and statements one may consult works of [7],[8],[9].

Quantum Computer is a new theoretical model of computation based on the laws of quantum mechanics. Such model of computation has been considered by R.Landauer [10], R.Feynman [11], C.Bennett [12], D.Deutsch [13] and P.Benioff [14]. In classical computers, the elementary information unit is a bit. The quantum analog of a bit called a *qubit*. A two state quantum system is described by a unit vector in the Hilbert space  $C^2$ . One of the two states will be denoted by  $|0\rangle$ , corresponds to the vector  $(1,0)$ . The other state, which is orthogonal to the first one, will be denoted by  $|1\rangle = (0,1)$ . These two states constitute an orthogonal basis to the Hilbert space. The state space for qubits, each with basis  $\{|0\rangle, |1\rangle\}$ , has basis  $\{|0\rangle \otimes |0\rangle, |0\rangle \otimes |1\rangle, |1\rangle \otimes |0\rangle, |1\rangle \otimes |1\rangle\}$ , which can be written compactly as  $\{|00\rangle, |01\rangle, |10\rangle, |11\rangle\}$ .

One possible realization of qubits, which is founded on the ion trap is consider in [15].

A basis for a three qubit system is  $\{|000\rangle, |001\rangle, |010\rangle, |100\rangle, |011\rangle, |101\rangle, |110\rangle, |111\rangle\}$  and in general an  $n$  qubit system has  $2^n$  basis vectors, since tensor product arbitrary vector spaces  $F_1$  and  $F_2$  has dimension  $\dim F_1 \times \dim F_2$ .

The state  $|00\rangle + |11\rangle$  is an example of a quantum state that cannot be described in term of the state of each of its components. In other words, we cannot find  $a_1, a_2, b_1, b_2$  such that

$$(a_1|0\rangle + b_1|1\rangle) \otimes (a_2|0\rangle + b_2|1\rangle) = |00\rangle + |11\rangle$$

since

$$(a_1|0\rangle + b_1|1\rangle) \otimes (a_2|0\rangle + b_2|1\rangle) = a_1a_2|00\rangle + a_1b_2|01\rangle + b_1a_2|10\rangle + b_1b_2|11\rangle$$

and  $a_1b_2=0$  implies that either  $a_1a_2=0$  or  $b_1b_2=0$ . States which cannot be decomposed in this way are called *entangled* states.

More generally, we write  $|i\rangle$  to mean  $|i_{n-1}, \dots, i_0\rangle$  where  $|i_j\rangle$  are the binary digits of the number  $i$ . This representation allays us to use our quantum systems being a computer. The general state which describes this system is a complex unit vector in the Hilbert space, called

the superposition  $\sum_{i=0}^{2^n-1} c_i |i\rangle$ , where  $\sum_{i=0}^{2^n-1} |c_i|^2 = 1$ . The initial state will correspond to the input

for the computation. We will then perform elementary operations on the system. The operations will correspond to the computational steps in the computation, just like logical gates are the elementary steps in classical computers. Assume that all the operations are performed on an isolated system, so the evolution can always be described by  $n$  unitary matrix operating on the state of the system.

**Definition 1.** A quantum gate on  $k$  qubits is a unitary matrix  $U$  of dimension  $2^k \times 2^k$ .

The example of a simple quantum gate operating on one qubit is

$$NOT = \begin{pmatrix} 0 & 1 \\ 1 & 0 \end{pmatrix}$$

where operate on the superpositions by wall:

$$NOT(c_0|0\rangle + c_1|1\rangle) = c_0|1\rangle + c_1|0\rangle.$$

In general,  $NOT$  gate operates on the first qubit in a system of  $n$  qubits, in the state  $\sum_i c_i |i_1 \dots i_n\rangle$

this state transforms to  $\sum_i c_i (NOT|i_1\rangle) |i_2 \dots i_n\rangle = \sum_i c_i |-i_1 i_2 \dots i_n\rangle$ .

Another quantum gate is the controlled  $NOT$  gate acting on two qubits, which computes the classical function:  $(a, b) \mapsto (a, (a+b) \bmod 2)$ ,  $a, b \in \{0,1\}$ .

This function can be represented by the  $4 \times 4$  matrix  $CNOT : C^2 \otimes C^2 \rightarrow C^2 \otimes C^2$  and

$$CNOT = \begin{pmatrix} 1 & 0 & 0 & 0 \\ 0 & 1 & 0 & 0 \\ 0 & 0 & 0 & 1 \\ 0 & 0 & 1 & 0 \end{pmatrix}$$

The  $CNOT$  gate cannot be decomposed into a tensor product of two single-bit transformation.

Quantum gates can perform more complicated tasks than simply computing classical functions. An example of such a quantum gate, which is not a classical gate is a gate which applies a general rotation on one qubit:

$$U_{\theta, \varphi} = \begin{pmatrix} \cos \theta & \sin \theta e^{i\varphi} \\ -\sin \theta e^{-i\varphi} & \cos \theta \end{pmatrix}$$

To perform quantum computation, we allow a sequence of elementary quantum gates on the qubit in our system. Suppose, that we have applied all the quantum gates in our algorithm, and computation has come to an end. The state which was initially a basis state has been rotated to the state  $|a\rangle \in C^{2^n}$ .

Consider a measurement of a qubit in the state  $|a\rangle = c_0|0\rangle + c_1|1\rangle$ . This qubit is neither in the state  $|0\rangle$  nor in  $|1\rangle$ . The measurement postulate asserts that when the state of qubit is observed, it must decide on one of the two possibilities. This decision is made non-deterministically. The classical outcome of the measurement would be 0 with probability  $|c_0|^2$  and 1 with probability  $|c_1|^2$ . After the measurement, the state of qubits is either  $|0\rangle$  or  $|1\rangle$  in consistency with the classical outcome of the measurement.

**Quantum Program.** The quantum analogy to Newton's Third Law is the Schrodinger equation

$$H\psi(r, t) = i\hbar \frac{\partial}{\partial t} \psi(r, t) \quad (1.1)$$

which determines the dynamics of a particle system. The Hamiltonian operator  $H$  describes the

total energy of the system at a given time.

If we take the simple case of a particle in a static potential  $V$ , equation (1.1) can be written as

$$\left(-\frac{\hbar^2}{2m}\nabla^2 + V(r)\right)\psi(r,t) = i\hbar\frac{\partial}{\partial t}\psi(r,t).$$

If the quantum state  $\psi(r,t)$  is of the form  $\psi(r,t) = \psi(r)\phi(t)$ , with  $|\phi(t)| = 1$ , then  $\rho = \psi^*(r)\psi(r)$  is time-independent and we get

$$E\phi(t) = i\hbar\frac{\partial}{\partial t}\phi(t) \quad (1.2)$$

$$H\psi(r) = E\psi(r)$$

(1.2) is solved by  $\phi(t) = e^{-i\omega t}$  with  $\omega = \frac{E}{\hbar}$ , where  $E$  is energy of the state.

The remaining eigenvalue problem  $E\psi = H\psi$  is also called the time-independent Schrodinger equation.

If we have the initial value problem with  $\psi(0) = \psi_0$  we can define an operator  $U(t)$

such that  $HU(t)|\psi_0\rangle = i\hbar\frac{\partial}{\partial t}U(t)|\psi_0\rangle$  and  $U(0)|\psi\rangle = |\psi_0\rangle$ . We get the operator equation

$HU = i\hbar\frac{\partial}{\partial t}U$  with the solution  $U(t) = e^{-\frac{i}{\hbar}Ht}$ .  $U$  is the operator of temporal evolution and satisfies the condition  $U(t)|\psi_0(t)\rangle = |\psi(t_0 + t)\rangle$ .

If  $|\psi\rangle = \sum_i c_i|i\rangle$  is a solution of the time-independent Schrodinger equation, then

$$|\psi(t)\rangle = U(t)|\psi\rangle = \sum_i c_i e^{-i\omega_i t}|i\rangle,$$

with  $\omega_i = \frac{E_i}{\hbar}$  is the corresponding time dependent solution.

Since the temporal evolution of a quantum system is described by a unitary operator and  $U^*(t) = U(-t)$  it follows that the temporal behavior of the quantum system is *reversible*, as long as no measurement is performed.

Since it is not possible to non-destructively measure a quantum system and we are only interested in the result of a computation, it is not necessary that a labeling is defined for a computation, i.e. it is not required to watch the temporal evolution of the system, as long as a labeling for the input-and output-state  $\psi_0$  and  $\psi_n$  is given. While the transitions  $\psi(t_i) \rightarrow \psi(t_{i+1})$  still have to correspond to simple operations  $U_i$  from an enumerable instruction set of quantum transformations, the operators  $U_i$  don't have to directly correspond to Boolean functions in classical computation theory.

We have shown that the temporal evolution of a quantum system is mathematically described by unitary operators, so a *quantum program* -  $prog = \{U_0, U_1, \dots, U_{n-1}\}$  is a composition of elementary unitary transformations.

A *quantum circuit* is a directed acyclic graph, where each node in the graph is associated with a quantum gate. This is exactly the definition of classical Boolean circuits, except that the gates are quantum. The input for the circuit is a basis state, which evolves in time according to the operation of quantum gates. At the end of the computation we apply measurements on the output qubits. The string of classical outcome bits is the classical output of the quantum computation. This output is in general probabilistic. This concludes the definition of model.

Let us now build a repertoire of quantum computations step by step. We have seen that classical gates can be implemented quantumly, by making the computation reversible.

Let me define the model of *quantum Turing Machine* (QTM) which is the quantum

analog of the classical Turing machine. The difference is that all the degrees of freedom become quantum: Each cell in the tape, the state of the machine, and the reading head of the tape can all be in linear superpositions of their different possible classical states. By definition a *quantum Turing machine* is:

1. A finite alphabet  $A = \{\#, 0, 1, \dots\}$  where  $\#$  is the blank symbol.
2. A finite set  $K = \{q_0, q_1, \dots, q_s\}$  machine states, with  $h, s \in K$  two special states.
3. A transition function  $\delta : Q \times \Sigma \times Q \times \Sigma \times \{-1, 0, 1\} \mapsto F$ .

As in classical *TM*, the tape is associated a head that reads and writes on that tape. A classical configuration,  $c$ , of the Turing machine is specified by the head's position, the contents of the tape and the machine's state. The Hilbert space of the *QTM* is defined as the vector space, spanned by all possible classical configurations  $\{|c\rangle\}$ . The dimension of this space is infinite. The computation starts with the *QTM* in a basis state  $|c\rangle$  which corresponds to the following classical configuration: An input of  $n$  symbols is written in positions  $1, \dots, n$  on the tape, all symbols except these  $n$  symbols are blank ( $\#$ ) and the head is at position  $1$ . Each time step, the machine evolves according to an infinite unitary matrix which is defined in the following way.  $U_{cc'}$  the probability amplitude to transform from configuration  $c$  to  $c'$  is determined by transition function  $\delta$ . If in  $c$ , the state of the machine is  $q$  and the symbol in the current place of the tape head is  $\sigma$  then  $\delta(q, \sigma, q', \sigma', \epsilon)$  is the probability amplitude to go from  $c$  to  $c'$ , where  $c'$  is equal to  $c$  everywhere except locally. The machine state in  $c'$ ,  $q$  is changed to  $q'$  the symbol under the head is changed to  $\sigma'$  and the tape head moves one step in direction  $\epsilon$ . Note that the operation of the Turing machine is local, i.e. it depends only on the current state of the machine and the symbol now read by the tape.

**Definition 2.** A unitary matrix  $U$  is said to be approximated to within  $\epsilon$ . by a unitary matrix  $U'$  if  $|U - U'| \leq \epsilon$ .

**Definition 3.** A set of gates,  $G$ , is called universal if for any  $\epsilon$  and any unitary matrix  $U$  on any number of bits,  $U$  can be approximated to within  $\epsilon \geq 0$  by a sequence of gates from  $G$ . In other words, the subgroup generated by  $G$  is dense in the group of unitary operators  $U(n)$ , for all  $n$ .

D. Deutsch was the first to show a universal elementary gates, which operates on three qubits [13]. E. Bernstein and V. Vazirani [16] give another proof of universality in terms of QTM. It was then shown by D.P. DiVincenzo [17] that two-qubit gates are universal. Note that one qubit gate is certainly not enough to construct all operations. An improvement of DiVincenzo's result was achieved later by A. Barenco et. al. [18], where it was shown that the classical controlled not gate, together with all one-qubit gates construct a universal set as well. In fact, one 1-qubit gate and the controlled not gate will do. This is perhaps the simplest and most economic set constructed so far.

**Theorem 1.** Let the matrices  $U_1, \dots, U_r \in SU(n)$  generate a dense subset in  $SU(n)$ . Then any matrix  $U$  in  $SU(n)$  can be approximated to within  $\epsilon$  by a product of  $\text{poly}\left(\log\left(\frac{1}{\epsilon}\right)\right)$  matrices from  $U_1, \dots, U_r, U_1^*, \dots, U_r^*$ .

Let  $SU(n)$  is the set of  $n \times n$  unitary matrices with determinant 1. Given a universal quantum set, we can easily convert it to a set in  $SU(n)$  by multiplying each matrix an overall complex scalar of absolute value 1, namely a phase. This overall phase does not effect the result of any measurement, so any gate can be multiplied by a phase without affecting the computation. We thus have:

**Corollary 1.** The approximation rate of any universal set of quantum gates is exponential.

Consider following set of  $2 \times 2$  -matrices:

$$I = \begin{pmatrix} 1 & 0 \\ 0 & 1 \end{pmatrix}, \sigma_x = \begin{pmatrix} 0 & 1 \\ 1 & 0 \end{pmatrix}, \sigma_z = \begin{pmatrix} 1 & 0 \\ 0 & -1 \end{pmatrix}, \sigma_y = \begin{pmatrix} 0 & -i \\ i & 0 \end{pmatrix},$$

where  $\sigma_x, \sigma_y, \sigma_z$  are Pauli matrices. Denoted by

$$H = \frac{1}{\sqrt{2}}(\sigma_x + \sigma_z), \sigma_z^\alpha = \begin{pmatrix} 1 & 0 \\ 0 & e^{i\alpha} \end{pmatrix}.$$

Then we have

$$\sigma_x = H\sigma_z H, \sigma_x = i\sigma_x \sigma_z, \sigma_y = \sigma_z^{\frac{1}{2}} \sigma_x \sigma_z^{\frac{1}{2}}.$$

Denoted by  $\Lambda_k U$  the controlled  $U$  operator with control bits (see A.Barenco, C.H.Benet and at.[18]), then  $CNOT$  is  $\Lambda_1(\sigma_x)$ .

**Theorem 2. 1.** *The operators  $H, \sigma_z^{\frac{1}{2}}, \Lambda_1(\sigma_x)$  are fault-tolerant, but not universal.*

2. *The set of basis  $\left\{ \Lambda_1\left(\sigma_z^{\frac{1}{2}}\right), H \right\}$  is universal (A.Kitaev)[19].*
3. *The set of basis  $\left\{ \Lambda_2(\sigma_x), H, \sigma_z^{\frac{1}{2}} \right\}$  is fault-tolerant (P.Shor [6]).*
4. *The basis  $\left\{ \Lambda_1\left(\sigma_z^{\frac{1}{2}}\right), H \right\}$  and  $\left\{ \Lambda_2(\sigma_x), H, \sigma_z^{\frac{1}{2}} \right\}$  are not equivalent.*
5. *The operators  $H, \sigma_z^{\frac{1}{4}}, \Lambda_1(\sigma_x)$  are universal and fault-tolerant basis for quantum computation.*
6. *The basis  $\left\{ \Lambda_2(\sigma_x), H, \sigma_z^{\frac{1}{2}} \right\}$  and  $\left\{ H, \sigma_z^{\frac{1}{4}}, \Lambda_1(\sigma_x) \right\}$  are not equivalent [16].*

**The general procedure of the fault tolerant creation of the encoded eigenstate.** Suppose that the fault-tolerant operator  $U_\eta$  operates on the state  $|\eta_i\rangle$  as follows:  $U_\eta|\eta_i\rangle = (-1)^i|\eta_i\rangle$ . Then the vectors  $|\eta_i\rangle$  are the eigenstates of the operator  $U_\eta$  with eigenvalues  $\pm 1$ . Let as we have access to a vector  $|\psi\rangle = \alpha|\eta_0\rangle + \beta|\eta_1\rangle$ . We show that using only bitwise operations, measurement, and this state  $|\psi\rangle$ , the eigenvectors  $|\eta_i\rangle$  obtained. Denote by

$$|cat\rangle = \frac{1}{\sqrt{2}}|00\dots 0\rangle + \frac{1}{\sqrt{2}}|11\dots 1\rangle.$$

Applying  $\Lambda_1(U_\eta)$  bitwise, on  $|cat\rangle \otimes |\psi\rangle$  we obtain

$$\begin{aligned} \Lambda_1(U_\eta)(|cat\rangle \otimes |\psi\rangle) &= \alpha \left( \frac{1}{\sqrt{2}}|00\dots 0\rangle + \frac{1}{\sqrt{2}}|11\dots 1\rangle \right) |\eta_0\rangle + \\ &+ \beta \left( \frac{1}{\sqrt{2}}|00\dots 0\rangle - \frac{1}{\sqrt{2}}|11\dots 1\rangle \right) |\eta_1\rangle \end{aligned}$$

Therefore, fault-tolerant measurement can be made to distinguish  $\left( \frac{1}{\sqrt{2}}|00\dots 0\rangle + \frac{1}{\sqrt{2}}|11\dots 1\rangle \right)$  from  $\left( \frac{1}{\sqrt{2}}|00\dots 0\rangle - \frac{1}{\sqrt{2}}|11\dots 1\rangle \right)$ .

## 2. Gauge theory and quantum computation.

Let  $E$  be a fibre bundle with base space  $X$  and fiber  $F$ . Let  $G$  be a group and suppose we have left action of  $G$  on  $F$  and let  $\rho : G \rightarrow Aut(F)$  the group homomorphism. Suppose the

transition function  $h_{ij} : U_i \cap U_j \rightarrow \text{Aut}(F)$  belong in  $\rho(G)$  for all  $x \in U_i \cap U_j$  and all  $i, j$  with  $U_i \cap U_j \neq \emptyset$ , then we say that  $G$  is the *structure group* of the bundle. Consider a fiber bundle  $\pi : E \rightarrow M$  with fiber  $F$ . At each point  $x \in E$  there is a canonical subspace  $V_x E \subset T_x E$  of the tangent space at  $x$  to  $E$  called the vertical subspace consisting of all vectors  $v$  such that  $d\pi v = 0$ . These are vectors tangent to fiber  $F_{\pi(x)}$ , which is a submanifold. A *connection* on  $E$  we mean a smooth choice at each  $x \in E$  of a subspace  $H_x E \subset T_x E$  complementary to  $V_x E$ . One has  $T_{(x,y)}(U \times F) \cong T_x U \times T_y F$ . Let  $(\xi, y) \in T_x U \times T_y F$ . Such a vector is vertical if and only if  $\xi = 0$ . Thus  $\pi_{\text{ver}}^{\text{hor}}$  must have the form  $\pi_{\text{ver}}^{\text{hor}}(\xi, y) = (0, \Gamma(x, v)\xi)$ , where  $\Gamma(x, v)$  is linear map  $T_x U \rightarrow T_y F$ . From this follows that  $\pi_{\text{ver}}^{\text{hor}}(\xi, y) = (\xi, -\Gamma(x, v)\xi)$ . The differential of this map must interwrite the local representatives of  $\pi^{\text{hor}}$ , the projection maps on the vertical tangent subspaces, specifically,  $d\psi_{(x,v)} \circ \pi_{(x,y)}^{\text{ver}} = \pi_{\psi(x,y)}^{\text{ver}} \circ d\psi_{(x,v)}$ . One has

$$dh_{vU}(x)(v)(x, y) = (\xi, d_1 h_{vU}(x)(v)\xi + d_2 h_{vU}(x)(v)y)$$

The intertwining relation with  $\pi^{\text{hor}}$  gives us

$$d_1 h_{vU}(x)(v) + \Gamma_U(x, h_{vU}(x)(v)) = d_2 h_{vU}(x)(v) \Gamma_U(x, v). \quad (2.1)$$

One can use (2.1) to define a connection.

**Theorem 3** (see [21]). *Let  $\pi : E \rightarrow X$  be a bundle with fiber  $F$ . Suppose we have a set of trivializations  $h_U : \pi^{-1}(U) \rightarrow U \times F$  such that the open sets  $U$  cover  $X$ . Suppose that for each trivialization and each  $(x, v) \in U \times F$  we have linear maps  $\Gamma_U(x, v) : T_x U \rightarrow T_y F$  varying smoothly with respect to  $(x, v)$  and such that relation (2.1) is satisfied for each pair of trivializations such that  $U_i \cap U_j \neq \emptyset$ . Then there is a unique connection of the bundle for which the representative with respect to the given trivialisations are the given  $\Gamma_U(x, v)$ .*

In a locally trivialized vector bundle using the mentioned identification  $T_{(x,v)}(U \times F) \cong T_x U \times T_y F \cong T_x U \times F$  for a connection to be linear one must have  $\Gamma_U(x, v)\xi = \Gamma(x)(\xi)v$  where  $\Gamma(x)$  can now be interpreted as a linear map  $T_x U \rightarrow \text{End}(F)$ , in other words an  $\text{End}(F)$ -value 1-form on  $U$ .

Let  $P$  be a principal  $G$ -bundle over a base space  $X$ . A *gauge transformation* is a bundle isomorphism  $\varphi : P \rightarrow G$  that commutes with right action. For this commute with right action it is necessary and sufficient that  $(pg)\gamma(pg) = (p\gamma(p))g$  and so

$$\gamma(pg) = g^{-1}\gamma(p)g. \quad (2.2)$$

Thus the set of all gauge transformations is the set of all maps  $\gamma : P \rightarrow G$  satisfying (2.2). The set of all gauge transformations of  $P$  is called the gauge group of  $P$  and we denote it by  $G(P)$ .

Consider a connection on  $E \rightarrow X$  with vertical tangent space projectors  $\pi_x^{\text{ver}}$ . A smooth curve in  $E$  is said horizontal if at each points its tangent lies in the horizontal tangent space of that point. To be horizontal is to be an integral curve of a differential equation. In fact consider a parametrized smooth curve in  $E$  and consider its image  $u(t) = (x(t), v(t))$  in a trivialization  $U \times F$ . One has  $\pi^{\text{ver}}(u'(t)) = (0, v'(t) + \Gamma(x(t), v(t))x'(t))$  and so the condition for being horizontal is

$$v'(t) + \Gamma(x(t), v(t))x'(t) = 0.$$

This is local coordinates in an ordinary differential equation for  $u(t)$ . Note that only the components  $v(t)$  are required to obey a differential equation and that  $x(t)$  can be given with arbitrary parametrization. This allows us to determine  $v(t)$  from  $x(t)$ . Given a smooth curve  $\sigma$  in  $X$  a horizontal lifting of  $\sigma$  is a horizontal curve  $\tilde{\sigma}$  in  $E$  such that  $\pi(\tilde{\sigma}) = \sigma$ . In a

trivialization this means that once  $\sigma$  is parametrized, then  $\tilde{\sigma}$  satisfies inheriting a parametrization from that of  $\sigma$ . By the existence, uniqueness and regularity theorems for solutions of ordinary differential equations, any smooth curve in  $X$  has at least a local unique horizontal lifting passing through any point  $v \in F_x$  for any  $x \in \sigma$ .

Let  $\sigma$  smooth curve in  $X$  with initial point  $x_0$  and end point  $x_1$ . Let  $v_0 \in F_{x_0}$  and assume that there is a global horizontal lifting of  $\sigma$  with initial point  $v_0$ . The endpoint  $v_1 \in F_{x_1}$  of  $\sigma$  is called the parallel transport of  $v_0$  along  $\sigma$ . It is obviously unique if it exists. If the parallel transport exists for all  $v_0 \in F_{x_0}$  then the map  $v_0 \mapsto v_1$  defines a diffeomorphism  $F_{x_0} \mapsto F_{x_1}$  is a linear isomorphism.

It is useful to have explicit forms for the parallel transport map. This is given by a construction known as time-ordered exponential integrals. Let  $F$  be a finite dimensional vector space and consider the following non-autonomous differential equation in  $F$ :

$$\frac{dv(t)}{dt} = A(t)v(t) \quad (2.3)$$

where  $A(t)$  is a linear operator which is a  $C^\infty$ -function of  $t$ . By the existence, uniqueness and regularity theorems for solutions of ordinary differential equations, for any  $v \in F$ , there is a unique solution  $v(t)$  with  $v(a)$  given. In differential equation theory, one generally introduces what is known as the *fundamental solution* of (2.3), that is, an  $End(F)$  valued function  $\Phi(t, a)$  which satisfies

$$\begin{aligned} \frac{\partial}{\partial t} \Phi(t, a) &= A(t)\Phi(t, a), \\ \Phi(a, a) &= I. \end{aligned}$$

One now has

$$v(t) = \Phi(t, a)v(a).$$

Other representation of the  $v(t)$  is:

$$v(t) = T \exp\left(\int_a^t A(s) ds\right)v(a)$$

where called *time-ordered exponential integral*.

Let now  $A$  be an  $End(F)$ -valued 1-form on a manifold  $X$  and let  $\sigma$  be a smooth oriented curve in  $X$ . One can also define the *path-ordered exponential integral*

$$P \exp\left(\int_\sigma A\right) = \lim_{N \rightarrow \infty} P \prod_{i=1}^N \exp\left(\int_{\sigma_i} A\right)$$

where the curve  $\sigma$  has been partitioned into successive arcs  $\sigma_1, \sigma_2, \dots, \sigma_N$  each one inheriting its orientation from  $\sigma$ . Then limit is to be understood in relation to a fixed parametrization of  $\sigma$  with the maximum parameter length of the  $\sigma_i$  tending to zero. Such a path-ordered exponential integral is an element of  $End(F)$ .

We can now use path-ordered exponential integrals to express the effect of parallel transport. In a trivialisation of a vector bundle the parallel transport equation reads

$$\frac{dv(t)}{dt} = \Gamma(x(t))(x'(t))v,$$

where  $x(t)$  is a parametrized path  $\sigma$  in  $U$  with initial point  $x(0)$  and final point  $x(1)$ . Thus we have

$$v(1) = T \exp\left(-\int_0^1 \Gamma(x(t))(x'(t)) dt\right)v(0) = P \exp\left(\int_\sigma \Gamma\right)v(0)$$

and so  $P \exp\left(\int_\sigma \Gamma\right)v(0)$  is the parallel transport operator for the oriented curve  $\sigma$ .

Finally, let  $G$  be a Lie group with Lie algebra  $\mathfrak{g}$  and  $\mathbf{A}$  a  $\mathfrak{g}$ -1-form on an open set  $U$

in a manifold  $M$ . Such a path exponential integral solves the parallel transport equation for a principal  $G$ -bundle with an invariant connection. In fact, consider a trivialization  $U \times G$  of such a bundle and a parametrized curve  $p(t) = (x(t), g(t))$  in it. The tangent vector at  $p(t)$  is  $(x'(t), g'(t)) \in T_{x(t)}U \times T_{g(t)}G$ . With  $T_{g(t)}G$  identified with  $\mathfrak{g}$  by right action we represent this tangent vector now by  $(x'(t), g'(t)g(t)^{-1}) \in T_{x(t)}U \times \mathfrak{g}$ . A vector is horizontal if and only if  $g(t)^{-1}(\mathbf{A}(x'(t)) + g'(t)g(t)^{-1})g(t) = 0$  that is, if and only if  $\mathbf{A}(x'(t)) + g'(t)g(t)^{-1} = 0$ . Thus the parallel transport equation in a principal  $G$ -bundle with an invariant connection is

$$\frac{dg(t)}{dt} = \mathbf{A}(x(t))(x'(t))g(t).$$

It is now easy to see that

$$g(t) = T \exp\left(-\int_0^t \mathbf{A}(x(s))(x'(s))ds\right)g(0).$$

The effect of parallel transporting a group element over an oriented curve  $\sigma$  in  $U$  is to multiply it on the left by  $P \exp\left(-\int_{\sigma} \mathbf{A}\right)$ .

This result shows that *parallel transport is globally defined as the path-oriented exponential integral exists for any compact oriented curve with end points.*

Let  $\sigma$  be a loop in  $X$  at point  $x_0$ :

$$\sigma : [0, 1] \rightarrow X, \sigma(0) = \sigma(1).$$

For this  $\sigma$  a *holonomy operator*  $\Omega_A(\sigma) = P \exp\left(-\int_{\sigma} \mathbf{A}\right)$ .

This acts on the fiber  $F_{x_0}$  at  $x_0$  of the vector bundle  $E \rightarrow X$  as follows:

$$v \mapsto \Omega_A(\sigma)v.$$

If  $\sigma$  and  $\sigma'$  are homotopic, then  $\Omega_A(\sigma) = \Omega_A(\sigma')$ . Therefore, we obtain the map  $\Omega_A : \pi_1(M, x_0) \rightarrow \text{Aut}F_{x_0}$  which is homomorphism of the groups. The subgroup  $\Omega_A(\pi_1(M, x_0)) \subset \text{Aut}F_{x_0}$  is called a *holonomy group* induced by the connection  $\mathbf{A}$ . Let

$F(\mathbf{A}) = d\mathbf{A} + \mathbf{A} \wedge \mathbf{A}$  a curvature. Then the first Chern number  $c_1(E) = \frac{1}{2\pi i} \int_M F(\mathbf{A})$  is

topological invariant of the bundle. It means, that if  $\mathbf{A}$  and  $\mathbf{A}'$  are gauge equivalent, then correspondently holonomy groups  $\text{Hol}_A, \text{Hol}_{A'}$  are conjugative in  $\text{Aut}F_{x_0}$  and holonomy group is independent to on choice of the connection.

Suppose  $\Omega_A(\sigma) \in U(n)$  and fibre of the bundle is isomorphic  $\mathbf{C}^2 \otimes \mathbf{C}^2 \otimes \dots \otimes \mathbf{C}^2$ . In this case we can talk about *quantum computer*.

*In the gauge quantum computer the encoding space of information is the fibre  $F_0$  of the vector bundle  $E \rightarrow X$  and processing of information is the holonomy operator defined by connection  $\Gamma$  of this bundle.*

**Physical terminology.** If physical system or theory is described by the principal bundle  $P \rightarrow M$ , with structural group  $G$ , then we talk that have *gauge theory*. The group  $G$  call *gauge group*. The choice of a trivialization of the principal bundle call *gauge*. Analog classical elementary field in gauge theory, which is a connection on the principal bundle called *gauge field* or *vector potential*. *Gauge transformation (change of gauge)* is a automorphism of the principal bundle which covers the identity of the base manifold. Maxwell's electro-magnetism (U(1)-gauge theory) and Yang-Mills theory are examples correspondently abelian and nonabelian gauge theories.

**Main result in gauge quantum computation.** Let an evolution of the physical systems is described non-autonomous system of differential equations (2.3). Then above from mentioned follows, that (2.3) induces the representation  $\rho : \pi_1(M, x_0) \rightarrow GL(n, \mathbf{C})$ . By theorem of covering homotopy  $\rho$  defines vector bundle on  $M$  and  $\Omega = \Phi^{-1}d\Phi$  is connection

of this bundle. Suppose  $\tau \in \text{Im} \rho$  and  $\exp(i\tau) \in U(n)$ . For any unitary transformation  $U$  there exists  $\sigma \in \pi_1(M, x_0)$  such that  $\|\Gamma_\Omega(\sigma) - U\| < \varepsilon$  for the arbitrary small  $\varepsilon$ . It means, we proofed the following main result in gauge quantum computation.

**Theorem 4.** Any computation code can be realized by connection  $\Omega$ .

### 3. Optical holonomic quantum computation as gauge quantum computation.

Below we shall consider one of the quantum optics models and show in that model appears homomorphism from the parameter space in to group of unitary operators of suitable Fock space. It gives possibility to construct bundle on parameter space with connections.

First we consider *geometric* or *Berry phase*, where input M. Berry in [22]. (For review *geometric phase* see book [23].)

A phase is, for our purposes, not a state of matter but a complex number of unit modules, an element of the group  $U(1)$  or more general elements of matrix group  $U(N)$ . The phases is obtained often with cyclic evolution of a physical system. Cyclic variation of external parameters often leads to a net evolution involving a phase depending only on the geometry of the path traversed in parameter space. The natural mathematical context for geometric phases in the theory of  $U(N)$  fibre bundles. There one defines a phase, known as *holonomy*, that depends on the geometry of a loop, and is independent of any coordinate choice.

Example of geometric phases a bound in many areas of physics: in optics, Pancharatnam's phase led to measurable interference effects; in molecular physics, the molecular Aharonov-Bohm effect was found to have a significant effect on molecular dynamics near to degenerate the universal significance of these phases, to show that whenever an adiabatic approximation applies, we may expect to find a geometric phase. The crucial role of adiabatically is not make sure that the cyclic variable of parameters leads to cyclic evolution.

In work [24] F. Wilczek and A. Zee consider non-Abelian phases associated with adiabatic evolution of *degenerate Hamiltonians*. This basic idea used P. Zanardi and M. Rasetti [1] for enabling quantum computation.

Let  $M$  smooth manifold, where our case play the role of parameter space. Let given a family of Hamiltonians  $H_\lambda$  depending continuously on parameters  $\lambda \in M$ , all of which have a set of  $n$  degenerate levels. By a simple renormalization of the energies we can suppose that these levels are at  $E=0$ .

We use adiabatic theorem:

**Theorem 5** [24]. If the parameters are slowly varied from an initial value  $\lambda_0$  to some final value  $\lambda_1$  over long time interval  $T$ , and the given space of degenerate levels does not cross other levels, then solitons of

$$H_{\lambda_0} \psi(t) = 0 \quad (3.1)$$

are mapped onto solution of

$$H_{\lambda_1} \psi(t) = 0$$

by solving the time-dependent Schrodinger equation

$$i \frac{\partial \psi(t)}{\partial t} = H(\lambda(t)) \psi(t)$$

with the boundary conditions

$$\lambda(0) = \lambda_0, \lambda(T) = \lambda_1.$$

Consider  $\lambda$  as the map  $\lambda : [0, T] \rightarrow M$  and suppose  $\lambda(0) = \lambda(T)$ . If the space of the solutions of is  $n$ -dimensional space  $F_0$ , with the basis  $\{|\psi_1(t)\rangle, |\psi_2(t)\rangle, \dots, |\psi_n(t)\rangle\}$  then we obtain the *holonomy transformation* of  $F_0$ . By theorem 3 there exists the connection  $A$  on the bundle  $M \times F_0$ , such that this transformation is equal to  $\Gamma_A(\sigma)$ , for any  $\sigma$ .

Now consider real physical system in quantum optic.

Consider coherent states based on the Lie algebras  $su(n+1)$ , which play a important role in multiphoton processes in quantum optics. These sates can be identified with eigenstates of Hamiltonians that are essentially number operators in appropriate Fock space, that correponding levels are equally spaced.

Let  $a, a^\dagger$  be the annihilation and creation operators correspondently of the harmonic oscillator and  $N = a^\dagger a$  a number operator. Then we have following relations:

$$[N, a^\dagger] = a^\dagger, [N, a] = -a, [a, a^\dagger] = 1. \quad (3.2)$$

Let  $H$  be a Fock space generated by  $a$  and  $a^\dagger$ . Assume  $|n\rangle, n = 0, 1, \dots$  be its basis. The actions  $a$  and  $a^\dagger$  on  $H$  are given by

$$a|n\rangle = \sqrt{n}|n-1\rangle, a^\dagger|n\rangle = \sqrt{n+1}|n+1\rangle, \quad (3.3)$$

where  $|0\rangle$  is a vacuum, i.e.  $a|0\rangle = 0$ .

Consider the system of  $n+1$ -harmonic oscillators. For any  $1 \leq j \leq n+1$  we set

$$a_j = 1 \otimes \dots \otimes 1^j \otimes a \otimes 1 \dots \otimes 1,$$

$$a_j^\dagger = 1 \otimes \dots \otimes 1 \otimes a^\dagger \otimes 1 \otimes \dots \otimes 1,$$

$$N_j = a_j^\dagger a_j.$$

Then

$$[a_i, a_j] = [a_i^\dagger, a_j^\dagger] = 0, [a_i, a_j^\dagger] = \delta_{ij}, i, j = 1, 2, \dots, n+1.$$

The Fock space of  $n+1$ -harmonic oscillators is the  $n+1$ -tensor product  $\mathfrak{S}^{(n+1)} = \mathfrak{S} \otimes \dots \otimes \mathfrak{S}$ , and each  $a_j$  and  $a_j^\dagger$  acts on  $j$ -components of  $\mathfrak{S}^{(n+1)}$  as (3.3).

Consider nonlinear interaction Hamiltonian product by a Kerr medium

$$H = \hbar X N(N-1),$$

where  $X$  a constant proportional to the third order nonlinear susceptibility,  $\chi^{(3)}$ , of the medium.

Degenerate eigenstates of  $H$  are  $|0\rangle$  and  $|1\rangle$ . In the case two laser beams, with annihilation operators  $a_1$  and  $a_2$  respectively, the total Hamiltonian is given by the sum

$$H^{12} = \hbar X N_1(N_1-1) + \hbar X N_2(N_2-1). \quad (3.4)$$

Its degenerate eigenstate are the tensor product of the eigenstates of each subsystem:

$|i_1 j_2\rangle = |i_1\rangle \otimes |j_2\rangle$  for  $i_1, j_2 = 0, 1$  with  $|i_1\rangle$  and  $|j_2\rangle$  the degenerate states of each beam.

On state  $|\psi\rangle$  of a laser beam with annihilation operator  $a$ , the following operators can act

$$\text{Displaced operator: } D(\lambda) = \exp(\lambda a^\dagger - \bar{\lambda} a),$$

$$\text{Squeezer operator: } S(\eta) = \exp(\eta a^{\dagger 2} - \bar{\mu} a^2),$$

where  $\lambda, \eta$  are an arbitrary complex parametrs. Note, that the displacing device that implements  $D(\lambda)$  is a simple device that performs a linear amplification to the light field components. The squeezing operator can be implement in the laboratory by a degenerate parametric amplifier.

The displacer  $D(\lambda)$ , transforms the operators  $a, a^\dagger$  and any analytic function  $f(a, a^\dagger)$ , for any choice of parameters  $\lambda$ , as follows

$$\begin{aligned}
D(\lambda)aD^\dagger(\lambda) &= a - \lambda, \\
D(\lambda)a^\dagger D^\dagger(\lambda) &= a^\dagger - \lambda, \\
D(\lambda)f(a, a^\dagger)D^\dagger(\lambda) &= f(a - \lambda, a^\dagger - \lambda);
\end{aligned}$$

Similarly for the squeezing operator have:

$$\begin{aligned}
S(\eta)aS^\dagger(\eta) &= \cosh(2r)a - e^{-i\theta}\sinh(2r)a^\dagger, \\
S(\eta)a^\dagger S^\dagger(\eta) &= e^{-i\theta}\sinh(2r)a + \cosh(2r)a^\dagger \\
S(\eta)f(a, a^\dagger)S^\dagger(\eta) &= f(S(\eta)aS^\dagger(\eta), S(\eta)a^\dagger S^\dagger(\eta));
\end{aligned}$$

where  $\eta = re^{-i\theta}$ , with  $r > 0$  and  $-\pi < \theta \leq \pi$ .

On general state of two lasers  $|\psi_1, \psi_2\rangle = |\psi_1\rangle \otimes |\psi_2\rangle$  with corresponding annihilation operators  $a_1$  and  $a_2$ , the following operators can act

$$\begin{aligned}
\text{Two mode displacer: } U(\xi) &= \exp(\xi a_1^\dagger a_2 - \bar{\xi} a_1 a_2^\dagger), \\
\text{Two mode squeezer: } V(\zeta) &= \exp(\zeta a_1^\dagger a_2^\dagger - \bar{\zeta} a_1 a_2).
\end{aligned}$$

The operator  $V(\zeta)$ , can be implemented in the laboratory by a non-degenerate parametric amplifier.

The operators  $D(\lambda)$  and  $S(\eta)$  acting on a single laser beam will result, after a closed loop is performed in their parameter space, into rotations in the state space spanned by  $|0\rangle$  and  $|1\rangle$ , according to adiabatic theorem 5.  $U(\xi)$  and  $V(\zeta)$  are transformation between two laser beams that produce, after performing adiabatically a loop in their parametric space, coherent transformations into the two qubit state space spanned by  $|00\rangle, |01\rangle, |10\rangle$  and  $|11\rangle$ . These transformations on the states of the laser beams can be produced by  $SU(2)$  or  $SU(1,1)$  interferometers, according to the algebra which their generators belong to. For instance, each one  $\lambda a_j^\dagger - \bar{\lambda} a_j$  and  $\xi a_1^\dagger a_2 - \bar{\xi} a_1 a_2^\dagger$  belongs to an  $su(2)$ , while  $\eta a^{12} - \bar{\eta} a^2$  and  $\zeta a_1^\dagger a_2^\dagger - \bar{\zeta} a_1 a_2$  belong into  $su(1,1)$  algebras.

Consider general case the system of  $n+1$  particles, the Hamiltonian analogically (3.4) have form:

$$H = \sum_{j=1}^{n+1} \hbar X N_j (N_j - 1).$$

The  $0$ -eigenstate of this Hamiltonian becomes therefore

$$F_0 = \text{Vect}\{|0\rangle, |1\rangle\} \otimes \dots \otimes \text{Vect}\{|0\rangle, |1\rangle\} \cong C^2 \otimes \dots \otimes C^2 \cong C^{2^{n+1}}.$$

Construct unitary coherent operators  $U_j(\xi_j)$  and  $V_j(\zeta_j)$  for arbitrary  $1 \leq j \leq n$  based on  $su(2)$  and  $su(1,1)$  respectively:

$$\begin{aligned}
U_j(\xi_j) &= \exp(\xi_j a_j^\dagger a_{n+1} - \bar{\xi}_j a_{n+1}^\dagger a_j); \\
V_j(\zeta_j) &= \exp(\zeta_j a_j^\dagger a_{n+1}^\dagger - \bar{\zeta}_j a_{n+1} a_j);
\end{aligned}$$

For  $\xi = (\xi_1, \xi_2, \dots, \xi_n)$  and  $\zeta = (\zeta_1, \zeta_2, \dots, \zeta_n)$  we define:  $U(\xi) = \prod_{j=1}^n U_j(\xi_j)$  and  $V(\zeta) = \prod_{j=1}^n V_j(\zeta_j)$ ,

then

$$W(\xi, \zeta) = U(\xi)V(\zeta) \in U(\mathfrak{S}^{(n+1)})$$

Suppose  $\lambda = (\xi, \zeta)$  is parameter and  $M$  parameter space, which is smooth manifold. Let as  $pr: M \rightarrow Gr_m(\mathfrak{S})$  projector:

$$pr(\lambda) = W(\lambda) \left( \sum_{j=1}^m v_j v_j^\dagger \right) W(\lambda)^{-1},$$

then we have the pullback bundles  $P \rightarrow M$  with fibre  $U(m)$  and  $E \rightarrow M$  with fibre  $C^m$  [25].

The vector bundle  $E \rightarrow M$  have canonical connection  $A = W(\lambda)^{-1}dW(\lambda)$ . Therefore we can talk about the gauge quantum computation. In [3] is calculated analytically the connection  $A$  by the entangled formula obtained in [26]. To be founded on the theory is taken  $H(\lambda) = W(\lambda)HW(\lambda)^{-1}$  isospectral family of Hamiltonians and is used adiabatic theorem 5.

#### 4. Conclusion

Let  $E \rightarrow CP^1$  be a holomorphic bundle with fibre  $F = (C^2)^{\otimes n}$ . It is known  $E$  decomposes into a direct sum of line bundles  $E \cong O(k_1) \oplus \dots \oplus O(k_n)$ . From physical considerations possibly only stable bundles are interesting, i.e. those for which the condition  $|k_i - k_j| \leq 1$  holds for any  $i, j$ . Suppose  $E$  satisfies this condition. If the bundle  $E$  has a holomorphic connection, then  $k_i = 0$  for all  $i$ . Then the bundle is  $E$  is holomorphically trivial and the holonomy is the identity transformation. Hence this case is not interesting for us. Let us consider the nontrivial case. Let  $\Omega$  be the connection matrix with regular singularities of points  $z_1, \dots, z_m$ . This determines a representation

$$\rho : \pi_1(CP^1 - \{z_1, z_2, \dots, z_m\}, z_0) \rightarrow GL(n, C)$$

$\gamma_1, \gamma_2, \dots, \gamma_n$  be generators of  $\pi_1(CP^1 - \{z_1, z_2, \dots, z_m\}, z_0)$ . It is interesting to obtain a quantum algorithm for the monodromy matrices  $\rho(\gamma_1), \dots, \rho(\gamma_m)$  of the system of differential equations  $df = Af$ . This will give possibility to model the holonomic quantum theory [27] on a quantum computer.

It is also interesting to consider from the point of view of quantum computations systems of differential equations of Fuchs type on  $CP^m$  [28].

#### 5. Acknowledgments

The author is grateful to prof. G.Kharatishvili for the interest expressed in this work; also he thanks Dr. M. Jibladze and Z.Pipia for numerous useful conversations.

#### References

- [1]. P. Zanardi, M. Rasetti. Holonomic Quantum Computation. Los Alamos Physics Preprint Archive, quant-ph/9904011.
- [2]. J.Pachos, P.Zanardi, M. Rasetti. Non-Abelian Berry connections for quantum computation. Los Alamos Physics Preprint Archive, quant-ph/9907103.
- [3]. K. Fujii. Mathematical foundations of holonomic quantum computer. Los Alamos Physics Preprint Archive, quant-ph/0004102.
- [4]. G.Giorgadze. On the Riemann-Hilbert problems. Los Alamos Physics Preprint Archive, math.cv/9804035.
- [5]. M. H. Freedman, A. Kitaev, Z. Wang. Simulation of topological field theories by quantum computer. Los Alamos Physics Preprint Archive, quant-ph/0001071.
- [6]. P. W. Shor. Algorithms for quantum computation: Discrete log and factoring. In Proceedings of the 35th Annual Symposium on Foundations of Computer Science. I.E.E.C. pp.124-134, 1994.
- [7]. E. Rieffel, W. Polak. An introduction to quantum computing for non-physicists. Los Alamos Physics Preprint Archive, quant-ph/9809016.
- [8]. B. Omer. Quantum programming in QCL. 2000, <http://tph.tuwien.ac.at/~oemer>.
- [9]. D. Aharonov. Quantum computation. Los Alamos Physics Preprint Archive, quant-ph/9812037.
- [10]. R. Landauer. IBM J. Resw. Develop. 3,183, 1961.
- [11]. R.Feynman. Quantum mechanical computations. Optics News. February 1985, N11,p.11.
- [12]. C.H. Bennett. Logical Reversibility of computation. IBM J.Res.Dev. 6, p.525-532, 1979.
- [13]. D. Deutsch. Quantum theory, the Church-Turing principle and the universal quantum

- computer. Proceedings of the Royal Society of London. Ser.A 400, pp.97-117, 1985.
- [14]. P.Benioff. Models of quantum Turing Machines.Los Alamos Physics Preprint Archive, quant-ph/9708054.
- [15]. T.Medoidze, Z.Melikishvili, G.Tsintsadze. Quantum dynamics of qubit with polarization switch. Proceeding IC, vol.1,N2, 2000, pp.101-107.
- [16]. E. Bernstein, U. V. Vazirani.Quantum complexity theory. Society for Industrial and Applied Mathematics Journal on Computing. Vol.26, No.5, pp.1411-1473.
- [17]. D.DiVincenzo. Quantum computation. Sciences 270, pp.255-261,1995.
- [18]. A.Barenco, C.Bennett, R.Cleve, D.DiVincenzo, N.Margulus, P.Shor, T.Sleator, J.Smolin, H.Weinfurter. Elementary gates for quantum computation. Phys.Rev. A, 3457-3467,1995.
- [19]. A.Kitaev. Quantum computation: algorithms and error correction. Russian Mathematical Surveys, 52(6), pp.1191-1249, 1997.
- [20]. P.O. Boykin, T. Mor, M. Pulver, V. Roychowdhury, F. Vatan. On universal and Fault-Tolerant quantum computing: A novel basis and a new constructive proof of universality for Shor's basis. In Proceedings of the 40th Annual Symposium on Foundations of Computer Science.IEEE Comp.Soc. Press, Los Alamitos. pp.486-494, 1999.
- [21]. G. Svetlichny. Preparation for gauge theory. Los Alamos Physics Preprint Archive, math-ph/9902027.
- [22]. M.Berry. Quantal phase factors accompanying adiabatic changes. Proc. Royal Soc. London, A 392, 45-57, 1984.
- [23]. A. Shapere, F. Wilczek Eds. Geometric phases.in physics,World Scientific, 1987.
- [24]. F. Wilczek, A. Zee.Appearance of gauge structure in simple dynamical systems. Phys.Rev.Lett.52,2111 (1984).
- [25]. J.Milnor, J.Stasheff. Characteristic Classes. Princeton University Press, 1974.
- [26]. K. Fujii.More on optical holonomic quantum computer. Los Alamos Physics Preprint Archive, quant-ph/0005129.
- [27]. M.Sato, T.Miwa, M.Jimbo. Holonomic quantum field.I. Publ. RIMS, Kyoto Univ., 14 (1978), pp.223-267.
- [28]. V. Golubeva, V. Leksin. J.Diff. Equation (in russian). Vol.27, N 9, 1991.



## **A Representation of Gaussian Random Processes in the Form of Stochastic Series and its Application for Modeling**

**Zurab Piranashvili**  
*Institute of Cybernetics*

In practice, we often meet systems which input and output can be considered as random process. For these systems arises a problem: we know probabilistic characteristics of input random processes and transforming operator of input process into output process; It is necessary to find out probabilistic characteristics of output random processes (the problem of system analysis).

Solution of this problem is entirely depended on the structure of input process, the form of transforming operator and on the probabilistic characteristics of output processes.

As it is known, for some private cases it is easy to solve such problems, but, in general, there arise principle analytical difficulties. Real possibility for solving of such problems gives method of statistical modeling, the content of which is following: on the basis of observed values of input process, we construct its mathematical model, then we construct one or more independent realizations of input random process. After passing them through the system, we obtain suitable realizations of output process by the transforming operator; then the required probabilistic characteristics of output process are determined by the method of statistical estimation.

Such method gives possibility of comparably easier solution a problem not only system analysis, but also control problem in the case when the transforming operator contains control parameters. In this case, the set of possible values of control parameters we cover with net, in network points of which we find realizations of output process, then we estimate statistically probabilistic characteristics of output process, which are entered into the optimality criteria and at that we choose the best ones, in the sense of optimality criteria, from the said points. So, we obtain approximate values of control parameters. These values will be as close to the true values, as the cells of network are narrower, i.e. the network ties are close to each other (that means, that the value expressing the optimality criteria is continuously depended on the control parameters).

During the investigation and solution of stochastic systems analysis and control problems, by the method of statistical modeling, one of the basic stages is modeling of input process by using the information, which is given in observed values of input process.

Unfortunately this information is not sufficient. Such lack of information must be filled with bringing in any hypothesis. One of these hypotheses is following: the multidimensional distribution of any finite number depended random variables, one-dimensional distribution functions of which are normal, let be normal.

This supposition is conditionally called  $N$  hypothesis and random process for which  $N$  hypotheses is thru is called random process of class  $N$  [5], [9].

The random process of class  $N$  obtains by one-to-one transformation of Gaussian random process with zero mean and unit variance. This transformation is expressed by the one-dimensional distribution function of Gaussian process and one-dimensional distribution function of random process of class  $N$ . The random process of class  $N$  is wholly characterized by its one-dimensional distribution function and its correlation function. Those last characteristics may be estimated quite well, based on the statistical materials.

So, modeling of random process of class  $N$  reduces on the modeling of Gaussian process with (0,1) parameters.

Bellow are given various representations of Gaussian random process in the form of stochastic series, giving the possibilities of modeling of random process of class  $N$  (it is clear, that Gaussian process is random process of class  $N$  itself and there are some non-Gaussian processes belonging to class  $N$ ).

Suppose  $\xi(t)$  is second order real-valued random process which zero mean and covariance function  $B(t,s)$ :

$$B(t,s) = \sum_{k=1}^n \int_{a_k}^{b_k} f_k(t,\lambda) f_k(s,\lambda) dF_k(\lambda), \quad (1)$$

where  $F_k(\lambda)$ ,  $k = \overline{1,n}$  are continuous increasing functions such that  $0 \leq F_k(\lambda) \leq 1$ ,  $F_k(a_k) = 0$ ,  $F_k(b_k) = 1$

By substituting  $F_k(\lambda) = U_k$  in (1) we have

$$B(t,s) = \sum_{k=1}^n \int_0^1 f_k(t, F_k^{-1}(u_k)) f_k(s, F_k^{-1}(u_k)) du_k, \quad (2)$$

where  $F_k^{-1}(u_k)$  is the inverse function of  $u_k = F_k(\lambda)$ . (2) may be rewritten in the form:

$$B(t,s) = \sum_{k=1}^n \int_0^1 f_k(t, F_k^{-1}(u)) f_k(s, F_k^{-1}(u)) du. \quad (3)$$

Then, on the strength of Karunen's theorem [1] random processes  $\xi(t)$  will have such form:

$$\xi(t) = \sum_{k=1}^n \int_0^1 f_k(t, F_k^{-1}(u_k)) dZ_k(u), \quad (4)$$

where  $Z_k(u)$ ,  $k = \overline{1,n}$  are real-valued random processes, with one-correlated increments and

$$E[dZ_k(u)]^2 = du, \quad E[dZ_k(u)dZ_m(v)] = 0, \\ 0 \leq u, v \leq 1, \quad k \neq m.$$

When  $\xi(t)$  is real-valued Gaussian random process, then  $Z_k(u)$ ,  $k = \overline{1,n}$  are independent standard Wiener processes. In the right side of (4) by „integration by parts” (taking into account  $Z_k(0) = 0$ ,  $k = \overline{1,n}$ ) [2],[3]:

$$\begin{aligned} \xi(t) &= \sum_{k=1}^n \left[ f_k(t, b_k) Z_k(1) - \int_0^1 \left( \frac{\partial f_k(t, k)}{\partial \lambda} \right)_{\lambda=F_k^{-1}(u)} Z_k(u) dF_k^{-1}(u) \right] = \\ &= \sum_{k=1}^n \left[ f_k(t, b_k) Z_k(1) - \int_0^1 \varphi_k(t, F_k^{-1}(u)) Z_k(u) dF_k^{-1}(u) \right] = \\ &= \sum_{k=1}^n \left[ f_k(t, b_k) Z_k(1) - \int_{a_k}^{b_k} \varphi_k(t, \lambda) Z_k(F_k(\lambda)) d\lambda \right] \end{aligned} \quad (5)$$

where  $\varphi_k(t, \lambda) = \frac{\partial f_k(t, \lambda)}{\partial \lambda}$ .

As all sampling functions of Wiener's process  $Z_k(u)$ ,  $k = \overline{1,n}$  and all functions  $F_k(\lambda)$  ( $0 \leq F(\lambda) \leq 1$ ) are continuous, so integrals

$$\int_0^1 \varphi_k(t, F_k^{-1}(u)) Z_k(u) dF_k^{-1}(u) = \int_{a_k}^{b_k} \varphi_k(t, \lambda) Z_k(F_k(\lambda)) d\lambda$$

exist for almost every sampling function, if there are derivatives  $\varphi_k(t, \lambda) = \frac{\partial f_k(t, \lambda)}{\partial \lambda}$  and functions  $\varphi_k(t, \lambda)$  are continuous with respect to  $\lambda$ , or are bounded and almost everywhere continuous in the Lebesgue's sense correspondingly at the intervals  $[a_k, b_k]$ .

If we use orthogonal decomposition of Wiener's process [4]; insert this decomposition in (5), make term-by-term integration of series [5], then we obtain:

$$\xi(t) = \frac{\sqrt{2}}{\pi} \sum_{k=1}^n \left[ \sum_{m=0}^{\infty} \frac{(-1)^m}{m+0,5} f_k(t, b_k) Z_m^k - \int_{a_k}^{b_k} \varphi_k(t, \lambda) \sum_{m=0}^{\infty} Z_m^k \frac{\sin[(m+0,5)\pi F_k(\lambda)]}{m+0,5} d\lambda \right] = \dots + \dots \quad (6)$$

$$= \frac{\sqrt{2}}{\pi} \sum_{k=1}^n \sum_{m=0}^{\infty} \frac{1}{m+0,5} [(-1)^m f_k(t, b_k) + C_m^k(t)] Z_m^k$$

where  $C_m^k(t) = - \int_{a_k}^{b_k} \varphi_k(t, \lambda) \sin[(m+0,5)\pi F_k(\lambda)] d\lambda$ .

and  $\{Z_m^k\}$ ,  $k = \overline{1, n}$ ;  $m = 0, 1, \dots$  – are independent sequences of Gaussian independent random variables with parameters (0,1) (here and further  $k$  is index, not the exponent).

The (5) we can write in following form:

$$\xi(t) = \sum_{k=1}^n \left[ f_k(t, b_k) Z_k(1) - \int_0^1 Z_k(u) d_u f_k(t, F_k^{-1}(u)) \right].$$

If  $f_k(t, F_k^{-1}(u))$  are functions with bounded variations with respect to  $u$ , then integrals

$$\int_0^1 Z_k(u) d_u f_k(t, F_k^{-1}(u)), \quad k = \overline{1, n}$$

exist for almost every sampling functions.

Analogously, in this case we have

$$\xi(t) = \frac{\sqrt{2}}{\pi} \sum_{k=1}^n \sum_{m=0}^{\infty} \frac{1}{m+0,5} [(-1)^m f_k(t, b_k) + D_m^k(t)] Z_m^k, \quad (7)$$

where

$$D_m^k(t) = - \int_0^1 \sin[(m+0,5)\pi u] d_u f_k(t, F_k^{-1}(u)),$$

and  $\{Z_m^k\}$ ,  $k = \overline{1, n}$ ;  $m = 0, 1, \dots$  again are independent sequences of Gaussian independent random variables with parameters (0,1).

To estimation of remainder term of representation (6) let note

$$\xi_v(t) \equiv \sum_{k=1}^n \left[ f_k(t, b_k) \frac{\sqrt{2}}{\pi} \sum_{m=0}^v \frac{(-1)^m}{m+0,5} Z_m^k - \int_0^1 \varphi_k(t, F_k^{-1}(u)) \frac{\sqrt{2}}{\pi} \sum_{m=0}^v Z_m^k \frac{\sin[(m+0,5)\pi u]}{m+0,5} dF_k^{-1}(u) \right].$$

It may be written

$$\begin{aligned}
E[\xi(t) - \xi_v(u)]^2 &= E \left\{ \sum_{k=1}^n \left( f_k(t, b_k) \left[ Z_k(1) - \frac{\sqrt{2}}{\pi} \sum_{m=0}^v \frac{(-1)^m}{m+0,5} Z_m^k \right] - \int_0^1 \varphi_k(t, F_k^{-1}(u)) \left[ Z_k(u) - \frac{\sqrt{2}}{\pi} \sum_{m=0}^v \frac{(-1)^m}{m+0,5} Z_m^k \right] dF_k^{-1}(u) \right)^2 \right. \\
&\quad \left. + \left( \int_0^1 \varphi_k^2(t, F_k^{-1}(u)) \left[ Z_k(u) - \frac{\sqrt{2}}{\pi} \sum_{m=0}^v \frac{(-1)^m}{m+0,5} Z_m^k \right] dF_k^{-1}(u) \right)^2 \right\} \leq 2nE \left\{ \sum_{k=1}^n \left( f_k^2(t, b_k) \left[ Z_k(1) - \frac{\sqrt{2}}{\pi} \sum_{m=0}^v \frac{(-1)^m}{m+0,5} Z_m^k \right]^2 + \right. \right. \\
&\quad \left. \left. + \int_0^1 \varphi_k^2(t, F_k^{-1}(u)) \left[ Z_k(u) - \frac{\sqrt{2}}{\pi} \sum_{m=0}^v \frac{(-1)^m}{m+0,5} Z_m^k \right] dF_k^{-1}(u) \right)^2 \right\} \leq \frac{4nR_v}{\pi^2} \sum_{k=1}^n \left[ f_k^2(t, b_k) + (b_k - a_k) \times \right. \\
&\quad \left. \times \int_0^1 \varphi_k^2(t, F_k^{-1}(u)) dF_k^{-1}(u) \right] = \frac{4nR_v}{\pi^2} \sum_{k=1}^n \left[ f_k^2(t, b_k) + (b_k - a_k) \int_{a_k}^{b_k} \varphi_k^2(t, \lambda) d\lambda \right], \quad (8)
\end{aligned}$$

where  $\frac{1}{v+1,5} < R_v < \frac{1}{v+0,5}$  [7].

When functions  $f_k(t, b_k)$  and integrals  $\int_{a_k}^{b_k} \varphi_k^2(t, \lambda) d\lambda, k = \overline{1, n}$  are finite, then (8) shows,

that representation (6) is true in mean square sense, with probability 1 and consequently for almost every sampling functions, if we require  $\xi(t)$  process being separable in case of continuous  $t$ .

Analogously is obtained estimation of remainder term of (7). For this, note

$$\tilde{\xi}_v(t) \equiv \sum_{k=1}^n \left[ f_k(t, b_k) \frac{\sqrt{2}}{\pi} \sum_{m=0}^v \frac{(-1)^m}{m+0,5} Z_m^k - \int_0^1 \frac{\sqrt{2}}{\pi} \sum_{m=0}^v \frac{(-1)^m}{m+0,5} Z_m^k \sin[(m+0,5)\pi u] d_u f_k(t, F_k^{-1}(u)) \right].$$

In this case we also may write

$$\begin{aligned}
E[\xi(t) - \tilde{\xi}_v(t)]^2 &= E \left\{ \sum_{k=1}^n \left( f_k(t, b_k) \left[ Z_k(1) - \frac{\sqrt{2}}{\pi} \sum_{m=0}^v \frac{(-1)^m}{m+0,5} Z_m^k \right] - \int_0^1 \left[ Z_k(u) - \frac{\sqrt{2}}{\pi} \sum_{m=0}^v \frac{(-1)^m}{m+0,5} Z_m^k \right] d_u f_k(t, F_k^{-1}(u)) \right)^2 \right. \\
&\quad \left. + \left( \int_0^1 \left[ Z_k(u) - \frac{\sqrt{2}}{\pi} \sum_{m=0}^v \frac{(-1)^m}{m+0,5} Z_m^k \right] d_u f_k(t, F_k^{-1}(u)) \right)^2 \right\} \leq \\
&\quad \leq 2nE \left\{ \sum_{k=1}^n f_k^2(t, b_k) \left[ Z_k(1) - \frac{\sqrt{2}}{\pi} \sum_{m=0}^v \frac{(-1)^m}{m+0,5} Z_m^k \right]^2 + \right. \\
&\quad \left. + \left( \int_0^1 \left[ Z_k(u) - \frac{\sqrt{2}}{\pi} \sum_{m=0}^v \frac{(-1)^m}{m+0,5} Z_m^k \right] d_u f_k(t, F_k^{-1}(u)) \right)^2 \right\} \leq \\
&\quad \leq \frac{4nR_v}{\pi^2} \sum_{k=1}^n \left[ f_k^2(t, b_k) + \left( \int_0^1 d_u f_k(t, F_k^{-1}(u)) \right)^2 \right],
\end{aligned}$$

where last integral express full variation of function  $f_k(t, F_k^{-1}(u))$ .

Here, we can make conclusion about convergence of series (7) analogous to (6).

Obtained results can be formulated in the form of following theorem:

**Theorem 1.** If  $\xi(t)$  is a real-valued Gaussian random process with zero mean and covariance function  $B(t, s)$ , represented in the form (1), then, when  $f_k(t, b_k)$  and integrals

$\int_{a_k}^{b_k} \varphi_k^2(t, \lambda) d\lambda, k = \overline{1, n}$  are finite, we have the (6) stochastic series decomposition of

$\xi(t)$  process. When  $f_k(t, b_k)$  and integrals  $\int_0^1 d_u f_k(t, F_k^{-1}(u))$ ,  $k = \overline{1, n}$  are finite, then we have

the decomposition (7) for  $\xi(t)$ . Both, (6) and (7) representations are true in mean square sense, with probability 1 and hence, for almost every sampling functions, if for continuous t is required separability of  $\xi(t)$ .

When  $\xi(t)$  is stationary Gaussian real-valued process with zero mean and continuous bounded spectrum, then

$$B(t, s) = \int_0^a \cos(t-s)\lambda dF(\lambda) = \int_0^a \cos t \lambda \cos s \lambda dF(\lambda) + \int_0^a \sin t \lambda \sin s \lambda dF(\lambda), \quad n = 2,$$

$$F_1(\lambda) = F_2(\lambda) = F(\lambda), \quad a_k = 0, \quad b_k = 0, \quad f_1(t, \lambda) = \cos t \lambda, \quad f_2(t, \lambda) = \sin t \lambda,$$

$$\varphi_1(t, \lambda) = -t \sin t \lambda, \quad \varphi_2(t, \lambda) = t \cos t \lambda, \quad f_1(t, b_1) = \cos at, \quad f_2(t, b_2) = \sin at,$$

$$C_m^1(t) = t \int_0^a \sin(t\lambda) \sin[(m+0,5)\pi F(\lambda)] d\lambda,$$

$$C_m^2(t) = -t \int_0^a \cos(t\lambda) \sin[(m+0,5)\pi F(\lambda)] d\lambda$$

and from (6) we have

$$\xi(t) = \frac{\sqrt{2}}{\pi} \sum_{k=0}^{\infty} \frac{1}{k+0,5} \left\{ (-1)^k \cos(at) + t A_k(t) \right\} Z'_k + \left\{ (-1)^k \sin(at) - t B_k(t) \right\} Z''_k \quad (9)$$

where

$$A_k(t) = \int_0^a \sin(t\lambda) \sin[(k+0,5)\pi F(\lambda)] d\lambda,$$

$$B_k(t) = \int_0^a \cos(t\lambda) \sin[(k+0,5)\pi F(\lambda)] d\lambda$$

and  $\{Z'_k\}$ ,  $\{Z''_k\}$  are independent sequences of independent Gaussian random variables with parameters (0,1).

When  $\xi(t)$  is stationary random sequence i.e.  $t = 0, \pm 1, \pm 2, \dots$ , then  $a = \pi$ . In this case  $\cos(\pi t) = (-1)^t$ ,  $\sin(\pi t) = 0$ ;  $t = 0, \pm 1, \pm 2, \dots$ , and (9) will have the form:

$$\xi(t) = \frac{\sqrt{2}}{\pi} \sum_{k=0}^{\infty} \frac{1}{k+0,5} \left\{ (-1)^{k+t} + t A_k(t) \right\} Z'_k + t D_k(t) Z''_k, \quad t = 0, \pm 1, \pm 2, \dots, \quad (10)$$

where

$$A_k(t) = \frac{1}{2} \int_0^{\pi} \cos[t\lambda - (k+0,5)G(\lambda)] d\lambda - \frac{1}{2} \int_0^{\pi} \cos[t\lambda + (k+0,5)G(\lambda)] d\lambda, \quad (11)$$

$$D_k(t) = -B_k(t) = \frac{1}{2} \int_0^{\pi} \sin[t\lambda - (k+0,5)G(\lambda)] d\lambda - \frac{1}{2} \int_0^{\pi} \sin[t\lambda + (k+0,5)G(\lambda)] d\lambda, \quad (12)$$

$$G(\lambda) = \pi F(\lambda) = 2\pi \frac{\hat{F}(\lambda) - \hat{F}(0)}{\hat{F}(\pi)}, \quad \hat{F}(\lambda), \quad -\pi \leq \lambda \leq \pi, \text{ is spectral function.}$$

When  $\hat{F}(\lambda)$  is unknown and only observed values  $x_1, x_2, \dots, x_T$  of  $\xi(t)$  are known, then in place of  $\hat{F}(\lambda)$  will be taken its estimation (see [8], pp. 476-479):

$$\hat{F}_T^*(\lambda) = \int_{-\pi}^{\lambda} I^*(\omega) d\omega,$$

where

$$I^*(\omega) = \frac{1}{2\pi} \sum_{r=-(T-1)}^{T-1} C_r^* \cos(\omega r), \quad -\pi \leq \omega \leq \pi,$$

$$C_r^* = C_{-r}^* = \frac{1}{T} \sum_{t=1}^{T-r} (x_t - \bar{x})(x_{t+r} - \bar{x}), \quad r = 0, 1, \dots, T-1, \quad \bar{x} = \frac{1}{T} \sum_{t=1}^T x_t,$$

Sampling spectral function  $\hat{F}_T^*(\lambda)$  is consistent estimate for  $\hat{F}(\lambda)$  at the point of continuity and  $\sqrt{T}(\hat{F}_T^*(\lambda) - \hat{F}(\lambda))$  has limit normal distribution (see [8], p. 537).

Since

$$\int_{-\pi}^{\lambda} \cos(\omega r) d\omega = \begin{cases} \frac{\sin(\lambda r)}{r}, & \text{when } r \neq 0, \\ \lambda + \pi, & \text{when } r = 0, \end{cases}$$

therefore from (13) we have

$$\begin{aligned} \hat{F}_T^*(\lambda) &= \int_{-\pi}^{\lambda} I^*(\omega) d\omega = \frac{1}{2\pi} \sum_{r=-(T-1)}^{T-1} C_r^* \int_{-\pi}^{\lambda} \cos(\omega r) d\omega = \frac{1}{2\pi} \sum_{r=-(T-1)}^{T-1} C_r^* \frac{\sin(\lambda r)}{r} + \frac{1}{2\pi} C_0^* (\lambda + \pi) = \\ &= \frac{1}{\pi} \sum_{r=1}^{T-1} \frac{C_r^*}{r} \sin(\lambda r) + \frac{C_0^*}{2\pi} \lambda + \frac{C_0^*}{2} \end{aligned}$$

So, when the spectral function  $\hat{F}(\lambda)$  is unknown and only observed values of  $\xi(t)$  process  $x_1, x_2, \dots, x_T$  are known, then in formulae (11) and (12) we shall take the value  $G_T^*(\lambda)$  instead of  $G(\lambda)$ :

$$G_T^*(\lambda) = 2\pi \frac{\hat{F}_T^*(\lambda) - \hat{F}_T^*(0)}{\hat{F}_T^*(\pi)} = \frac{2}{C_0^*} \sum_{r=1}^{T-1} \frac{C_r^*}{r} \sin(\lambda r).$$

From here, algorithm of numerical modeling of real-valued stationary Gaussian random sequence with zero mean and continuous spectrum is obtained based on (10).

Following statements easily are proved also:

**Theorem 2.** When  $\xi(t)$  is stationary Gaussian random process with unbounded spectrum, then for any  $\varepsilon > 0$  there exists stationary Gaussian random process  $\xi_1(t)$  with bounded spectrum such, that

$$\sup E|\xi(t) - \xi_1(t)|^2 < \varepsilon.$$

Modeling of approximating process  $\xi_1(t)$  will be realized based on the (9).

**Theorem 3.** If  $\xi(t)$  is real-valued stationary Gaussian random process with zero mean, unit variance and spectral function  $F(\lambda)$  (discrete spectrum):

$$F(\lambda) = \sum_{k=1}^{\infty} a_k I(\lambda - \lambda_k),$$

$$I(\lambda) = \begin{cases} 0, & \lambda \leq 0 \\ 1, & \lambda > 0, \quad a_k > 0, \quad k = 1, 2, \dots, \end{cases}$$

then for  $\xi(t)$  in mean square sense, with probability 1 and so, for almost every sampling functions, the following representation is correct:

$$\xi(t) = \sum_{k=1}^{\infty} \sqrt{a_k} (\cos(t\lambda_k) u_k + \sin(t\lambda_k) v_k), \quad (14)$$

where  $\{u_k\}$  and  $\{v_k\}$  are independent sequences of Gaussian random variables with parameters  $(0,1)$ . In case of continuous  $t$  is required separability of  $\xi(t)$  process.

For the case, when the spectrum contains discrete and continuous parameters, then modeling of processes with discrete and continuous spectrum will take place separately, by above described methods and the results of modeling will be added together. The above

mentioned method gives possibility of modeling of more wide class random processes, namely of random processes of class  $N$  [5], [9].

### References

- [1]. K.Karhuner, Uber lineare methoden in der wahrscheinlinchkeitsrechnung, Ann. Acad. Sci Fennicae, Ser. A, I, 37, 1947, p.p. 3-79.
- [2]. N.Wiener, Nonlinear problems in random theory, John Wiley and Sons, New York, 1958.
- [3]. K.J.Astrom, Introduction to stochastic control theory, Academic Press, New York, 1970.
- [4]. I.I.Gikhman, A.V.Skorokhod, The theory of random processes, v.I, M., 1971, (Russ.).
- [5]. Z.A.Piranashvili, On one class of random processes, Proceed. Inst. of Appl. Math of Tbilisi stateUnivers. N1, 1969, pp.25-37.
- [6]. Z.A.Piranashvili, O.G.Petriashvili, On one method of modeling stationary Gaussian random processes, Bulletin of the Georgian academy of sciences,v.96, N2, 1979, pp.301-304.
- [7]. Z.A.Piranashvili, O.G.Petriashvili, On representation of stationary Gaussian random processes, Bulletin of the Georgian academy of sciences,v.99, N3, 1980, pp.557-560.
- [8]. T.W.Anderson, The statistical of time series, New York, 1971.
- [9]. Z.A.Piranashvili, Some questions of statistical-probabilistic modeling of continuous random processes, Tbilisi, "Metsniereba", 1966, pp.53-91.



## Optoelectronic processor for artificial intellect problems

**Goderdzi Lezhava**

*Institute of Cybernetics*

In the last few decades a serious effort has been mounted to tackle problems concerning the create of

1. Optical computing machinery – optical supercomputer and
2. Artificial intellect.

The above lines of research, in spite of notable advance, have not been as successful as one might expected. Below we shall try to investigate the cause of the above – mentioned failure. Also we shall try to define possible role of optical computations.

Optical signals, being data carriers, are known to have major advantages over electronic signals. This makes it possible to employ a variety of physical phenomena for information encoding and conversion. [ 1, 2, ].

Nevertheless, all attempts to devise optoelectronic computing machinery have met with failure. We are of the opinion that the chief cause of the above-mentioned failure is that of an ideological nature.

To prove this view let us find out what is it that forms the basis of electronic computer engineering. The essentials are as follows:

1. Logic;
2. Mathematics;
3. Mathematical logic;
4. The idea of programmed control;
5. Technology.

Ideological as well as theoretical foundations of computer engineering have been elaborated over a long period of time within the framework of logic and mathematics. These foundations constitute:

1. The notion of formal symbolic-deductive system, developed in the works of George Boole and further updated by Gotlib Frege.
2. The concept of algorithm and computability, the fresh approach employed to their interpretation being associated with the names of Church, Turing and Markov [ 3, 4, 5 ].

The well-known abstracts of Church, Turing and Markov, defining essentially computable mathematical objects, are mutually equivalent.

Equivalent to them is also the so-called cybernetic thesis or to put it otherwise, the principle of computer – aided computability, that reads as follows:

“Each finite computable (in particular, logical deductive) procedure, characterized by determinacy in execution can be in principle carried out by a digital computer provided that the latter features reasonably high-speed internal performance (enough ran time) [ 6 ].

This means that a computer-assisted solution may be obtained to any problem that is clearly and unambiguously stated.

The validity of the above statement seems to be corroborated by practice. There is much speculation that there is no principal reason for failing to obtain a computer-assisted solution other than insufficient volume of particular computer memory or inadequate inner performance.

At any rate, there is, conceivably, potential as well as factual computability. We have two cases here:

1. Some problems that are potentially computable on a computer, while being practically incapable of computation today might well lend themselves to computation tomorrow as a consequence of improvements done to the computer.

2. Some problems that are principally computable with the aid of a computer, will never be practically computable (A chess-playing computer with a program based on the full search of the so called "Game tree" is a good case in point. Shannon believes that there is no way of computerized search for the  $10^{120}$  options he has counted).

There were a few dissenters from this view, though.

Some major arguments supporting the above view are cited below.

- It is evident from Gyodel second theorem that the axiomatic-deductive method is by no means absolute and some problems may crop up even in elementary arithmetic of natural numbers that are incapable of solution within any particular axiomatic system [ 7 ].
- While investigating the question of obtaining computer-aided solution of an intricate problem – in particular, the simulation of brain neuro structures, Fon Neyman came to the conclusion that in case of a system achieving a certain limit of complexity, its description and hence its mechanical model cannot be less complicated than the system itself. This means that the mechanical model of a brain should be identical to the brain in sophistication [ 8 ].
- At first, Marvin Minski was an adamant proponent of the approach involving a computerized investigation of artificial intellect through the creation of suitable "intellectual" programs. But this approach has run into insurmountable obstacles. Many years of research have met with only limited success. Chess programs and expert systems that have been created so far can only conventionally be considered as "intellect" carriers. Minski himself has changed his opinion stating that according to his current views, the breakthrough in the creation of intellectual machines may occur with devices that have much in common with perceptrons [ 9 ].
- From psychology it is known that intellectual objects consist, as a rule, of two independent systems: sensor perception system, whereby one can perceive the environment, and character (sign) processing system whereby one can process information on the environment.

The arguments adduced legitimately lead to the following line of reasoning:

1. Employing optoelectronic inductive derivation associative system in hybrid systems along with digital computer will make it possible to considerably shift the boundary between actually computable and actually incapable of computatione.
2. In order for the computer to become "reasonable", that is, in order to achieve much progress toward the creation of artificial intellect, it is necessary to ensure the coupled operation of a computer – symbolic deductive derivation system and inductive derivation associative system. The argument about inductive derivation system being programmed-realizable within a computer fails because the complication of a problem is limitless while the capabilities of a computer are restricted by the so-called Fon Neyman limitation of a crucial nature and, as the problem gets more and more complicated, there will be the overlapping of practically computable and practically incapable of computation, which makes the solution of the problem impossible.
3. Electronics is best suited for the technical realization of symbolic deductive derivation systems. Any formula of symbolic logic is known to have one-to-one relation to electronic rectifier-containing circuit. Microelectronics technological potentialities are also well-appreciated [10].
4. The same cannot be said of optical systems; Optical means are unsuitable for symbolic deductive systems. Then again, optical means do possess great potential for the realization of preliminary precomputer processing systems – associative inductive derivation systems that are an analogue of sensory perception.

From the above line of reasoning it would be worthwhile to devise a computing system relying on optoelectronics to process effectively the specifications of objects or situations obtained by sensor perception and represented as a multidimensional vector and to correlate each specification with a particular character from the given alphabet.

This kind of optoelectronic processor is to carry out the comparison between the specification of some input object or a situation and the specifications of objects and situations fixed previously in the memory.

Let us assume that object or situation specification are represented as multicomponent vectors:  $\bar{x} = \{x_i\}$ ,  $i = 1, \dots, d$ ;

The so called a priori information, or teaching information, or information based on past experience that is represented as N number of specifications of that kind is fixed in processor on-line storage in advance:  $[\bar{x}_1, \bar{x}_2, \dots, \bar{x}_j, \dots, \bar{x}_N]$ .

When some input object or situation specification is fed to the processor

$$\hat{x} = \{ \hat{x}_i \}, i = 1, \dots, d,$$

the latter will compare it with all specifications of a priori information – all vectors of  $\bar{x}_j$  set.

This comparison may be effected in parallel so that the processor will produce simultaneously the output results of the comparison between  $\hat{x}$  vector  $\bar{x}_j$  set and all vectors, or the measure of similarity. Generally, they may be represented as

$$D(\hat{x}, \bar{x}_j) = \sum_{i=1}^d f(\hat{x}_i - x_{ij}), j = 1, \dots, N.$$

The comparison criterion – the nature of comparison is determined by the form of function f. In fact, these are distances in some d-dimensional metric space between the points  $\hat{x}_i$  and  $\bar{x}_{ij}$  (Fig. 1).

With Euclidean space, the above distances may be expressed as

$$D'(\hat{x}, \bar{x}_j) = [ \sum_{i=1}^d (\hat{x}_i - x_{ij})^2 ]^{1/2}, i = 1, \dots, d; j = 1, \dots, N.$$

The squares of the distances will acquire the form

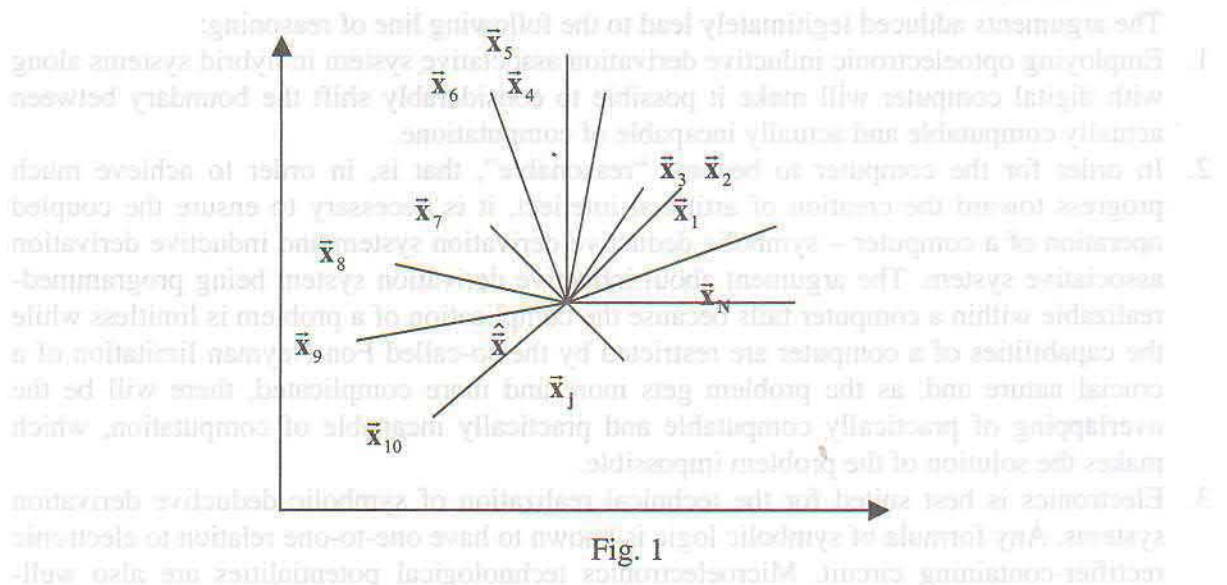


Fig. 1

$$D'(\hat{x}, \bar{x}_j) = \sum_{i=1}^d (\hat{x}_i - x_{ij})^2, i = 1, \dots, d; j = 1, \dots, N.$$

Sometimes, the so – called Hemming or Manhattan or “City section metric” [11] space is more convenient for practical realization, the distance in that case being represented as follows

$$D'(\hat{\bar{x}}, \bar{x}_j) = \sum_{i=1}^d |\hat{x}_i - x_{ij}|, \quad i=1, \dots, d; \quad j=1, \dots, N.$$

As stated above, the distances between points  $\hat{\bar{x}}$  and  $\bar{x}_j$  could be interpreted as the measure of proximity or similarity. In a sense, any expression  $A + B\{F[D(\hat{\bar{x}}, \bar{x}_j)]\}$  could also be thought of as the measure of similarity, with  $F$  being monotonously increasing function

$$G(\hat{\bar{x}}, \bar{x}_j) = A + B\{F[D(\hat{\bar{x}}, \bar{x}_j)]\},$$

where  $G(\hat{\bar{x}}, \bar{x}_j)$  denotes the measure of similarity.

It is pertinent to note that all these  $N$  distances, being inter-independent values, could be calculated in parallel and simultaneously [12].

A processor that implements such a function is, in a sense, an associative system of inductive derivation. As pointed out above, the need for a system like that arises extensively when facing practical problems, especially those dealing with artificial intellect.

The formal apparatus of such problems is characterized by operations in a multidimensional space and in particular, by repeated assessment of distances in the above space, performing which by means of a computer is in many instances unfeasible in real time.

The existing elemental base makes it possible for optoelectronic processor to be realized in multiple versions.

Information conversion process taking place in the processor is represented schematically in fig. 2. Here, plane 1 corresponds to storage system containing a priori information.

Information presentation special arrangement in optical system is known to be of great importance in contrast to electronics.

A priori information in a processor is represented as a set of matrices. Each row of all the matrices of this kind – data page – corresponds to vector representation of one object or one situation, while the columns correspond to the components of the same vectors.

$$\begin{matrix} X_{11} & X_{21} & X_{31} & \dots & X_{i1} & \dots & X_{d1} \\ X_{12} & X_{22} & X_{32} & \dots & X_{i2} & \dots & X_{d2} \\ X_{13} & X_{23} & X_{33} & \dots & X_{i3} & \dots & X_{d3} \\ \vdots & \vdots & \vdots & \ddots & \vdots & \ddots & \vdots \\ X_{1j} & X_{2j} & X_{3j} & \dots & X_{ij} & \dots & X_{dj} \\ \vdots & \vdots & \vdots & \ddots & \vdots & \ddots & \vdots \\ X_{1N} & X_{2N} & X_{3N} & \dots & X_{iN} & \dots & X_{dN} \end{matrix}$$

Data pages of a priori information could be stored in holographic storage system as Fourier holograms. In that case, it is possible for each matrix (data page) to be derived simultaneously in parallel in the processor [14]. Then again, the priori information may, in principle, be stored on a magnetic disk.

In the event of analogous realization the values included in data page may be encoded as intensity, phase or polarization relief.

Fourier hologram retrieval is effected in accord with the problem to be solved. This retrieval may be interpreted as the retrieval of the prearranged structure or a frame of the data (knowledge) related to the given problem.

The fetch time from a hologram system is  $10^{-5} \div 10^{-6}$  sec. It is during this time that the retrieved hologram – fixed data page is being reconstructed (in our case it is a concrete matrix  $\bar{x}_{ij}$  of a priori information) and projected on plane 2. The said plane is the input of the processor itself.

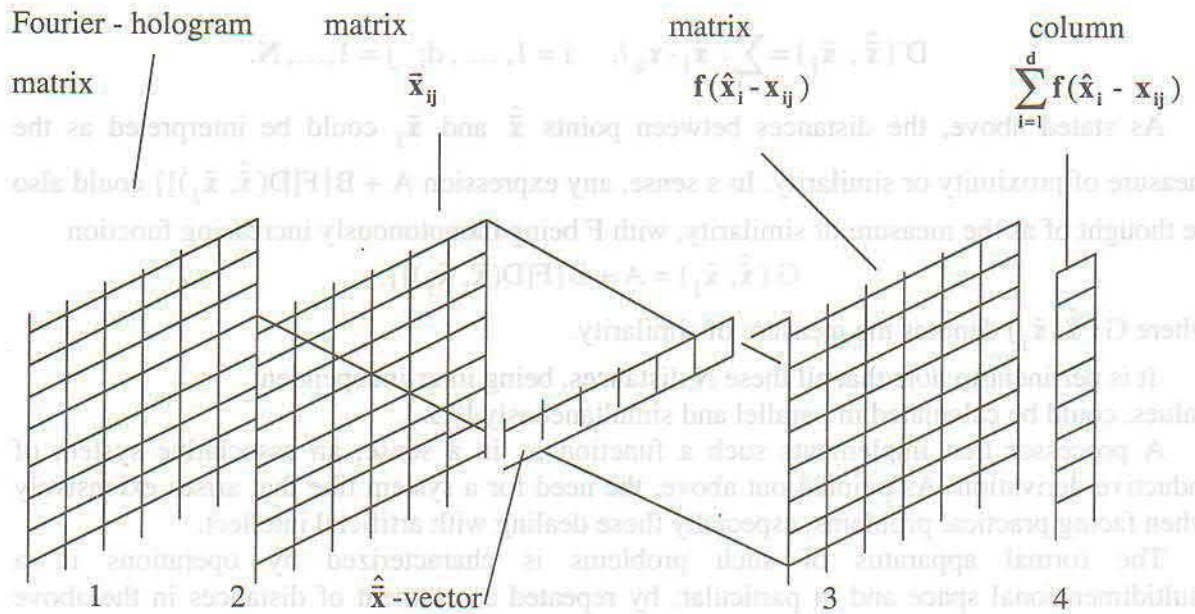


Fig. 2

The basic operation that is being accomplished in the processor is the conversion of  $\bar{x}_{ij}$  matrix into that of  $f(\hat{x}_i - x_{ij})$  values as a result of the interaction between matrix  $\bar{x}_{ij}$  and vector  $\hat{x}_j$ .

For this conversion there is the corresponding plane 2 transformation into plane 3 in fig. 3. The said transformation may be effected by the so-called PCEM (photo - conductor - electrooptical material) structure. Among the said structures are, for example, "Phototitus" (Photo Tube Image Transparency Variable Spatio-temporal), "Prom" (Pockels Readout Optical Memory or Modulator), liquid-crystal spatio-temporal light modulator etc. [14]. They are distinguished by modulation characteristics being of the following form

$$I = I_0 \sin^2 \frac{\pi \Gamma}{\lambda},$$

where  $I_0$  is the intensity of light incident on the modulator,

$I$  - the intensity of light transmitted through the modulator,

$\lambda$  - light wavelength,

$\Gamma$  - electric voltage - induced crystal path-length difference.

The subtraction operation  $\hat{x}_i - x_{ij}$  on charge carrier level is readily realized on photoconductive layer of the said structure, with  $\hat{x}_i$  and  $x_{ij}$  being analogously represented by intensities. The index of refraction will be suitably modulated and the light transmitted through each structural element  $ij$  will be proportional to  $\sin^2 k(\hat{x}_i - x_{ij})$ . Thus we obtain

$$f(\hat{x}_i - x_{ij}) = \sin^2 k(\hat{x}_i - x_{ij}).$$

As for the last 3 - 4 conversion, it may easily be effected by means of cylindrical optics that transfers the matrix of  $\sin^2 k(\hat{x}_i - x_{ij})$  values into a column. For each element of the column we shall have  $\sum_{i=1}^d \sin^2 k(\hat{x}_i - x_{ij})$ , or there will be a sequence

$$G(\hat{x}, \bar{x}_j) = A + B \sum_{i=1}^d \sin^2 k(\hat{x}_i - x_{ij}),$$

which in the above-mentioned context is the assemblage of the measures of similarity of  $\hat{x}$  and  $\bar{x}_{ij}$  vectors (the specifications of objects or situations).

It is evident, that the discussed example of optoelectronic processor realization is neither unique nor the best. Seeking technical solutions of practical value is a subject of special research.

It has been known that there are certain "General intellectual" procedures or, in other words, metaprocedures, that are common for varied intellectual activity.

Among these are, for example:

- problem solving or the purposeful search procedure in the maze of possibilities. It is related to the classical programs "Logician theorist" and GPS (General Problem Solver) developed by Nuel, Simon and Show and relies on the search of the "final state" or a goal in the so-called "state space". The latter involves repeated measurement of distances in multidimensional space [15]. It is apparent that the processor is well suited for this kind of problem.
- Metaprocedure is a known psychological phenomenon of insight or "brightening up" involving the change of frame in the course of problem solution; The term we use for it is the change of a priori information or the change of vector  $\bar{x}_j$  set [ 16 ]. This procedure is also readily realizable with the aid of a processor.
- As early as 1959, the metaprocedure of pattern recognition was at first devised by Selfridge as the problem vector or point classification in the multidimensional attribute space [17]. This metaprocedure too, is readily realizable by means of a processor.

A processor can be used in complex industrial or military facilities control systems as well as in those employed in dealing with high-speed processes. In particular, yet another area of processor application is unmanned navigation.

Thus, from the above discussion it appears that there is a rather extensive class of topical practical problems that defy solution by means of ordinary computers.

Among such problems are: artificial intellect problems involving the repeated assessment of distances in multidimensional space; the control of complex industrial, military and other facilities as well as various high-speed processes, unmanned navigation etc.

There is good reason to assume that the optoelectronic processor, implementing simultaneously a speedy assessment of distances in state space, would cause a marked shift of the boundary between practically solvable and that incapable of computation, while operating with ordinary computer.

Rapid concurrent assessment of distances in state space is hard to carry out by means of electronic devices. But then again, it can be successfully realized by optoelectronic means.

Hence, it is advisable to discuss such processor designs as provide maximum of compatibility with the existing computers and ensure the computer-aided solution of more or less broad spectrum of problems.

Furthermore, it would be a good idea to discuss also the purely electronic versions of a processor. The electronic designs of a processor are far more advantageous than the programmed designs, yet they do not compare with optoelectronic designs in efficiency.

### References

- [1]. Winston E. Kock, Optical Computing, Example of Change, Proceeding IEEE, vol. 65, № 1, pp. 6-9, January, 1977.
- [2]. Alexander A. Sawchuk, Digital Optical Computing, Proceeding IEEE, vol. 72, № 7, pp. 758-779, July, 1984.
- [3]. Turing A. M., On computable numbers, with an application to the Entscheidungsproblem. "Proceedings of the London Mathematical Society", ser. 2, vol. 42, 230-265, 1936.
- [4]. A. A. Марков. Теория алгоритмов. Труды математического института АН СССР, т. XLII, М. – Л, 1954
- [5]. Church A., An unsolvable problem of elementary number theory, "American Journal of Mathematics," vol. LVIII, № 2, 345-363, 1936
- [6]. Michael A. Arbib, Brains, Machines and Mathematics, New York, McGraw Hill, 1964.

- [7]. Godel K., Uber formal unentscheidbare Satze der Principia Mathematica und verwandter Systeme I, *Monat. Math. und Phys.*, 38, 173-198, 1931.
- [8]. Дж. Фон Нейман. Теория самовоспроизводящихся автоматов – М.: Мир, 1971
- [9]. Artificial Intelligence Computer Images, bay the Editor of Time-Life Books, Time-Life Books, Amsterdam 1986.
- [10]. К. Шенон. Символический анализ релейных и переключательных схем. – В кн.: Работы по теории информации. – М.: ИЛ, 1963
- [11]. A. Faure, Perception et reconnaissance des formes, Editests, 1985.
- [12]. Lezhava G. G., Kamkamidze I. Sh. Method for Pattern Recognition and Optoelectronic Processor for Performing Thereof, *Official Bulletin of the Industrial Property*, 5(14), Tbilisi, 40-41, 1997.
- [13]. Geylord T. K., Storage Optical Information, *Handbook of Optikal Holography*, Academic Press, 414-451, 1979.
- [14]. D. Casasent, Spatial light modulators, *Proceeding IEEE*, vol. 65, № 1, pp. 143-157, January, 1977.
- [15]. Earl B. Hunt, Artificial Intelligence, Academic Press, Inc., 1975.
- [16]. M. Minsky, Aframework for Representing Knowledge. In the Psychology of Computer Vision, 211-277, 1975.
- [17]. Selfridge O. Pandemonium. A paradigm for learning. *Proceedings of the Symposium on the Mechanization of Thought Processes*. London, 1959.

#### References

- [1] Winston E. Koch, *Digital Optical Computing*, Proceeding IEEE, vol. 65, no. 1, pp. 6-8, January, 1977.
- [2] Alexander A. Savchuk, *Digital Optical Computing*, Proceeding IEEE, vol. 72, no. 7, pp. 758-779, July, 1984.
- [3] Turing A. M., On computable numbers, with an application to the Entscheidungsproblem, *Proceedings of the London Mathematical Society*, ser. 2, vol. 42, 230-265, 1936.
- [4] A. A. Mikhlin, *Точные методы решения нелинейных задач*, М.: ИЛ, 1954.
- [5] Church A., An unsolvable problem of elementary number theory, *American Journal of Mathematics*, vol. LVIII, no. 2, 345-363, 1936.
- [6] Michael A. Arbib, *Brains, Machines and Mathematics*, New York: McGraw Hill, 1964.



## Theoretical Principles of the Pattern Recognition Systems and some of Expert Systems

Nelly Tkemaladze  
*Institute of Cybernetics*

### Introduction

Two automatized systems of pattern recognition are suggested. The first of them is the system of pattern recognition with learning (PRL) and the second one - the system of unsupervised (without teacher) pattern recognition (UPR). The system PRL or UPR is used depending on the type of initial information.

If the initial information is given as learning descriptions in such case the problem of pattern recognition with learning is arisen and will be used the system PRL. The learning description is a sequence of parameter values (features), characterizing such objects for which the class this object belongs to is known beforehand [1,2].

If we imply that between objects and their learning descriptions single-valued interrelations exist then, the description  $G_i$  of the object  $Q_i$  of the class  $S_v$  may be represented as follows

$$G_{iv} = \{q_{1iv}, q_{2iv}, \dots, q_{Miv}\} \quad (1)$$

where  $q_{jiv}$  is the  $j$ -th parameter value characterizing the  $i$ -th object of the  $v$ -th class,  $M$  is the number of parameters.

If the initial information is given as object descriptions but for these objects the classes to which they belong to are not known beforehand, the problem of unsupervised pattern recognition is arisen and will be used the system UPR.

Two expert systems and the method on the basis of which they are constructed are suggested as well. The first expert system DEOP determines and estimates object parameters and the second one EOB – estimates objects.

### 1. Automatized System of Pattern Recognition with Learning (PRL)

The problem of Pattern Recognition with Learning is put forward as follows:

The  $L$  numbers of unlapped classes (subsets) of objects, descriptions of which are represented as (1) are given. On the basis of this information (learning descriptions) must be determined such knowledge base and data base (or decision function) by using of which will be recognized new objects from the given list of classes.

For solving this problem the system PRL [3,4] which consists of two subsystems is elaborated. The first subsystem is the learning model (LM), the second one is the model of recognition (MR).

The aim of the learning model is to determine knowledge bases and data bases on the basis of initial parameter values, i.e. learning descriptions which consist of features (parameter values). To accomplish this goal in the learning model are decided 9 problems.

The first problem of the LM is arisen when initial information is not given as learning descriptions, parameters are the functions of time and their values are given in the definite period of time for objects of each class. By solving this problem are determined such initial parameters, sequences of values of which are learning descriptions. At the same time each description consists of parameter values not only in the fixed time but also in relation to different time intervals. This problem is especially important for prediction of different

phenomena, natural calamities.

By solving the second problem of the LM by means of random numbers and slipping control procedure from the learning descriptions at first are singled out the control descriptions (after recognition of which the effectiveness of work of the system PRL is determined), then are determined different variants of learning and recognizable descriptions to determine different knowledge bases and data bases. For the system PRL the both problems are the auxiliary problems.

The method which is elaborated for solving the third problem - for separation of initial informative parameters uses balanced incomplete block-designs (BIB-designs) [5], correlation matrices, corresponding to the blocks of the indicated designs and vector-optimized method of choosing [6]. When the number of initial parameters are small this problem is not arisen.

The learning descriptions often consist of small informative initial parameter values (i. e. features). In such cases to use these features for characteristics of classes in that form in which they are given in the learning descriptions is impossible. In these cases for characteristics of classes must be considered connections existing among initial parameters. By solving the fourth problem are determined those connections - functions which are called artificial (formal) parameters. They show those inner hidden connections among initial parameters, which exist in reality, but in initial learning descriptions are given implicitly. Those parameters make it possible to expand the space of parameters when there are few initial parameters and otherwise narrow it down. In order to discover these hidden connections the method of determination of artificial parameter transforms learning descriptions into geometrical configurations after two-fold usage of BIB-designs. So tops of a geometrical configuration (for simplicity is supposed that it's a triangle) correspond to the blocks of the primary BIB-design which is composed of initial parameters. That's why artificial parameters are considered in relation with these blocks. From these connections - functions are chosen the best parameters, values of which characterize classes. Artificial parameters may be angular coefficients of straight lines passing through the tops of the geometrical configurations, trigonometrically functions etc. For instance one of the artificial parameters is

$$P = (b^2 + c^2 - a^2) / 2bc,$$

where  $a, b, c$  are lengths of sides of such triangle coordinates of tops of which are elements of blocks of the primary BIB-design. It must be mentioned that if correlation coefficients indicate the existence of connections between parameters (correlation between them), artificial parameters determine a form of these connections - functional dependence among parameters.

As it is possible parameters to have a large number of different values, the problem of determination of intervals of parameter values - the fifth problem is put forward. The algorithm of solving this problem takes into consideration that parameter values are elements of learning descriptions, which don't contain all parameter values. That's why this algorithm determines the intervals of parameter values and codes them. The number of codes are determined according to the parameter  $v$  of balanced or partially balanced incomplete block-design, i.e. configuration of type  $(v, b, k, r, \lambda)$  or  $(v, b, k, r, n_i, \lambda_i, p^i)$  which is used for solving the problem seven. Thus are obtained learning descriptions written in a new "language" (codes) [2].

By solving the sixth problem are chosen optimal parameters on the basis of coded learning descriptions. The method of solving this problem uses new artificial parameters (which exist in reserve), criteria of the choice of parameters and vector-optimized method of choosing. By using them after repeated coding the learning descriptions will be written in such "language" in which must be written recognizable descriptions as well.

So, by solving the problems 3÷6 is made preliminary transformation of learning descriptions.

Solving the seventh problem of the LM takes into account the transformation of coded learning descriptions into BIB- or PBIB(2)-design by using the following function of transformation

$$\forall q_\alpha \in B_\mu \in I : \begin{cases} q_\alpha \in G_i \Rightarrow q_\alpha \rightarrow q_\alpha \\ q_\alpha \notin G_i \Rightarrow q_\alpha \rightarrow -q_\alpha \end{cases} \quad (2)$$

where  $I$  is the BIB- or PBIB(2)-design,  $B_\mu$  - the  $\mu$ -th block of corresponding scheme.

Thus, the scheme  $I_{iv} \in I_v$  corresponds to each learning description  $G_{iv}$ . The elements of the blocks of the mentioned scheme are features (codes) with positive and negative signs. At the same time each description  $G_{iv}$  corresponds to  $b$  number of blocks. It means that the description  $G_{iv}$  will be partially reflected in each block. Characteristics of classes are determined on the basis of the learning descriptions, which are written in blocks. These characteristics are single features, their pairs, triplets (which are determined without a complete exhaustive search) and specific blocks of these schemes which are combinations of features characterizing and not characterizing classes [7]. Such feature, which characterizes objects of only one class, is called a maximal informative feature (MIF). If MIF characterizes all objects of a class, it is called a maxMIF. At the same time by this method are determined the measures of informativity of other features (not MIF) and that data which are necessary for the model of recognition to recognize objects.

By solving the eighth problem are calculated threshold measures. The MR uses them for object recognition on the basis of the measures of informativity of features.

The last ninth problem of the LM is determination of a well-grounded learning sampling, i.e. the necessary number of parameters, learning descriptions and optimal BIB- and PBIB(2)-designs which are used in the method of solving the seventh problem.

The method of solving the ninth problem uses result matrices, which are determined after recognition of objects of variants defined by the LM.

After solving the above-mentioned problems are received the knowledge bases and the data bases for the MR (the second subsystem).

The model of recognition for transformation of description of each recognizable object uses all knowledge bases, which are determined for every variant of objects determined by the LM. These knowledge bases are: the best parameters chosen from initial parameters; the formulae which determine the artificial parameters; intervals of parameter values and their codes – “language” in which are written learning descriptions. Besides, as the usage of different BIB and PBIB(2)-designs and different number of initial parameters is taken into account for each recognizable object is obtained corresponding number of descriptions written in codes. This means that one and the same object will be examined from different sides.

For making the decision which class a recognizable object belongs to the elaborated criteria must be based on the following types of data:

1. A number of MIF-s and the learning descriptions which contain these MIF-s;
2. Informative features and their corresponding measures of informativity;
3. Thresholds which are determined by the LM (problem 8) on the basis of such learning descriptions, which don't contain any MIF and maxMIF.

In the second subsystem on the basis of the above-mentioned are determined the criteria of three kinds. The criterion of the first kind makes decision only on the basis of the data of the first type. The criterion of the second kind uses the data of the first and the second types. The criterion of the third kind makes decision using the data of the second and the third types.

After recognition of object descriptions of different variants the MR determines result matrices. The LM determines a well-grounded sampling on the bases of result matrices (problem 9). On the basis of the knowledge bases and the data bases (which are determined according to the well-grounded sampling) primary decisions are received for each control description. On the basis of them is made the final decision which class  $S_v$  each object corresponding to control description belongs to with the degree of belonging

$$0 \leq \mu_j(Q_x) \leq 1.$$

The function of the MR is also to correct knowledge bases and data bases after recognition of objects. The correction of knowledge bases and data bases takes place after

determination of well-grounded sampling as well as when the MR makes decision about belonging such new objects to class which are not taken from the learning descriptions. The latter indicates the fact that the longer the system PRL will work the more effectively will work the system.

The ratio of the  $n_k$  number of correctly recognized control descriptions to the whole number  $n$  of control descriptions, i.e.  $E = n_k / n$  is considered as the degree of effectiveness of work of the system PRL.

In order to determine the detector of trust of the system PRL,  $E$  is considered as the first characteristic.

The ratio of number  $m_i$  of correctly recognized object descriptions of all variants in the process of learning to a number  $m$  of all recognizable object descriptions, i.e.  $A = m_i / m$  is considered as the second characteristic of the detector. The normalized length of the vector  $D$

$$D = (1/2(E^2 + A^2))^{1/2}$$

is called the detector of trust. It shows how a user of this system can trust the system PRL in future for recognition of new objects.

Our approach to the solution of the problem of pattern recognition with learning and accordingly the theoretical principles of the system PRL differs from all the works that we know. In the methods and algorithms of solving the problems of the system PRL are used the geometrical configurations; BIB- and PBIB(2)-designs, i.e.  $(v, b, k, r, \lambda)$  and  $(v, b, k, r, n_i, \lambda_i, p^i)$  type of configurations where  $v, b, k, r, n_i, \lambda_i$  are the parameters of the first kind and  $P^i = (P_{vt}^i)$  is the parameter of the second kind as it is given by a matrix; vector-optimized method of choosing; slipping control procedure and correlation matrices.

The suggested system PRL works effectively even in the cases when the following difficulties arise:

1. Descriptions of objects of one and the same class differ from each other more than descriptions of different classes;
2. Learning descriptions include a small or too large number of only less informative values of initial parameters;
3. Just the same parameter takes values over  $10^6$ .

In the system PRL for the first time were used BIB- and PBIB(2)-designs for determination of characteristics of classes majority of which are MIF and maxMIF. A great number of them stipulated a large per cent of correctly recognized objects - the high effectiveness of the system PRL. For the first time were also used the geometrical configurations and BIB-design for determination of such artificial (formal) parameters values of which draw together descriptions of the same class and move apart from each other descriptions of different classes. Such approach stipulated to remove the above-mentioned difficulties and that fact that functioning of the system PRL does not depend on the physical essence of the objects under investigation and a number of initial parameters. Therefore there is a great number of objects (different phenomena, situations) for recognition (prediction) of which may be used the suggested automatized system PRL.

The system PRL was often used successfully for recognition of objects of different classes. The results obtained after the work of the system PRL showed that in many cases this system on the basis of minimum initial information will be able to solve complicated problems of pattern recognition.

## 2. Automatized System of Unsupervised Pattern Recognition (UPR)

Let's admit  $Q = \{Q_i\}, i = \overline{1, N}$  is a set of objects which must be the sum of the classes (subsets)  $Q = \coprod_{v=\overline{1, L}} S_v$ ,  $G_i$  is the description of the object  $Q_i$ , i.e.  $G = \{G_i\}, i = \overline{1, N}$ , corresponds to the set  $Q$ . When initial information is given by the elements of the set  $G$ ,

which are not learning descriptions then the problem of unsupervised pattern recognition is arisen [8]. For solving this problem the automatized system of unsupervised pattern recognition (UPR) is elaborated. In the system UPR are solved 5 problems. After solving these problems this system uses the system PRL. Indeed, for unsupervised pattern recognition before determining the knowledge base and the data base the system UPR makes classification of object set  $Q = \{Q_i\}, i = \overline{1, N}$ . It makes possible to reduce the problem of unsupervised pattern recognition to the problem of pattern recognition with learning.

The aim of the first problem of the system UPR is to transform initial descriptions by using the artificial parameters. Utilization of the system PRL for recognition of different types of objects showed that there exist such artificial parameters, which are one and the same type of functions for them. These functions draw together the descriptions of objects of one and the same class and move apart from each other the descriptions of objects of different classes. This factor stipulates to write the descriptions  $G_i, i = \overline{1, N}$ , in such artificial parameter values. But here, as in the system PRL, the artificial parameters are used in relation with blocks of BIB-design. As initial information is not represented as learning descriptions, how well are chosen the artificial parameters will be revealed after solving the other problems of the system UPR or must be elaborated a special algorithm for choosing these parameters. It is possible these descriptions to contain also values of initial parameters.

The second problem of the system UPR is a determination of intervals of parameter values and their coding. For this purpose a sequence  $\overline{P_j}$  of values of any parameter  $p_j$  must

be divided into such intervals that  $\sum_{j=1}^n \text{card} \overline{P_j} = v$  and coded by the codes which are taken from

the sequences  $1, 2, \dots, v$ , where  $v$  is the parameter of BIB- or PBIB(2)-design, which is applied in the third problem. It is obvious that the more different values contains a parameter the more codes are singled out for it. These codes are new features. If among them are uninformative features (which characterize all objects – all elements of the set  $Q$ ) then they will be excluded and the remained features will be coded repeatedly or if the number of uninformative codes is small they will be considered as fictitious features.

The third problem consists in transformation of learning descriptions into BIB- or PBIB(2)-design by the function (2), the second condition of which must be changed as follows

$$\forall q_\alpha \in B_\mu \in I : q_\alpha \notin G_i \Rightarrow q_\alpha \rightarrow 0.$$

Thus, any description  $G_i$  corresponds to blocks of design  $I$ , which consists of zeroes and codes from the description  $G_i$ , which is written in the blocks. The transformation of objects into blocks gives possibility to determine a proximity (distance) among descriptions by blocks.

The aim of the fourth problem is just to determine the distances among the descriptions by the distances among the blocks.

Let's call the blocks of BIB- or PBIB(2)-design in which the first description is transformed the main blocks and the description itself - the main description. By the distances calculated between each  $j$ -th main block and the  $j$ -th blocks corresponding to other descriptions  $G_i, i = \overline{2, N}$ , is received a matrix

$$R_i = \{r_{ij}\}, j = \overline{1, b}, i = \overline{2, N}, \quad (3)$$

where  $b$  is the parameter of BIB- or PBIB(2)-design and notes the number of blocks in it. After determination of the minimal, maximal and mean values for each row of matrix (3) they are considered as components of a vector.

The lengths of these vectors are calculated and ordered according to the growth. Thus is obtained the sequence:

$$R_l = |r_{12}|, |r_{13}|, \dots, |r_{1N}|, \quad (4)$$

It shows the proximity between the first basic description and the other descriptions.

Let us assume, that the objects given by the descriptions which correspond to  $|r_{12}|$  and the lengths of its two (or more) following vectors belong to one and the same class. After this will be determined the average of the lengths of these three (or more) vectors and will be calculated

$$T_{1t} = \left( n_k^{-1} \sum |r_{1k}| - |r_{1t}| \right)^2, t = \overline{(n_k + 1), N},$$

where  $n_k$  is a cardinal number of the set of those objects which are regarded to belong to one and the same class. Thus is received a sequence  $R_1^*$  arranged according to the growth of the deviations  $T_{1t}$ . The description corresponding to the last member of this sequence is considered as the second main description. The same procedure will be carried out for it as for the first main description and will be received the sequence  $R_2$  which is analogous to (4) and consequently is received the sequence  $R_2^*$ . The sequence  $R_3$  is received in the same way, but as the first element of the sequence  $R_3$  will be regarded as that element which will approximately equally be remote from the first element of the sequences  $R_1^*$  and  $R_2^*$ . For each sequence  $R_1, R_2, R_3$  will be separately calculated the difference between each following element  $(T_{\mu+1}, T_{\mu})$  and will be chosen the maximal difference for each of them

$$\max(T_{\mu+1} - T_{\mu}) = d_{\mu+1}(\mu), \mu = \overline{1, 3}. \quad (5)$$

In the sequences  $R_1, R_2, R_3$  according to the numbers of classes, the maximums of the differences determined by (5) will be considered in turn. According to these maximums the objects corresponding to the elements of each sequence are divided into classes.

Thus, by using the sequences of the (4) type and (5) are received different variants of the primary classification. As it's possible to have a great number of initial parameters and as already we have a great number of artificial parameters, it should be advisable to group them and then to use these groups separately. This will increase the number of variants. After determining the variants of the primary classification is arisen the problem of numbering the classes identically according to the numbered classes in the first variant, of choosing admissible variants and of determining which class the objects belong to with the degree of belonging - the fifth problem. For solving this problem in the first time the classes in variants are numbered and then are determined the admissible variants. Those variants will be regarded as admissible variants in which the number of minimal objects in any class  $n \leq \alpha L$ , where  $L$  is a number of all classes.  $\alpha < 1$  is chosen according to the number of all classes. Thus are received different variants (or variant) of classification  $B_k, k = \overline{1, n}$ . Some of them can coincide with each other, but in some variants classes were intersected. On the basis of admissible variants will be determined the final variants of classification, each element (object) of which will have the degree of belonging to the corresponding class

$$\mu_{Q_i}(v) = m(Q_{iv})/n, \quad (6)$$

$m(Q_{iv})$  shows the number of those variants in which the object  $Q_i$  belongs to the  $v$ -th class,  $n$  is the number of all variants. The object  $Q_i$  will belong to the  $v$ -th class to  $\mu_{Q_i}(v)$  degree in case if the condition

$$\mu_{Q_i}(v) > 0.5 \text{ and } (\mu_{Q_i}(v) - \mu_{Q_i}(k)) < 0.25 \quad \forall k \neq v$$

is fulfilled. Otherwise the belonging of the object  $Q_i$  will be determined by using the system PRL /3,4/.

Thus, objects will be classified without a teacher. In this case some objects belong exactly to the concrete class, some of them - with the degree of belonging (6).

After classification of objects the descriptions of them will be given to the system PRL as the learning descriptions. On the basis of them the system PRL will determine the

knowledge bases and data bases for recognition of new objects. At the same time by the system PRL is determined how much correctly is made the object classification and in case of necessity will make corrections in it.

The system UPR suggested by us, unlike the existing works, at first requires preliminary transformation of descriptions - writing descriptions in the values of artificial parameters (obtained by using geometrical configurations and BIB-designs), dividing their values into intervals, encoding them, transformation encoded descriptions into BIB- or PBIB(2)-designs. Then it requires usage of the concept of proximity by means of the approach, which is unlike existing works and the system PRL for determination of a knowledge base and a data base.

The advantage of the determination of the distances between the blocks for the classification of objects is that in this case not only separate features are compared, but also their certain combinations.

### 3. Expert Systems

Let's consider two problems the solving method of which is used in the suggested expert systems:

1. Determination and estimation of object characteristics (problem A);
2. Estimation (also recognition) of objects by using the characteristics determined by means of solving the first problem (problem B).

For solving the both problems one and the same main approach is used. It is accordingly modified taking into account the specificity of these problems.

Let's assume that any object is given. We must determine the characteristics - features of this object taking into account experts' opinions.

The procedure of solving this problem consists of three stages.

On the first stage each expert  $\exists_j, j = \overline{1, m}$  determines a set of those features (characteristics) which to his/her mind characterizes the object  $Q, P_j = \{ p_{jt} \}, t = \overline{1, t_j}$ . By using them is determined a set  $P' = \prod P_j$  of the features of the object  $Q$ .

On the second stage each expert will choose the set  $P'_j, j = \overline{1, m}$  of permissible features from the set  $P'$ . From these sets will be chosen such elements (features) which are chosen at least by two experts. Let's number the chosen features and mark their set this way  $P = \{ p_i \}, i = \overline{1, n}$ .

On the third stage experts order the elements of the set  $P$  according to preference from the point of view of informativity [9]. If we consider informativity as a fuzzy concept and a set of informative features as a fuzzy set, the measure of infirmativity of features will be considered as a degree of belonging to a fuzzy set  $\mu_p(p_i)$  [2,10].

Thus the problem is reduced  $\forall p_i \in P$  to determine the function  $\varphi(p_i) = \mu_p(p_i), i = \overline{1, n}$ . For ordering the elements of the set  $P$  is used the following term-set

$$T(\omega) = \{ \omega_i \}, i = \overline{1, 5},$$

where  $\omega_1 \triangleq \succ \succ -$  much more preferable,  $\omega_2 \triangleq m \succ -$  much preferable,  $\omega_3 \triangleq \succ -$  preferable,  $\omega_4 \triangleq \geq -$  preferable or equal,  $\omega_5 \triangleq \sim -$  equal. (7)

(A number of elements of the set  $T(\omega)$  may be increased as well as decreased).

Let's mark the ordered sets (sequences) offered by the expert  $\exists_j, j = \overline{1, m}$ , in the following way  $\Pi_j = [P, \omega]$ . If we number the sequence  $\omega$  separately from the sequence  $\Pi_j$  we'll have n-1 element in it so, that before the element  $p_i \in \Pi_j$  which is the  $v$ -th element in it, will be the  $(v-1)$ -th element from the sequence  $\omega$ . If we determine the distance

between two elements of the set  $\Pi_j$  as a function of  $\omega - r(\omega)$ , the distance between the features placed on the first and the  $v$ -th place in the set  $\Pi_j$  will be determined as follows:

$$\rho_v = \rho(\rho_j^1, \rho_j^v) = \sum_{i=1}^{v-1} r(\omega_i), \quad (8)$$

where the function  $r(\omega) \forall \omega_i$  elements transforms into  $[0,1]$  interval so that

$$r(\omega_i) = \begin{cases} 1 & \text{if } \omega_i = \gg \\ 0.75 & \text{if } \omega_i = m > \\ 0.5 & \text{if } \omega_i = \Rightarrow \\ 0.25 & \text{if } \omega_i = \geq \\ 0 & \text{if } \omega_i = \sim \end{cases} \quad (9)$$

If we consider the set  $P$  as an abstract set, then  $card T(\omega) = 1$  and  $r(\omega_i) = 1 \forall i$ . While determining the sequence  $\Pi_j \forall \vartheta_j$  expert must put on the first place a fictitious element which must correspond to the best feature and in its relation must order all the elements (objects) taking into account (9). On the basis of the sums of the values of  $r(\omega_i)$  which are determined by (9) from the sequences  $\Pi_j, j = \overline{1, m}$  is formed one sequence  $\Pi$  in which will already be taken into account opinions of all experts. It's obvious that the further will be the  $i$ -th element from the best ones (from the element placed on the first place) in the sequence  $\Pi$  the less must be its measure of informativity (weight function) - a degree of belonging to a fuzzy set for determination of which we use the following normalized function [2]

$$\varphi(p_i) = (\rho - \rho_i) / \rho, \quad (10)$$

where  $\rho = \max_j \max_i \{\rho_{ij}\} + \varepsilon, \varepsilon > 0$  is any small number,  $\rho_i$  is the deviation of the  $i$ -th element from the first place in the sequence  $\Pi$  and  $\rho_{ij}$  is the deviation of the same element in the sequence  $\Pi_j$ . Thus is determined the function  $\varphi(p_i) = \mu_p$ , which transforms  $[p, \omega]$  into the interval  $[0,1]$ . Such approach makes possible to estimate experts as well and determine their competence by means of the following two characteristics [2,11].

The first of them is connected with the weight functions of parameters offered by the expert  $\vartheta_j$

$$X(\vartheta_j) = \frac{1}{\Phi} \sum_{i \in (I | p_i \in P_j \cap P)} \varphi(p_i), \quad \Phi = \sum_{i=1}^n \varphi(p_i),$$

for determination of the second characteristics of the  $j$ -th expert must be taken into account deviation of the sequence  $\Pi_j$  from the sequence  $\Pi$  taking into consideration weights (measures of informativity) of features, i.e. is determined

$$\delta_j = \frac{1}{n} \sum_{i=1}^n \varphi(p_i) \Delta r_{ij}, \quad \Delta r_{ij} = |r_i - r_{ij}|, \quad (11)$$

where  $r_i$  is deviation of  $p_i$  from the first place in the sequence  $\Pi$  and  $r_{ij}$  - in the sequence  $\Pi_j$ . On the basis of (11) is determine the set  $\Pi[\vartheta_j]$  ordered according to experts' preference. On the basis of the sequence  $\Pi[\vartheta_j]$  by analogy with (10) is determined the second characteristics of experts  $\vartheta_j, j = \overline{1, m}$

$$Y(\vartheta_j) = (\delta - \delta_j) / \delta, \quad \delta = \max_j \{\delta_j\} + \varepsilon, \varepsilon > 0.$$

If we consider  $X(\vartheta_j)$  and  $Y(\vartheta_j)$  as the components of the vector  $K$ , we call the normalized length of this vector the competence of the expert  $\vartheta_j$ . We can determine  $K$  as a

linear combination of  $X(\varepsilon_j)$  and  $Y(\varepsilon_j)$ . For estimation of coefficients in this combination we can use the method of determination of features with the help of experts.

When the number of features is large it's not convenient to order the elements of the whole set  $P$  simultaneously. In such case we use BIB-designs or tactical configurations (the blocks of which besides pairs contain also triplets of one and the same quantity). In this case the presentation of knowledge is matrix form unlike the previous case when the form of presentation of knowledge is linear. This is conditioned by the factor that experts have to order according the preference not the whole set  $P$ , but the elements of each block, which make peculiar corrections in the method and at the same time specifies feature weights. An algorithm of determination of expert competence requires correction as well. In this case is determined the third characteristics of experts which concern the deviations of the cardinal numbers of a set of such blocks of BIB-designs in which one and the same elements are placed in the first place. This conditions the addition of the third characteristic  $Z(\varepsilon_j)$  for the determination of expert competence. By means of these three characteristics is determined the competence of the expert  $\varepsilon_j$

$$K(\varepsilon_j) = \sqrt{(X(\varepsilon_j)^2 + Y(\varepsilon_j)^2 + Z(\varepsilon_j)^2) / 3} \quad (12)$$

This is that main method (approach), which is used in expert systems (ES) [12]. In general the following main problems must be solved for constructing expert systems:

1. To acquire knowledge using the specialists of the corresponding branches;
2. To choose a form of representation of knowledge (to determine the knowledge base) and form the data base;
3. On the basis of the existing knowledge base and data base to work out a decision-making mechanism and make a decision.

Two expert systems are elaborated for solving the problems A and B. The ES DEOP is elaborated for solving the problem A - to determine and estimate the parameters (characteristics), which are characteristic to objects. For the ES DEOP knowledge is acquired on the first stage of the method described above. The form of representation of knowledge (linear or matrix) is chosen and the data base is formed on the second stage and the decision-making mechanism is worked out and characteristics are finally chosen and estimated on the third stage. The expert system uses the algorithm of estimation of the experts described above to determine the competence of experts. The expert system DEOP is used to determine and estimate characteristics of any objects, situations, competitive projects; of ergonomically demands; of criteria etc.

For solving the problem B (for estimating objects) the ES EOB takes into account the characteristics determined by the DEOP, weight functions of characteristics of those objects estimations of which are the goal of the expert system EOB.

Let's have objects, which must be estimated - competitive projects, educational books, information about regions, where may be expected conflict situations etc. Experts must have the list of parameters of the objects under investigation which are determined by the ES DEOP. Every  $j$ -th  $j = \overline{1, m}$  expert must fill a matrix, the firsts row of which corresponds to the sequence of parameters  $p_i, i = \overline{1, n}$  and the first column - to the sequence of objects  $Q_k, k = \overline{1, N}$ . Thus every expert  $\varepsilon_j$  will determine the matrix  $T^j$  the element  $a_{ik}^j$  of which shows how much the  $i$ -th parameter characterizes the  $k$ -th object by means of the opinion of the  $j$ -th expert. The element  $a_{ik}^j$  receives values from the interval [0.1]. Thus is obtained the  $m$  number of matrices. From matrices  $T^j, j = \overline{1, m}$  is determined the matrix an element of which is determined as follows:

$$a_{ik} = \frac{1}{m} \sum_{j=1}^m \varphi(p_i) a_{ik}^j,$$

where  $\varphi(p_i)$  is determined by the formula (10). For any  $k$ -th object is determined

$$\varphi(Q_k) = \frac{1}{n} \sum_{i=1}^n a_{ik},$$

which is the first characteristic of the object  $Q_k$ . For determining the second characteristic the ES EOB will use presentation of matrices form for knowledge and so will determine the weight function  $\psi(Q_k)$  of the object  $Q_k$ , which is considered as the second characteristic. By these two characteristics the normalized weight function of the objects  $Q_k$  is determined

$$\phi_k = \sqrt{((\varphi(Q_k))^2 + (\psi(Q_k))^2) / 2}.$$

If we wish to determine the weight of the object  $Q_k$  only by means of the expert  $\varepsilon_j$ , for the first characteristic of the object  $Q_k$  is considered  $\phi_j(Q_k)$ , which is determined on the basis of the sequence ordered by the expert  $\varepsilon_j$  according to the preference of elements (objects). For the second characteristic is considered the weight  $\psi(Q_k)$  which is determined on the basis of blocks of BIB-design ordered by the  $j$ -th expert according to the preference of elements (objects). The normalized length  $\phi_k^j$  of the weight vector determined by these two characteristics is the weight of the object  $Q_k$  by means of the opinion of the  $j$ -th expert.

Thus, on the one hand is determined the weight  $\phi(Q_k)$  of the object  $Q_k$  in which is taken into account the parameter weights which are previously calculated by the ES DEOP and the common opinions of experts and on the second hand - the weight  $\phi_k^j$  of the object  $Q_k$  determined only by means of the opinions of the experts  $\varepsilon_j, j = \overline{1, m}$ .

By the differences between them for all objects is determined a lie detector for every expert  $\varepsilon_j$

$$L^j = \frac{1}{N} \sum_{k=1}^N |\phi_k - \phi_k^j|,$$

usage of which by analogy with (10) the characteristic of the  $j$ -th expert is determined

$$\gamma_j = (L - L^j) / L \quad \forall j,$$

where  $L = \max_j L^j + \varepsilon, \varepsilon > 0$ . What concerns other characteristics they are calculated by the

algorithm of estimation of experts as the second and the third characteristics as well. By these three characteristics the competence of experts is calculated by analogy with (12). The first ES suggested by us besides the fact that prepares information for the second ES is also used for determination of initial parameters for the system PRL. It will help the system PRL to determine object parameters by means of experts for determination of learning descriptions by these parameter values.

The both ES in dialogue regime can use any natural language. The systems PRL, UPR and expert systems DEOP and EOB are realized on the PC Pentium-133 by the collaborators of the Department of Classification of Complex Systems.

### References

- [1].G. Sebestyan. Decision-making Process in Pattern Recognition. Technics. Kiev. 1965. (Russian).
- [2].N.T.Tkernaladze. Recognition, Classification, Estimation. Mecniereba. Tbilisi. 1990. (Russian).
- [3].N.Tkernaladze. Bull. Georg. Acad. Sci. 159, 1. 1999. 42-44.
- [4].N.Tkernaladze. Automated System of Pattern Recognition with Learning. Lega.Tbilisi. 2000. (Georgian. Russian and English annotations).
- [5].M.Hall. Combinatorial Theory. Mir. M. 1970. (Russian).

- [6]. M.A. Aizerman, A.V. Malishevsky. Automatics and Telemechanics. N2. 1981. 65-83. (Russian).
- [7]. V.V. Chavhanidze. Works of IY IUC about Artificial Intelligence. Tbilisi. 1976. 7-77. (Russian).
- [8]. N. Tkemaladze. Some Problems of Pattern Recognition and Experts Systems. Intellect. Tbilisi. 1998. 42-49. (Georgian. Russian and English annotations).
- [9]. N.T. Tkemaladze. Certain Problems of Pattern Recognition and Graph Theory. Tbilisi. Mecniereba. 1972. 37-48. (Russian).
- [10]. Z.A. Kikvidze, N.T. Tkemaladze. Bull. Acad. Sci of GSSP. N2. 1979. 317-120. (Russian. English summary).
- [11]. N.T. Tkemaladze, Z.A. Kikvidze. Management in the presence of Fuzzy Categories. Thez. of Reports. Perm. 1980. 49-51. (Russian).
- [12]. N.T. Tkemaladze, M. Menabde, V. Jikhvashvili. Some Problems of Pattern Recognition and Experts Systems. Intellect. Tbilisi. 1998. 50-57. (Georgian. Russian and English annotations).

## 1. INTRODUCTION

Most investigations of learning networks as any adaptive systems using recurrent procedures like perceptrons [1], ADALINE and MADALINE [2] or learning matrices [3] and so on are dealing with the systems in which processed information flows through them only into the one direction - from inputs to outputs without inner cycles. This circumstance makes it possible to avoid temporal correlations into the input sequences and consider separated samples of an input information as temporally independent from each another. These systems cannot process temporal sequences without a special arrangement with delay elements installed especially for this purpose.

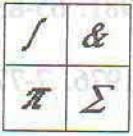
The present paper pursues the objective to clear up some principal abilities of the dynamic adaptive learning network the example of which is so-called cross-connected perceptron [1] with inner feedbacks.

First of all the dynamic system with inner feedback must be considered, on the one hand, as a system consisting of neuronlike elements with feedbacks and providing the spatiotemporal summation of input signals. Then they have various dynamic states. We will try to show how such a system could adapt to a periodically presented temporal sequence without any outer interference upon this system, or is able to be self-learning or self-organizing under certain conditions.

On the other hand such a system develops quite new abilities concerning a stable one in a sense of its complex behavior or interaction with an environment which means a further approximation towards understanding of brain mechanisms.

The perceptronlike systems were built 30 years ago by analogy with the topological structure of the visual neural system of a living organism. But here we omit such a question as localization of various specific functions like multidimensional controlling of an organism's motoric system [4], selective act [5] and so on which are really connected with a complex sequential behavior of an organism. Below we will only consider the hypothetical memory mechanism which is necessary for objectives of the present work.

Kalbfleiss, Hebb and others proposed the model of memory, which was effectively used



## Dynamic Adaptive Learning Networks

**Avtandil Kvitashvili**  
*Institute of Cybernetics*

### ABSTRACT

Most learning systems for pattern recognition using recurrent adaptive procedures are usually considered without inner feedbacks. That means they cannot process temporally correlated patterns without a special arrangement with delay elements. Besides such static systems do not have an ability to generalize patterns in a sense to maintain relations between visual, oral or other kind of stimuli.

The adaptive systems with inner feedback are to be considered as the dynamic systems with inner complex transient processes. The external and internal signals continuously changing the structure of systems. These systems have quite different character of functioning as distinct from static ones and there has been made an attempt to show whether they can be able to adapt to a temporally changing environment and learn certain relations between patterns or generalize complex stimuli. Simulation of such dynamic systems is also considered.

### 1. INTRODUCTION

Most investigations of learning networks as any adaptive systems using recurrent procedures like perceptrons [1], ADALINE and MADALINE [2] or learning matrixes [3] and so on are dealing with the systems in which processed information flows through them only into the one direction - from inputs to outputs without inner cycles. This circumstance makes it possible to avoid temporal correlations into the input sequences and consider separated samples of an input information as temporally independent from each another. These systems cannot process temporal sequences without a special arrangement with delay elements installed especially for this purpose.

The present paper pursues the objective to clear up some principal abilities of the dynamic adaptive learning network the example of which is so-called cross-connected perceptron [1] with inner feedbacks.

First of all the dynamic system with inner feedbacks must be considered, on the one hand, as a system consisting of neuronlike elements with feedbacks and providing the spatiotemporal summation of input signals. Then they have various dynamic states. We will try to show how such a system could adapt to a periodically presented temporal sequence without any outer interference upon this system, or is able to be selfadapting or selflearning one under certain conditions.

On the other hand such a system develops quite new abilities concerning a static one in a sense of its complex behavior or interaction with an environment which means a further approximation towards understanding of brain mechanisms.

The perceptronlike systems were built 30 years ago by analogy with the topological structure of the visual neural system of a living organism. But here we omit such a question as a localization of various specific functions like multidimensional controlling of an organism's motoric system [4], selective sets [5] and so on which are really connected with a complex sequential behavior of an organism. Below we will only consider the hypothetical memory mechanism, which is necessary for objectives of the present work.

Kalbertson, Hebb and others proposed the model of memory, which was effectively used

in various learning systems [6,7]. This mechanism suggested a correlation between an afferent synapse and an efferent neuron so that the transmission ability of the synapse is increasing with a positive correlation and vice versa. Investigation of synapses show also that the each previous depolarization of a given synapse increases the action of subsequent ones but after a certain excitatory sequence there are coming so called periods of facilitation which may have three phases [8]. For instance, the last of these phases may continue for many seconds. The depression phases are also coming after each facilitation.

Number of investigations the dynamics of a synaptic transmission show that the interconnected neurons determine a temporal perception and they could memorize such temporal patterns for a certain period of time [9].

Perhaps, the mechanism, which could be used as a neural model has to be substantially simple but on the other hand it should provide some complexity of behavior of a living system. From this point of view a simple adaptive learning system like ADALINE, MADALINE, perceptron or learning matrix [10] were as an attempt to investigate abilities of a homogeneous associative system with an extremely simplified memory mechanism, minimum structural differentiation and without any internal feedback which means that they are the static systems only but not dynamic.

Meanwhile a neuron network as a model of a part of brain is supposed to be making it possible appearance of some psychological phenomena according to the structural complexity of a network. Concerning the static adaptive learning networks we can say that they have the simplest psychological phenomenon - to distinguish of stimuli. This property of a system uses the difference between environmental stimuli reflected on the sensory input of the system. It is obvious that almost all pattern recognition systems are based on such an external differentiation of stimuli on the sensory input.

The generalization of stimuli we can accept as the following psychological phenomenon which is suppose to be an ability of invariance of the system concerning various transformations of input stimuli and this property rather expresses a detection of relations between stimuli than they have common input components. Therefore, from this point of view talking of the simple distinguishing the term „generalization” is fairly often used not quite properly. As it was shown such an ability partly had the multilayer perceptrons and the systems with inner feedbacks or so called cross - connected perceptrons [1].

The third important psychological phenomenon is connected with introduction of a temporal factor or it is ability to recognize the temporal sequences. In other words it means the temporal invariance of the system to in the time-correlated inputs. This property is principal ability of living organisms for interaction with changing environment. We should note that this property is organically connected with the systems with inner feedbacks.

Finally we can say that the above mentioned three properties of the brain with such a complex phenomenon as the selective set [11] which is intended to be a programmed controlling of perception that may probably lead us to understanding of more and more higher levels of the human brain's activity expressed as self-consciousness, creative activity and so on.

Therefore the substantial difference between the adaptive learning models corresponding to the first psychological phenomenon - to distinguish or classify by impute differences and the transitional dynamic systems with inner feedbacks having quite different abilities is obvious. Usually almost any recurrent adaptive pattern recognition or decision making procedures are concerning the first simple static models while we will try to show as the dynamic ones could able to generalize input stimuli as to recognize temporal sequences. Here we should note that the ability of temporal pattern separation can also include the first static recognition as its special case.

Before we will consider the dynamic adaptive systems it seems to be reasonable to analyze some properties of neuron networks dealing with a spatiotemporal summation of input signals.

## 2. SPATIOTEMPORAL SUMMATION OF INPUT SIGNALS AND CHANGING STRUCTURE OF THE DYNAMIC NETWORK

As we know one of the important mechanisms participating in neural information processing is the input of a neuron the-synapse [12]. Some details connected with synaptic transformation of the electric input signals into the chemical mediator and its further transform into the postsynaptic potential here will be omitted. Though this process is very important to investigate the synaptic conductivity which we will consider later as the weight or transmission coefficient of the separate synaptic input.

The input signal comes to a synapse of the neuron and participates into creation of the postsynaptic potential. This potential stipulates the excitement of the neuron. In general the action one or even several synapses is hardly reflected on the postsynaptic potential so that the response of the neuron is determined by the total sum of all the excited synapses.

The phenomenon characterized by a summation of signal sequences on the one synapse during a short time interval; as a matter of fact it is an integration in the time and is known as the property of temporal summation of input signals. On the other hand the postsynaptic potential is a result of summation of input signals coming on the several synapses at the same time or almost at the same time. Such an action is known as the property of spacial summation of input signals coming on the several synapses at the time or almost at the time. Such an action is known as the property of spacial summation of input signals.

Quantitative description of the above mentioned processes undoubtedly presents fairly hard problem but some investigations had shown that we can assume with a certain approximation that the spatiotemporal summation of the synaptic signals has linear character [13].

If we suggest that  $V(t)$  is the postsynaptic or membrane potential caused by an action of the given synapse at the time  $t - \tau$  and this potential is exponentially dropping after each activation of the synapse [14] we could have

$$V(t) = \int_0^t \alpha e^{-\beta(t-\tau)} \lambda(\tau) d\tau \quad (1)$$

where  $\lambda(\tau)$  is a mean pulse intensity coming to the given synapse,  $\alpha$  and  $\beta$  are constants depending on the synaptic electrochemical properties. The equation could be rewritten as

$$\frac{dV(t)}{dt} + \beta V(t) = \alpha \lambda(t) \quad (2)$$

These equations are approximately describing a transformation of the input pulse sequence intensity into the membrane potential under conditions of both the linear summation of input signals and the exponential decrease of postsynaptic potential. In fact the spatiotemporal summation has much more complex character.

Now if we suppose that transmission of an information from one to another neuron occurs without any distortion or is linear it will turn out that the transform operator of an input-output is

$$T = \frac{k}{\alpha} \left( \frac{d}{dt} + \beta \right)$$

where  $k$  -is some constant and presents a ratio factor between membrane potentials of serially connected two neurons or  $V_2(t) = kV_1(t)$ . This means that the intensity of generated pulses by the neuron as well as input pulses, should be proportional to both the membrane potential of this neuron and the rate of potential change.

Now let us consider an isolated neuron on the inputs of it are coming pulse sequences  $\lambda_1(t), \lambda_1(t), \dots, \lambda_i(t), \dots, \lambda_m(t)$ . According with neurophysiology the transmission function of a neuron does basically depend on the character and duration of input influences. These input sequences are causing a change of the synaptic conductivity or a synaptic weight change. Such changes are to be short-term changes. Then the transmission function of a neuron could be written as  $W[\lambda_1(t), \lambda_1(t), \dots, \lambda_i(t), \dots, \lambda_m(t)]$ . Now suppose we have an arbitrary network

consisting of above-mentioned neurons and having internal feedbacks. In general case each neuron is supposed to be having a part of inputs from outside environment relating to this network and another part of inputs coming from any other neurons of this network. Now for any component of this network  $\lambda_i(t)$  which can be an input as well as an output of any neuron of this network we can write

$$\frac{d\lambda_i(t)}{dt} = F_i[\lambda_1(t), \lambda_2(t), \dots, \lambda_1(t), \dots, \lambda_m(t)] \quad (3)$$

which means that an arbitrary chosen part of this network could be considered as the autonomous dynamic system [15]. Later we will consider some properties of such systems.

Here we should note that the weight changes in the static adaptive learning systems is assumed to be made by an instructor from outside after what these weights can be left unchanged as long as it is required. However in such a system as the dynamic cross-connected neuron network, as distinct of the static one, the weight coefficients are permanently changing even if input signals are absent. Then we can observe a dynamic equilibrium of the system. The weight changes depend on a local activity of groups of neurons. It means that such a system can autonomously rechange its structure without any outer interference. One may suggest that the instructor's action upon the weights of static systems is corresponding to the outer information flows coming to the living neural system. For instance, the oral, tactile and so on information channels could serve as an instructive inputs for the visual neural network.

Therefore, we can affirm that the variation of the neuron transmission into the learning or adapting neuron subnetwork occurs depending on a character and duration of the temporal input signals upon this subnetwork.

There are some works dealing with a pulse circulation in neuronlike networks [16,17]. According to them the time while a pulse track is existing into a circulation loop determines the circulation's further existence. In other words if the time of track existence surpasses some time interval we have the fixed changes into the loop during the time much longer than the track existence time, or there is a dynamic memorization of a pulse sequence for a while.

### 3. ACTIVITY OF THE DYNAMIC NEURON NETWORK AND ADAPTATION

There are known some investigations of an activity of neuron networks with internal feedbacks [18,19]. More distinguished results on this matter were shown by D. Smith and S. Davidson [20]. Though in this work as in many others the statistic qualitative analysis was used for the randomly connected neuron network activity to establish relations between a degree of activity and the network parameters. Because of complexity even statistic analysis of such a system with nonlinear elements connected transmission coefficients between neurons and the second limitation supposed absence of the input signals to this network. In other words there was investigated the isolated system with an arbitrary initial state from which the system has been started its motion. As a matter of fact it turned out that the system was always coming up to the same ultimate state independently on its initial state. However this final state was conditioned by only the parameters of the system.

There was shown also despite the neurons can have considerably varying thresholds there is always existing a stationary network activity having the definite oscillation cycle and the period of this cycle is widely varying depending on values of thresholds. In other words the weight changes could be reduced and considered as the adequate threshold changes. Hence we can conclude that for any connected neuronlike network with considerably varying weighted connections there is the precisely determined oscillation cycle or sequence of excitations for neuron subsets which does not depend on the network's initial state.

Therefore such systems are autonomous and their motion trajectory in the phase space and the ultimate equilibrium state when  $t \rightarrow \infty$  does depend on the parameters of the system. It is obvious the oscillation and cycling activity is to be the basis of a dynamic memory. Since an investigation of such a system interacting with an environment and undergoing structural changes happens to be very important problem. For such a case the activity levels of a dynamic network has to be changing as it was shown by W. Ross Ashby [21].

Let us consider the network shown in Fig.1 which is consisting of  $n$  neurons. The weighted signals from all the neurons are coming to the inputs of each neuron. The total input signal  $\alpha_i(t)$  for  $i$ -th neuron is corresponding to the above mentioned neuron's membrane potential  $V(t)$  and the output signal  $\beta_i(t)$  is respectively corresponding to the pulse intensity in an axon  $\lambda_i(t)$ . Then the transform operator  $\Omega$  according with equation (2) will be

$$\left(\frac{d}{dt} + \gamma\right), \text{ where } \gamma \text{ is constant.}$$

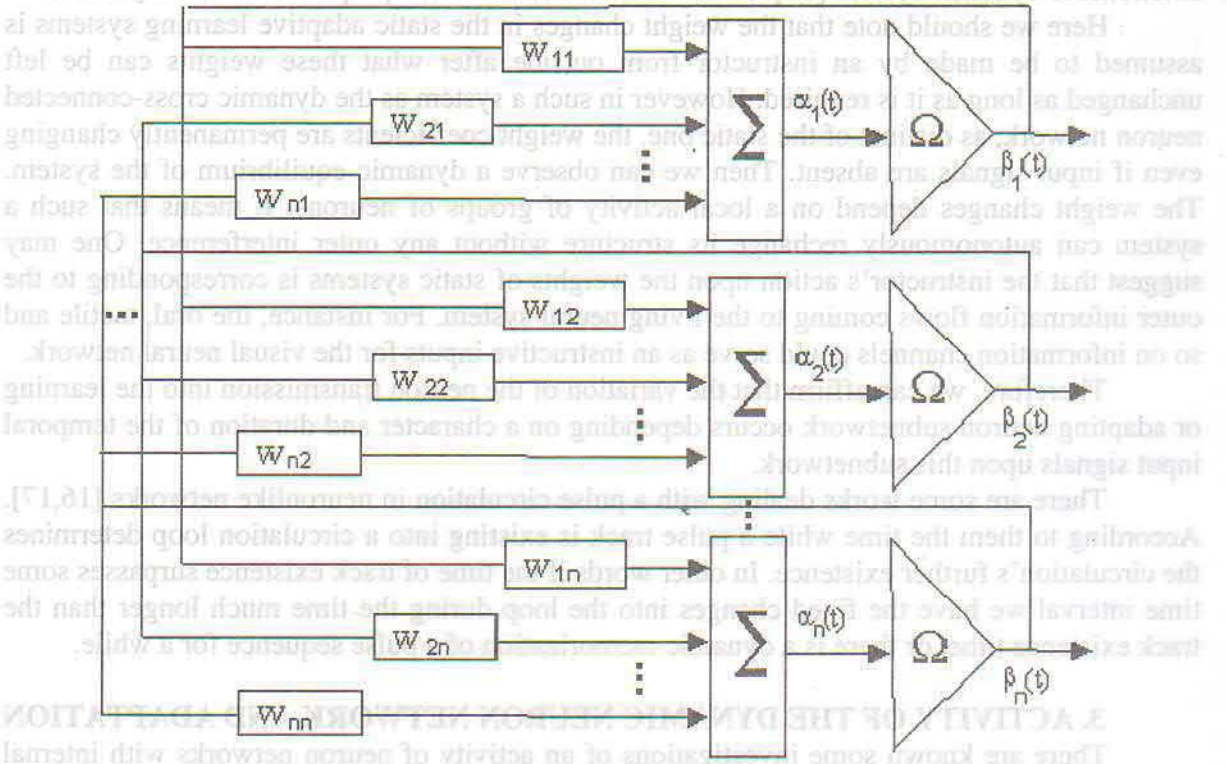


**Fig.1- THE ENTIRELY INTERCONNECTED DYNAMIC NETWORK**

Now we suggest that the synaptic coefficient  $w_{ij}$  between the  $i$ -th and  $j$ -th neurons are automatically changing as a certain given function of current values of the  $i$ -th and  $j$ -th neuron outputs. For instance this coefficient could get some positive increments to strengthen the correlation between neurons excited at the same time while these increments may be negative for the neurons, excitations of which are not coinciding. The system with such automatic weight changes presents the dynamic adaptive learning network. The state of the system is characterized by motion of the representative point into the  $n$ -dimensional space of inputs or the  $n^2$ -dimensional trajectory into the space of input components.

The operator  $\Omega$  is realized by a neuron according to equation (20), which expresses the relation between the change rate and value of the total input signal and the output signal and the output signal of neuron. It makes possible to consider such networks as autonomous dynamic systems. The network remains autonomous if the  $\Omega$  operator happens to be either the threshold function realizing the permanent output when the total input overpasses the threshold or some nondecreasing function of the total input.

Therefore in case of the network consisting of  $n$ -neurons and the total inputs are differentiated time functions  $\alpha_i(t)$ , where  $I = 1, 2, \dots, n$ , we have the canonical presentation of the system:

$$\frac{d\alpha_i(t)}{dt} = F_i(\alpha_1, \alpha_2, \dots, \alpha_n) \quad (4)$$

Such a presentation of the system where  $F_i$  is a singlevalued but necessarily continuous function makes it possible to eliminate some variables by introducing derivatives of these variables. The system (4) could be written in the finite differences if we have temporally quantized variables.

Investigation of an autonomous system stability showed that in case of the linear or nonlinear system increasing number of connections between elements leads to the instability of whole system. We should note that if  $F_i$  are nonlinear differentiated functions they have to be considered as linear in an area of closeness to the equilibrium points.

Let us now consider a neuron network with certain thresholds. It is easy to show that the introduction of thresholds in such a system is equal to consider the system with variables  $\alpha_1, \alpha_2, \dots, \alpha_m$ , which are piecewise constantly changing in time and  $\alpha_{m+1}(t), \alpha_{m+2}(t), \dots, \alpha_n(t)$  are continuously changing variables in time. Now we can prove the theorem: any system of  $(n - m)$  variables does remain autonomous on the permanent intervals of  $m$  variables [23]. Therefore the threshold elements involving addition or elimination of constant functions does not change autonomosness of the system. They only change the phase space and stability of the system. It is obvious that a unification of several autonomous systems forms a new autonomous system as well.

We should also note that the unification of autonomous subsystems in some cases may give a stable system while in other cases we can get unstable systems for one and the same input. It is also easy to show that a unified system has more wide choice of behavior than a system consisting of the same but isolated subsystems [21].

Let us consider the neuronlike network (see Fig.2) consisting of  $n$ -neurons and each of them is connected with all of the rest. Now suppose the weights of these connections  $w_{ij}$  can change continuously depending on the state of connected neurons at the definite moments of time. The changes of a total input signal  $\alpha_i$  happens by leaps and a transient of the system between these leaps will correspond to behavior of an autonomous system because all the weight changes are explicit functions of outputs  $\beta_i$  and hence of inputs  $\alpha_i$ . However there are  $n^2$  subspaces conditioned by  $n$  threshold elements and states of the system where the system can make such a leap is called the critical states of the system.

Let us now suggest that we have an outer input vector consisting of the piecewise constant time functions as components of  $X[k] = X\{x_1[k], x_2[k], \dots, x_n[k]\}$  where  $k = 1, 2, \dots, z$  is number of discrete intervals on which the components  $x_i$  remain constant. Now if such a vector is applied to the autonomous system then for such an interval exists its respective phase space or there is a certain correspondence between the input vector and state spaces. However this relation is not singlevalued because for one and the same phase space we can have the set of input vectors.

If the weights of connections are increasing between correlated neurons and decreasing between all the rest ones then we can observe a tendency of formation the quite definite strongly connected neuron subsets. As it was said earlier such dynamic system comes to its periodical or cyclic activity if there is no outer input signal and weight changes of feedbacks [20]. An addition of feedback weight changes leads to a motion of the system into the subspaces continuously and makes it possible to find a stable equilibrium state in one of these subspaces. In other words the system is adapting with its structural changes during the cycles.

To converge motion of the system to a stable equilibrium state there are necessary and sufficient conditions depending on the feedbacks changes [21]. Such a state corresponds to the definite stable subset of excited neurons and changing input variables. The representative point of the system is into respective phase subspace and is not overcoming stability borders of the system.

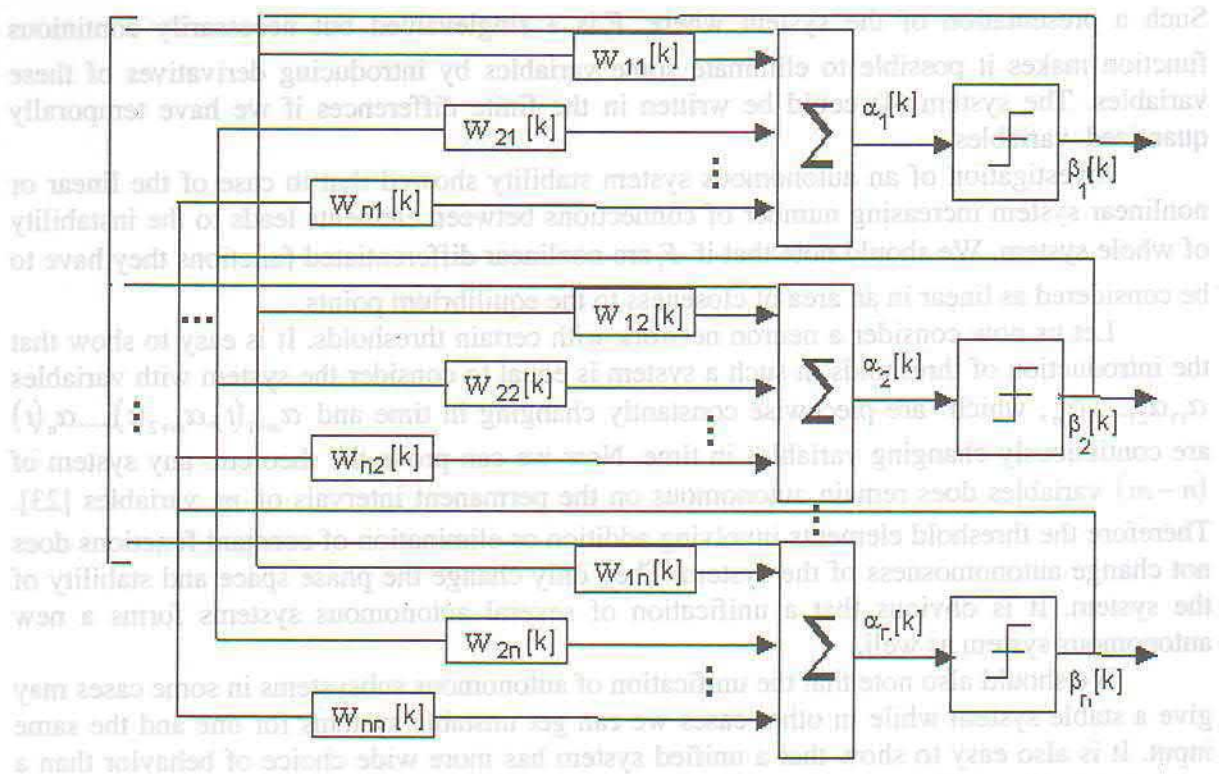


**Fig. 2- THE DYNAMIC NEURON ADAPTIVE NETWORK**

time independability of variables, which is equivalent to a separation of the system into the parts and substantially shortens a transient of the system.

As distinguished from the systems with fixed weight coefficients in the system with automatically changing weights the ultimate activity of the system depends on both the system's initial state or initial values of weights and the input vector  $X[k]$  which is constant at the interval  $T_x$ . Therefore if the state of network is  $S[k]$  and accordingly the weight vector of the system is  $W[k]$  where  $k$  is number of discrete time intervals then for  $k \rightarrow \infty$  we have

$$S[\infty] = \Psi\{X[\infty], T_x, W[0], S[0]\}$$

Now it is easy to show that if the time interval  $T_x$  is less than transient time of the neuron or weight element of the system and the same input  $X$  is periodically coming on the system with a period much longer than the transient of whole system then the system comes to such equilibrium subspace from where the same input  $X$  cannot lead out the system any more. It means that having a certain metrics and continuity of the phase space one and the same periodically repeated impingement will be shifting the representative point on less and less distance which corresponds to gradual decreasing of changes of weight vector components. Such a fact shows stability of an utmost equilibrium state of the system to the weak irregular input signals. This phenomenon was experimentally shown by F.Rosenblatt [1]. If the neurons have three or more inputs from the outputs of other ones not depending on a number of input components the system quickly "forgets" any irregular changes into the input regular sequence. However there are cases when such changes might be easily detected with eliminating the negative inner feedbacks between neurons.

Hence the dynamic connected network like cross-connected perceptron presents a selfadapting autonomous network which can find out the respective stable areas remote from critical points during its interaction with a periodically repeated input. For instance, for two various periodical sequences such a system can respectively find out two stable areas into the different phase subspaces. Overlapping between excited neurons for different sequences shows a closeness of external stimuli according to "the point of view" of this system.

Therefore the dynamic cross-connected system accumulates an external information by a periodically acting environment. Besides the system changes its inner structure or

weights because it has to be adapted to an environment. Such an adaptation could be rather considered as selfadaptation or selflearning ability of the system.

We should not that such an ability is entirely absent in the static systems without inner feedbacks which is to be the principal difference between the static and dynamic systems.

### 3. CHANGING ENVIRONMENT AND LEARNING OF THE DYNAMIC SYSTEM

Existence of the time factor into a real physical environment should be respectively reflected on behavior of the system perceiving some changes of this environment. From this point of view, first of all, there is arising the question of a temporal accordance of the environmental changes with the internal system transients as well as any kind of interactions between environmental objects and the system. Hence if the brain is considered as a dynamic system so it could perceive such environmental changes the rate of changes of which roughly saying is less than the rate of internal system transients. The time constants are usually conditioned by properties of neurons. We should note that under the rate of movement of a changing environment we will mean the reduced rate of movement to the sensor or receptive field which actually is a relative value. For instance, under the reduced rate of a moving airplane or car being observed by a man should be understood the airplane's or car's projection rate on the retina of an observer.

Perhaps the living organisms worked out their watching ability the principal sense of which (except widening of watching angle) is the ability of reduction an object's projection rate on the retina. The watching process is continuously occurring as a result of coming of controlling signals from the brain. It is too complex process, which presents the objective of the separate investigations [4].

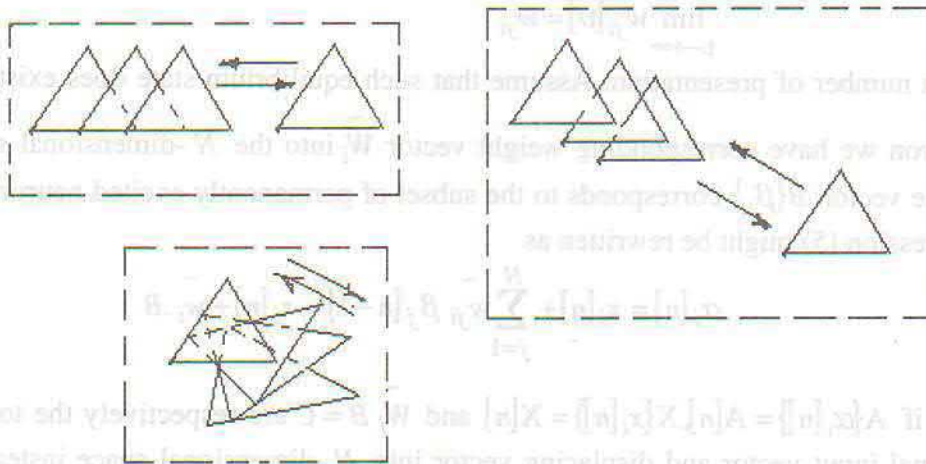


**Fig.3 – THE MOVING TRIANGLE ON THE INPUT FIELD**

Let us now consider a sequence of images reflecting a motion of one and the same image on the retina. For convenience suppose that the top margin of retina is prolongation of the bottom one. Therefore the part of image outgoing from the bottom margin has to be appearing at the margin of the retina and vice versa. Now if the time is quantified or  $t = 1, 2, \dots, n$ , then the motion of an image for  $n$ -intervals might be presented by an image sequence caused by successive shifting or turning of the one initial image.

A direction of shifting of the center of gravity of an image determines the motion direction and a linear angular distance between two subsequent images respectively determines a linear or angular rate of movement. The possible versions of shifting and turning motion of the triangle on the retina is shown in Fig.3.

Suppose the number of neurons of the connected network is equal to  $N$ . Then the sequence of images  $U_k^n \{u_k^1, u_k^2, \dots, u_k^n\}$  corresponds to the time vector-function

$$X^k[n] = X^k \{x_1^k[n], x_2^k[n], \dots, x_n^k[n]\}$$

where  $x_i^k[n]$  is the total input signal on the  $i$ -th neuron from the  $k$ -th fragment of the  $n$ -th time interval. Then in accordance with Fig.2 for the  $n$ -th moment of time we can write

$$\alpha_i[n] = X_i[n] + \sum_{j=1}^N w_{ji}[n] \beta_j[n-1] \quad (5)$$

Here we have to take into consideration that the neuron realizes a signal delay for one time interval and we have as well

$$\beta_i[n] = \begin{cases} 1, \alpha_i[n] \geq \theta \\ 0, \alpha_i[n] < \theta \end{cases} \quad (6)$$

However according to (5) the weight coefficient

$$w_{ji}[n] = w_{ji}[n-1] + \Delta w_{ji}[n] \quad (7)$$

where the increment  $\Delta w_{ji}[n]$  depends on both the  $\beta_j[n-1]$  and  $\beta_i[n]$ . Hence the sum of multiplications  $w_{ji}[n] \beta_j[n-1]$  is the nonlinear function of  $\beta_j$ .

Now suppose all the weights  $w_{ji}[n]$  are changing in accordance with a certain rule or algorithm [23]. As some investigations show we always can choose such weight change transients that during only one presentation of the  $U_k^n$  sequence the increments  $\Delta w_{ji}[n]$  could be such a small that we can consider the input as a constant for a given autonomous system. Then if there is a steady solution or respective steady equilibrium state for the system as a result of multiple presentation of the same sequence there should exist a limit of weight components:

$$\lim_{v \rightarrow \infty} w_{ji}[v] = \tilde{w}_{ji}$$

where  $v$ -is a number of presentation. Assume that such equilibrium state does exist and for the  $i$ -th neuron we have corresponding weight vector  $\tilde{W}_i$  into the  $N$ -dimensional space. In addition if the vector  $B\{\beta_j\}$  corresponds to the subset of permanently excited neuron outputs then the expression (5) might be rewritten as

$$\alpha_i[n] = x_i[n] + \sum_{j=1}^N \tilde{w}_{ji} \beta_j[n-1] = x_i[n] + \tilde{w}_i \cdot B \quad (8)$$

Now if  $A\{\alpha_i[n]\} = A[n]$ ,  $X\{x_i[n]\} = X[n]$  and  $\tilde{W}_i \cdot B = C$  are respectively the total input vector, external input vector and displacing vector into  $N$ -dimensional space instead of (8) we can have

$$A[n] = X[n] + C \quad (9)$$

As it was said earlier an adaptation of a system has to be characterized by permanence of some parameters during the presentation of on  $++\#$  and the same image sequence because of threshold elements. Therefore as a result of learning or adaptation of a given dynamic system to the  $U_k^n$  image sequence the system's motion into  $N$ -dimensional space of inputs will be cyclic when repeating the sequence. This cyclic activity will be conditioned by the displacing vector  $C$  (9), into the immediate closeness of which the cycle will be closed. However this cycle will not be outgoing from one  $N$ -dimensional subspace limited from above by the hypercube having the side equal to the threshold of neuron.

Hence a learning process of the dynamic network means a reduction of the image space by complex nonlinear transforms so that to place all the repeated learning image sequence into the proper subspace with a corresponding center of gravity.

The above mentioned says of principal difference between learning procedures into the static adaptive systems and the systems with inner dynamics. According to formed

systems we can have rigid nonlinear previous transforms of input information and later linear separation into classes. In recent work we showed how it is possible to find out minimum learning adaptive network for a given recognition problem by sorting out procedure of nonlinear transforms which have been done by the supervisor [22]. However in the dynamic system to a certain extent similar sorting out procedure of transform operators is automatically occurring without any supervisor's interference. It is obvious as well that the dynamic system has wide possibilities of choice of an input space transformation but then arises very important question-under what conditions could the system optimally move to the respective equilibrium steady state.

We should note that the constants of weight changes or weight algorithm parameters have a great deal with convergence of a learning process. While a maximum rate of image changes will be determined by the system's temporal characteristics or boundary of perception. Thus a learning process in dynamic systems is substantially connected with temporal factor and there are to be considered temporally correlated image sequences. So the dynamic system itself recognizes temporal sequences when it is gradually adapting to the periodically repeated "memorized" sequence. The duration of such a sequence depends as well on transit time of the system. Some random deviations or irregular input noises does not influence the main trend of a system to reach a proper steady state.

F. Rosenblatt has made an attempt to show how the dynamic neuronlike network can generalize environmental stimuli [1], which is also very important psychological phenomenon as it was said earlier. In other words this is the property of invariance concerning the transformation groups of inputs which is probably also connected with temporal correlation into the transformation groups. It follows from some experiments of simulation of the dynamic neuron networks [1, 23]. Even these experiments with poor and very simplified dynamic neuron adaptive networks to a certain extent showed the ability of generalization. The digital computers have been operating very long time (about several hours) to get a learning curve. The need of long simulation is conditioned by serial processing of a lot of weight changes.

As a rule the temporal input sequence presented to the dynamic network consisted of such couples as an image and its some one to one transform, another image and it's the same transform, the third one with the same transform and so on. These transforms is supposed to be shifting, turning or continuous deformation of one and the same image. There were used two kinds of images. The first group derived from randomly chosen digits on the retina and the second one supposed to use also random but congruent images. The ten experiments were carried out for each kind of images. The generalization ability was observable for all the cases but the congruent images had some advantage before random incongruent ones. It is important that here was appearing a steady excited neuron subset corresponding to rather a given transform or transition from any image to its transform than the overlapping of images at the retina as it usually happens in the static systems. Moreover as it was shown in other experiments of simulation the images of one class can have no overlapping with each another but may have considerable overlapping with representatives of other classes. In these cases the dynamic neuron network has learned proper recognition which is absolutely impossible for the static systems.

The ability of generalization, as it might be expected, should be much more expressed with simulation of large interconnected dynamic systems.

Not stopping here on consideration of the possible feedbacks to the inputs of system from the outputs of network elements, which perhaps could not change the main properties of the system, however it can add some new abilities. Probably just such connections could control the input information channel transmission to realize the phenomenon of "selective set" as we noted earlier.

And finally we can draw the conclusion that there still are large number of experiments to be done to clear up all the items of temporal interactions between the system and changing environment. It should be a principal stimulus to penetrate into the brain

mechanisms and it also would be a significant step towards creation of the systems with artificial intelligence having reasonable goal oriented behavior.

#### REFERENCES

- [1]. F.Rosenblatt, Principles of Neurodynamics. Washington, D.C.: Spartan Books, 1962.
- [2]. B.Widrow, Generalization and information Storage in Networks of ADALINE Neurons. In: Self-Organizing Systems, Yovits, Jacoby, Golstein (eds.), Washington, D.C.: Spartan Books, 1962.
- [3]. K.Steinbuch, Automat und Mensch. Berlin, Heidelberg, New York: Springer-Verlag, 1965.
- [4]. H.Milsum, Biological Control systems Analysis. New York, San Francisco, London: McGraw-Hill Book Company, 1966.
- [5]. K.S.Lashley, The Problem of Serial Order in Behavior. In: Cerebral Mechanisms in Behavior. New York: J.Wiley, 1951.
- [6]. I.T.Culbertson, Consciousness and Behavior. Brown, Dubuque, Iowa, 1950.
- [7]. D.O.Hebb, The organization of Behavior. New York: J.Wiley, 1949.
- [8]. A.Mallart, A.R.Martin, Analysis of Facilitation of Transmitter Release at the Neuromuscular Junction of the frog, Journ. Phys., London: p. 193, 1967.
- [9]. L.p.Kreisler and oth., Nekotorye Modely Circulyacionnich System Pamyati Problemy Neurokibernetiki, Rostov on Don, (in Russian), 1965.
- [10]. A.A.Kvitashvili, Cross-Connection Neuron Network Learning and Self-learning Ability. In: Progress of Cybernetics, London, New York, Paris, Gordon and Breach Sci. Publ.-s, 1971.
- [11]. H.A.Simon, Motivation and Emotional Controls of Cognition, Psychological Review, 74, N4, PP. 29-39, 1967.
- [12]. C.f.Stevens, Physiology of Synapses, Proc. IEEE, 56,6, 1968.
- [13]. D.Rall, Distinguishing Theoretical Synaptic Potentials Computed for Different Soma-Dendritic butions of Synaptic Input, Journ. Neurophysiology, V. 20, 1967.
- [14]. B.Katz, R.Miledi, The Release of Acetylcholine from Nerve Endings by Graded Electric Pulses, Proc. Roy. Sc., London, 167, 1967.
- [15]. I.M.Horowitz, Synthesis of Feedback Systems. New York, London: Academic Press, 1963.
- [16]. A.R.Cox, W.L.Smith, Superposition of Several Strictly Periodic Sequences of Events, Biometrika, 40,1,1953.
- [17]. P.Muller and oth., General Principles of Operations in Neuron Nets and their application for Acoustic Pattern Recognition, In: Biological Prototypes and synthetic Systems, New York, Plenum Press, 1962.
- [18]. C.H.Davidson, D.R.Smith., Oscillation Characteristics of Large Neural Networks, Proc. 15-th Annual Conf. Of Ass. Comput. Mach., Milwaukee, 1960.
- [19]. D.R.Smith, C.H.Davidson, Maintained Activity in Neural Nets, Journ. ACM, 1962.
- [20]. D.R.Smith, C.H.Davidson Activity, Levels and Various Kinds of Hesitation in Neural Nets, Biological Prototypes and Synthetic Systems, New York: Plenum Press, 1962.
- [21]. W.Ross Asbly, Design for a Brain, London: Chapman and Hall Ltd., 1960.
- [22]. A.A.Kvitashvili, A.Heuristic Approach to Design of the Minimum Adaptive Learning Network, Proc. 1-st International Joint Conf. On Pattern Recognition, Washington, D.C., 1973.
- [23]. A.A.Kvitashvili, Dynamicheskie Perceptrony. In: Perceptron Systema Raspoznavania Obrazov. Kiev: Naukova dumka (in Russian), PP. 199-242, 1975.



## Decision Making: Superiority Degree

Vladimer Zhukovin, Zurab Alimbarashvili  
*Institute of Cybernetics*

### Abstract

It is introduced the concept of Superiority Degree one competitive decision over another. On the basis of this concept the mathematics – theoretic structure is developed, which is part of pairs – comparisons branch in modern decision making theory. It will be useful for practice and interesting for scientific research.

**Key words:** Decision making, Pairs comparison, Superiority Degree, Incomplete information.

### 1. Introduction.

The famous American cybernetics F. George, analysing in his book: "The Foundations of Cybernetics" the stages of cybernetics' development in future, writes: That we may expect progress in all schools, but essentially in creation of the computer programs keeping decision making principles on the analogy of the same ones in humans .

The correspondent investigation on decision making has been conducting in the Institute of Cybernetics of Georgia from the very beginning of its foundation. As this paper would has been writing for the collection devoted to 40<sup>th</sup> jubilee of our Institute, let us turn back to history.

The year 1967, The Third All - Union Symposium on Cybernetics organised by the Institute of Cybernetics of Georgia - "Decision making in humans" was one of the three problems being discussed. The thesis's book has been published.

The year 1972, The Sixth All - Union Symposium on Cybernetics organised by the Institute of Cybernetics of Georgia - devoted clear to "Decision making in humans' all kind activities. Six volumes of thesis were published.(Russian).

The year 1979, The Soviet-American Symposium on the subject of Normative and Descriptive Models of decision making, Tbilisi, the Institute of Cybernetics of Georgia was one among the organisers. The book of accounts named similarly has been published(English and Russian).

The year 1985, Berlin, Symposium on System Analysis and Simulation. Many accounts devoted to the decision making systems (complex) opposite decision making procedures were presented. The plenary report has been suggested from the Institute of Cybernetics of Georgia.

There were other International Forums included always the decisions making sections.

Every 2-3 years during the 70-80<sup>th</sup> the Seminar on the Operation Research and System Analysis has been conducting by the laboratory of "Decision Making Theory", very popular among the decision making specialists as it was the sole in USSR wholly devoted to multicriteria decision making problems. It was conducted in Kutaisi or Batumi as usual and was named by ORSA-N.

Overlooking the numerous of our publications including foreign ones, note that the most resonance has been attended in the main to our investigations on Fuzzy Multicriteria Decision Making Problems. However we have at once interesting results in other branch of the Decision making theory. There are investigations associated with concept of the superiority degree of one decision over another. Such conception has been introduced at first in [1] in context of group (social) decisions of the modern Decision making theory which are very

wide and multiform. The pair-comparison branch of this theory is one of the most important being the basic for other ones. We have presented in this paper the theoretic-mathematical construction (the ABC of theory) of the degree superiority for the pair-comparison.

## 2. Preference Relations

In scientific research on decision making problems preference relations occupy the most part as research tools. They are defined and noted first by Fishborn [3]. It is no wonder because they allow to compare one decision with other so as to choose better of them in some concrete situation of decision making. Theory of preference relations is elaborated now already [2,7]. This theory, which is necessary for this article.

Let  $X$  is set of competitive decisions (alternatives), it is finite. Then  $E = X \times X$  is set of all ordered pairs of decisions. Mathematically preference relation is defined as  $R \subseteq E$ , i.e. it is also set and all set theory operations may be used on  $R$ . Any preference relation is binary relation. Inverse preference relation  $R^{-1}$  corresponds to any  $R$  in the following way: if pair  $(x, y) \in R$ , then pair  $(y, x) \in R^{-1}$ . Inverse preference relation  $R^{-1}$  has all those characteristics which corresponding preference relation  $R$  has. Any  $R$  is composed by two components: identity relation  $R^e = R \cap R^{-1}$ , strict preference relation  $R^s = R \setminus R^{-1}$  and, it is clear, that  $R = R^e \cup R^s$ , but  $R^e \cap R^s = \emptyset$ . If each of them is transitive, then  $R^e$  is equivalence relation and  $R^s$  is strict order. One of them may be empty. But if both preferences are non-empty, then  $R$  is non-strict preference relation or quasi-order when it is transitive. Any preference relation  $R$  may be connected or disconnected. It is connected when all decisions pairs from  $E$  are comparable by  $R$ , i.e.  $(x, y) \in R$  or  $(y, x) \in R^{-1}$  are fulfilled simultaneously. Some set  $X_{\Pi}(R) \subseteq X$  corresponds to preference relation  $R$ . It is its core, which contains maximal or effective decisions. We name it Pareto-set similarly with multicriteria decision making problems. It may be empty, but if  $R$  is transitive then always  $X_{\Pi}(R) \neq \emptyset$ . Let present also following results:

1. For two preference relations  $R_1$  and  $R_2$  if condition  $R_1^s \subseteq R_2^s$ , then  $X_{\Pi}(R_2) \subseteq X_{\Pi}(R_1)$ .

2. Preference relation  $R_1$  is coordinated with preference relation  $R_2$  if conditions  $R_1^s \subseteq R_2^s$  and  $R_1^e \subseteq R_2^e$  fulfill simultaneously. In this case  $X_{\Pi}(R_2) \subseteq X_{\Pi}(R_1)$ .

We shall present the other results and notions when they will be needed.

2. **Superiority Degree (SD).** Let present two classes of functions:

$$H = \{ \Psi(x, y) | \Psi(x, y) = -\Psi(y, x) \} \quad (1)$$

They are skew - symmetric functions.

$$T = \{ \varphi(x, y) | \varphi(x, z) + \varphi(z, y) = \varphi(x, y) \}, \quad (2)$$

this is a condition of transitivity.

Functions  $\Psi(x, y)$  and  $\varphi(x, y)$  are scalar and  $x, y, z$  are from  $X$  - set.

**Definition 1.** Let note any scalar function  $\varphi(x, y)$  defined on the set  $E$  as **superiority degree** of one competitive decision  $x \in X$  over other competitive decision  $y \in X$  if it is skew-symmetric, i.e.  $\varphi(x, y) \in H$ .

**Basic characteristics of SD:**

- $-\varphi^* \leq \varphi(x, y) \leq \varphi^*$ , where  $\varphi^* = \max_{(x, y) \in E} \varphi(x, y)$
- $\varphi(x, y) + \varphi(y, x) = 0$
- $\varphi(x, x) = 0$ . If  $\varphi(x, y) = 0$ , then  $x$  and  $y$  are identical.

$$d) \sum_{x \in X} \sum_{y \in X} \varphi(x, y) = 0, \quad (3)$$

$$\sum_{x \in X} \sum_{y \in X} \lambda(x) \lambda(y) \varphi(x, y) = 0,$$

where  $\lambda(x) \geq 0$  and  $\sum_{x \in X} \lambda(x) = 1$ .

The coefficients  $\lambda(x)$  are interpreted as "weights" or coefficients of significance of decisions.

In contrast to rations scale all results in this article, stated by using SD, will be given in differences scale. We make a remark because all known publications on these problems use rations scale.

**Definition 2.** Let note following scalar function  $F(x, y)$  defined on the set  $E$  as Integral (global) Superiority Degree (ISD):

$$F(x, y) = \sum_{z \in X} \lambda(z) [\varphi(x, z) - \varphi(y, z)], \quad (4)$$

where  $\varphi(x, y)$  is SD, i.e.  $\varphi(x, y) \in H$ .

In this case two decisions  $x$  and  $y$  are compared with one another non-directly but by means of third decision (reference point)  $z$ . Because  $\varphi(x, y)$  is difference estimation the difference in formula 4 don't contradict to common sense. **Basic characteristics of ISD:**

1.  $F(x, y) = -F(y, x)$ , i.e.  $F(x, y) \in H$  and it is superiority degree.
2. Hence it possesses all characteristics of SD (formulae 3),
3.  $F(x, y) \in T$  always independently of corresponding characteristic for  $\varphi(x, y)$ ,
4. But if  $\varphi(x, y) \in T$ , then  $F(x, y) = \varphi(x, y)$ .

The last two characteristics are most significant. ISD possesses many positive aspects, which will be presented in this article. But it possesses negative aspect too. Crossing out or addition decisions in  $X$  in general influence on comparison of decisions. We take into consideration this fact and try to neutralize it by control actions.

3. **Interconnection SD and ISD with preference relation  $R$ .** Let given any preference relation  $R$ . Now we can form several SD connected with this  $R$ .

This connection is based on following concept:

**Definition 3.** Scalar function  $\varphi(x, y) \in H$  is named as coordinated with preference relation  $R$  if the conditions:

$$\begin{aligned} (x, y) \in R^s &\rightarrow \varphi(x, y) > 0, \\ (x, y) \in R^e &\rightarrow \varphi(x, y) = 0 \end{aligned} \quad (5)$$

These conditions may be used for ISD too, i.e. for function  $F(x, y)$ .

On other hand, if initial information received by experts inquiry or by any other way is presented as SD, the corresponding preference relation may be formed always by following formula:

$$R(\ell) = \{(x, y) \in E \mid \varphi(x, y) > \ell\}, \quad (6)$$

where constant  $\ell \geq 0$ . This is a binary preference relation, which we name as  $\ell$ -level preference relation and analyze it later.

**Affirmation 1.** If some preference relation  $R$  is coordinated with  $R(0)$ ; given by formula 6, then it is coordinated with  $\varphi(x, y)$ , too (definition 3).

Proofs of affirmations we don't present in this article.  $R(0)$  is always connected because  $\varphi(x, y)$  is defined for all pair  $(x, y) \in E$ . Mean while  $R$  may be disconnected. Therefore in formula 5 arrows are directed only to one side.

4. **Utility Function (UF).** Initial information for decision making problem is obtained by comparison of decisions pairs. Comparison means may be different.

But results are  $R$  or  $\varphi(x, y)$ . Since some superiority degree is connected with any preference relation one can assume, that initial information is presented as scalar skew-symmetric function  $\varphi(x, y)$ , i.e. SD is presented. One of most difficult problem is the ordering of set  $X$  on the basis of the results of pairs comparisons. The ordering means to define utility function on  $X$ .

**Affirmation 2.** If  $\varphi(x, y) \in H \cap T$  (formulae 1 and 2) then it can be represented as the difference  $\varphi(x, y) = f(x) - f(y)$ , where  $f(x)$  is some potential function [4]. And following formula takes place:

$$f(x) = \sum_{y \in X} \lambda(y) \cdot \varphi(x, y) \quad (7)$$

In partial case we may assume, that  $\lambda(y) = \frac{1}{n}$ , where  $n$  is number of competitive decisions in  $X$ . Potential  $f(x)$  order set  $X$  and thus it is **utility function**. Many way are of conversion of pairs comparisons into UF. But they use intuition, experience, common sense and concrete of decision making situation. That is why we attach very importance this result (affirmation 2, formulae 7). This affirmation introduces in foregoing problem generality (universality), formal basis, completeness and it defines those conditions, which are necessary for problem solving. In practical work usually  $\varphi(x, y) \notin T$ , i.e. the transitive condition is infringed (formulae 2).

But then we can form (formulae 4) and use ISD with  $F(x, y)$ , we know, that  $F(x, y) \in H \cap T$  always fulfils. Hence using affirmation 2 we may write following formulae:

$$F(x, y) = q(x) - q(y) \quad (8)$$

where  $q(x) = \sum_{y \in X} \lambda(y) \cdot F(x, y)$

The last one is utility function defined on  $X$ . Thus we can order  $X$  always on the basis of data of pairs comparisons. Allowed transformations for  $f(x)$  and  $q(x)$  are linear: they don't infringe initial order given on  $X$ .

**Affirmation 3.** If SD  $\varphi(x, y) \in T$  (transitive condition), then  $q(x) = f(x)$ .

### 5. Multicriteria utility.

Multicriteria Decision Making Problems (MDMP) are the most wide-spread and very significant class of decision making problems in modern decision making theory. In this case each decision is estimated on the basis of several criteria. And then we have the set  $\Phi$  of scalar functions, defined on  $E$ :

$$\Phi = \{ \varphi_1(x, y), \dots, \varphi_j(x, y), \dots, \varphi_m(x, y) \}. \quad (9)$$

**Affirmation 4.** If  $\varphi_j(x, y) \in H$  for all  $j = \overline{1, m}$  then  $\varphi(x, y) \in H$ , where

$$\varphi(x, y) = \sum_{j=1}^m \lambda_j \varphi_j(x, y). \text{ If } \varphi_j(x, y) \in T \text{ for all } j = \overline{1, m}, \text{ then } \varphi(x, y) \in T.$$

Let  $\varphi(x, y) \in H \cap T$ , then on the basis of Affirmation 2 multicriteria utility function defined on  $X$  may be presented by following formulae:

$$L(x) = \sum_{y \in X} \lambda(y) \sum_{j=1}^m \lambda_j \varphi_j(x, y) \quad (10)$$

Let us prove that it is the linear convolution known in multicriteria decision making problems.

$$L(x) = \sum_{j=1}^m \lambda_j K_j(x) \quad (11)$$

where  $K_j(x) = \sum_{y \in X} \lambda_j(y) \varphi(x, y) = f_j(x)$ . This is a some effectiveness criterion of "win"

type, moreover,  $\lambda_j \geq 0, \sum_{j=1}^m \lambda_j = 1$ . Hence  $L(x)$  is Pareto-effective convolution [2]. Pareto-

set is formed by  $m$  effectiveness criteria  $K_j(x)$ .

6.  **$\ell$  - level preference relations.** They are connected with SD or ISD and is introduced by us (formulae 6). They are binary preference relations, i.e.  $R(\ell) \in E$  for all allowed value of  $\ell \geq 0$ . If  $\varphi(x, y) \in H$ , then reverse preference relation is:

$$R^{-1}(\ell) = \{(x, y) \in E | \varphi(x, y) \leq -\ell\}. \quad (12)$$

If  $\ell \neq 0$ , then  $R(\ell)$  is strict, disconnected and, in general, non-transitive, preference relation. If  $\ell = 0$ , then it is connected, non-strict and also non-transitive preference relation. Now we shall formulate transitivity conditions for  $R(\ell)$ .

**Affirmation 5.** If SD  $\varphi(x, y) \in T$  (formulae 2), then  $R(\ell)$  is transitive for all allowed  $\ell \geq 0$ . This means that for  $\ell \neq 0$  it is strict, disconnected order, but for  $\ell = 0$  it is linear quasi-order (or linear order).

On the basis of  $\varphi(x, y)$  may be introduced identity relation  $R^e = \{(x, y) \in E | \varphi(x, y) = 0\}$ . If  $\varphi(x, y) \in T$ , then it is equivalence relation. Let introduce non-strict  $\ell$ -level preference relation:

$$Q(\ell) = R^e \cup R(\ell), \quad \ell \neq 0 \quad (13)$$

For  $\varphi(x, y) \in T$   $Q(\ell)$  is non-strict  $\ell$ -level order. Let remark that for both cases it is disconnected.

**Affirmation 6.** If  $\ell_2 > \ell_1$ , then  $R(\ell_2) \subseteq R(\ell_1)$  and  $X_{\Pi}(\ell_1) \subseteq X_{\Pi}(\ell_2)$ .

For  $\varphi(x, y) \in T$  the Pareto-sets are non-empty. Hence we have formed the mathematical structure imbedding one into other non-empty Pareto-sets. This is conveniently for elaboration of dialogue procedures on computer ( $\ell$  is control parameter).

$$X_{\Pi}(0) \subseteq X_{\Pi}(\ell_1) \subseteq X_{\Pi}(\ell_2) \subseteq X_{\Pi}(\ell^*) = X, \quad (14)$$

where  $0 < \ell_1 < \ell_2 < \ell^*$ . All  $\ell > \ell^*$  haven't meaning.

### 8. Similarity with fuzzy preference relations.

**Affirmation 7.**  $R(\ell_1) \cap R(\ell_2) = R(\ell)$ , where  $\ell = \max\{\ell_1, \ell_2\}$ , and  $R(\ell_1) \cup R(\ell_2) = R(\ell)$ , where  $\ell = \min\{\ell_1, \ell_2\}$ . Thus all  $\ell$ -level preference relations, formed on the basis of the same SD  $\varphi(x, y)$ , are closed under operations of join and intersection.

Let introduce yet one class of functions:

$$S = \{\varphi(x, y) | \varphi(x, y) > \max\{\varphi(x, z), \varphi(z, y)\}\}. \quad (15)$$

**Affirmation 8.** If  $\varphi(x, y) \in S$ , then  $R(\ell)$  is transitive for all allowed values of level  $\ell$ .

These facts are similar on some results from fuzzy sets theory. In future we want to determine more profound connection of superiority degree with decision making fuzzy problems.

### 9. Example: group decisions.

Initial data for group (social) decisions are described as  $\langle X, N, R \rangle$ , where  $X$  is finite set of competitive decisions (alternatives);  $N$  is number of experts in group (their indices are

$v = 1 + N$ );  $R$  is Vectors Preference Relation (VPR) obtained by experts inquiry and defined on set  $X$ ;  $R$  consists of  $N$  components:

$$R = \{R^{(1)}, R^{(2)}, \dots, R^{(v)}, \dots, R^{(N)}\}, \quad (16)$$

where  $R^{(v)} \subseteq E$  is ordinary (usual) scalar binary preference relation, which map preference structure of expert with index  $v$ . But  $E = X \times X$  is set of all ordered pairs of decisions. Group decisions itself is defined as result of some procedure over  $R$ , that is:

$$G = \Pi(R), \text{ and also } G \subseteq E. \quad (17)$$

Symbol  $\Pi$  haven't mathematical meaning, it's procedure notation. Let us introduce next function:

$$\delta_{ij}^{(v)} = \begin{cases} 1, & \text{if } (x_i, x_j) \in R^{(v)}, \\ \frac{1}{2}, & \text{if } (x_i, x_j) \in R^{(v)} \ \& \ (x_j, x_i) \in R^{(v)}, \\ 0, & \text{if } (x_j, x_i) \in R^{(v)}. \end{cases} \quad (18)$$

This function is defined on decisions pairs, i.e.  $(x_i, x_j) \in E$  and other, where  $x_i \in X$  and  $x_j \in X$ .

It is coordinated with preference relation  $R^{(v)}$  in view of specific sense. We don't require transitivity of preference relations  $R^{(v)}$ ,  $v = \overline{1, N}$ . For describing data, received fully from experts group, let us determine next function also defined on the decision pairs:

$$n_{ij} = \sum_{v=1}^N \delta_{ij}^{(v)} \quad (19)$$

Now two known (traditional) group decisions can be determined in view of context of our article.

**Voting by majority:**

$$G_V^s = \{(x_i, x_j) \in E \mid n_{ij} > n_{ji}\}. \quad (20)$$

This is a strict preference relation, it isn't transitive in general case. Identities relation corresponds to it and is also non-transitive:

$$G_V^e = \{(x_i, x_j) \in E \mid n_{ij} = n_{ji}\}. \quad (21)$$

These two preference relation form voting by majority:

$$G_V = G_V^s \cup G_V^e, \quad (22)$$

if they will be joined (together).

**K-procedure (правило Копленда):**

let us introduce following  $K$ -index for  $x_i \in X$

$$\varphi_i = \sum_{j=1}^m (n_{ij} - n_{ji}), \quad (23)$$

where  $m$  is number of decisions in  $X$ . Using it we can write following group decision  $K$ -procedure:

$$G_k = \{(x_i, x_j) \mid \varphi_i \geq \varphi_j\}. \quad (24)$$

This is a linear order, it is transitive,  $K$ -procedure is more progressive than voting by majority, because each decision is compared with all other decisions from set  $X$ . But it is true that it is not ideal.

Let introduce following number function, defined on pairs of decisions:

$$Z_{ij} = n_{ij} - n_{ji} \quad (25)$$

It is obvious that it is SD, because  $Z_{ij} = -Z_{ji}$ . Let introduce ISD too:

$$F_{ij} = \sum_{s=1}^m (Z_{is} - Z_{js}) \quad (26)$$

It is easy to prove that following condition takes place:

$$F_{ij} = V_i - V_j, \quad (27)$$

where  $V_i = V(x_i)$  is number potential function, defined on the set  $X$  and given on difference scale. It is (formulae 8 and 13):

$$V_i = \sum_{s=1}^m Z_{is} = \varphi_i, \quad K\text{-index} \quad (28)$$

Let determinate now  $\ell$ -level preference relation:

$$G(\ell) = \{(x_i, x_j) \in E \mid F_{ij} \geq \ell\}, \quad (29)$$

where  $\ell \geq 0$ . This is a disconnected, strict order when  $\ell \neq 0$  and it is a linear order when  $\ell = 0$ . Level  $\ell$  of preference relation  $G(\ell)$  can be selected on the bases of practical considerations as in work [3] for example.

The interesting results can be formulated at once:

1.  $G(0)$  is  $K$ -procedure.
2. Condition  $Z_{ij} = Z_{is} + Z_{sj}$  is sufficient condition for transitivity of Voting by Majority.
3. When this condition takes place then  $K$ -procedure and Voting by Majority are equivalent [6].

As soon as  $\ell$ -level group preference relation  $G(\ell)$  is formed one can define  $\ell$ -level group decision - this is a core of  $G(\ell)$ , i.e. Pareto-set, which will be noted by  $X_{\Pi}(\ell)$ . Two interesting results can be proved connected with Pareto-set:

4.  $X_{\Pi}(\ell) \neq \emptyset$  for any value of level  $\ell$ .
5. If two  $\ell$ -level group preference relations are with levels  $\ell_1$  and  $\ell_2$  correspondingly and  $\ell_1 > \ell_2$  then condition  $X_{\Pi}(\ell_2) \subseteq X_{\Pi}(\ell_1)$  (affirmation 6).

Thus we can form the structure of imbedding one to an other non-empty Pareto-sets.

Let remark only that the foregoing problems presented in this article deal with complete initial information.

Now we present one variant of using of SD and ISD in decision making problems with incomplete initial information.

**10. Incomplete information: disconnected preference relation.** In practical work the situations with incomplete information arise very often when some part of decisions pairs remain incomparable. The reasons of this fact may be very different: subjective as well as objective one. Disconnected preference relations correspond to this situation in mathematics.

Let disconnected preference relation  $NC \in E$  is given on the set  $X$ .

Let take also any decision  $x \in X$ . With respect to it the set  $X$  will be separated in two parts (two subsets):  $X_1(x)$  and  $X_2(x)$ . First subset contains decisions, comparable with  $x$  and second subset contains decisions, in comparable with  $x$ . For any  $x \in X$  following conditions holds:

$$\begin{aligned} X_1(x) \cup X_2(x) &= X, \\ X_1(x) \cap X_2(x) &= \emptyset, \\ x &\in X_1(x). \end{aligned} \quad (30)$$

Superiority degree may be introduced also in this case.

**Definition 4.**

- a) Let name as Upper Superiority Degree (USD) following value:

$$u(x, y) = \begin{cases} \varphi(x, y), & \text{if } y \text{ is comparable with } x, \\ \varphi^*, & \text{if } y \text{ is incomparable with } x, \end{cases}$$

b) Let name as Lower Superiority Degree (LSD) following value:

$$d(x, y) = \begin{cases} \varphi(x, y), & \text{if } y \text{ is comparable with } x, \\ -\varphi^* & , \text{if } y \text{ is incomparable with } x, \end{cases}$$

where  $\varphi(x, y) \in H$  on the set  $X_1(x)$ ,  $\varphi^*$  is maximal value of SD  $\varphi(x, y)$  - formulae (30, 1) are used.

We shall explain this definition. If decisions  $x$  and  $y$  are comparable, then value  $\varphi(x, y)$  for this pair belongs to interval  $[-\varphi^*, \varphi^*]$ . For incomparable decisions pairs we take the extreme values of this interval: very successful and very unsuccessful one.

**Characteristic of USD and LSD:**

1.  $u(x, y) > d(x, y)$  always.
2.  $u(x, y) = -d(y, x)$  and  $d(y, x) = -u(x, y)$ ,
3.  $u(x, x) = d(x, x) = 0$ ,
4.  $u(x, y) > 0$  and  $d(x, y) < 0$  always.

Now let introduce following utility functions:

$$f_d(x) = \sum_{y \in X} \lambda(y) \cdot d(x, y)$$

$$f_u(x) = \sum_{y \in X} \lambda(y) \cdot u(x, y)$$

where  $\varphi(x, y) \in T$  on the set  $X_1(x)$  - formulae (30,2) and affirmation 2 are used.

Thus now the interval estimation is given for each  $x \in X$  on the basis of incomplete initial information (disconnected preference relation NS):

$$\Delta(x) = [f_d(x), f_u(x)]. \tag{34}$$

We remark only that  $f_u(x) \geq f_d(x)$ , and equality correspond to the point estimation of  $x$ .

Now we must order the set  $X$  on the basis of interval estimations. Such problem is studied in detail by us in publications [5,8] and we don't present them here: only a little information. The disconnected, strict order with corresponding non-empty Pareto-set is formed on  $X$ . When new additional information is received the previous intervals are transformed into the intervals, which have diminished lengths. We don't take into consideration the case of false information. When we receive complete information then the lengths of all intervals  $\Delta(x)$  will be equal to 0, and we shall deal with point estimations of  $x \in X$  (affirmation 2).

Let correct the formulae 33 and 34:

$$f_d(x) = \sum_{y \in X_1(x)} \lambda(y) \cdot \varphi(x, y) - \sum_{y \in X_2(x)} \lambda(y) \cdot \varphi^* = \varphi(x) - \Lambda(x) \cdot \varphi^*, \tag{35}$$

where  $\varphi(x)$  is some constant value corresponding received information. It is transformed only when additional information is obtained. And  $\Lambda(x) \geq 0$  is characteristic of missing information. It tends to 0, when additional information is obtained and is equal to 0 under complete information.

Similarly we may write and discuss:

$$f_u(x) = \varphi(x) + \Lambda(x) \cdot \varphi^*. \tag{36}$$

Criteria for the estimation of missing information size can be introduced, which will be useful possibly for practical work, by this way. We present three variants:

1.  $\Lambda_{mean} = \sum_{x \in X} \lambda(x) \cdot \Lambda(x)$ ,
2.  $\Lambda_{max} = \max_{x \in X} \Lambda(x)$
3.  $\Lambda_{sum} = \sum_{x \in Q} \lambda(x)$ , where  $Q = \bigcup_{x \in X} X_2(x)$ .

They are equal to 0 under complete information. Let present yet some more several results.

**Affirmation 9.**

a) If the transitivity condition  $d(x, y) = d(x, s) + d(s, x)$ , i.e.  $d(x, y) \in T$ , for all allowed  $x, y, s$ , then

$$d(x, y) = f_d(x) - f_u(y). \quad (37)$$

b) If  $u(x, y) \in T$ , then

$$u(x, y) = f_u(x) - f_d(y). \quad (38)$$

**Definition 5.**

a) Let note as Integral (global) Upper Superiority Degree (IUSD) following value:

$$U(x, y) = \sum_{r \in X} \lambda(r) \cdot [u(x, r) - d(y, r)]. \quad (39)$$

b) Let note as Integral (global) Lower Superiority Degree (ILSD) following value:

$$D(x, y) = \sum_{r \in X} \lambda(r) \cdot [d(x, r) - u(y, r)]. \quad (40)$$

**Affirmation 10.** Following results always take place.

$$\begin{aligned} U(x, y) &= f_u(x) - f_d(y), \\ D(x, y) &= f_d(x) - f_u(y). \end{aligned} \quad (41)$$

Let present now the characteristic of IUSD and ILSD:

1.  $U(x, y) > D(x, y)$ .
2.  $U(x, y) = -D(y, x)$  and  $D(x, y) = -U(x, y)$ .
3.  $D(x, y) = d(x, y)$  if transitivity condition, i.e.  $d(x, y) \in T$  for all  $x, y, s$ ,  
 $U(x, y) = u(x, y)$ , if  $u(x, y) \in T$  for all  $x, y, s$ .
4.  $U(x, r) + U(r, y) = U(x, y) + U(r, r)$ ,  
 $D(x, r) + D(r, y) = D(x, y) + D(r, r)$ .
5. In general  $U(r, r) \neq 0$  and  $D(r, r) \neq 0$ .

$D(r, r) = -U(r, r)$  and  $D(r, r) \leq 0$ . If all decisions pairs are comparable, then  $U(r, r) = D(r, r) = 0$ . It is variant with complete information.

**11. Again about group decisions: incomplete information.** The group consists of  $N$  experts. Let pick out one decisions pair  $(x, y) \in E$ . Vector Preference Relation (VPR)  $R = \{R^{(1)}, \dots, R^{(i)}, \dots, R^{(N)}\}$  corresponds to each pair. Analysis of it for picked out pair will give following result:

1.  $a(x, y)$  experts have voted for  $x$ .
2.  $b(x, y)$  experts have voted for  $y$ .
3.  $p(x, y)$  expert couldn't compare  $x$  to  $y$ .

All these values are the functions determined on  $E$  on the basis of  $R$ , and their sum is  $N$  for one pair. Now let form following values:

$$\begin{aligned} d(x, y) &= (a(x, y) - b(x, y)) - p(x, y), \\ u(x, y) &= (a(x, y) - b(x, y)) + p(x, y). \end{aligned} \quad (42)$$

First of them is LSD and second is USD. This fact can be proved. Using the affirmation 10 we have:

$$\begin{aligned} f_d(x) &= \sum_{y \in X} \lambda(y) \cdot \varphi(x, y) + \sum_{y \in X} \lambda(y) \cdot p(x, y), \\ f_u(x) &= \sum_{y \in X} \lambda(y) \cdot \varphi(x, y) - \sum_{y \in X} \lambda(y) \cdot p(x, y), \end{aligned} \quad (43)$$

where  $\varphi(x, y) = a(x, y) - b(x, y)$  and  $\varphi(x, y) \in H$ .

Thus the interval  $\Delta(x) = [f_d(x), fu(x)]$  corresponds to any  $x \in X$  and then we shall order the set  $X$  using these interval estimations [2,5]. Let remark also that  $\varphi(x, y) = \frac{1}{2} [d(x, y) + u(x, y)]$ .

**12. Conclusion.** Some very simple ideas and concepts permit us to develop and to present you the mathematics -theoretic structure (the basis of theory ) for superiority degree and connected with its problems. This structure is part of pairs comparison branch in modern decision making theory. It will be useful for practical work and interesting for scientific research. Many unsolved problems are in this field yet.

### References

- [1]. В.Е. Жуковин. К проблеме группового выбора.- Сообщения АН ГССР, Тбилиси, 99, №2, 1980.
- [2]. В.Е. Жуковин. Многокритериальные модели принятия решений с неопределенностью, Тбилиси: Мецниереба, 1983, с.104.
- [3]. Фимберн П. Теория полезности для принятия решений - М., Наука, 1978.
- [4]. Жуковин В.Е., Черняев С.П., Шахнов И.Ф. Потенциальные нечеткие отношения и их использование в задачах упорядочения объектов. - Известия АН СССР, Техническая кибернетика. - М., 1988, с.с.182-189.
- [5]. Бокучава И.Т., Жуковин В.Е., Топчишвили А.Л. Интервальные оценки для многокритериальных задач принятия решений с неполной информацией.- Сборник трудов ИСУ АН Грузии, Тбилиси, 1999, с.с.20-22.
- [6]. В.Е. Жуковин. Об эквивалентности некоторых групповых решений.- Сообщения АН ГССР, Тбилиси, 85, №1, 1977.
- [7]. Миркин Б.Г. Проблема группового выбора. - М., Наука, 1974.
- [8]. Seminar on decision making: theory and practice (V. Zhukovin ed.), -Tbilisi, Institute of Cybernetics of Georgian Academy of Sciences, IC preprint №05-2000.
- [9]. Подиновский В.В. Методы многокритериальной оптимизации -М., 1971.
- [10]. Ларичев О.И. Наука и искусство принятия решений - М., Наука, 1961.
- [11]. Нормативные и дескриптивные модели принятия решений. - М., Наука, 1981.



## **Decision Making on the Example of Informational System Projecting**

**Irina Bokuchava, Nanuly Chkhikvadze, Zurab Alimbarashvili**

*Institute of Cybernetics*

### **Abstract**

Local informational nets are considered, which may be represented as tree-like graphs. The procedure is worked out for such nets which permits us to solve the problem of minimal cost net search as a multicriteria problem of the effective decision choice. Here is given the algorithm, which finds Pareto set from the given set. Pareto sets contains all those alternatives each of what is a graph of minimal value. The expert system has been developed on the basis of T. Saaty's hierarchy analytic method. The system puts according to each element of Pareto set some meaning of the weight or probability.

**Key words:** Net, Process of choosing, Tree-like graph, Alternative, Pareto, Vector criterion, Algorithm.

### **1. Pareto set formation algorithm for minimal cost network**

#### **1.1. Introduction**

Under the investigation of problems for the formation of local informational networks with definite designation, such as, for seismic stations networks of observation, networks for the meteorological services, or networks of processing the information thrown down from the flying apparatus, it's become evident, that all of them have similar structures and can be described as oriented non cycled graph without of surplus arcs, i.e. tree-type graph with one root.

Such circumstance has allowed us to estimate the number of possible networks of the given type with the given number  $n$  of communication information sources and with one data processing centre of information, also to construct an algorithm of choosing of the minimal cost network.

This article describes the process of network's construction for  $n$ -independent information sources with the united centre of its processing. The process is presented as a process of ordering the set of possible networks and choicing from them an optimal the (one) optimal in some way by many criterions.

#### **1.2. Multicriteria problem of choosing of minimal cost network**

The process of choosing of information transmission minimal cost network, according to the vector criterion, is given as the union of this criterion, net estimation and models of net structure, sources and channels. In the model the transmission net of information is discussed as communication network, where among  $(n+1)$  nodes  $n$  ones are information sources and one node is common data processing center (PC).

The net structure is presented by tree-like graph, i.e. by the connective, plane graph without loop, which has one rooted and  $n$  - independent node [1-3].

Each node of such graph may have from 0 to  $n$  input ribs and only one output rib. The rooted node PC has only input ribs. Every node is called as predecessor for the given node if it is situated before this node on any way to the PC.

The line drawn between some two nodes of net presents the communication channels.

Each channel has some length  $\ell$  and minimally necessary capacity  $p$ .

The length  $\ell(ab)$  of channel between  $a$  and  $b$  nodes is defined as the distance between  $a$  and  $b$  nodes. The node  $a$  is called initial,  $b$  - final. Each separate channel capacity  $p$  depends on concrete net structure and it is determined by the number of predecessor nodes for initial node  $a$  of channel.

A quality of any set  $s$  is characterized by the vector criterion  $K(s) = K\{k_1, \dots, k_m\}$  and is estimated by some scalar function  $C(s) = C(k_1, \dots, k_m)$  of this criterion. This function conditionally is called cost function of net [4,5].

The net given in such way gives the possibility to from the problem of choosing as follows.

Assume, that we have  $(n+1)$  point with  $(x_0 y_0, \dots, x_n y_n)$  coordinates on the plane. Let us consider the set  $S = S(s_1, \dots, s_N)$ ,  $N = n(n+1)/2$  of all tree-like graphs with  $n$  nodes in the points and one rooted nodes in  $(x_0 y_0)$  point. This set is finite and is the set  $S$  of alternatives for choosing of graph that is optimal in certain sense.

Every  $\ell(ab)$  ribs of  $s_i \in S$  graphs has some length  $\ell$  and weight  $p$ . The weight  $p$  depends upon the structure of element  $s_i \in S$  in which the rib is located and is proportional  $p$  to the number of predecessor nodes for node  $a$ . Every element  $s_i \in S$  characterized by two dimensional vectorial criterion  $K(s_i) = \{K_1(s_i), K_2(s_i)\}$   $K_1(s_i)$  is the summation of lengths of all ribs of elements  $s_i$  and is equal to  $K_1(s_i) = \sum_{(ab)} \ell(ab) = L_i$ . That corresponds to

physical expenditures while net efficiency is characterized by  $K_2(s_i) = \sum_{(ab)} p(ab) \ell(ab) = P_i$ .

Thus for the data transformation network which is represented by graph  $s_i$ ,  $L$  is a common length and  $P$  - is a resulting capacity of net for the case, when generation of information occurs in all nodes according to Poisson distribution law with mean intensity  $\bar{\nu} = 1$ .

Let define on set  $s$  cost function of alternative  $s_i$  as follows;

$$C(s_i; \hat{\alpha}) = c(L_i + \hat{\alpha}P_i) = c \left( \sum_{(ab)} \ell(ab) + \hat{\alpha} \sum_{(ab)} \ell(ab)p(ab) \right) = c \sum_{(ab)} \ell(ab)(1 + \hat{\alpha}p(ab)).$$

Here  $c$  is a cost of the rib, for which  $\ell = 1$  and  $p=0$ , the  $\hat{\alpha}$  defines cost increasing of the rib according to increasing of its weight,  $(ab)$  is a pear of any different nodes of graph, when are different from each others.

Therefore, the problem of choosing of minimal cost net is reduced to problem of finding such set  $S^* \subseteq S$ , for every element  $s_i$  of which cost function  $C(s_i, \hat{\alpha})$  takes minimal value at the certain value of  $\hat{\alpha}$ .

The relation of preference is used to determine the  $S^*$  set. In our case the problem is as follows: to every  $s_i \in S$  is put according the point of quality index space with coordinates

$$K_1(s_i) = L_i, \quad K_2(s_i) = P_i$$

Then preference relation on the set  $S$  is defined:

$$R_k = \{(s_i, s_j) | K_1(s_i) \leq K_1(s_j) \& K_2(s_i) \leq K_2(s_j)\},$$

$$R_c(\alpha) = \{(s_i, s_j) | C(s_i, \alpha) \leq C(s_j, \alpha)\}, \quad \alpha \in [0, 1].$$

$R_k$  relation defines the quasi-order on  $S$  set,  $R_c(\hat{\alpha})$  - defines linear order. Each relation creates its Pareto-set (nucleus of relation). Let us denote them correspondingly as  $S_{\Pi}(R_k)$  and  $S_{\Pi}(R_c(\hat{\alpha}))$ .

These sets are not empty sets for any allowable  $\hat{\alpha}$ . Besides  $C(\hat{\alpha}) = \min C(s_i, \hat{\alpha})$  and this minimum is achieved on any  $s_i \in S^*$  alternative, where  $S^* \subseteq S$ . Then  $S_{\Pi}(R_k) = \{S^*\}$ .

If  $R_k$  is coordinated with  $R_c(\hat{\alpha})$  for any allowable  $\hat{\alpha}$ , then  $S_{\Pi}(R_k) \subseteq S_{\Pi}(R_c(\hat{\alpha}))$  it gives possibility to find the alternative, being optimal by  $R_c(\hat{\alpha})$ -sense, only in  $S_{\Pi}(R_c(\hat{\alpha}))$  set.

The algorithm given below gives possibility to find  $S_{\Pi}(R_c(\hat{\alpha}))$ .

### 1.3. Pareto set formation (construction) procedure

The formation procedure of searching  $S^*$  set of efficiency decisions, minimizing the cost function  $C(s_i, \hat{\alpha})$ , for all  $\alpha \in [0,1]$  can be shown in the following way:

Suppose the coordinates of (PC) and information source (IS) are given.

On the first step the set of graph's all ribs ordered by length must be formed:  $L^* = L \setminus \{\ell_i(ab)\} \quad i = 1, \dots, n(n+1)/2$ , where  $(ab)$  is any pear of different nodes.

On the 2nd step the graph of minimal length  $s_{min} \in S$  must be singled out from the set  $S$ . For this purpose from  $L^*$  will be chosen the first shortest  $n$  ribs so that they will have to create the graph without cycles. This graph will be the found graph  $s_{min}$ . For this graph, for alternative, the values of criteria  $K_1$  and  $K_2$  are denoted correspondingly by  $L_{min}$  and  $P_{min}$ .

In the 3rd step the algorithm singles out the graph  $s_{max} \in S$ , in which every node is connected with root, i. e. the graph is created by ribs of type  $\ell(0i), i \in [1, n]$ . For this alternative the values of criteria  $K_1$  and  $K_2$  are as follows:

$$K_1(s_{max}) = \sum_{i=1}^n \ell(0i) = L_{max}; \quad K_2(s_{max}) = 0.$$

The 2nd criterion is equal to 0, because all nodes in this graph (except root) are initial. In other words all nodes (except root) have no predecessor.

The cost of alternative  $s_{min}$  is equal to  $C(s_{min}; \hat{\alpha}) = c(L_{min} + \hat{\alpha}P_{min})$ , while the cost of alternative  $s_{max}$  -  $C(s_{max}; \hat{\alpha}) = cL_{max}$ .

So, any graph  $s_i \in S^*$ , for which  $L_i \geq L_{max}$  will not get into the set of alternatives  $S^*$ , because  $C(s_i; \hat{\alpha}) = c(L_i + \hat{\alpha}P_i) > C(s_{max}; \hat{\alpha}) = cL_{max}$ , for any  $\hat{\alpha}$ .

If the  $s_{min}$  and  $s_{max}$  are the same elements from  $S$ , then the  $s_{min}$  is the desired graph, to which the minimal cost net is corresponding for any  $\hat{\alpha} \in [0,1]$ .

If this condition is fulfilled, the problem will be considered as solved. If not - the next step of algorithm will be realized.

In this step the algorithm will involve the shortest rib in the graph  $s_{min}$  from the set  $\bar{L}^* = L^* \setminus \{\ell_1, \dots, \ell_n\}$ . By this operation the graph with cycle will be obtained as it will contain  $(n+1)$  nodes.

Then all ribs from the cycle, beginning from the longest one, will be removed one by one. So the series of graphs without cycles and with increasing  $L$  will be obtained, where the first one will be the graph  $s_{min}$ . On the graphs of this series the relation of the preference is checked and unrelated graphs are selected. These graphs belong to the found set  $S^*$  of alternatives.

The same procedure is repeated by the next rib of set  $\bar{L}^*$  for every graph which have already got into the set  $S^*$ . These process continues until the graph  $s_{max}$  will be obtained. It will be the last element of alternatives set, as the summary lengthy  $L$  of all next graphs

obtained by this algorithm will be more than  $L > L_{max}$ . If we take into account that  $p > 0$ , for them it is obvious that their cost will be more than  $C(s_{max})$ .

The set  $S^*$  obtained by this method contains all that and only that  $s_i$  alternatives, each of which is the graph of minimal cost for certain value of  $\alpha$  from  $[0,1]$  interval, and  $S^* \equiv S_{\Pi}(R_c(\alpha))$ .

More broadly the results of the represented work are given in paper [6,8].

On fig .2.1 the dependence diagram of cost function from  $\alpha$  for each element  $s_i \in S_{\Pi}(R_c(\alpha))$  is given when the searching problem of the net of minimal cost for  $n=5$  is solved.

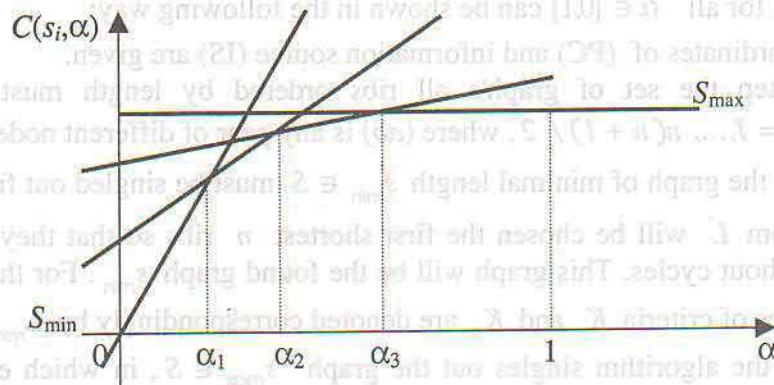


Fig. 2.1

The program realising this algorithm by personal computer is composed.

## 2. Experts System of Procedures Decision-Making for Multicriterion Problems

### 2.1. Introduction

After constructing the set  $S_{\Pi}(R_c(\alpha))$  we must get ranged row of a quantity meanings. For this purpose there has been worked out the expert system that is based on T. Saaty's analytic hierarchy method [7], as a result of which all elements of minimal cost network of  $S_{\Pi}(R_c(\alpha))$  set, will get (squire) some meaning of weight or probability. 2.2. The Method of Analytic Hierarchy Process

The method of analytic hierarchy process consists in decomposition of some problem in more simple components and in following expert-discussion of correlation between them in pairs the logically judgements on the basis of the results of pairwise comparison. Then the results of those judgements may be expressed in numbers on the definite 9-marks scale of relations and so the relative degrees of correlation between the components, as the priorities of some criterion may found. At the last step of procedure the generalized or global priorities of alternatives are defined but that may be carried out after the local priorities on each stage of hierarchy are defined.

Here we consider only a case of dominant hierarchy, the scheme of which looks like an overturned tree; the root of tree expresses the goal of problem. The hierarchy is complete if any element of a level functions as a criterion for all elements of level. According to principle of continuity of hierarchy all elements of a given level must be pairwise comparable, in respect of an arbitrary factor from previous level and so up to tope of hierarchy, i.e. -to the goal of problem.

The definition of goal of problem may be demand preliminary long talks here we don't consider this processes. We consider decision-making problems counting that already defined, the decision problem is formulated clearly and all alternatives are given. On the following step of procedure the priorities of criteria are determined for each alternative and by that the

most significance one is found.

For criteria priorities evaluation the method suggests to use process of pairwise comparison of elements' influences (or importance) of one level on the upper preceding elements. The pairwise comparison leads to reciprocal matrix eigenvector which expresses priorities of corresponding factors.

There is suggested in T. Saaty's method the following scale for expression in numbers the results of subjective estimation of pairwise comparison.

Based on the experts interviewing a reciprocal matrix  $C$  is constructed for the objects' quality, which reflects all pairwise comparison of the particular criteria. With this an arbitrary element  $c_{ij}$  of this matrix gives the expert result on the comparison of the particular criteria  $a_i$  and  $a_j$ . To establish this result the experts are asked to reply to the following question: How much is the criterion  $a_i$  more significant than the criterion  $a_j$  for the objects' (for a main goal) efficiency? It is sufficient to mean here a certain quality of the consumers' demands satisfaction under an "efficiency". The experts are asked to respond to the stated question taking into account only the following cases:

"Both  $a_i$  and  $a_j$  criteria are equally important for the object";

" $a_i$  criterion is slightly more important than  $a_j$  criterion for the object";

" $a_i$  criterion is considerably more important than  $a_j$  criterion for the object";

" $a_i$  criterion is much more important than  $a_j$  criterion for the object";

" $a_i$  criterion is absolutely prevalent than  $a_j$  criterion for the object";

Based on different investigators T. Saaty proposes to prescribe points 1, 3, 5, 7, 9 from the scale 1 to 9 for such gradation. Number 2, 4, 6, 8 are used for the rearrangement of compromises to make intermediate decisions and conclusions on the cases which slightly differ from the graded.

Ask the experts group as far as possible for them to achieve evaluation of comparison based on a concession rule. If it is unattainable then choose a score (on estimator) which has been proposed by the majority of experts.

By the results of the pairwise comparison we get  $n \times n$  dimensional matrix. It is essential to assume that  $c_{ii} = 1$  for all  $i = \overline{1, n}$ , when we compare the element  $a_i$  with itself, and when comparing the element  $a_j$  with the element  $a_i$  - to take the inverse value, i.e.

$c_{ji} = \frac{1}{c_{ij}}$ . Based on these assumptions we have to carry out only  $\frac{n(n-1)}{2}$  comparisons. It is

well-known that a maximal eigenvalue  $\lambda_{\max}$  of positive, reciprocal, ideally consistent matrix (a matrix is called as consistent if for any triple of its elements  $c_{ij}, c_{ki}, c_{kj}$  with have

$c_{ij} = \frac{c_{ki}}{c_{kj}}$  is equal to  $n$  (the number of activities in matrix) the closer  $\lambda_{\max}$  is to  $n$ , the more

consistent is the result. The inequality  $\lambda_{\max} \geq n$  holds for any positive reciprocal matrix. The

deviation from consistency has been represented by  $\frac{\lambda_{\max} - n}{n - 1}$ , which is referred to as a

consistency index (C.I). The consistency index of a randomly generated reciprocal matrix from the scale 1 to 9, is called a random index (R.I). The rates of C.I. to the average R.I for the same order matrixes called a consistency ratio (C.R.). Based on same comments (see ref [5, p. 21]) we consider the values of the experts pairwise evaluations only in the case when the consistency ratio for the constructed matrix is less than  $[0,1]$ . Otherwise it is recommended to interview the experts for second time and with this to keep the experts informed in details. May be it will be worth while to reorganized or to change the experts group too.

An eigenvalue  $\lambda$  of the matrix  $A$  is calculated from the vector equation  $Ax = \lambda x$ . An arbitrary solution  $x$  of this equation is referred as an eigenvector. If a matrix  $A$  is a consistent, reciprocal one and its diagonal elements are equal to 1, then the maximal eigenvalue  $\lambda_{\max} = n$ , and the more consistency is broken the more is the difference  $\lambda_{\max} - n$ , i. e. the consistency index. A maximal eigenvalue is called a principal eigenvalue, and the corresponding eigenvector is referred to as a principal eigenvector. It has been proved that if a principal eigenvector was normed then it can be considered as a priorities vector.

On base of subjective but thought out judgements experts fill in matrix with the results of pairwise estimation, then the set of local hierarchy must be defined. The priorities express the action, (or importance) of elements of given level hierarchy to the preceding elements on the upper level. In order to make that principal eigenvalues and eigenvectors for multi matrixes must be calculated and therefore using of Saaty's method reasonable only when numbers of hierarchy levels and elements are enough small (no more then 5-th for each of them). After that by some defined operations on matrixes and vectors the vector priorities for elements of each level, and for the last one among them, may be calculated. The priorities for the lowest level are just the global ones for alternative contesting decisions.

### 3. The expert system "Archevani"

For users helping the human-machine expert system "Archevani" has been developed. It is composed in the Delphi procedure language, which is based on object Pascal Procedure Language.

Dialogue with user in system keeps in Georgian.

Experts' system consists of the following sub- systems:

The first sub-system analyses the experts, determines their possibilities, independent opinion and limitations.

The second sub-system performs the decomposition of problems, helps a person who makes decision to define of a problem characteristics.

In the third sub-system there is the estimation of problems criterions in a dialogue regime according to the inquiry.

The fourth sub-system mathematically works our experts' data for getting the local and global probabilities of alternatives.

The programs is mode on a personal computer on Delphi System base.

We have chosen the Analytic Hierarchy Process method for construction of expert system for multicriterion decision-making procedures. The main point of this procedure is to obtain the general evaluation of main goal, by the weights of the elements of hierarchy scheme which present factors having an influence at the main goal. This weights, in their turn, are determined by the group of experts by means of comparison in pairs of elements for each upper pairwise elements in scheme and expression the results of the pairwise comparison of the 9-marks scales.

At the method demands from experts can to common statements when evaluating, the method is not a statistical procedure. At the same time, as the comparison of importance of elements are expressed in numbers, it makes possible to use for matrix of results of pairwise comparisons the tools of matrix analysis.

The Analytic Hierarchy Process method has been created by American scientific T. Saaty. It may be freely used for solution many practical problem, Saaty's procedure has been considered as the most solid logical and good one and that is why we have chosen it for our expert system.

For the decision-making person this system is first step in whole decision-making problem.

The expert system "Archevani" contains the following procedures:

- chosen of problems attributes (characters);
- hierarchy regulation of problems (characters);
- fixing of evaluations attributes or weights on the base of experts pairwise comparison;

- calculations of eigenvalues and eigenvectors and local priorities;
- definition of global priorities.



### References

- [1]. D. Bertsekas, R. Gallager. Data Networks, Frentice-Hall International, Inc., 1987R.
- [2]. Stanly. Enumerative Combinatorics. Voll, Wadsworn & Brooks /Cole. Advanced Books & Software Mouterey, California, 1998.
- [3]. Applied Combinatorial Mathematics, Editor E.E. Beckeubach John Wilay and Sons, Ing. New York, London, Sydney. 1964.
- [4]. V. Zhukovin. Decision making models and procedure, Tbilisi, Mecniereba, 1981. (in Russian)
- [5]. M. Salukvadze. Vector - Valued optimization problems in control theory. Academic Press, New York, 1976.
- [6]. I. Bockuchava, A. Topchishvili, N. Chkhikvadze. To one procedure of minimal cost net search. In: Proceedings of A.Eliashvili Institute of Control Systems of Georgian Academy of Sciences. Tbilisi. 1998.(in Georgian)
- [7]. T. L. Saaty. The Analytic Hierarchy Process. New York, McGraw-Hill, 1980
- [8]. I. Bokuchava, N. Chkhikvadze, Z. Alimbarashvili, Pareto Set Formation Algorithm for Minimal Cost Network, IC preprint № 05-2000.

Coordinated behavior of vast number of neurons – synchronization – is necessary condition for EEG formation. Existence of sequence of repetitive waves in EEG indicates that there exists rhythmical process and, accordingly, rhythm leader – pacemaker, initiator of the rhythmic activity.

Interaction between neurons is performed mainly via chemical synapses. Chemical substance – transmitter – released from presynaptic ending, changes permeability for specific ions in a postsynaptic membrane. The postsynaptic neuron excites or inhibits depending on for which ion of ions the membrane permeability have changed. So, various substances, acting on synaptic apparatus, would change interaction between neurons and, such a way, influence a degree of their synchronized behavior.

The purpose of this work was to investigate ability of controlling pacemaker mechanism and synchronization process using neurophysiologic tools.

Electrophysiological studies and those performed on mathematical models show that all of excitable membranes possess ability of autorhythmic activity (R, T, S, Z, N, neuron) or muscle fiber membrane needs only slight quantitative changes of its parameter to be switched from steady resting state to a state of autorhythmic activity.

Investigations performed on completely isolated molluscan neurons (7, 18) showed that some neurons without any synaptic connections exhibit autorhythmic activity. Of course, this is not to say that intercellular interaction is not important in organization of EEG rhythm in various regions of the brain (6, 11). Isolated pieces of tissue from hemisphere, for example, are not capable to produce spontaneous rhythmic activity (3, 2). However, our investigations revealed that single stimulation of thalamic ventral posterolateral (VPL) nucleus in cats induce large amplitude rhythmic waves in response to each stimulus (Fig. 1). Intracellular



## **Control of Pacemaker Mechanisms and Synchronization Processes**

**David Danelia, Naira Beckauri, Esmā Gonashvili**  
*Institute of Cybernetics*

### **Abstract**

Stimulation of VPL nucleus caused rhythmic activity in cortical neurons. Low-frequency stimulation of VPL nucleus caused synchronization of cortical neurons in somatosensor region of a cortex. The synchronization was reflected in EEG as rhythmic waves. Strychninization of thalamic nuclei caused asynchronous excitation of thalamic neurons due to inactivation of inhibitory synapses and asynchronous discharges in cortical neurons in response to asynchronous impulses arrived from thalamus. So, rhythmical cortical response to either single or low-frequency stimulation is the result of thalamic synchronization mechanism.

Experiments performed in calcium channel blockade conditions showed that  $Co^{2+}$  induced slight depolarization of neuronal membrane with subsequent rearranging of discharges in the groups.  $Cd^{2+}$  induced depolarization and conversion of tonic activity into PDS-like activity. The groups occurred in the both cases differ from bursts observed in neurons under normal conditions.

PTZ perfusion induced either hyperpolarization or depolarization or no changes of membrane potential in different neurons. Grouping of discharges was observed in the all cases independently to the sign of shift of membrane potential. After washing typical bursting activity occurred in all described cases.

Coordinated behavior of vast number of neurons – synchronization – is necessary condition for EEG formation. Existence of sequence of repetitive waves in EEG indicates that there exists rhythmical process and, accordingly, rhythm leader – pacemaker, initiator of the rhythmical activity.

Interaction between neurons is performed mainly via chemical synapses. Chemical substance – transmitter – released from presynaptic ending, changes permeability for specific ions in a postsynaptic membrane. The postsynaptic neuron excites or inhibits depending on for which ion or ions the membrane permeability have changed. So, various substances, acting on synaptic apparatus, would change interaction between neurons and, such a way, influence a degree of their synchronized behavior.

The purpose of this work was to investigate ability of controlling pacemaker mechanism and synchronization process using neurotrophic tools.

Electrophysiological studies and those performed on mathematical models show that all of excitable membranes possess ability of autorhythmic activity (8, 21, 22, 25). Neuronal or muscle fiber membrane needs only slight quantitative changes of its parameters to be switched from steady resting state to a state of autorhythmic activity.

Investigations performed on completely isolated molluscan neurons (7, 18) showed that some neurons without any synaptic connections exhibit autorhythmic activity. Of course, this is not to say that intercellular interaction is not important in organization of EEG rhythm in various regions of the brain (6, 11). Isolated pieces of tissue from hemisphere, for example, are not capable to produce spontaneous rhythmic activity (3, 5). However, our investigations revealed that single stimulation of thalamic ventral posterolateral (VPL) nucleus in cats induce large amplitude rhythmical waves in response to each stimulus (Fig. 1). Intracellular

recordings of a neuron in a somatosensor cortex (Fig. 2) make obvious that rhythmic waves appeared in response to single stimulation of VPL nucleus reflect rhythmic waves of postsynaptic potentials of cortical neurons. Fig. 2a represents response of a neuron to thalamic impulse – short-latency excitatory postsynaptic potential (EPSP) with a discharge on its top, followed by long inhibitory postsynaptic potential (IPSP). After the IPSP disappeared, EPSP with superimposed discharges was evoked again. With slower scanning oscilloscope (Fig. 2b) it is shown that these alterations were rhythmical.

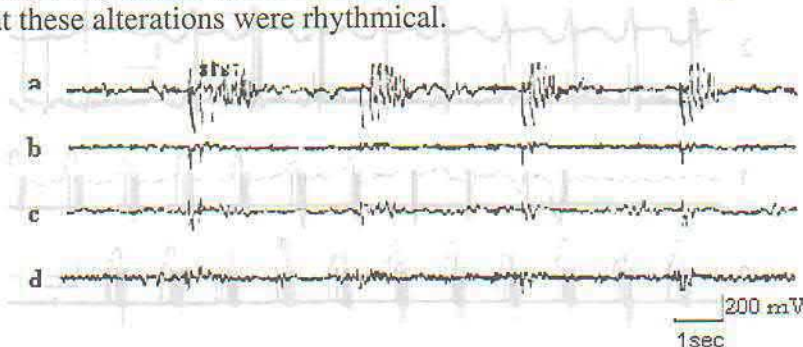


**Figure 1.** Rhythmical activity in somatosensor region of a cortex produced by single stimulation of VPL. a) Ipsilateral somatosensor region; b) Ipsilateral thalamic region; c) Contralateral somatosensor region; d) Contralateral thalamic region.

So, stimulation of the thalamic nucleus causes rhythmic activity in cortical neurons. P. Andersen and S. Anderson (1) and J. C. Eccles (13) developed the idea about thalamus as a rhythm leader. The authors considered thalamic nuclei are original and the only generator of rhythmical spindle-like activity in the brain. Rhythmical activity is determined by existence of negative feedback in the network of thalamic neurons. Impulses evoked with excitation of thalamocortical switcher neurons excite inhibitory interneurons via backward collaterals, and the latter ones cause IPSP in both excited and not excited thalamocortical neurons. Duration of these IPSP is 100-150 msec and, postanodal increase of excitation at the decay phase causes discharges in thalamic neurons, probably, via background excitability. Existence of

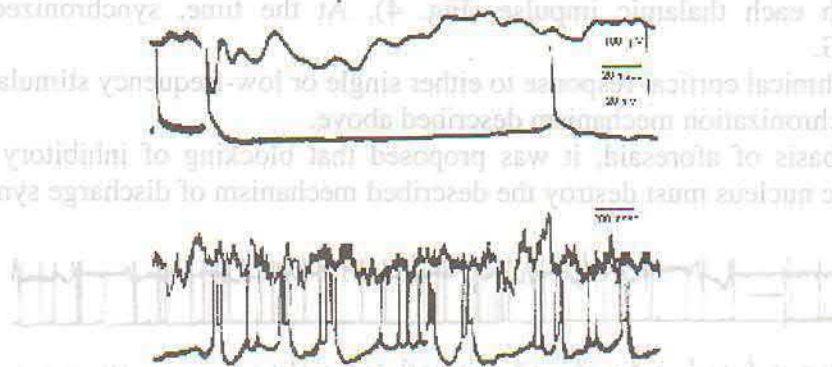


**Figure 2.** Response of a neuron in somatosensor region to single stimulus; Intracellular recording; a) Fast scanning oscilloscope; b) slow scanning oscilloscope; Upper curve: macroelectrode recording; lower curve: microelectrode recording.

positive feedback in the network of thalamic neurons makes synchronization of neighboring neuron's responses more possible. Rhythmical discharges of thalamic neurons passed through thalamocortical fibers form rhythmic activity in corresponding cortical zones. Besides, each particular thalamic nucleus controls activity of certain cortical region.

Our investigations showed that if VPL nucleus was stimulated electrically at 7-10 Hz then each stimulus induced either single or grouped discharges in 72% of cortical neurons in somatosensor region and there were no discharges between stimuli (Fig. 3).

Fig. 3a represents a simultaneous recording of activity in two neurons. It can be seen that the stimulation induces synchronization of the neurons. Fig. 3b represents an activity of a

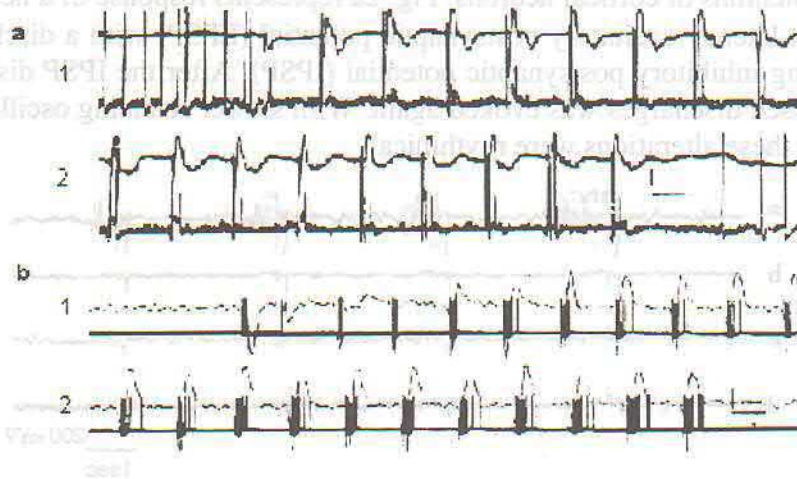


**Figure 3.** Responses of neurons at somatosensor region of a cortex to stimulation of VPL at 6 Hz. Intracellular recording; a) 1, 2: simultaneous recording of two neurons; b) continuous recording of neuron activity in pyramidal tract.

neuron from pyramidal tract. Well then, there is both quantitative and qualitative evidence, that low-frequency stimulation of specific thalamic nucleus induces synchronization of discharges in cortical neurons. It can be seen in intracellular recordings of activity of these neurons, that EPSP with superimposed discharge followed with long IPSP occurs, in



**Figure 4.** Intracellular recording of activity of a neuron at a somatosensor region of cortex in response to VPL stimulation at 6 Hz

accordance with each thalamic impulse (Fig. 4). At the time, synchronized activity is observed in EEG.

So, Rhythmical cortical response to either single or low-frequency stimulation is result of thalamic synchronization mechanism described above.

On the basis of aforesaid, it was proposed that blocking of inhibitory synapses in specific thalamic nucleus must destroy the described mechanism of discharge synchronization

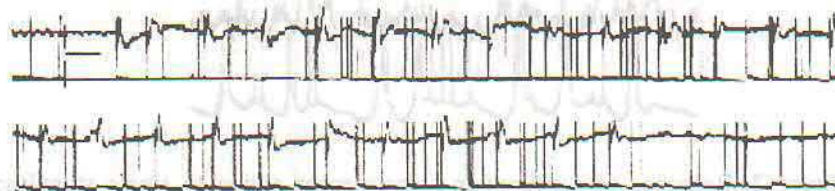


**Figure 5.** Response of a neuron at somatosensor region of cortex to low-frequency stimulation of strychninized VPL. Intracellular recording.

in cortical neurons. Some experiments were performed with strychninization of VPL nucleus. According with a great deal of data, strychnine effectively suppresses postsynaptic inhibition via competition with inhibitory transmitter glicin to occupy receptor regions (12,15,19,20,29). Our experiments showed that in all investigated neurons in cortical somatosensor region, disturbance of discharge's occurrence took place when VPL was stimulated low-frequently. From oscillograms representing intracellular recordings it is obvious that the

disturbance is the result of shortening of EPSP duration (Fig. 5). On the basis of the results we can propose that low-frequency stimulation of strychninized thalamic nucleus causes asynchronous excitation of thalamic neurons (except discharges evoked as direct responses to stimuli), because inhibiting pause absents between stimuli due to inactivation of inhibitory



**Figure 6 .** Typical bursting pacemaker activity of a neuron in right parietal ganglion of *Helix Asperca*. 10 sec; 40 mV.

synapses. In response to asynchronous impulses arrived from thalamus, cortical neurons also generate asynchronous discharges.

So, we can conclude, that blockage of inhibitory synapses in visual hillock nuclei suppresses synchronization processes in cortical neurons.

As it was already noted, many molluscan neurons exhibit endogenous pacemaker activity. In some ones a special type of activity – bursting activity is observed. These neurons generate groups of action potentials where the groups are separated from each other with relatively long intervals. Each group of impulses appears superimposed on a slow

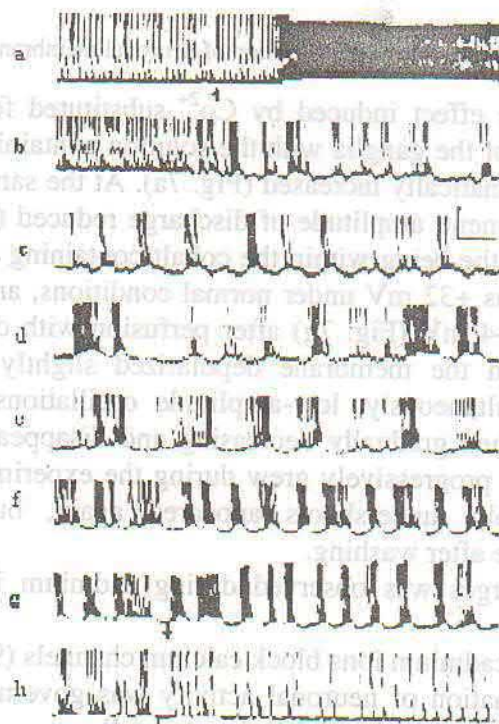


**Figure 7.** Effect of substitution  $Co^{2+}$  for  $Ca^{2+}$ . Here and in following figures:

↑ – application of testing saline; ↓ – washing; a-h: continuous records. 10sec; 40mV

depolarization wave followed by a long hyperpolarization (Fig. 6). It is clear in the figure that there are some regular changes of action potentials and interspike intervals within each group: overshoot gradually increases and undershoot gradually decreases, and interspike intervals gradually shorten at first and then increase again.

Now there already exists sufficiently reliable data concerning the endogenous nature of the described activity and its association with neuronal membrane and cytoplasm processes, that depends on many factors such as extracellular maintenance of one- and bivalent ions, pH, temperature, etc. (27). Also, it was shown in early works that hypocalcemic environment facilitates generation of action potentials in spinal cord



Figure 8 Effect of cadmium ions on molluscan neuron activity

motoneurons and skeletal muscle fibers (26).

These data are of particular interest due to specific features of calcium ions, which enables them to connect large organic molecules and regulate a course of biochemical reactions, which these molecules participate in (2, 4, 10).

A next series of experiments described in this paper were performed on snail neurons in membrane calcium channel blockade conditions achieved by adding of cobalt and cadmium ions into bath saline. In the first case  $\text{CaCl}_2$  of normal Ringer was substituted by equimolar concentration of  $\text{CoSO}_4$ , and in the other case 2 mM of  $\text{Cd}(\text{NO}_3)_2$  was added into a Ringer solution.



Figure 9. PTZ-induced hyperpolarization of neuronal membrane; 10 sec; 40 mV

Fig. 7 illustrates the effect induced by  $\text{Co}^{2+}$  substituted for  $\text{Ca}^{2+}$ . The neuron was depolarized after perfusion of the ganglia with the solution containing 7 mM  $\text{CoSO}_4$ , and the frequency of discharges dramatically increased (Fig. 7a). At the same time, apparently due to reduction of calcium component, amplitude of discharge reduced (Fig. 7a). The reducing of amplitude continued during the being within the cobalt-containing medium. In the illustrated case the overshoot value was +32 mV under normal conditions, and it became equal to +24 mV (Fig. 7b) and than to +4 mV (Fig. 7g) after perfusion with cobalt containing solution. Immediately after perfusion the membrane depolarized slightly and grouped discharges occurred (Fig. 7b-c). Simultaneously, low-amplitude oscillations of membrane potential, gradually increasing, and then gradually decreasing and disappearing emerged (Fig. 7b-f). The grouping of discharges progressively grew during the experiment. After washing, spike amplitude increased sharply, undershoots appeared again, but bursting activity was maintained for a certain time after washing.

Grouping of discharges was observed during cadmium ions were added into the Ringer solution (Fig. 8).

Because cobalt and cadmium ions block calcium channels (9, 14, 16, 17), it is unlikely that the observed transformation of neuronal activity was governed via activation of some bursting neurons, presynaptic respecting the registered cell.

Reduction of calcium ions' influx through the membrane at the outset was manifested in decreasing of the amplitudes of action potentials, and the grouping of action potentials, as well as recovery of initial activity, derived with some delay. In that we can propose the emergence of bursting activity is due to activation of any cytoplasm biochemical reactions that control ion channels and are regularable by calcium ions.

Transformation of neuronal activity into grouped rhythmical activity can be performed after a ganglion is perfused with pentylentetrazol (PTZ) - containing solution. According existent data a convulsive effect of PTZ is due to blocking of chloride permeability by an inhibitory neurotransmitter GABA (24). Due to reduction of inhibitory contribution in

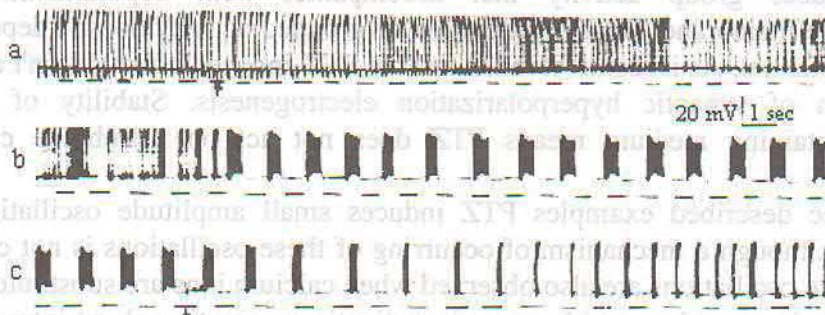


Figure 10. PTZ-induced depolarization accompanied with grouping;

summary effect of synaptic processes an excitation enhances on a postsynaptic membrane and after all convulsive state establishes (13). In other investigations it was shown that PTZ causes small amplitude oscillations of membrane potential and grouping of discharges in many isolated neurons. These data indicates that PTZ, besides reduction of synaptic activity, also acts on a neuronal membrane directly.

In experiments performed in our laboratory a majority of investigated neurons hyperpolarized after perfusion with PTZ-containing solution, and the hyperpolarization was followed with group rhythmical activity (fig. 9). In some neurons the emergence of the group rhythmical activity was preceded by a membrane depolarization with discharges becoming more and more frequent (fig. 10). The observed groups of discharges differed from typical grouping activity: instead of gradual increase of overshoot within each group of spikes significant decrease of overshoot took place (compare Fig. 6 and Fig. 10). It seems, we must regard such an activity as convulsive. After washing, grouped activity with increasing overshoot within each group was observed (Fig. 10b).

In some neurons PTZ did not cause significant changes of membrane potential before the emergence of grouped activity (Fig. 11). Although PTZ-induced grouped activity was not rhythmical in this case, as it was in the cases described above. Once PTZ was applied, convulsive activity emerged with some latency – paroxysmal depolarization shifts evoked, and high-frequency discharges with significantly decayed amplitudes at the tops were generated (Fig. 11 d, e). After washing, typical rhythmical activity was observed. Then, within each burst, number of spikes gradually decreased, interspike intervals increased and the process finished with recovery of initial activity (Fig. 11e).

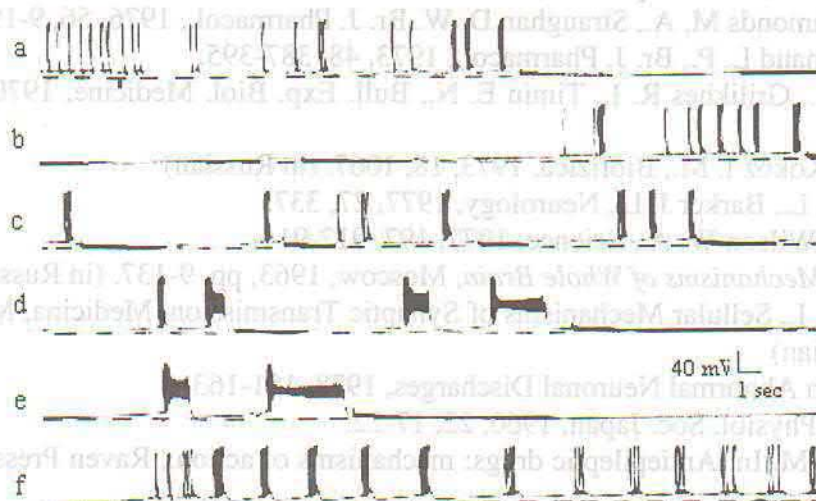


Figure 11. . PTZ- induced PDFs. Dotted line corresponds to -80 mV.

So, PTZ induces group activity that accompanies both depolarization and hyperpolarization of the membrane. Hence, generation of grouped activity doesn't depend on a shift of membrane potential. As it seems, it indicates that PTZ-induced effect doesn't depend directly on relaxation of synaptic hyperpolarization electrogenesis. Stability of action potentials in PTZ-containing medium means PTZ does not act on membrane calcium channels.

In the all three described examples PTZ induces small amplitude oscillations of membrane potential. Although a mechanism of occurring of these oscillations is not clear, it must be noted that these oscillations are also observed when calcium ions are substituted with cobalt ions. This fact is in accordance with recent investigations reporting about intracellular  $[Ca^{2+}]$  oscillations. The similarity of the influence of PTZ and cobalt ions is also expressed in after washing typical grouped activity occurs. Therefore, the results of the performed experiments give basis to suppose that PTZ activates reactions that are related to reactions flowed in a neuronal cytoplasm.

### References

- [1]. Andersen P., Anderson S. Physiological basis of alpha-rhythm, N. Y., 1968.
- [2]. Berrige M. J., *Neuron*, 1998, 21, 13-26.
- [3]. Bremer F. Cerebral and cerebellar potential, *Physiol. Rev.*, 1958, 38, 357-388.
- [4]. Bridge J. B., Ershler R., Cannel M. B., *J. Physiol.*, 1999, 518, N2, 469-478.
- [5]. Burns B. D. The mammalian cerebral cortex, Arnold, London, 1958.
- [6]. Calabrese R. L., *Current Opinion in Neurobiology*, 1998, 8, 710-717.
- [7]. Chen C., Baumgarten R., Hart O. *Pflugers Arch. Gen. Physiol.*, 1973, 345, 195.
- [8]. Cole K. *Membranes, Ions and Impulses*, Univ. California Press, Berkely and Los Angeles, 1968.
- [9]. Crisital O. A., *Rep. Acad. Sci. SSSR*, 1976, 231, N4, 1003-1005.
- [10]. Cseresnyes Z., Bustamante A. I., Shneider M. F., *J. Physiol.*, 1999, 514, N1, 83-99.
- [11]. O'Donovan M. J., *Current Opinion in Neurobiology*, 1999, 9, 94-104.
- [12]. Dreifuss J. J., Matthews E. K. *Brain Res.*, 1972, 45, 599-603.
- [13]. Eccles J. C. *Epilepsia*, 1965, 6, 89-115.
- [14]. Ecert R., Lux H. D., *J. Physiol*, 1976, N1, 129-151.
- [15]. Faber D., Klee M., *Brain Res.*, 1974, 65, 109.
- [16]. Gorman A. L. F., Thomas M. V., *J. Physiol.*, 1980, 308, N5, 258-285.
- [17]. Heyer C. B., Lux H. D., *J. Physiol.*, 1976, 262, N2, 319-348.
- [18]. Hild W., Takaki J., *J. Neurophysiol.*, 1962, 25, 277-304.
- [19]. Hill R. G., Simmonds M. A., Straughan D. W. *Br. J. Pharmacol.*, 1976, 56, 9-19.
- [20]. Kelly J. S., Renaud L. P., *Br. J. Pharmacol.*, 1973, 48, 387-395.
- [21]. Khodorov B. I., Grilikhes R. I., Timin E. N., *Bull. Exp. Biol. Medicine*, 1970, 4, 26. (in Russian)
- [22]. Krinski V. I., Kokoz I. M., *Biofizica*, 1973, 18, 1067. (in Russian)
- [23]. MacDonald R. L., Barker J. L., *Neurology*, 1977, 27, 337.
- [24]. Pellmar T. C., Wilson W. A., *Science*, 1977, 197, 912-914.
- [25]. Purpura D. in *Mechanisms of Whole Brain*, Moscow, 1963, pp. 9-137. (in Russian)
- [26]. Shapovalov A. I., *Sellular Mechanisms of Synaptic Transmission*, Medicina, Moscow, 1966. (in Russian)
- [27]. Takeuchi H., in *Abnormal Neuronal Discharges*, 1978, 151-163.
- [28]. Washizu Y. *J. Physiol. Soc. Japan*, 1960, 22, 17-22.
- [29]. Woodbury D. M. In: *Antiepileptic drugs: mechanisms of action.*, Raven Press, N. Y., 1980, 249-303.

## General Solution of Gauss Nonhomogeneous Hypergeometric Equation's of Particular Class

**Guram Kharatishvili**  
*Institute of Cybernetics*

Let consider Gauss nonhomogeneous hypergeometric equation

$$t(t-1)\ddot{x} + [(\alpha + \beta + 1)t - \gamma]\dot{x} + \alpha\beta x = f(t) \quad (1)$$

of particular class, defined by

$$\alpha + \beta = \alpha\beta + 1 \quad (2)$$

General solution of equation (1) with condition (2) has the form

$$x = (t-1)^{\gamma-\alpha\beta-1} t^{1-\gamma} \left[ c_1 + \int (t-1)^{\alpha\beta-\gamma} t^{\gamma-2} \left( c_2 + \int f(t) dt \right) dt \right], \quad (3)$$

where  $c_1, c_2$  are arbitrary constants.

For homogeneous equation (1) general solution has the form

$$x_0 = (t-1)^{\gamma-\alpha\beta-1} t^{1-\gamma} \left[ c_1 + c_2 \int (t-1)^{\alpha\beta-\gamma} t^{\gamma-2} dt \right].$$

General solution (3) is constructed by new method of solvation linear nonhomogeneous equations of the second order with variable coefficients, which is making ready for the press.

**Proof.** We have:

$$\begin{aligned} \dot{x} &= \frac{\gamma - \alpha\beta - 1}{t-1} x + \frac{1-\gamma}{t} x + \frac{1}{t(t-1)} \left( c_2 + \int f(t) dt \right) = \\ &= \frac{\gamma - 1 - \alpha\beta t}{t^2 - t} x + \frac{1}{t^2 - t} \left( c_2 + \int f(t) dt \right). \\ \ddot{x} &= \frac{-\alpha\beta(t^2 - t) - (2t-1)(\gamma - 1 - \alpha\beta t)}{(t^2 - t)^2} x + \\ &+ \frac{\gamma - 1 - \alpha\beta t}{t^2 - t} \left[ \frac{\gamma - 1 - \alpha\beta t}{t^2 - t} x + \frac{1}{t^2 - t} \left( c_2 + \int f(t) dt \right) \right] - \\ &\quad - \frac{2t-1}{(t^2 - t)^2} \left( c_2 + \int f(t) dt \right) + \frac{f(t)}{t^2 - t} = \\ &= \frac{(\gamma - 1 - \alpha\beta t)^2 - \alpha\beta(t^2 - t) - (2t-1)(\gamma - 1 - \alpha\beta t)}{(t^2 - t)^2} x + \\ &\quad + \frac{\gamma - \alpha\beta t - 2t}{(t^2 - t)^2} \left( c_2 + \int f(t) dt \right) + \frac{f(t)}{t^2 - t}. \end{aligned}$$



$$\begin{aligned}
 (t^2 - t)\ddot{x} + [(\alpha + \beta + 1)t - \gamma]\dot{x} + \alpha\beta x &= \\
 &= (t^2 - t)\ddot{x} + (\alpha\beta t + 2t - \gamma)\dot{x} + \alpha\beta x = \\
 &= \left[ \frac{(\gamma - 1 - \alpha\beta t)(\gamma - \alpha\beta t - 2t) - \alpha\beta(t^2 - t)}{t^2 - t} + \right. \\
 &\quad \left. + \frac{(\alpha\beta t + 2t - \gamma)(\gamma - 1 - \alpha\beta t)}{t^2 - t} \right] x + \\
 &+ \left[ \frac{\gamma - \alpha\beta t - 2t}{t^2 - t} + \frac{\alpha\beta t + 2t - \gamma}{t^2 - t} \right] \left( c_2 + \int f(t) dt \right) + f(t) + \alpha\beta x = f(t).
 \end{aligned}$$

(1) P.S. General solution (3) is constructed by new method of solvation linear nonhomogeneous equations of the second order with variable coefficients, which is making ready for the press.

$$(2) \quad \alpha + \beta = \gamma + 1$$

General solution of equation (1) with condition (2) has the form

$$(3) \quad x = (t-1)^{\gamma-\alpha\beta-1} \left[ c_1 + \int (t-1)^{\alpha\beta-1} c_2 + \int (t-1) dt \right],$$

where  $c_1, c_2$  are arbitrary constants.

For homogeneous equation (1) general solution has the form

$$x_0 = (t-1)^{\gamma-\alpha\beta-1} \left[ c_1 + c_2 \int (t-1)^{\alpha\beta-1} dt \right].$$

General solution (3) is constructed by new method of solvation linear nonhomogeneous equations of the second order with variable coefficients, which is making

ready for the press.

Proof. We have:

$$\begin{aligned}
 \dot{x} &= \frac{\gamma - \alpha\beta - 1}{t-1} x + \frac{\gamma - 1 - \alpha\beta t}{t-1} x + \frac{1}{(t-1)} \left( c_2 + \int (t-1) dt \right) = \\
 &= \frac{\gamma - 1 - \alpha\beta t}{t-1} x + \frac{1}{(t-1)} \left( c_2 + \int (t-1) dt \right) = \\
 \ddot{x} &= \frac{-\alpha\beta(t-1) - (\gamma - 1 - \alpha\beta t)}{(t-1)^2} x + \\
 &+ \left[ \frac{\gamma - 1 - \alpha\beta t}{t-1} x + \frac{1}{(t-1)} \left( c_2 + \int (t-1) dt \right) \right] - \\
 &= \frac{\gamma - 1 - \alpha\beta t}{(t-1)^2} x + \frac{1}{(t-1)} \left( c_2 + \int (t-1) dt \right) - \\
 &+ \frac{(\gamma - 1 - \alpha\beta t)^2 - \alpha\beta(t-1)(\gamma - 1 - \alpha\beta t)}{(t-1)^2} x + \\
 &+ \frac{\gamma - \alpha\beta t - \gamma}{(t-1)^2} x + \left( \int (t-1) dt \right) + c_2
 \end{aligned}$$



## On some relations between one-particle density and energy characteristics in the system of one-dimensional fermions.

**Roland Bakuradze**  
*Institute of Cybernetics*

### Abstract

A number of relations between one-particle density, one-particle levels of energy and wave functions of the  $2n$  fermion system has been obtained.

Hohenberg and Kohn [1] showed, that one can find the energy of the principal state in the multielectron system existing in the external field with local potential  $q(r)$ ,  $r = (x, y, z)$  as the lower bound of some functional  $E(\rho)$ , defined on a subset of sufficiently smooth non-negative functions satisfying the normalization condition

$$\int_{R^3} \rho(x, y, z) dx dy dz = N,$$

where  $N$  is number of particles. The function  $\rho = \rho(x, y, z)$  has the value of electron density and is defined by means of multielectron function  $\Psi(\tau_1, \dots, \tau_n)$  according to the following formula:

$$\rho(x, y, z) = N \int |\Psi(\tau_1, \tau_2, \dots, \tau_n)|^2 d\sigma_1 d\tau_2 \dots d\tau_n.$$

where  $\tau_j$  is Cartesian and spin coordinates of  $j$ -th particle  $\tau_j = (x_j, y_j, z_j, \sigma_j)$ . Integration is carried out by the variables  $(\tau_2, \dots, \tau_n)$  and  $\sigma_1$ ,  $(\tau_1 = \tau)$ .

In the work [1] it was also shown that if the principal state of Schrodinger's  $N$ -electron operator

$$H(q) = -\frac{1}{2} \sum_{i=1}^n \left( \frac{\partial^2}{\partial x_i^2} + \frac{\partial^2}{\partial y_i^2} + \frac{\partial^2}{\partial z_i^2} \right) + \sum_{i < j} \frac{1}{r_{ij}} + \sum_{i=1}^n q(r_i)$$

with the potential of the external field  $q(r)$  being non-degenerate  $q(r) \rightarrow 0, |r| \rightarrow \infty$  and  $\rho(r)$  is corresponding electron density, then the function  $\rho(r)$  can not be electron density for Schrodinger's nondecremente operator with a different potential:

$$\tilde{q}(r) = q(r)$$

In the works of March and co-authors [2-4] the problem of regeneration of one particle potential  $q(r)$  by the function  $\rho(r)$  is discussed as well as the possibility to make approximate estimations of the density  $\rho(r)$  by the potential  $q(r)$ .

In the present work we have considered one-dimensional case  $N = 2n$  of interacting fermions and obtained a number of simple relations between one-particle density, one-particle energies and wave functions.

2n one-dimensional fermion system with hamiltonian

$$H y(x_1, \dots, x_{2n}) = -\sum_{i=1}^{2n} \frac{\partial^2}{\partial x_i^2} y(x_1, \dots, x_{2n}) + \sum_{i=1}^{2n} q(x_i) y(x_1, \dots, x_{2n}) = \sum_{i=1}^{2n} h_i y(x_1, \dots, x_{2n})$$

is being considered.

The operator  $h_i$  acts on the coordinates of the  $i$ -th particle and has the form

$$hy(x) = -\frac{d^2}{dx^2}y(x) + q(x)y(x)$$

Let us denote by  $\lambda_i$  denote the one-particle levels of ( $\lambda_i < \lambda_{i+1}$ ),  $\varphi_i(x)$  are their corresponding wave functions normalized by the condition  $\int |\varphi_i(x)|^2 dx = 1$ .  $\tilde{\rho}(x)$  is fermion density in the principal state

$$\tilde{\rho}(x) = 2 \sum_{j=1}^n \varphi_j^2(x); \quad \rho(x) = \frac{1}{2} \tilde{\rho}(x) \quad (1)$$

$E$  is the energy of the principal state and  $E = 2 \sum_{i=1}^n \lambda_i$ .

1.  $q(x)$  and  $\rho(x)$  are assumed to be given. We claim that one-particle levels of energy  $\lambda_i$  and their respective wave functions  $\varphi_i(x)$  can be obtained by algebraic methods without solving Schrodinger's equation  $hy = \lambda y$ .

E.g. in the case of a one-dimensional potential box having infinitely high walls in the points  $x = 0$  and  $x = \pi$  the procedure of findings  $\lambda_i$  and  $\varphi_i(x)$  consists in the following: let  $A$  denote the operator

$$Af(x) = -\frac{1}{4}f''(0) - \frac{1}{4}f''(x) + \frac{1}{2}q(x)f(x) + \frac{1}{2} \int_0^x q(t)f'(t)dt \quad (2)$$

Then one-particle levels of energy are determined from the following system of equations:

$$\sum_{k=1}^n \lambda_k^i = \int_0^\pi A^i \rho(x) dx, \quad (i = 1, \dots, n) \quad (3)$$

if  $q(x) \equiv 0$ , then the density  $\rho(x) = \frac{2}{\pi} \sum_{k=1}^n \sin^2 kx$

The equation (3) in this case have the form:

$$\sum_{k=1}^n k^{2i} = \frac{-\pi}{(-4)^i} \rho^{(2i)}(0), \quad (i = 1, \dots, n).$$

That is why the formula (3) is easily checked directly.

The solution of the system of equations (3) is reduced by Newton's formulae to finding the solution of the polinomial of the  $n$ -th power  $Q_n(t)$  [5]. If we write  $Q_n(t)$  in the form

$$Q_n(t) = (-1)^n (t^n - P_1 t^{n-1} - P_2 t^{n-2} - \dots - P_n),$$

then its coefficients  $P_k$  can be calculated by the formulae

$$kP_k = a_k - P_1 a_{k-1} - \dots - P_{k-1} a_1, \quad (k = 1, \dots, n),$$

where  $a_k = \int_0^\pi A^k \rho(x) dx$ .

If  $\lambda_i$  are found, the squares of their corresponding wave functions are calculated by the following formula

$$\psi_i(x) = \frac{\begin{vmatrix} 1 & \dots & 1 & \rho(x) & 1 & \dots & 1 \\ \lambda_1 & \dots & \lambda_{i-1} & A\rho(x) & \lambda_{i+1} & \dots & \lambda_n \\ \dots & \dots & \dots & \dots & \dots & \dots & \dots \\ \lambda_1^{n-1} & \dots & \lambda_{i-1}^{n-1} & A^{n-1}\rho(x) & \lambda_{i+1}^{n-1} & \dots & \lambda_n^{n-1} \end{vmatrix}}{\prod_{m>i} (\lambda_m - \lambda_i)}$$

If we know the function  $\psi_i(x)$  we can find the corresponding wave function  $\varphi_i(x) = \pm \sqrt{\psi_i(x)}$ .

The sign of the solution is determined uniquely in the tegion located between any two neighbouring zeros of the function  $\psi_i(x)$  from the condition of continuity of the

derivative of the function  $\varphi_i(x)$ .

The number of zeros of the functions  $\psi_i(x)$  determines the ordinal number of the wave function.

2. It has been shown that the density  $\rho(x)$  and the potential  $q(x)$  are calculated by the equation

$$\prod_{i=1}^n (A - \lambda_i) \rho(x) = 0, \quad (4)$$

where the numbers  $\lambda_i$  are determined from the equations (3) and operator A by the formula (2).

If the density  $\rho(x)$  is known, then this equations (4) determines all the potential  $q(x)$  (to within additive constant) to which the given density  $\rho(x)$  corresponds. If we know that  $2\rho(x) = \tilde{\rho}(x)$  is the density for the principal state of some Schodinger's operator, then by the theorem Hohenberg-Kohn, as was mentioned above, there is only one such operator (and hence the potential  $q(x)$  as well).

### References

- [1]. P. Hohenberg, W. Kohn Phys. Rev. B. 136, 1964, 864-871
- [2]. J. C. Stoddart, A. M. Beattie, N. M. March Int. J. Quant. Chem., N4, 1971, 35-53
- [3]. N. H. March, W. H. Young Nuclear Phys. 70, 1979, 587-588
- [4]. D. K. Faddeev and W. N. Faddeeva, The calculation Methods of Linear Algebra (Fismatgis, Moscow, 1960).

$$\psi(x) = \frac{1}{\sqrt{2\pi \cdot \sigma^2}} \exp\left\{-\frac{x^2}{2\sigma^2}\right\} \exp\left\{-\frac{x^2}{2\sigma^2}\right\}$$

where  $\sigma$  is a known parameter.  
Then joint distribution of  $(\xi, \eta)$  random value is assigned by formula

$$\psi(\xi, \eta) = \int \psi(\xi - x) \psi(\eta - x) g(x) dx \quad (1)$$

where  $g(x)$  is a prior density function  $x$ .  
If we substitute  $\psi(\xi, \eta)$  into the expression (1) then we receive

$$\psi(\xi, \eta) = \int \frac{1}{\sqrt{2\pi \cdot \sigma^2}} \exp\left\{-\frac{(\xi - x)^2}{2\sigma^2}\right\} \exp\left\{-\frac{(\eta - x)^2}{2\sigma^2}\right\} g(x) dx \quad (2)$$

integrating equation (2) first by  $\eta$  and after by  $\xi$  we receive

$$\psi(\xi) = \int \frac{1}{\sqrt{2\pi \cdot \sigma^2}} \exp\left\{-\frac{(\xi - x)^2}{2\sigma^2}\right\} g(x) dx \quad (3)$$

$$\psi(\eta) = \int \frac{1}{\sqrt{2\pi \cdot \sigma^2}} \exp\left\{-\frac{(\eta - x)^2}{2\sigma^2}\right\} g(x) dx \quad (3')$$

If instead of  $\psi(\xi)$  we have only its evaluation  $\hat{\psi}(\xi)$  received on the basis of observable values, then (3) represents integral equation of the first kind with respect to  $g(x)$ .

$\int$	$\&$
$\pi$	$\Sigma$

## Numerical Method of Establishing Dependence Parameters Between Two Variables

Amiran Toronjadze, Lili Revishvili  
*Institute of Cybernetics*

### Abstract

In this article we can see the task of estimation the parametrs in the dependence between two variables, which were measured with a deviation. The parameters are estimated by the solution of the integral equation and also by using maximum likelihood method. The example of the dependence between two measured variables is constructed. Maximization of likelihood function is done by the computer.

Let us consider the task when there is a functional dependence between  $x$  and  $y$  characters

$$Y = f(x; \beta_1, \beta_2, \dots, \beta_k)$$

containing unknown parameters  $\beta_1, \beta_2, \dots, \beta_k$ ; and we should find by measured values  $\xi, \eta$  the most suitable estimation of the said parameters.

$\xi$  and  $\eta$  result from measuring  $x, y$  values, i.e.  $\xi = x + u, \eta = y + v$ , and  $u = \xi - x, v = \eta - y$  - random errors. Let us assume that  $u$  and  $v$  are independent and are distributed normally with parameters  $(0, \sigma_1), (0, \sigma_2)$  i.e. for  $(u, v)$  random bivariate we have density function

$$\Psi(u, v) = \frac{1}{\sqrt{2\pi} \cdot \sigma_1} \exp\left\{-\frac{u^2}{2\sigma_1^2}\right\} \frac{1}{\sqrt{2\pi} \cdot \sigma_2} \exp\left\{-\frac{v^2}{2\sigma_2^2}\right\}$$

where  $\sigma_1$  is a known parameter.

Then joint distribution of  $(\xi, \eta)$  random value is assigned by formula

$$\varphi(\xi, \eta) = \int_{-\infty}^{\infty} \Psi[\xi - x, \eta - f(x; \beta_1, \beta_2, \dots, \beta_k)] g(x) dx \quad (1)$$

where  $g(x)$  is a priori density function  $x$ .

If we substitute  $\psi(u, v)$  into the expression (1) then we receive:

$$\varphi(\xi, \eta) = \int_{-\infty}^{\infty} \frac{1}{\sqrt{2\pi} \cdot \sigma_1} \exp\left\{-\frac{(\xi - x)^2}{2\sigma_1^2}\right\} \exp\left\{-\frac{[\eta - f(x; \beta_1, \beta_2, \dots, \beta_k)]^2}{2\sigma_2^2}\right\} g(x) dx \quad (2)$$

integrating equation (2) first by  $\eta$  and after by  $\xi$ , we receive

$$\varphi_1(\xi) = \frac{1}{\sqrt{2\pi} \cdot \sigma_1} \cdot \int_{-\infty}^{\infty} \exp\left\{-\frac{(\xi - x)^2}{2\sigma_1^2}\right\} g(x) dx \quad (3)$$

$$\varphi_2(\eta) = \frac{1}{\sqrt{2\pi} \cdot \sigma_2} \cdot \int_{-\infty}^{\infty} \exp\left\{-\frac{[\eta - f(x; \beta_1, \beta_2, \dots, \beta_k)]^2}{2\sigma_2^2}\right\} g(x) dx \quad (3^1)$$

If instead of  $\varphi_1(\xi)$  we have only its evaluation  $\hat{\varphi}_1(\xi)$  received on the basis of observable values, then (3) represents integral equation of the first kind with respect to a

priori density function  $g(x)$ . In [1,2,3,] consistency estimate  $\hat{g}(x)$  of a priori density function  $g(x)$  is received by means of solution of integral equation of the first kind by A.N. Tikhonov's stable regularization method.

If we substitute  $\hat{g}(x)$  in (3') we receive density function

$$\varphi_2(\eta) = \frac{1}{\sqrt{2\pi} \cdot \sigma_2} \cdot \int_{-\infty}^{\infty} \exp \left\{ -\frac{[\eta - f(x; \beta_1, \beta_2, \dots, \beta_k)]^2}{2\sigma_2^2} \right\} \hat{g}(x) dx \quad (4)$$

with unknown parameters  $\beta_2, \beta_1, \beta_2, \dots, \beta_k$ . Let us estimate these parameters through likelihood method.

In [4] it was proved that estimates found through this method are consistent. So the task comes to finding a maximum of likelihood functions for these parameters. For this purpose we take  $f = ax$ ,  $\varphi_2(\eta) = \varphi(\eta)$ ,  $\sigma_2 = \sigma$  as functions and the values of  $\hat{g}(x)$  in discrete points  $x_1, x_2, \dots, x_{10} - \hat{g}(x_j)$ , resulted from integral equation (3). The density function will be:

$$\varphi(\eta; a, \sigma) = \frac{1}{\sqrt{2\pi} \cdot \sigma} \cdot \frac{1}{\sum_{j=1}^{10} \hat{g}(x_j)} \cdot \sum_{j=1}^{10} e^{-\frac{(\eta - ax_j)^2}{2\sigma^2}} \cdot \hat{g}(x_j) \quad (5)$$

and for observable values  $\eta_i (i=1, n)$  the likelihood function

$$L = \prod_{i=1}^n \varphi(\eta_i; a, \sigma)$$

Will look like

$$\ln L = \sum_{i=1}^n \ln \left( \frac{1}{\sqrt{2\pi} \cdot \sigma} \cdot \frac{1}{\sum_{j=1}^{10} \hat{g}(x_j)} \cdot \sum_{j=1}^{10} e^{-\frac{(\eta_i - ax_j)^2}{2\sigma^2}} \cdot \hat{g}(x_j) \right) \quad (6)$$

In the present paper we artificially construct, by means of Monte-Carlo method, the dependance between two variables. We hold fixed specific values  $a, \sigma$  and define the values  $(\xi, \eta)$  by the table of random numbers. We process the data  $(\xi, \eta)$  obtained by means of the above mentioned theoretical method and we receive the parameters' estimates.

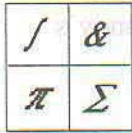
In the constructed example  $n=200$  i.e. we have 200 pairs of values  $(\xi_i, \eta_i)$ . According to  $\xi_i$  values we solve the integral equation thus receiving the following values of  $g(x)$ :  $(-2.7, 0.01), (-2.1, 0.09), (-1.5, 0.12), (-0.9, 0.19), (-0.3, 0.35), (0.3, 0.26), (0.9, 0.20), (1.5, 0.19), (2.1, 0.10), (2.7, 0.03)$ .

Further in compliance with  $\eta_i$  values the likelihood function is constructed. Maximization of likelihood function is done on a computer (Matlab, Optimization Toolbox,  $f_{\min}$ ). Results are  $a=0.9839$ ,  $\sigma=3.00679$  (in our artificial example  $a=1.0$ ,  $\sigma=3.0$ ). The results of computations are quite satisfactory.

We are kindly thankful to A.Zhuzhunashvili for the help.

### References

- [1].Ревишвили Л.В. Оценка априорного закона распределения. Тр. Института прикладной математики ТГУ, т.1,Тб.,1966,стр.127-130
- [2].Ревишвили Л.В. Оценка априорной плотности распределения методом регуляризации А.Н.Тихонова. "Сообщения АН ГССР",Тб.,86, №I,1977,стр.41-44.
- [3].Ревишвили Л.В. Оценка априорной плотности распределения методом регуляризации А.Н.Тихонова. Информационный бюллетень осФАП,7(51),1982,стр.55
- [4].Ревишвили Л.В. О двумерной задаче регрессии, когда обе переменные наблюдаются. Тр. Института прикладной математики ТГУ.,т.1,Тб.,1969,стр.131-136



## Heterogeneous Biological Systems

**Liana Andriadze**

*Institute of Cybernetics*

Important sphere of biological investigations is connected with study of mechanisms of collection and work of information from outside area with living systems. Such functions execute organs consist of different kind of receptors and analysators. Their functional variety is conditioned by special structural properties of their composite membranes, which determine passive and active transport, generation of excitation, bioenergetics of cell etc. And physiological process, as nerve impulse transference contraction of muscles, optic perception proceed by agreement of interaction of many structures. Only due to of natural and artificial achievements of molecular biology in membrane structures is possible intensification of research in receptor and analisator's sphere.

As example of application of biological principle of receptors action in technical systems by building miniature sensibility sensors different signals are following: acoustic, thermal, electrical, optical etc.

Biosystem exists and functions based on the refined balanced molecular interaction in heterogenic medium. Biological phenomena in whole cell is determined of electron conformational processes which are developing on the molecular level, on the level of lipoprotein's complex.

In all membranes phosphalipids is obligatory component and membrane's property in important step are defined of phospalipids entering in her composition. Micelles structure made by phosphalipids and interaction of this micelles with proteins has foundation meaning for construction of membrane's

Phosphalipids entering in membrane's construction, belong to group of natural surface active materials and can exist in special liquid crystal structure. This structure capable for different structural transitions and they have now important role in cell's function.

Unbroken proceeding structural changes of lipid components of lipoprotein complex of membrane may be, possible consequence of change chemical nature of their lipid molecules. They call conformation changes of protein component, which bring on change of her biological activity.

High degree of organization and continuous of structural changes of lipoprotein formations make difficult direct research in such systems. Therefore where interaction of components such systems worth while study on simple model's systems. Liposomes can be such model as one of liquid crystal state of phosphalipides, as structure made on spherulites type, which is obtained by mixture phosphatides with water.

Interaction of liposomes with proteins now studies very intensive. Phospatide as more complicated substance of lipids own faculty have high possibility of orientation on protein molecules. Twisted in water solution molecule of enzyme can not show all her potential activity, which it discovers unfolding on surface of phosphalipide micelle.

Modeling of fermentative kinetic in lipid water systems help us understand passage of chain of biochemical reaction of metabolism in heterogeneous condition of cell, where paramount role has space rapprochement enzymes and substrate.

By influence of phospatide liposome, detergent oxidants and reductors, two and three components liposome on activity of glikolitic ferment aldolase we want study one from

possible ways of regulation of this enzyme by participation phosphalipides of membrane. Enzyme's interaction with natural surface-active phosphatides made in heterogeneous condition, where is having also influence of division surface.

We obtained liposomes from phosphatidylcholin of cattle's brain, eggs and soy. In structure of two and three components liposomes were entered ganglioside and cholesterol. Enzyme aldolase was obtained from the rabbit's muscles.

Electromicroscopic studies show that liposome and proteoliposomes are on form spherullite, often they form united system of membranes layer. Liposomes-spherulites present discrete partially aggregated bodies 10 nm in size, composed by concentric layers, which have a dimension of aproximately 4 nm and periodicity of about 7nm. After desintegration by sonar influence creates close by size particles which after addition the protein, stand more densitive and discrete. Fig. (1,2) [1,2].



Fig.1. Liposomes. Phosphatidylcholine from brain PH 7,0 X 170.000

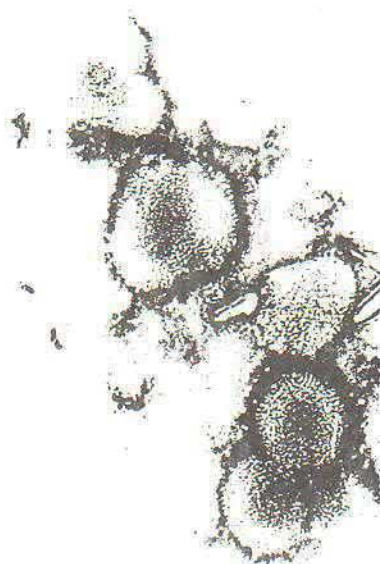


Fig.2. Proteoliposomes. Phosphatidylcholine from eggs PH 7,0 X 170.000

Obtained proteoliposomes perhemental activity of protein depended on state of lipide's component. By tight contact of proteins with lipides between them easily proceed oxiden-reduce reaction. By oxigenation lecithine in proteoliposomes changes her redox-potential and by contact with protein changes conformation of enzyme and passage actively oligomer in dimmer and monomer form [3]. Oxidized and in non-oxidized lipides in

proteoliposomes differently influence on activity of aldolase. Non-oxidized form of lipids increases activity of protein, when the oxidized form inhibites her [4,5].

Phospholipide liposome are natural substances for organism and by entering them into the organism they take part in metabolism and do not accumulate: and do not provoke toxikal and allergical reactions.

We have obtained liposomes with ferromagnetic particles - magnetocontroler liposomes, which can be controlled from out with outer magnetic field [6]. In magnetoliposome we put in biological active materials from medical herbs: kalanchoe, plantain.

Now, liposomes are very successful model of membrane for study and change of biological objects. The foundation of this is that, that their various composition in sizes and other parameters, determining variety of possible interaction of liposomes with cells. Investigation of heterogeneous biological systems are perspective for biocybernetics, biochemistry, biophysics and for practical medicine as well.

### References

- [1]. Andriadze L.I., Shtein-Margolina V.A., Serebrovskaia KB., Oparin A.I., Jour. evol. biochemistry and physiol. XI v, 333-339, 1975.
- [2]. Andriadze L.I., in collect. liposomes and their interaction with cell and tissue, M. science 143-152, 1981.
- [3]. Andriadze L.I., inf. ASGR, biological serie, v. VI, N4, 299-305, 1980.
- [4]. Andriadze L.I., inf. ASGR, biological serie, v. XIII, N6, 390-395, 1987.
- [5]. Andriadze L.I. in collect. 'Biocybern, Bioph.', Tbilisi, Mecniereba, 51-59, 1988.
- [6]. Akhalaya M. Kakiashvili M. Perel'man M. "Medico-biological effects of influence of ultradispersive magnetite results and perspectives,, Tbilisi Collections of reports. Georgian symposium for projet development and conversion. May 15-18, 244-246, 1995.

Fig. 1. Liposomes Phosphatidylcholine from brain PH 7.0 X 170.000



Fig. 2. Proteoliposomes Phosphatidylcholine from eggs PH 7.0 X 170.000

Obtained proteoliposomes pharmaceutical activity of protein depends on state of lipide's component. By tight contact of proteins with lipides between them easily proceed oxidize-reduce reaction. By oxygenation lactate in proteoliposomes changes her redox-potential and by contact with protein changes conformation of enzyme and passage activity oligomer in dimer and monomer form [3]. Oxidized and in non-oxidized lipides in



## Selection of Artificial Parameters for Unsupervised Object Classification

Makvala Kuridze, Viola Jikhvashvili  
 Institute of Cybernetics

In the problem of unsupervised pattern recognition, in distinction from the pattern recognition with learning, initial information is given by such object descriptions for which the classes these objects belong to are not known beforehand [1,2]. For that reason it is necessary to carry out the object classification in advance.

Let us suppose that  $Q = \{Q_i\}$ ,  $i = \overline{1, N}$  is a set of objects and  $G = \{G_i\}$  - the set of the corresponding object descriptions. The object descriptions may be represented in the following manner:

$$G_i = \{q_{1i}, q_{2i}, \dots, q_{mi}\}, \quad (1)$$

where  $q_{ki}$  is the  $k$ -th parameter value in the  $i$ -th object description. The purpose of the algorithm suggested by us is such previous transformation of descriptions given by (1) which draws together the object descriptions of one and the same class and move apart from each other the object descriptions of different classes. For that purpose it is appropriate to use the artificial parameters. Defining these parameters is considered to be one of the most important problems of the automatized system PRL [3,4]. The artificial parameters are defined by two-fold using balanced incomplete block-designs (BIB-design) and by transforming learning descriptions into geometrical configurations [2,3] during the process of learning.

These parameters show the functional connection that exist between the initial parameters, but are not given clearly in primary descriptions. Let us suppose that  $P = \{p_j\}$ ,  $j = \overline{1, M}$  is a set of parameters, the sequences of values of which compose the learning descriptions for the system PRL. This is the basis on which the artificial parameters are determined. The learning model of the system PRL will select the best different artificial parameters for different types of objects. Let us denote the set of selected parameters for all corresponding types by  $P^* = \{p_j^*\}$ ,  $j = \overline{1, M^*}$ . Our purpose is to choose the best artificial parameters from this set. For each  $j$ -th parameter is defined the following characteristics:

1.  $A_j = n_j / N$ ,

where  $n_j$  represents the number of those types of objects during the investigation of which the  $j$ -th parameter was chosen by the learning model of the system PRL.

2.  $B_j = \max_t \{b_{jt}\}$ ,  $b_{jt} = v_{jt} / V_t$ ,  $t = \overline{1, T}$ ,

where  $v_{jt}$  is the number of those variants in case of the  $t$ -th type of objects in which was chosen the  $j$ -th parameter.

3.  $C_j = \max_t \{c_{jt}\}$ ,  $c_{jt} = \max_k \{r_{jkt} / R_{kt}\}$ ,  $t = \overline{1, T}$ ,  $k = \overline{1, v_t}$ ,

where  $r_{jkt}$  is for the  $t$ -th type of objects such maximal number of descriptions which include the codes, corresponding to the maximal informativity features (MIF), but  $R_{kt}$  denotes the number of object descriptions of the corresponding class. MIF is called such features, which characterize objects of only one class (4).

$$4. \quad D_j = \max_t \{d_{jt}\}, \quad d_{jt} = \max_k \{m_{jkt} / M_{jkt}\}, \quad t = \overline{1, T}, \quad k = \overline{1, v_t},$$

where  $m_{jkt}$  is in case of  $t$ -th type objects the maximal number of MIF codes corresponding to the  $j$ -th parameter in the  $k$ -th variant, but  $M_{jkt}$  is the common number of the  $j$ -th parameter for the  $t$ -th type of objects.

If we consider  $A_j$  and  $B_j$  as  $X_j$  vector components, then the normalized length of this vector is called the first main characteristic of the parameter  $P_j$ . Like the first main characteristic, by the third and the fourth characteristics defined the second main characteristic  $Y_j$ .

By using the vector-optimized method of choosing [5] and the main characteristics  $X_j$  and  $Y_j$  the best artificial parameters are determined. For the weight of the  $j$ -th artificial parameter is considered the normalized length of vector determined by the characteristics  $X_j$  and  $Y_j$ .

$$\phi_j = \sqrt{(X_j^2 + Y_j^2)} / 2. \quad (2)$$

This is the way the artificial parameters are selected. The statistic shows that the number of artificial parameters is large. That's why it is advisable to divide the set of the selected parameters by groups and use them separately. The parameters the weight of which meet the following criteria

$$\phi_j \geq \gamma, \quad 0.5 < \gamma < 1$$

are called admissible parameters. Let's mark such parameter set by  $P'$ . For formation of the artificial parameter groups  $B_t$ ,  $t = \overline{1, b}$  by the elements of the set  $P'$  is chosen a BIB-design i.e. a configuration of type  $(v, b, k, r, \lambda)$  [6], parameter  $k$  of which must satisfy the condition  $k = \text{card} B_t$ , where  $B_t$  is a block of a BIB-design. If  $k < \text{card} B_t$  the correction of the blocks must done on the basis of the initial parameters. This will give us a possibility to consider the initial and artificial parameters simultaneously. It is a possibility that the parameter pairs the weights of which are defined by formula (2) will be admissible. According to this formula each component corresponds to the parameter pairs. In this case both of the parameters will be admissible. It is obvious that both of them participate together at least in one variant. A BIB-design guarantees this. If the parameter pair is admissible the each parameter in it is admissible as well and the weight of both of them will grow. The weight of the blocks will be estimated by using the weights of parameters.

$$\phi(B_t) = \sum_{j \in \{j | P_j \in B_t \subset P'\}} \phi_j / k,$$

where  $k$  is a number of block elements. On the basis of these weights the blocks that will meet the following criteria

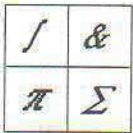
$$\phi(B_t) \geq 0.75$$

will be chosen.

As BIB-design is composed by the set  $P'$ , the  $b$  number of variant of set descriptions is received, where the initial descriptions given in the form (1) are written in the selected artificial parameters.

#### References

- [1]. J.Tou, R.Gonzalez. Pattern Recognition Principles. Mir. M.1978. (Russian).
- [2]. N.Tkemaladze. Some Problems of Pattern Recognition and Experts Systems. Intellect. Tbilisi. 1998. 42-49. (Georgian. Russian and English annotations).
- [3]. N.T.Tkemaladze. Recognition, Classification, Estimation. Mecniereba. Tbilisi. 1990. (Russian).
- [4]. N.Tkemaladze. Bull. Georg. Acad. Sci. 159, 1. 1999. 42-44.
- [5]. M.A. Aizerman, A.V. Malishevsky. Automatics and Telemechanics. N2. 1981. 65-83. (Russian).
- [6]. M.Hall. Combinatorial Theory. Mir. M. 1970. (Russian).



## Expert System of Class Formation

**Mzia Menabde, Meri Khanjalashvili, Eteri Buchukury**

*Institute of Cybernetics*

A set of objects  $Q = \{Q_i\}$ ,  $i = \overline{1, N}$  is given. It is represented by sum of the unlapped object subsets (classes)  $Q = \coprod S_k$ ,  $k = \overline{1, n_k}$ . Let's call this kind of set  $Q$  divided by classes the primary classification. As an additional information we may have  $G = \coprod S'_k$  - set of the descriptions corresponding to the objects of the set  $Q$  or other information about classes. It is necessary to unite the classes in-groups  $T_l$  according to the certain purpose or feature that the following conditions must be met:

- $Q = \coprod T_l$ ,  $l = \overline{1, n_l}$ ,  $n_l < n_k$
- $T_l = \coprod S_{l_i}$ ,  $i = \overline{1, n_l}$ ,  $1 \leq n_l < n_k$

The knowledge base by the multiple dialogue with the experts is formed. These are the sequences of specially ordered classification variants (CV)  $W = \{W_j\}$ ,  $j = \overline{1, n_w}$  ( $j$ -th index of which is a code of the corresponding classification variant) and the groups of these variants  $V = \{V_l\}$ ,  $l = \overline{1, n_v}$ . The classification variants must meet the conditions (1).

The  $i$ -th expert  $i = \overline{1, n_e}$  orders codes of classification variants by preference in a lineal or matrix regime. The matrix regime is more appropriate in the case when the number of the variants  $n_w > 4$ . In this case each expert orders the classification variant codes according to the block elements of BIB-design [1]. In both regimes the row ordered by the  $i$ -th expert is represented as follows:

$$N_{i1} \Omega_{i2} N_{i2} \dots \Omega_{in_w} N_{in_w},$$

where  $N_{i\alpha}$  is a classification variant code and  $\Omega_{i\alpha} \in T(\omega)$ ,  $T(\omega) = \{\omega_\alpha\}$ ,  $\alpha = \overline{1, n_\omega}$  is the term-set, which represents the preference degrees [2].  $n_\omega = 5$  in our case. On the term-set  $T(\omega)$  is determined the numerical function

$$R(\omega_\alpha) = (n_\omega - \alpha) / (n_\omega - 1),$$

which is the estimation function of preference degree of  $\omega_\alpha$ .

By this function expert system (ES) determines the deviation function

$$r_i(W_j) = \sum_{l=1}^l R(\Omega_{il}). \quad (2)$$

The  $i$ -th expert uses this function to estimate the preference degree of the  $j$ -th CV. In (2)  $l$  is determined by the condition  $N_{il} = J$ .

The ES determines also the normalized weight function [3]

$$P_i(W_j) = (\rho - r_i(W_j)) / \rho,$$

where  $\rho = \max_{i,j} r_i(W_j) + \varepsilon$ ,  $\varepsilon > 0$  any small number and

$$f_1(W_j) = \frac{1}{n_e} \sum_{i=1}^{n_e} P_i(W_j), \quad (3)$$

which is a joint estimation of the  $j$ -th CV.

The multiple dialogue with the experts permits to precise the joint estimation of classification variants. Besides (2) the ES determines joint estimation of elements of set  $V = \{V_p\}$ . For estimation of the group  $V_p$  by the  $i$ -th expert is used the sequence  $\{\beta_{ip}^k\}$ ,

$k = \overline{1, n_\beta}$ , where  $n_\beta$  is the number of dialogues (in our case  $n_\beta = 3$ ).

$$\beta_{ip}^k = \begin{cases} 1, & \text{if the } i\text{-th expert has named the } p\text{-th group in } k\text{-th dialogue.} \\ 0, & \text{otherwise} \end{cases}$$

Let's define the function

$$\varphi_i(V_p) = \left( \sum_{l=1}^{n_\beta} 2^{n_\beta-l} \beta_{ip}^l \right) / \sum_{l=1}^{n_\beta} 2^{n_\beta-l}.$$

This function presents the normalized estimation of the group  $V_p$  by the  $i$ -th expert. By using this function is determined the joint estimation of the group  $V_p$

$$F(V_p) = \frac{1}{n_e} \sum_{i=1}^{n_e} \varphi_i(V_p). \quad (4)$$

After this the function

$$f_2(W_j) = \frac{1}{n_j} \sum_{l=1}^{n_j} F(V_l^j) \quad (5)$$

will be considered as the second component of the joint estimation of the CV  $W_j$ . In the formula (5)  $V_l^j$  is the  $l$ -th group of the CV  $W_j$ ,  $n_j$  is a number of the groups in the  $j$ -th CV.

By means of the components  $f_1$  and  $f_2$  the final joint estimation for the classification variant  $W_j$  is determined by the formula

$$f(W_j) = \sqrt{(f_1^2(W_j) + f_2^2(W_j)) / 2}.$$

The best classification variant  $W_{j_0}$  is determined by the condition

$$f_{j_0} = \max\{f(W_j)\}.$$

Furthermore, the ES estimates the competence of experts as well. For this ES besides the other components [3], as an additional component, uses the function

$$\psi_i(W_j) = \sum_{l=1}^{n_{ij}} F(V_l^{ij}) / \sum_{l=1}^{n_j} F(V_l^j),$$

where  $V_l^{ij}$  is the  $l$ -th group named by the  $i$ -th expert at the final dialogue in the  $j$ -th CV  $n_{ij}$  is a number of the groups in the  $j$ -th CV, named by the  $i$ -th expert,  $F(V_p)$  is determined by the formula (4), but  $V_l^j$  and  $n_j$  have the same mean as in formula (5).

## References

- [1]. M.Hall. Combinatorial Theory. Mir. M. 1970. (Russian).
- [2]. N.T.Tkemaladze, M.Menabde, V. Jikhvashvili. Some Problems of Pattern Recognition and Expert Systems. Intellect. Tbilisi. 1998. 50-57. (Georgian. Russian and English annotations).
- [3]. T.Tkemaladze. Recognition, Classification, Estimation. Mecniereba. Tbilisi. 1990. (Russian).



## The mechanism and function of pacemaker potential

**Besarion Partsvania**  
*Institute of Cybernetics*

Specific class of neurons was researched – so called pacemaker neurons. Pacemaker neurons can be divided into two main classes: actual and latent neurons. Actual neurons are background actives. They generate impulses rhythmically. Generally latent neurons are silent. They become activated if a stimulus is applied to them.

It was repeated the experiment of neuron's complete isolation and was confirmed that in such cases, pacemaker neuron retains background activity. This activity is a result of the existence of pacemaker potential. The experiment proved that pacemaker potential is neuron's internal feature and is not connected to synaptic input.

Neuron's pacemaker activity was studied. It is a result of existence of pacemaker locus on the neuronal membrane. Pacemaker locus was investigated. It is located on the membrane segment between soma and axon. It was shown, that density of calcium ion channels on this area is higher than their density on the apical segments of membrane.

Was established that some of latent pacemaker neurons represent so-called command neurons. The control of animal's some simple behavioral processes is realized by these pacemaker neurons. For instance, defensive reaction of mollusk "Helix Pomatia" is controlled by single pacemaker neuron.

Was studied the process of habituation and facilitation in different types of neurons. Mechanism of these events for pacemaker neurons differs from the mechanism of synaptic habituation or facilitation. Their dynamics and temporary development are also different. First of all, in the neuron habituation or facilitation takes place on the pacemaker level. The synapsis are involved in these processes later. Besides this, habituation or facilitation depends on the stimulus parameters. It was shown, that habituation and facilitation play great role in main control processes.

Researches show, that pacemaker potential is an amplifier of synaptic inputs. One and the same stimulus causes weak reaction in common neuron, while, this stimulus switches on long-term pacemaker activity in pacemaker neuron.

In terms of intracellular stimulation of latent pacemaker neuron, it was shown that neuronal response corresponds to the parameters of stimulus. This event may be regarded as information coding by means of pacemaker potential.

The frequency plasticity of pacemaker neuron was revealed. During the rhythmic stimulation of pacemaker neurons, plastic modification of neurons own frequency takes place. When stimulus frequency is much lower than neuron's own pacemaker frequency, neuron perceives each stimulus as separate one and responds to each of them with phase binding. When the stimulus frequency is increased, but is still less than neurons own pacemaker frequency and changes plastically and becomes coordinated with stimulus frequency. When stimulus frequency is higher than neuron's own pacemaker frequency, in this case plasticity is expressed in filtration effect, when neuron responds only on the part of stimulus.

Besides, the influence of some biological active substances on the neuron bio-electric activity was studied. For instance, action of ethyl spirits, insulin and some peptides on the neuronal activity was investigated. Ethyl spirits in low concentration improves neuronal activity, while, in high concentration it inhibits this activity. As for insulin – it inhibits

neuronal activity.

Now we investigate the influence of high frequency electromagnetic radiation on the neuron's bio-electrical activity. The results show that this radiation suppresses neuronal activity.

The object of investigation is mollusk neurons system or the single neuron isolated from this system. Choice of this object was conditioned by acknowledged opinion, that processes that take place in neuron's system of mollusks are relevant models of the processes in vertebrate animal's neuron's system.

The following methods were used in the experiment: 1. Microelectrode technique. 1,2 or 3 microelectrodes were immersed in the neuron, depending on the experiment requirements; 2. Potential clamp method; 3. Patch clamp at non-complete contact.



## Photo- and Thermo-sensitive Systems

**Kokhta Japaridze, Zaza Elashvili, Jimsher Maisuradze,  
Lali Devadze, Nino Sepashvili**  
*Institute of Cybernetics*

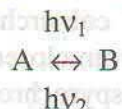
One of the main problems of contemporary science and techniques is to produce such substances and systems, which under influence of external factors (electric, magnetic, thermal and acoustic fields, mechanical influence, electromagnetic radiation, orientating substances and others) change characteristics. Especially interesting are systems with reversible changed characteristics, applied in solving the problems related with recording, representation and processing of information.

High-sensitive reversible systems attract an interest of many scientific centers and firms of world.

In the past century the attention of scientists were attracted by compounds being colourless or slightly coloured became coloured under sunlight radiation but in darkness spontaneously return to initial position. This reversible colourchanging was called as photochromism and compounds- photochroms.

Later it appeared that different organic and inorganic compounds have photochromic properties.

The photochromic transformation is accepted to represent as inter transition between two states of photochromic compounds-A (coloured) and B (colourless)



Photochromism can be determined as reversible photoinduced transition of compounds from one stable state to the other, which is accompanied with absorption spectra changes.

The ability of photochromic compounds to reverse colour, provides the possibility of their application in many areas of science and techniques. One of the important applications of photochromic materials is creation of fixer and optical information accumulators.

For special aims successfully applied materials are those which possess a number of advantages in comparison with ordinary photomaterials (cheapness, high resolution and so on).

Especially interesting are photochrome materials, which without developing a film are able of multiple "recording" and "deleting" the information by light.

In spite of that phototransformation of photochromical compounds occurs with quantum yield less then one and to obtain the image with suitable contrastivity it is required a fairly great doze of light energy (0,01-0,2 j/cm<sup>2</sup>), the sensibility reached to our days is quite enough for major tasks.

The most convenient form for application of reversible photosensitive materials is transparent polymer film containing photochromic compounds. As distinguished from usual photomaterials they have very high-resolution ability – above 1000 line/mm. Furthermore they allow to obtain from original both - positive and negative image at will.

Photochromic films as distinguished from usual photomaterials keep substances in molecular dispersion state. The development of film in usual sense is not presented here, the

image appears in consequence of molecular transition from visible light "transmission state" to the "absorption state" that is coloured state or alternatively-from "absorption state" to the "transmission state".

The photochromic materials are successfully applied to holographic recording of information [1]. The regeneration of initial information occurs by means of rays, wavelength of which coincides with coloured film absorption maximum. These rays are photoactive and cause bleaching of films, therefore when reading off it takes place certain paling of image (but there are such materials, which do not bleach while reading).

Among variety of photochrome materials the spirochromens hold a prominent place.

The investigation of spirochromens is of significant interest, because among other types of photochromic compounds they differ by high sensitivity and show photochromism in solution as well as in polymer materials, which are available for practical utilization.

In spite of numerous investigations, which throw light on various aspects of phototransformation mechanism, the structure and nature of colourless and coloured forms of spirochromen, many questions are still open.

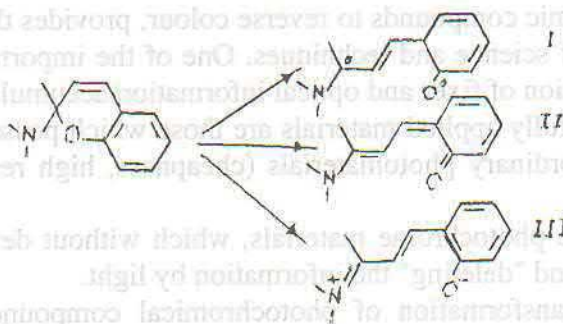
We managed to observe spirochromen photochromism in amorphous and crystalline state, which allowed elucidating some questions about coloured form's structure of those compounds.

More than 200 compounds were synthesized as part of the study which made it possible to watch the influence of substitutions and solutions on thermodynamics, kinetics and spectral characteristics and also to clear some questions on chemical and photochemical stability of given spirochromens.

Exhibition of photochromical properties in amorphous and crystalline states and also obtaining compounds with increased sensibility and solubility made it possible to observe IR and PMR spectral alternations during photoinduced colour changes.

The subject of photosensitive materials remains one of the important directions of the Institute of Cybernetics from its foundation and observed results are admitted as an original [2-33].

For the better understanding of colourchanging nature in spirochromens let us consider energy balance when transiting from closed to open form without going into details of molecular structure. Let us assume that spirochromen molecule during C-O bond breaking can turn into one of the following states:



The formation of biradical (1) is related to C-O bond breaking, energy of which can be assumed as 75 k-cal/mol (the energy of C-O bond in ethers). However the interaction of noncoupled electrons with  $\pi$ -electron molecular system can bring to extra stability to about 10-15 k-cal/mol. As a result the formation of biradical (configuration of which is near to initial molecule) from spirochromen requires the spare of about 60-65 k-cal/mol. Obviously this biradical has short lifetime and can not determine colour of spirochromen solution at usual conditions. Actually neither by chemical methods nor by EPR spectra can be proved the existence of biradicals in coloured form.

The chinoide form (II) is energetically approximately at 15-20 k-cal/mol higher than closed structure (when calculating by data of bond break and formation of bond, taking into account stability energy losses in benzene ring and the increase of conjugation of molecule's  $\pi$ -electron system). The energy of zwitterion (III) formation calculated by the additive scheme is higher than for biradical and chinoid forms. However if consider the interaction possibility of groups between each other, with groups of neighbor molecules and with solvent molecules, then it seems reasonable to give the preference to ionic form.

It is necessary to underline the role of solvation and association energies in the thermochromic spirochromens. Generally accepted schemes of thermo- and photochromizm do not reflect this, it produces an impression that the colour formation is the property of isolated molecule. In fact the energetical difference between coloured and colourless forms of molecule is so great, that it is difficult to imagine the presence of appreciable amount of coloured form in the state of equilibrium with colourless form.

Let us try to estimate the salvation energy of spirochromens in polar (ethanol) and nonpolar (toluene) solvents.

By way of example we consider 6-nitrosubstituted indolinspirochromen.

Denoting by A colourless form and by B coloured form of spirochromen



Where  $\Delta H_0$  is the difference of isolated molecule enthalpy for B  $\rightarrow$  A transition



Where S is solvent, W- salvation energy,  $\Delta H$ - difference of enthalpy when bleaching of solvateted molecule. From (2), (3) and (4) it follows:



The comparison with (1) results:



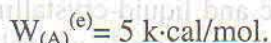
For ethanol (e) and toluene (t):



From (6a) and (6b) is got

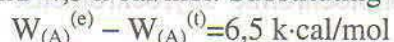


Taking into account that spirochromen's closed form is "ordinary" organic compound, structure of which is arranged in the framework of organic chemistry classic conception, the difference between salvation heats can be equated to the colouring process (A  $\rightarrow$  B) activation energy difference in ethanol and toluene. For nitroderivative indolinospirochromen this difference equals to 4 k-cal/mol. It is interesting to note that according to data [34], the difference in energies in photoactive triplet state in ethanol and toluene in the same compound is 5,7 k-cal/mol. Therefore it is sure that closed form of spirochromen in ethanol is stabilized by ~4 k-cal/mol stronger than in toluene. The salvation energy of organic molecules in such inert solvents as toluene is ~1 k-cal/mol. Thus we can write



This value of salvation energy may seem great, but taking into account that ethanol can generate hydrogen bond with oxygen and nitrogen atoms of spirochromen, the energy confirming with each of them will be on an average 1,8 k-cal/mol.

The thermal effects ( $-\Delta H$ ) of B  $\rightarrow$  A process in ethanol and toluene accordingly are equal to 2 k-cal/mol and 4,5 k-cal/mol. Substituting these data into(7), we obtain



From (6a) and (6b) follows



and  $W_{(B)}^{(0)} = - (3,5 + \Delta H_0) \text{ k-cal/mol}$

The spectral analyze of the mentioned above materials in gaseous condition shows that at temperatures 200-250<sup>0</sup>C the equilibrium is practically shifted to colourless direction. The simple estimation shows that  $\Delta H_0 < -8$ .

Then

$W_{(B)}^{(e)} > 11 \text{ k-cal/mol}$   
and  
 $W_{(B)}^{(0)} > 4,5 \text{ k-cal/mol}$

These estimations were obtained at assumption that spirochromen molecule' s opened form has the same structure in both solvents and energy deficit is partly covered by solvation energy when opening the cycle. In the case of ethanol such a great solvation energy can be explained by generating hydrogen bond and strong polar molecule of spirochromen' s opened form. There are known cases, when solvation energy of strong polar compounds in alcohols reaches 30 k-cal/mol. As for solvation energy in toluene, it's value (>4,5 k-cal/mol) seems abnormally high. It is possible that polar groups of coloured molecules may interact with toluen' s  $\pi$ -electron system and generate something like  $\pi$ -complex, but even for such complex this energy - 4,5 k-cal/mol is too high.

Therefore it may be assumed that in nonpolar solvents the molecules of spirochromens are associated. Only in such case it can be represented the existence of measurable quantity of coloured form molecules in the equilibrium with colourless form. The coupling of molecules having oppositely charged groups obviously can cover energy deficit when opening the cycle. The same conclusion results from following: dipole moments of "coloured" molecules do not differ from "colourless" [35,36].

Solvation, which is expressed in strong influence of solvent nature on the absorption spectra, plays the specific role in polar solvents.

The common considerations on possible structure of coloured spirochromens show that opened form of spirochromen is nearer to zwitterion than to chinoidal or byradical forms. The literature data on bond and conjunction energy in organic compounds make it possible to conclude, that nonassociated or not strongly solvated spirochromen molecule' s coloured form in comparison with molecules with closed form are energetically non profitable. The qualitative considerations and conclusions were confirmed by quantum-mechanical calculations [37].

The nature of sensitiveness of spirochromen' s two states is defined by molecular structure variation under light influence, which is accompanied by system' s physico-chemical property changes. It is possible to alter molecular as well as supermolecular structures by means of external excitors. By such properties are characterized wide class of substances, which possess liquid crystalline phases and can be easily operated by external excitors.

Many investigations were carried out to create photochromale liquid-crystalline photochemically reversible systems combining ability of easy changing molecular and supermolecular structures were carried out.

Considering importance of photochromic and liquid-crystalline substances, it were carried out a lot of studies to obtain effective systems, especially optically active compounds\*, causing formation of specific supermolecular systems. It was synthesized more than hundred optically active compounds with definite geometrical characteristics.

In the framework of investigation of electric field influence on the systems possessing both photochromic and liquid-crystalline properties, there were studied mixtures of nematic liquid crystals (NLC) and photochromic spirochromens. It was expected that

\* By using these compounds it were carried out wide investigations in the Liquid Crystals Optics department of the Institute of Cybernetics.

liquid-crystalline matrix structurization would effect on kinetic characteristics of photoinduced photochrom spontaneous bleaching, thereby leading to understanding field influence on chemical (biochemical) processes proceeding mechanism.

Photoinduced coloured photochroms are known to undergo dark bleaching with definite speed. Speed constant of given spirochromen depends on the solvent and temperature [35].

The bleaching speed constant of spirochromens dissolved in NLC is appeared to be depended also upon the applied electric field. The speed constant increases by enlarging of field.

NLC possess high electrical resistance. Introduction of spirochromens in NLC does not effect on resistance but UV high photoinduction increases the conductivity of mixtures. The value of electric current depends upon the concentration of coloured molecules. NLC including dinitroderivative spirochromens (in which thermodynamical equilibrium is shifted to the coloured form) mixtures, under irradiation by visible rays with reducing the concentration of coloured molecules increases the resistance.

It is necessary to note that local heating by electric current and also electrochemical destruction (which could contribute the increasing of bleach speed constant) are excluded in present experiment conditions.

The influence of electric field (~ tens of kv) on indoline spirochromens mixtures was investigated [38]. On basis of experimental data authors concluded that under UV light photoinduction dimers and agglomerates are generated in mixtures. The falling out of A and B ions from agglomerates takes place when applying the electric field. It was more likely falling out of A ion, as on anode is precipitated coloured powder whereas cathode is remained colourless. Electric conductivity of spirochromen salts coloured mixtures and its dependence on incident rays intensity were investigated [39].

The increase of electric conductivity when bleaching mixture by visible rays the authors connect with formation of mobile  $H^+$  ion instead of less mobile spirochromen cation. Therefore electric conductivity of colourless form is less than coloured one.

The coloured form of spirochromen represents zwitterion, which during ionization forms system with opposite charges, as distinguished from ordinary ionogens. Thus "ion" with opposite charges on each side is joined by chemical bond. This system due to compensated charge can not move in electric field. If ionradicals are formed in system, naturally electroconductivity is increased. One can suppose that when discharging on electrode, the obtained excess of molecular energy contributes process  $B \rightarrow A$  and increasing of rate constant effective meaning.

The following mechanism is not excluded: if on one end of the molecule is excess of charge resulting from different ionization degree of both parts of molecule, then zwitterion molecule's coloured form moves. This assumption was born out by experimental data. Dinitroderivative spirochromen's electroconductivity is higher than nitroderivative's one. This is related with high polarity of nitroderivative spirochromens.

Thus the variation of spirochromen's bleaching rate is not related with NLC matrix structural changes on applied electrical field. The increase of rate constant is not connected with field effect, but is a result of electric current passing through the system.

The studied mixtures of NLC and spirochromen behave like photoconductors: by UV and visible rays it is possible to regulate the current intensity passing through the system.

Upon the photochrome processes abrupt changes of geometrical as well as electron structure of molecules take place. By incorporation of photochrome material possessing also thermochrome properties, into liquid crystal (LC) matrix with helical substructure, while irradiating and varying of temperature, the change of helical pitch was expected i.e. change of LC system selective reflection spectrum.

With the aim of refining the colour-contrast characteristics of LC systems and thermoindicator films, we intended to investigate the influence of different dopants geometrical and electron peculiarity upon LC systems.

Considering difficulty of finding out the role of photochromic compound molecules two forms of which are able reciprocally to convert during the experiment, we begin to examine the dopants with definite stable geometrical and electron characteristics.

In intermediate states (blue phase, TGB phases) with phase transitions isotrope→chiral→smectic A and C (I→Ch→SmA and SmC) in chiral liquid-crystalline systems are known in certain conditions. This transitional phases exhibit optical properties typical for helical structures.

In present work it was studied the influence of compounds synthesized by us – derivatives of 1-menthol-tigogenin, spyrocompounds and so on, on cholesteric and nematochiral systems near transition Ch→Sm. On investigation of such systems (for example mixture of cholesteriloleat, cholesterilpelargonate and mentioned above compounds of dopants), on samples with thickness 100 μm, regime of cooling, at certain temperature, we observed phase transition, which was accompanied by short-wave shift of Bragg band reflection and noticeable increase (to 100%) of intensity. The phase is temperature-sensitive and exists in narrow range (1-1,5°C). This new state we named as St (strange) phase [40-43]. The generation of new phase was confirmed by microcalorimetric measurements too.

For recognizing compounds forming St phase it were studied mixtures of a series of cholesterilalkanoats  $C_nH_{2n+1}COO$  Chol.  $n=1-9,11,13,17$  with cholesteriloleat and different dopants. In investigated compositions the first five terms of cholesterilalkanoats did not form St phase. In cholesterilalkanoats with middle radical length ( $C_5-C_{10}$ ) it was observed St phase formation. This phenomenon is related with the absence of smectic phase in the first five terms of homological range cholesterilalkanoats and their mixtures with cholesteriloleate. Cholesterilalkanoats with middle radical length side by side with cholesteric phase have also smectic phase and their mixtures with cholesteriloleates are smectogenic. Therefore smectogenicity of matrix together with chirality is necessary but insufficient for St phase forming.

Alkanoats with radicals higher then  $C_{10}$  in spite of their smectogenicity, in mentioned above conditions do not generate St phase. Apparently it is due to great twist power of spiral (i.e. short pitch) and high smectogenicity.

Addition of nonsmectogen cholesterilchlorid with right spiral to smectogenic cholesterics with left spiral can cause the reduction of smectogenicity and weakening of twist power (i.e. increasing of pitch). The result appeared positive: by adding 10-15% of cholesterilchlorid in the mixture of cholesterilalkanoats with radical  $> C_{10}$ , cholesteriloleate and 0,25-3% of 1-menthol derivatives, formation of St phase was observed in certain conditions.

The systems studied by us contain bent and volume molecules [44]. Bent molecule is cholesteriloleate, radical of which has cis-configuration. To show up the role of bent fragment in the formation of St phase, cholesterine ester of elaidin acid was synthesized. The elaidin acid ( $C_{17}H_{33}COOH$ ) is trans isomer of olein acid and by geometry is near to stearin acid. It was expected that by substitution of cholesteriloleate for cholesterilelaidinate mentioned above mixture would lose the property of St phase formation. However St phase was formed in the mixtures with cholesterilelaidinate, though to find it out appeared to be complicated. Consequently for St phase generation it is enough even slight shift (due to double bond) of elaidine acid radical fragments to each other (0,032 nm). It has been confirmed by following: in the same conditions the substitution of cholesterilelaidinate by cholesterilstearate prevents St phase formation. The generation of St phase prevented also, by adding mentioned above mixtures rigid linear molecules such as alkilcianbifenile.

For full presentation the role of bent molecule on St phase generation, cholesterin ester of linol acid was synthesized. The linol acid  $C_{17}H_{31}COOH$  includes in position 9-12 two double bonds and has cis-cis configuration. St phase formation was observed in mixtures of cholesterillinoleates with other cholesterilalkanoats without bulky molecule dopants. Evidently cholesterillinoleate molecules due to double bent cause so strong geometrical disturbance in LC system that it is no necessary of presence of bulky molecule.

The molecules of unsaturated fat acid have cis-configuration and therefore, bent form. The molecules of l-menthol derivatives include terpen fragment, situated in two plans. In the spirocompounds the fragments are perpendicular to each other. Alongside with steroid skeleton the molecules of tigogenin derivatives include spiran fragment, therefore molecules of all observed dopants have bulky shape. The presence of bent and bulky molecules or fragments in mixtures cause their geometrical incompatibility, consequently, probably elastic bend constant decreases. Whereby arise conditions for generation St phase. It is necessary to note that bulky molecules compounds might be either optically active or not active.

The generation of St phase we observed also in nemato-chiral composition: matrix-p-butoxybenziliden-p-butylanilin (BBBA), dopants - synthesized esters of tigogenin\* [43,44].

On account of experimental data, we propose that in cholesteric and nematochiral mixtures for generation of St phase it is necessary: chirality, smectogenity and geometrical incompatibility of mixture components, also to be apt to formation of tilt structure.

In region of cooling, at certain temperature (T) and wavelength ( $\lambda$ ) which depends on concentration of dopants,  $d\lambda/dT$  changes the sign which points to beginning of St phase formation. The run of process we observed in transmission and reflection regimes. St phase, as well as TGB phases, is formed on the boundary of the transition Ch-Sm. As distinguished from TGB phases, the system in St phase reflects light of any polarization while normal incidence. In case of reflection circularly polarized light, the sign of polarization direction changes, while incidence of linear polarized ray initial polarization is retained. The difference between the intensity of left and right hand circular polarized reflected light decreases and tends to zero, on formation of St phase. Therefore the system in St phase reflects left and right hand polarized identically. If just over the cell with sample is placed linear polarizer, the axis of which coincides with the line of ray sound polarization, then on transition the system into St phase the reflected intensity significantly increases in comparison with Ch phase, that is polarization lines coincide.

In case of left-hand polarized light incident on system in Ch phase (left helix), the reflected light will be also polarized on left- hand circular. Accordingly the same polarizer, giving circular polarization of incident light, will transmit the reflected light. The polarizer in fact gives the coding operation with the incident light. With forming the St phase, in the same conditions, intensity of the reflected light band decreases to zero, that is when reflecting from St phase system the reversion of code occurs, due to the polarizer, which serves as analyzer, blocks the reflected light.

Thus spectral and polarizational investigations indicate the generation of new phase with properties inherent for multilayer system. It makes some difficulty in explaining the nature of new phase in framework of helical structures.

In spite of evidently likeness of St phase optical properties with variable reflection index systems, we propose that we have concerned with unusual helical structure. This proposal is based on structure preceding St phase and rate direction of shift of Bragg reflection band maximum in cooling regime. On achieving certain temperature  $T_{St}$  (Ch $\rightarrow$ St transition temperature) at isothermal conditions, it begins gradual spontaneous forming of St phase, which is followed by shift and rise of Bragg reflecting band intensity. The formation of St phase is completed in 8-10 minutes. St phase is temperature-sensing. Lowering the temperature Bragg reflection band initially shifts to long-wave region ( $d\lambda/dT < 0$ ) then to short-wave region ( $d\lambda/dT > 0$ ).

As a result of equilibrium state the band maximum appears to be shifted to short-wave region. Thus as distinguished from cholesterics  $d\lambda/dT > 0$  in St phase. The kinetic of process shows double influence of temperature on system, which is exhibited in, divided on time long-wave and short-wave Bragg reflection band shift. Red shift occurs nearly three times faster than blue one. The slow process is more effective and in consequence approaching the equilibrium the band appears to be shifted to blue region.

\* Later similar phase was observed in other nematochiral mixture with tigogenin caprate[45].

According to generally accepted presentation of the Gennes [46] in smectogenic cholesterics field generated by smectic clusters near phase transition  $Ch \rightarrow Sm$ , causes helical pitch increasing. Analogous phenomenon observed in systems with positive dielectrical anisotropy when applied electric field perpendicular to helical axis, is explained in the framework of de Gennes and Mayer [47]. As Mayer has shown the application of electric field which is parallel to the helical axis can cause conical deformation [48]. The process is accompanied by shift of Bragg reflection band to short-wave region (blue shift). It is possible when elastic bend constant is far less than elastic twist constant  $K_3 < K_2$ . (As a rule,  $K_3 > K_2$  in liquid-crystalline systems).

We assumed that on drawing near transition  $Ch \rightarrow Sm$ , elastic constant temperature dependence is not same and at certain conditions  $K_3 < K_2$ . It is necessary the existence of components (bent and bulky molecules [49]) favoring decreasing  $K_3/K_2$  ratio in system for this.

The whole complex of mentioned above considerations and facts enable us to suggest that conically deformed system may be generated by means of internal field. This state is not a change of texture but a new phase with particular optical properties not typical for helical systems.

Studying the behavior of system at different angles of incidence of light on the cell shows that Bragg reflection is of first order. Molecular arrangement in St phase can be represented as smecto-like double spiral which is generated by molecules tilted to plain which is normal to spiral axis, at the same angle but in different directions forming the conic structure.

On account of experimental data and generally accepted presentation we propose that near  $Ch \rightarrow Sm$  phase transition when  $K_3 < K_2$ , smectic field at the same time together with untwisting of spiral can cause conical deformation. As a result St phase is generated with unusual for helical structure high coefficient of Bragg reflection at any angle of light incidence and anomalous for helical structure polarizational properties.

### References

- [1]. K.G. Japaridze, J.P. Maisuradze, V.V. Mumladze, N.M. Ramishvili, E.B. Tecaev, V.V. Chavchanidze - *Optica i spectroscopia* XXXIII, 3, 579 (1972) Rus.
- [2]. A.I. Nogaideli, K.G. Japaridze, M.I. Brodzeli, L.V. Devadze, J.P. Maisuradze, E.L. Kercman, M.I. Chubabria - *Bulletin of the Academy of Sciences of the Georgian SSR*, 40, N3, 607, 1965 (Rus).
- [3]. A.I. Nogaideli, K.G. Japaridze, M.I. Chubabria, L.V. Devadze - *ZhOrKh* 3, 75, 1967 (Rus).
- [4]. A.I. Nogaideli, K.G. Japaridze, I.P. Mzhavanadze, L.V. Devadze - *Bulletin of the Academy of Sciences of the Georgian SSR*, 47, N2, 315, 1967 (Rus).
- [5]. G. Balny, K. Djaparidze, P. Douzou - *Comp. Rendus, S. C.* 265, 1149, 1967 (Fr).
- [6]. J.P. Maisuradze, A.I. Nogaideli, K.G. Japaridze - *Bulletin of the Academy of Sciences of the Georgian SSR*, 49, N1, 75, 1968 (Rus).
- [7]. J.P. Maisuradze, A.I. Nogaideli, K.G. Japaridze - *Bulletin of the Academy of Sciences of the Georgian SSR*, 50, N1, 77, 1968 (Rus).
- [8]. K.G. Japaridze, E.G. Akhalkatsi, L.P. Shishkin - *Bulletin of the Academy of Sciences of the Georgian SSR*, 52, N2, 351, 1968 (Rus).
- [9]. Z.M. Elashvili, L.V. Devadze, K.G. Japaridze - *Bulletin of the Academy of Sciences of the Georgian SSR*, 52, N2, 351, 1968 (Rus).
- [10]. K.G. Japaridze, A.I. Nogaideli, J.P. Maisuradze *Avt. Svidetelstvo*, cl.12, r.2, 107, 216730, 1968 (Rus).
- [11]. K.G. Japaridze, E.S. Gomelauri, J.P. Maisuradze - *Bulletin of the Academy of Sciences of the Georgian SSR*, 55, N2, 301, 1969 (Rus).
- [12]. K.G. Japaridze, I.P. Pavlenishvili, M.T. Gugava, J.P. Maisuradze - *Bulletin of the Academy of Sciences of the Georgian SSR*, 56, N3, 577, 1969 (Rus).

- [13]. K.G. Japaridze, I.P. Pavlenishvili, M.T. Gugava, J.P. Maisuradze - ZhOKh, XL1,N3, 582, 1970 (Rus).
- [14]. K.G. Japaridze, Z.M. Elashvili, L.V. Devadze - Bulletin of the Academy of Sciences of the Georgian SSR, 57, N1, 77, 1970 (Rus).
- [15]. L.V. Devadze, Z.M. Elashvili, Ts.G. Khugashvili, K.G. Japaridze - Bulletin of the Academy of Sciences of the Georgian SSR, 58, N3, 585, 1970 (Rus).
- [16]. K.G. Japaridze - " Nekotorie voprosi fotokhromizma v spirokromenakh" Dokladi mezhdunarodnogo kongressa po photographicheskoi nauke, seksia "E",H, 1970 (Rus).
- [17]. K.G. Japaridze, E.S. Gomelauri - Proceedings of the Academy of Sciences of the Georgian SSR, Chemical Series, 2, N2, 1976 (Rus).
- [18]. K.G. Japaridze, I.A. Mzhavanadze- Proceedings of the Academy of Sciences of the Georgian SSR, Chemical Series, 73, N2, 1974 (Rus).
- [19]. K.G. Japaridze, L.V. Devadze - Proceedings of the Academy of Sciences of the Georgian SSR, Chemical Series, 74, N3, 1974 (Rus).
- [20]. K.G. Japaridze, I.I. Pavlenishvili - Proceedings of the Academy of Sciences of the Georgian SSR, Chemical Series, 1, N2, 1976 (Rus).
- [21]. K.G. Japaridze, N.I. Mamistvalova - Proceedings of the Academy of Sciences of the Georgian SSR, Chemical Series, 62, N1, 69, 1971 (Rus).
- [22]. K.G. Japaridze, I.A. Mzhavanadze- Proceedings of the Academy of Sciences of the Georgian SSR, Chemical Series, 63, N2, 325, 1971 (Rus).
- [23]. K.G. Japaridze, I.A. Mzhavanadze- Proceedings of the Academy of Sciences of the Georgian SSR, Chemical Series, 62, N3, 585, 1971 (Rus).
- [24]. K.G. Japaridze, J.P. Maisuradze, G.G. Gachechiladze, E.S. Gomelauri - Kh.G.S. 775, 1971 (Rus).
- [25]. Z.M. Elashvili, K.G. Japaridze - Zh.G.S. 1491, 1971 (Rus).
- [26]. J.P. Maisuradze - Kand. dissertatsia, Tbilisi, 1968 (Rus).
- [27]. Z.M. Elashvili- Kand. dissertatsia, Tbilisi, 1968 (Rus).
- [28]. I.I. Pavlenishvili - Kand. dissertatsia, Tbilisi, 1970 (Rus).
- [29]. M.J. Chubabria - Kand. dissertatsia, Tbilisi, 1970 (Rus).
- [30]. E.G. Akhalkatsi - Kand. dissertatsia, Tbilisi, 1971 (Rus).
- [31]. E.S. Gomelauri - Kand. dissertatsia, Tbilisi, 1971 (Rus).
- [32]. L.V. Devadze - Kand. dissertatsia, Tbilisi, 1971 (Rus).
- [33]. I.A. Mzhavanadze - Kand. dissertatsia, Tbilisi, 1971 (Rus).
- [34]. G.I. Lashkov, A V. Shablia - Izv. A.N.SSSR, ser. phiz. t XXXII, N3, 1968 (Rus).
- [35]. K.G. Japaridze - "Spirochromeni" izd "Metsniereba", Tbilisi, 1979 (Rus).
- [36]. J.P. Maisuradze - Doktorskaia dissertatsia, 1997 (Georg.).
- [37]. M.T. Gugava, K.G. Japaridze, I.I. Pavlenishvili - Proceedings of the Academy of Sciences of the Georgian SSR, t.15, N2, 1989 (Rus).
- [38]. V.A. Krongauz, A.A. Parshutkin - Photochemistry and Photobiology. 19, 503, 1972.
- [39]. Takao Nakayama, Isamu Shimizu, Hiroshi Kokado and Eiichi Inoue - Bulletin of the Chemical Society of Japan. Vol 43, N7, 1970.
- [40]. Vashakidze E.I., Japaridze K.G., Zurabishvili Ts.I., Chelidze G.Sh., Elashvili Z.M. - Proceedings of the Academy of Sciences of the Georgian SSR, Chemical series, t.15, 1989, 15, N3, 225 (Rus).
- [41]. Japaridze K., Vashakidze E., Metonidze M., Sepashvili N., Devadze L., Elashvili Z. - Saertashoriso konpherentsia chimiashi, mokhsenebis thezisebi, 1994, Tbilisi, gv 12 (Georg).
- [42]. Japaridze K.G., Vashakidze E.J., Metonidze M.S., Sepashvili N.O., Devadze L.V., Elashvili Z.M - Proceedings of the Georgian Academy of Sciences, 1996, 22, N1-4, s.97 (Rus).
- [43]. Japaridze K., Elashvili Z., Devadze L., Sepashvili N., Metonidze M. - Bulletin of the Georgian Academy of Sciences, 1999, 159, N1, 90 (Eng).
- [44]. Elashvili Z.M - Doktorskaia dissertatsia, Tbilisi, 1993 (Georg).

- [45]. Chilaia G., Petriashvili G., Chanishvili A. and Sikharulidze D. - Mol. Materials, 1997, 8, 245.
- [46]. P. de Zhen "Phizika zhidkikh kristallov" Moskva, Mir, 1977 (Rus).
- [47]. Mayer R.B. Appl. Phys. Lett. 1968, 12, 9.
- [48]. Mayer R.B. Appl. Phys. Lett. 1969, 14, 208.
- [49]. Gruler H. - J. Chem. Phys., 1974, 61, 5408.

**Figures:**

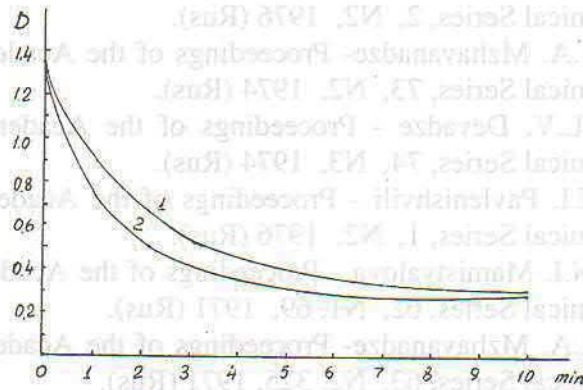


*Fig.1.*

The dark reaction kinetic curves of film. Layer thickness-80  $\mu\text{m}$ .

- 1)  $V=0$
- 2)  $V=15v$

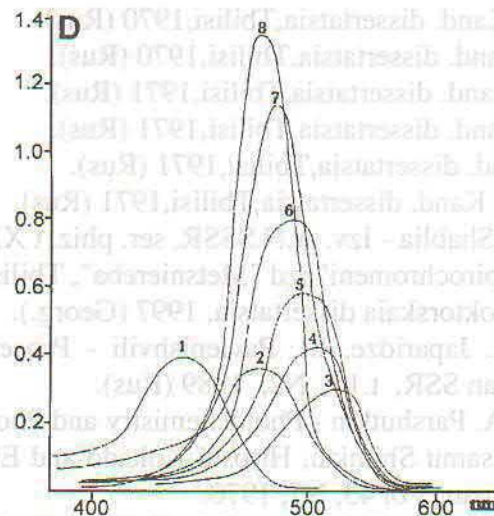


*Fig.2.*

The temperature dependence of Bragg reflection bands corresponding to St phase formation process:  
 1-  $t=31^{\circ}\text{C}$ , 2-  $t=30^{\circ}\text{C}$ , 3-  $t=29^{\circ}\text{C}$  - cholesteric phase;  $t=29^{\circ}\text{C}$  St phase formation  
 $\tau=8\text{min}$ ; (mixture of cholesteriloleate-cholesterilpelargonate 1,8:1 (mass)); 2,5% l-mentil-p-ethoxy-cinnamate as dopant).

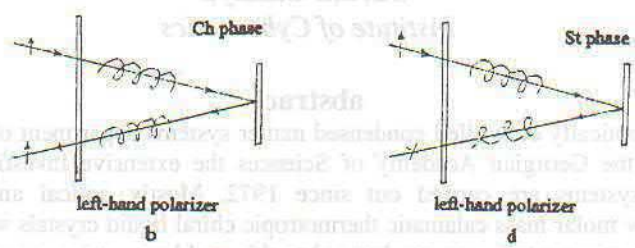
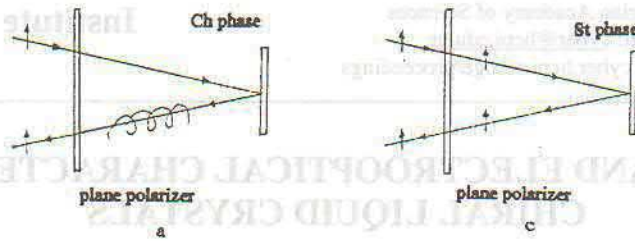


Fig.3

The polarization characteristics of Ch phase (a) and (b); St phase - (c) and (d).

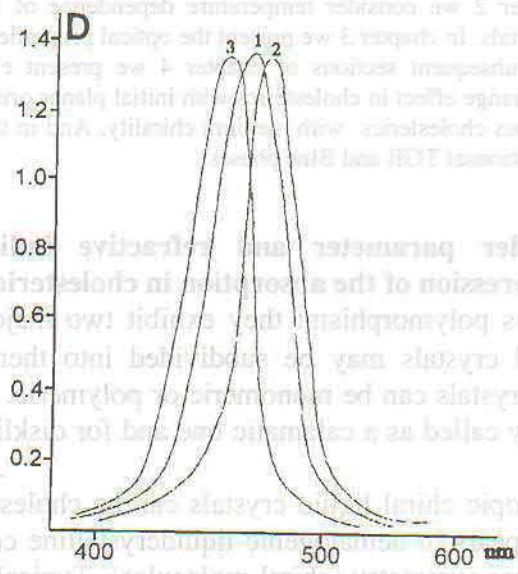


Fig.4

The time dependence of Bragg reflection band corresponding to St phase:

- (1)  $t = 26,5^{\circ}\text{C}$ ; (2)  $t = 26^{\circ}\text{C}$   $\tau_1 = 95$  sec; (3)  $t = 26^{\circ}\text{C}$   $\tau_2 = 775$  sec mixture of cholesteriloleate-cholesterilpelargonate 1,8:1 (mass); 3,5% 1-mentil-p-ethoxy-cinnamate as dopant).

We can consider the cholesteric structure as a special case of a nematic structure when the director  $n$  describes a helix. A nematic LC with a uniform alignment of the director  $n$  behaves like a uniaxial crystal with positive optical anisotropy  $n_e > n_o$  (where  $n_e = n_{||}$  is the reflection index for the extraordinary beam and  $n_o = n_{\perp}$  is the reflection index for the ordinary beam). The optical anisotropy in CLC is negative, i.e.  $n_{e\perp} > n_{e\parallel}$  and  $n_{o\parallel} = n_{o\perp}$  are the refractive indices for the extraordinary and the ordinary beams respectively. The index  $n_{e\parallel}$  indicates that the macroscopic optical axis corresponds to the direction of the pitch axis. If the local nematic refractive indices are given by  $n_x$  and  $n_y$ , the average refractive indices with respect to the helix  $h$  can be written as  $n_{e\parallel} = n_x = n_y = n_o$  and  $n_{e\perp} = (n_x^2 + n_y^2)^{1/2}$ .



## OPTICAL AND ELECTROOPTICAL CHARACTERISTICS OF CHIRAL LIQUID CRYSTALS

Guram Chilaya  
*Institute of Cybernetics*

### abstract

In the optically controlled condensed matter systems department of the Institute of Cybernetics of the Georgian Academy of Sciences the extensive investigation of chiral liquid crystal systems are carried out since 1972. Mostly optical and electrooptical properties of low molar mass calamatic thermotropic chiral liquid crystals were studied. We would like to propose a review paper devoted to this problem, paying a special attention to the results obtained in this department.

In chapter 1 we consider general optical properties of cholesterics: orientational order parameter and refractive indices; induced circular dichroism and suppression of the absorption. In chapter 2 we consider temperature dependence of the pitch in induced cholesteric liquid crystals. In chapter 3 we present the optical properties of chiral smectic C liquid crystals. In subsequent sections of chapter 4 we present electrooptic effects in cholesterics: colour change effect in cholesterics with initial planar orientation; bistability in cholesterics; amorphous cholesterics with medium chirality. And in the last 5<sup>th</sup> chapter we consider two pretransitional TGB and Blue phases.

### 1. Orientational order parameter and refractive indices; induced circular dichroism and suppression of the absorption in cholesterics

Liquid crystals possess polymorphism: they exhibit two major classes- nematics and smectics [1-3]. The liquid crystals may be subdivided into thermotropic and lyotropic. Thermotropic chiral liquid crystals can be monomeric or polymeric. If liquid crystals formed by elongated molecules, they called as a calamatic one and for disklike molecules as discotic liquid crystals, accordingly.

Monomeric thermotropic chiral liquid crystals can be cholesterics and chiral smectic C. The cholesteric phase appears in nematogenic liquidcrystalline compounds which consist of molecules without mirror symmetry (chiral molecules). Typical representatives of these compounds are derivatives of cholesterol. Thus, chiral nematic liquid crystals are generally called cholesteric liquid crystals, although the name chiral nematic is more correct. The cholesteric structure occurs not only in pure chiral compounds, but also in mixtures of achiral nematics with optically active (chiral) mesogenic or nonmesogenic dopants (induced cholesteric systems) [4-9].

We can consider the cholesteric structure as a special case of a nematic structure when the director  $\mathbf{n}$  describes a helix. A nematic LC with a uniform alignment of the director  $\mathbf{n}$  behaves like a uniaxial crystal with positive optical anisotropy  $n_e > n_o$  (where  $n_e \equiv n_{||}$  is the refraction index for the extraordinary beam and  $n_o \equiv n_{\perp}$  is the refraction index for the ordinary beam). The optical anisotropy in CLC is negative, i. e.  $n_{oh} > n_{eh}$ , where  $n_{eh} \equiv n_{||h}$  and  $n_{oh} \equiv n_{\perp h}$  are the refractive indices for the extraordinary and the ordinary beams, respectively. The index  $\mathbf{h}$  indicates that the macroscopic optical axis corresponds to the direction of the pitch axis. If the local nematic refractive indices are given by  $n'_e$  and  $n'_o$ , the average refractive indices with respect to the helix axis  $\mathbf{h}$  can be written as:  $n_{eh} = n'_o$ ,  $n_{oh} = (n'^2_e + n'^2_o)^{1/2}$ .

Precise measurements of the refractive indices of racemic (nematic) and the optically active (cholesteric) form of the *p*-methoxybenzilidene - (*p'* - isopentacil) amyl show, that the refractive indices fulfill this theoretical expectation within experimental error ( $\pm .0005$ ) [11,12] (Fig. 1a and 1b).

The same results for another materials have been obtained by Pelzl [13]. The optical anisotropy of the LC phase is determined by the anisotropy of the polarizability of the molecules and by the degree of their order which is described by the order parameter *S*. The obtained results indicate that the orientational order parameter *S* in a layer of a CLC is the essentially the same as in the nematic phase occurring in the corresponding racemic mixture.

In various cholesteric systems, the period of the supermolecular structure (helical pitch) takes values in a wide range (from 0.1  $\mu\text{m}$  to several hundred  $\mu\text{m}$ ). For short pitch, when the wavelength of light  $\lambda$  and *P* are comparable, a selective reflection in the visible range can be observed. If the light propagates parallel to the helical axis of the planar cholesteric texture, according to the Bragg's law the maximum of the selective reflection is observed at  $\lambda_B = P * n$ , where *n* is a mean refractive index. For oblique light incidence, the Bragg wavelength is given by  $\lambda_B = P * n * \cos \varphi$ , where  $\varphi$  is the incidence angle.

Direct observation of eigen waves dispersion law was observed in cholesteics. The refractive indices for the right and left polarized light -  $n_R$  and  $n_L$  in cholesteric phase of 4-*p*-hexyloxyphenyl ester of 4' (2"- methylbutyl) biphenyl 4-carboxylic acid (CE-3, Merck) was measured by goniometer using the wedge method [14,15] (Fig.2).

The suggest method for determining local refractive indices according to the measurements of eigen wave refraction has a number of advantages.

If a small amount of dye, possessing linear dichroic absorption, is dissolved in a CLC, the helical arrangement transforms the linear dichroism into a circular one. The induced circular dichroism is given by  $D = (I_l - I_r) / (I_l + I_r)$ , where  $I_l$  and  $I_r$  are the light transmission coefficients for left-handed and right-handed circularly polarized light, respectively. Several authors studied Induced circular dichroism [16-21]. It was investigated even for a dye possessing simultaneously both positive and negative dichroism [21]. With the sign inversion of the linear dichroism, the sign of circular dichroism is changed, as well.

The data given in [16-21] were obtained for structures where the pitch was greater than the absorption wavelength of the dye. However, the absorption is suppressed when the wavelengths of absorption and selective reflection coincide. Since the arrangement of the molecules is helical, the absorption of light with the diffracted polarization undergoes an abrupt change near the region of selective reflection. On the short wavelength side of Bragg reflection, the electric vector is perpendicular to the long axis of the molecules, i. e. to the absorbing effective oscillators in dyes with positive dichroism. As mentioned in [17], this effect is analogous in many respects to the anomalous absorption of x-rays (Borrmann effect) that occurs as a result of diffraction in ordinary crystals. Some measurements and the corresponding theoretical works [22-25] show a quantitative agreement between the theory and the experiment [25].

When the pitch of the cholesteric LC is larger than the wavelength of the visible light and if the linear birefringence is also large, it is possible to observe the forward diffraction [26]. For a cholesteric layer between crossed polaroids, the presence of forward scattering is manifested in the form of selective dependence of the transmission coefficients on the wavelength of light. Experimental studies on a well planar oriented CLC with certain parameters confirm the forward diffraction effect [27].

## **2. Temperature dependence of the pitch in induced cholesteric liquid crystals**

The helix pitch is very sensitive to external influences, and in particular it may strongly depend on the temperature. The property of cholesteric liquid crystals to change the reflected color with temperature (due to the temperature dependence of the pitch) is known for a long time, and CLC are successfully used as a thermochromic material. The practical

importance of the application of thermo-optical effect of cholesterics is extensive: medical diagnostics, nondestructive testing, temperature indicators, various detectors, and even in jewelry [28]. A number of new chemically stable thermochromic nematic-chiral mixtures proposed [29-31].

The temperature dependence of the pitch is an advantage for thermometric applications, but it can be a major problem for the use of cholesteric liquid crystals as an electro-optic material. In the latter case, it is necessary to obtain mixtures with operating voltages, which is independent of the temperature. For this purpose, systems with designed pitch-temperature dependence  $P(T)$  are needed.

The temperature dependence of the helix pitch in induced cholesteric phases is quite complex and so far not completely understood. A comprehensive theory of the temperature dependence of helical pitch is yet to be developed. The statistical model for the temperature dependence of the pitch in induced cholesteric liquid crystals was proposed in [32].

Induced cholesteric mesophases formed by nematic liquid crystals (NLC) with optically active dopants (OAD) exhibit, as a rule, a weak increase of helical pitch  $P$  with temperature [33]. For nematic-cholesteric ester mixtures, the slope of the  $P(T)$  curve is also very small. Significant negative values of  $dP/dT$  are obtained only with large amounts ( $\geq 40\%$ ) of cholesteric esters forming the smectic-A mesophase [34]. If smectogenic substance is used as a nematic host, the typical picture of pretransitional phenomena is observed [35-38] in a complete analogy with cholesterol esters forming the smectic-A mesophase. The divergence of the helical pitch near the cholesteric-smectic A phase transition theoretically was considered by de Gennes as an analogy between superconductors and smectic A [39].

However, as will be shown lower, the main problem for investigator is the obtaining of chiral induced mixture for electro-optic application with designed pitch-temperature dependency  $dP/dT$ . Five ways of the thermostabilization of the threshold electric field are discussed in [40].

The first reentrant cholesteric mixture was observed in [41]. The mixtures exhibit a low temperature reentrant cholesteric phase, near room temperature, for which the pitch variation against temperature is opposite to classical systems. This property, from a practical point of view, stimulates the fabrication of liquid-crystalline thermoindicators giving blue light reflection at low temperature and red one at high temperature.

### 3. Chiral smectic C liquid crystalline phase

Chiral smectic C phases exhibit analogous optical properties to cholesterics [22]. The experimental investigations of optical properties of chiral smectic C phase had been unavailable because appropriate samples don't exist. The Bragg diffraction for normal and oblique incident of light in chiral smectic C liquid crystal (CE3, BDH) was observed for the first time and investigated. [42-46]. In Fig.3 the temperature dependence of the maximum wavelength of Bragg reflection ( $\lambda_B$ ) for normal incidence of light in CE-3 for smectic C\* and cholesteric phases is shown.

For the determination of the dielectric tensor of a chiral smectic C liquid crystal (CE3) in [47,48] carried out calculations of the principal values  $\epsilon_1, \epsilon_2, \epsilon_3$  of the dielectric tensor, the pitch  $P$  and director tilt angle  $\theta$ . These values were calculated from the experimentally determined values:  $n_{oc}$ ,  $n_{ec}$  ordinary and extraordinary indices of uniaxial chiral smectic C liquid crystal;  $n_R$ ,  $n_L$  refractive indices for the right and the left polarized light, respectively, and the maximum wavelength of Bragg reflection  $\lambda_B$  (Fig.4).

The two component mixture which consists of the achiral liquid crystal 4,4'-diheptyloxyazobenzene (HOAB) and the optically active dopant 2,5-bis-[4-(2-chloropentanoxy)-phenyl]-pyrimidine (OAD) [49] was studied. Mixtures with concentrations of 40% - 60% OAD exhibit wide temperature ranges of chiral smectic C phase.

Using oblique incident light both second-order and first-order Bragg reflections [4,22,50] and resulting minima in the transmission spectrum for the wavelength  $\lambda_0$ , satisfying the Bragg condition, occur:

$$m\lambda_B = 2 R n \cos \varphi \quad (1)$$

where  $m$  - is the diffraction order,  $\varphi$  - is the angle of incidence,  $n$  - is the mean refractive index of medium and  $R$  - is the period which for chiral smectic C liquid crystal is equal to full pitch. Experimental measurements of second and first order diffraction for oblique incidence light allowed calculating an extremely small value of pitch of  $0.145 \mu\text{m}$  [51,52].

From data of  $\lambda_B$  of the both diffraction order the pitch was calculated, taking for  $n$  the value equal to 1.55. The pitch decreases strongly with decreasing temperature as shown in figure 6. The small difference between the pitch values calculated for first and second order diffraction becoming evident at  $74^\circ\text{C}$  might be due to neglecting of refractive index dispersion.

Additionally to the short pitch the investigated mixture shows high values of the spontaneous polarization up to  $P_S = 400 \text{ nC}/\text{cm}^2$  and might be therefore of interest for application e.g. in deformed helix ferroelectric (DHF) effect [50,53].

Several theoretical studies of oblique reflection from helical phases have been made, particularly in [54-61] and there is a good agreement between numerical calculations and experimental results.

Electrooptics of chiral smectic C liquid crystals, mostly of ferroelectric  $S^*_C$ , are reviewed in [50]. The temperature and concentration dependencies of pitch in chiral induced smectics, dielectric properties, spatial light modulators in structure of type metal-insulator - semiconductor-  $S^*_C$  LC were studied (see References 51,83, 84; 60,61; 148 in [50]).

#### 4. Electrooptic effects in cholesterics

Several types of electrooptic effects have been observed in cholesteric LCs depending on surface treatment (boundary conditions), helical pitch  $P$ , thickness to pitch ratio  $d/P$ , dielectric anisotropy  $\Delta\epsilon$  and the frequency of the applied field, droplet size and different anchoring conditions in case of polymer-dispersed liquid crystal (PDLC) films [1-4]. These effects are caused by texture changes. Thus, many influences lead to a variety of electrooptic effects in cholesteric LCs, promising as materials for new generations of display devices.

Cholesteric liquid crystals with negative dielectric anisotropy  $\Delta\epsilon < 0$  show a dynamic scattering for electric fields with low frequency [62]. A transparent field-off state can be obtained by preparing a planar texture. The electric field induces hydrodynamic instabilities, which cause a diffuse scattering appearance. Under appropriate conditions, the scattering state is maintained after removal of the field, thereby providing an optical memory effect ("storage mode"). The stored scattering state can be erased by the application of a high frequency electric field, which reorganizes the planar structure. The hypothesis that this effect is connected with the transition of a confocal texture to a planar texture was firstly expressed in [63]. Experiments show that the erasure frequency is inverse proportional to the dielectric relaxation time [64].

##### 4.1. Colour change effect in cholesterics with initial planar orientation

In CLC with positive dielectric anisotropy, an electric field-induced cholesteric-nematic phase transition was theoretically predicted [65,66] and experimentally observed [67,68]. If the electric field  $E$  is applied perpendicular to the helix axis  $h$  of a cholesteric LC, the helix unwinds. At sufficiently high field strength, the homeotropic nematic structure is stabilized. The critical field strength  $E = E_{CN}$  depends on the zero-field pitch  $P_0$ , the dielectric anisotropy  $\Delta\epsilon$ , and the twist elastic constant  $K_{22}$ .

$$E_{CN} = (\pi^2 / P_0) (K_{22} / \epsilon_0 \Delta\epsilon)^{1/2}, \quad (2)$$

where  $\epsilon_0$  is the vacuum permittivity

If the electric field is applied parallel to the helix, the situation is more complicated. For short pitch, a shift of the reflection peak to shorter wavelengths (blue shift) can be observed [69-72]. It was assumed that above a threshold field, a conical deformation of the planar texture leads to a contraction of the pitch, and thus  $\lambda_B$  is shifted to shorter wavelength [72]. However, it could be shown that the blue shift of the selective reflection results from a periodic distortion of the texture, rather than from a pitch contraction [66]. Using the continuum theory, a field induced pitch gradient in the cholesteric LC cell has been proposed [73]. The latter effect would result in a shorter pitch, which provides an alternative explanation for the field-induced wavelength shift.

The detail study of this effect was made in [74,75]. For increasing voltage, a sequence of structures (planar - quasiplanar - confocal - homeotropic) can be observed in cholesterics with positive  $\Delta\epsilon$ . During the planar - quasiplanar transition that begins at the threshold field  $E_{TH}$  (see Figure 7) the color of the samples is changed to shorter wavelengths. The characteristics of this transition depend on the initial pitch and the strength of the applied electric field. If the electric field is switched off, the sample returns to the planar state. Was observed that the samples with shorter initial pitch are more stable against the field-induced transformation into the confocal texture. For the initial pitch in the green region, the displacement of  $\lambda_B$  to the direction of shorter wavelengths is much greater than for the case of  $P_0$  in the red region (see Figure 8). However, this effect depends on the duration of the application of the electric field. After some seconds the structure is deformed.

Experiments on dual frequency addressable mixtures with a low crossover frequency lead to new conclusions on the origin of blue shift. It was shown that both a blue shift and a red shift occur in the same system. These two processes have different relaxation times. A reversible color change can be realized by the switching between the low and the high frequency, especially in the more stable systems with the shorter pitch. As shown in Figure 9, a higher frequency preserves the planar state with the initial pitch because of the negative sign of  $\Delta\epsilon$ . For lower frequencies the Bragg wavelength is shifted. This is also shown in Figure 6 for the transmission mode. The value of the shift is again higher in the dual frequency addressable samples with shorter pitch.

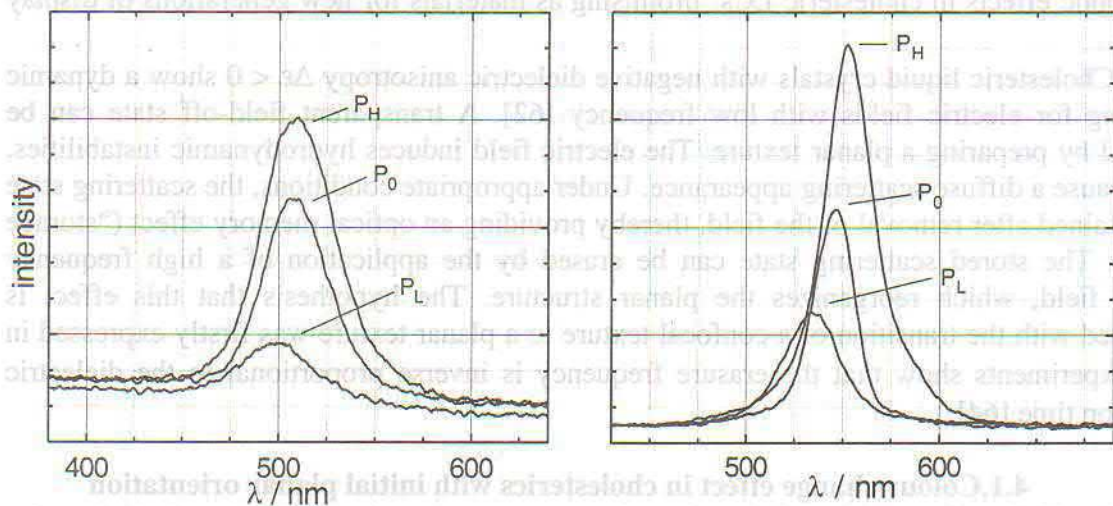


**Figure 9.** Reflection spectra of VGU 6/ChO-ChP;  $d = 5 \mu\text{m}$ ; left part: unipolar impulses,  $P_0$ : without applied voltage,  $P_L$ :  $f = 200 \text{ Hz}$ ,  $V = 40 \text{ V}$ , and  $P_H$ :  $f = 36 \text{ kHz}$ ,  $V = 60 \text{ V}$ ; right part: alternating application of low and high frequencies,  $P_0$ : without applied voltage,  $P_L$ :  $f = 200 \text{ Hz}$ ,  $V = 80 \text{ V}$ , and  $P_H$ :  $f = 115 \text{ kHz}$ ,  $V = 150 \text{ V}$ .

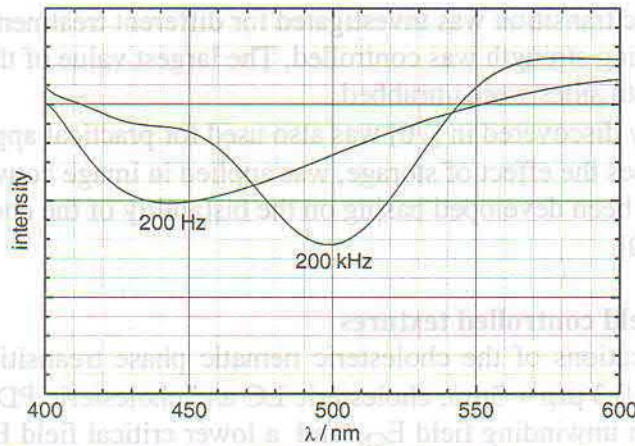


Figure 10. Transmission spectra of VGU 6/ChO-ChP for low and high frequency.

The study of the dynamic process (alternating application of low and high frequency fields) gives a more detailed picture. During the application of the low frequency field,  $\lambda_B$  is shifted to shorter wavelengths. After the switching from low to high frequency, the reflection peak is displaced from this short-wave position into a long-wave position as shown in Figure 10. This position corresponds to a pitch that is greater than  $P_0$ . The initial pitch is restored by a longer application of the high frequency.

These observations can be discussed assuming an inclined planar structure with increased (slightly unwound) pitch in the low frequency field. A slight distortion of the helix takes place because of the widening of the spectrum in this case. Till now, the blue shift was explained by the inclination of the helical structure only. In our investigations, the removal of the inclination is a fast process because of the application of the high frequency field. The increase of the pitch ( $P > P_0$ ) observed additionally is, probably, not induced by the high frequency field because this field stabilizes the initial structure. Therefore, the pitch should be increased during the application of the low frequency. At the switching to the high frequency field the planar structure is restored, but the increased pitch remains for some time. Only after a second relaxation the pitch takes its initial value. For switching off the low frequency field, without the application of the second field, the increase of the pitch has, probably, not been observed because here the removal of the inclination is also a slow process.

#### 4.2 Bistability in cholesterics

For normal (homeotropic) surface orientation, a bistability effect appears, i. e. the intensity-versus-voltage curve shows a large hysteresis [76]. As a matter of fact, the occurrence of a bistability is possible in all cases of surface treatment (including non-treated, non-rubbed cells), provided that the cell thickness  $d$  of the cholesteric sample is comparable to the helical pitch  $P$  [4,77].

The appearance of certain textures depends on the boundary conditions, the value of the pitch, the thickness-to-pitch ratio, and the regime of the applied voltage. A deformed spiral superstructure, the so-called strain (scroll) texture, is organized under certain conditions [77,78]. Various pitch-thickness ratios have been investigated [79,80]. A CLC doped with dyes can even show a tri-stability effect if the pitch is large [81].

The expression (3) for  $E_{CN}$  was calculated for infinitely thick films without taking into account the boundary conditions. However, the cholesteric to nematic phase transition was investigated for different thickness [82,83]. The influence of the surface orientation was taken into account [83] by introducing a surface free energy per unit area  $F$  that leads to the following expression for  $V_{CN}$

$$V_{CN} = (8\pi^2 d^2 K_{22} / P_0^2 \epsilon_0 \Delta\epsilon \pm 8Fd / \epsilon_0 \Delta\epsilon)^{1/2}, \quad (3)$$

The anchoring energy has a remarkable influence on  $V_{CN}$  [84-86]. The bi-stability behavior of

the cholesteric-nematic transition was investigated for different treatments of the surface [87]. Additionally, the rubbing strength was controlled. The largest value of the hysteresis width was obtained when both sides were unrubbed.

The bi-stability discovered in [76] was also used for practical applications. The strain texture, which possesses the effect of storage, was applied in image converters [88]. A color projection display has been developed basing on the bistability of the cholesteric –nematic phase transition [89,90].

### 4.3 Electric field controlled textures

Another applications of the cholesteric nematic phase transition was discovered in [91,75] : for pitch  $P = 0.3 \mu\text{m} + 3\mu\text{m}$ , cholesteric LC and cholesteric PDLC in applied field  $E$ , in the interval between unwinding field  $E_{CN}$  and a lower critical field  $E_{FC}$ , diffractive grating texture arises. This texture was named as a “new texture”. Was shown the possibilities a voltage controlled color shift and a laser beam deflection (up to  $30^\circ$  for He-Ne laser). Was noted that the arrangement of helicoidal structure with the helical axis parallel to the surfaces is a result of the specific balance between the influence of the electric field and the twisting forces. The principle arrangement for the investigation of the spectral characteristics and some results are given in Figures 12-15.

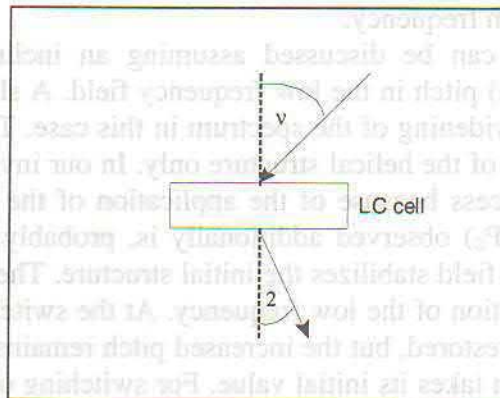


**Figure 12.** Experimental arrangement for the investigation of the light scattering;  $\phi$  - angle of incidence,  $\theta$  - observation angle.

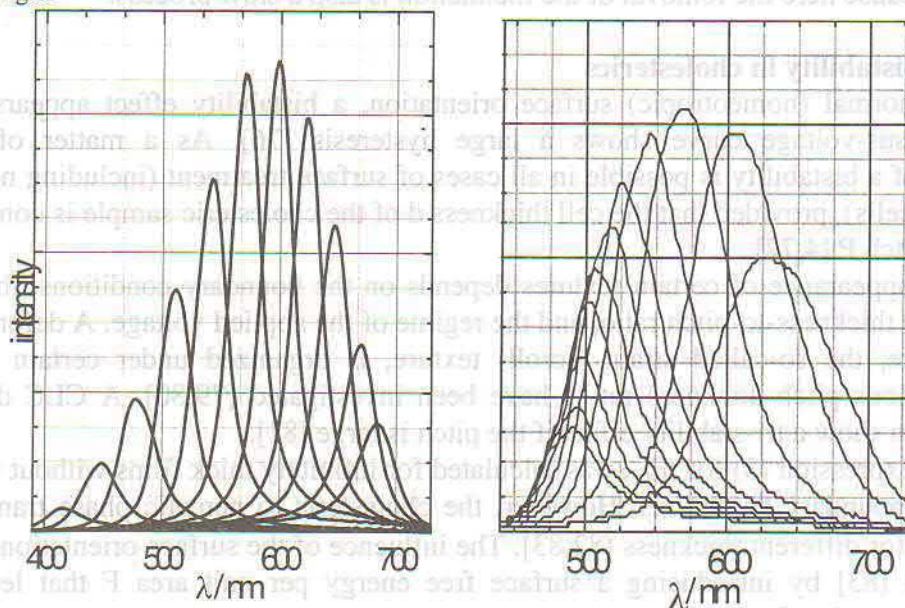


**Figure 13.** Dependence of the color on the observation angle and the applied voltage; mixture MLC 6023/S811,  $d = 5 \mu\text{m}$ ,  $\phi = 40^\circ$ ; left part:  $\theta$  is  $15^\circ$  for the left curve and is increased in  $5^\circ$  steps,  $V = 15 \text{ V}$ ; right part:  $V$  is  $20 \text{ V}$  for the right curve and is decreased in steps of  $2 \text{ V}$ ,  $\theta = 40^\circ$ .

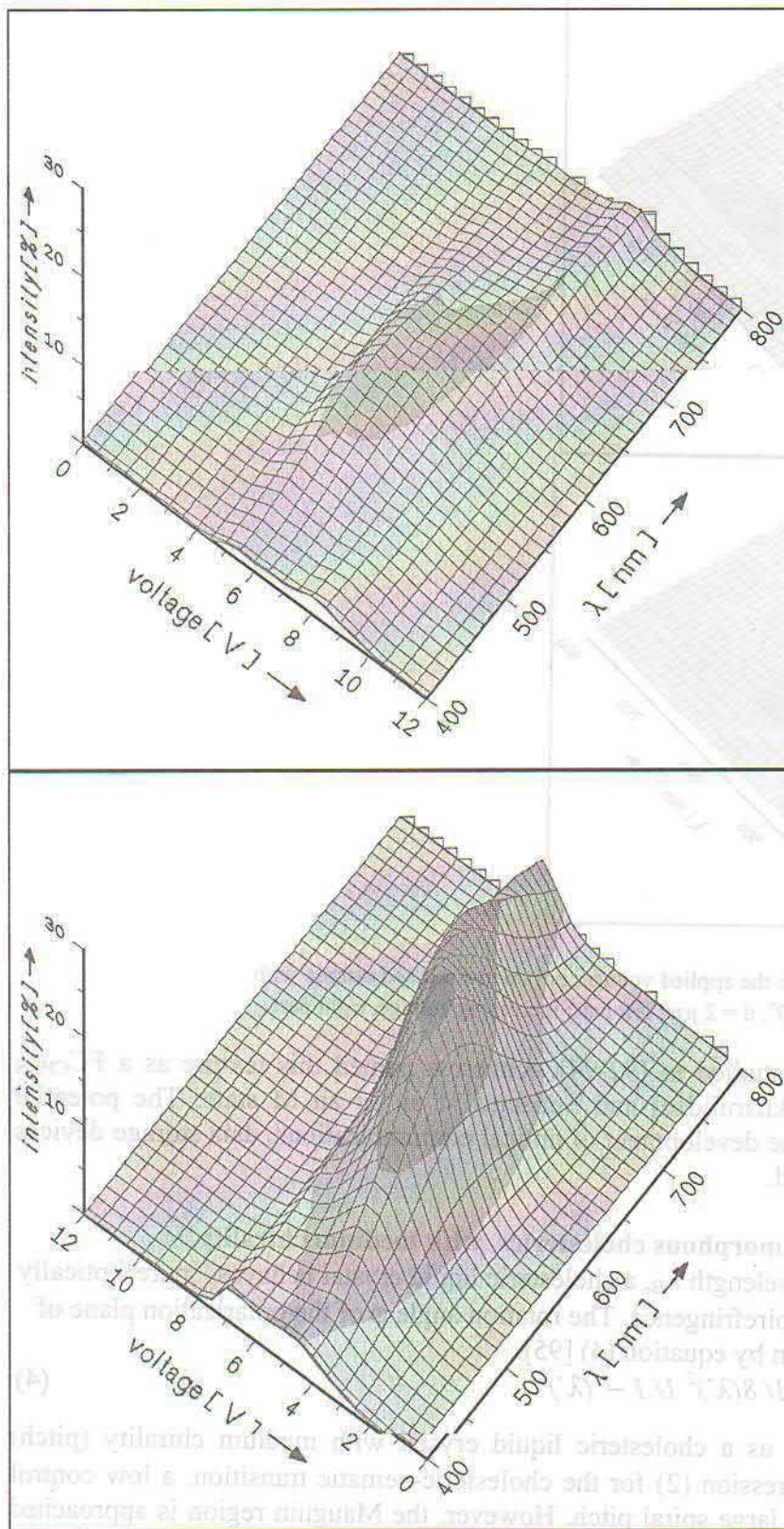


**Figure 14.** Dependence of color on the applied voltage; mixture E7/S811;  $\phi = 40^\circ$ ,  $\theta = 20^\circ$ ,  $P = 1.1 \mu\text{m}$ ; left part: increasing voltage, right part: decreasing voltage.

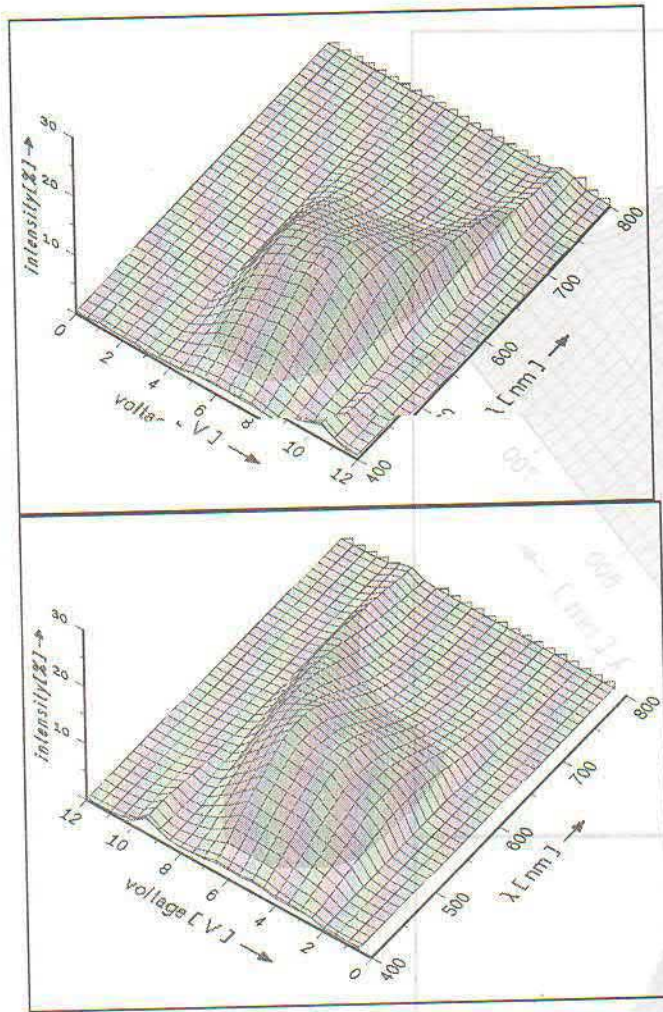


**Figure 15.** Dependence of color on the applied voltage; polymer-dispersed sample with E7/S811;  $\varphi = 40^\circ$ ,  $\theta = 20^\circ$ ,  $d = 2 \mu\text{m}$ ; left part: increasing voltage, right part decreasing voltage.

Later, this effect was studied in [92-94]. Kitzerow named this texture as a  $FC_{CHKS}$  (Chilaya, Hauck, Koswig, Sikharulidze) and Subacius at al. as an M state. The potential applications of this effect in the development of optical communications, data storage devices and holography were discussed.

#### 4.4 Electrooptics of amorphous cholesterics with medium chirality

Close to the Bragg wavelength  $\lambda_B$ , a cholesteric liquid crystal behaves "pure" optically active, i. e. it shows no linear birefringence. The rotation angle  $\varphi$  of the polarization plane of normally incident light is given by equation (4) [95]:

$$\varphi = \frac{2\pi d}{P} \frac{(n_e^2 - n_o^2 / n_e^2 + n_o^2)^2}{1/8(\lambda')^2} \frac{1}{1 - (\lambda')^2} \quad (4)$$

where  $\lambda' = \lambda / \lambda_B$ .

This case is denoted as a cholesteric liquid crystal with medium chirality (pitch) [31,96-99]. According to expression (2) for the cholesteric-nematic transition, a low control voltage can be obtained for a large spiral pitch. However, the Mauguin region is approached on increasing  $P$ . This is evident by an increase of the optical anisotropy (linear birefringence) of the structure. To avoid uncontrolled deformations of the pitch caused by the cell walls called strain textures [77,78]; the condition  $P > d$  must be satisfied. Estimating the influence of linear birefringence near the Mauguin's region, the general conditions for the optically active structure are  $\lambda \geq \Delta n P / 2$  and  $P > d$  [97].

Most frequently, a planar orientation of CLC is obtained by the rubbing technique. However, in cells coated with polyamide (without rubbing), a new cholesteric state, called

“amorphous” cholesteric structure, is formed [31,96-98]. The surface, covered by polyamide, orients the molecules parallel to the surface, but without any preferable direction in the surface plane. Thus, a structure with random orientation of liquid crystal molecules and a helical axis oriented normal to the surfaces is obtained (Fig. 16).

All parts of the amorphous cholesteric structure with medium chirality rotate the polarization plane by the same angle. The whole structure can be considered as optically active. In this case, the angle of rotation is independent of the direction of the polarization plane of the incident light. This is the basic property used for electrooptic application of the amorphous cholesteric structure with medium chirality. Characteristic features of this effect are: 1) low demands on the surface conditions (non-rubbed cell), 2) an ability to function in any position between crossed polarizers, 3) wide and uniform viewing angle, 4) rise times less than 10 ms and the decay times of 12- 20 ms. The electrooptic effect was also studied in polymer dispersed liquid crystal (PDLC) films [99]. With respect to non-chiral nematic PDLC films, the transmission is lower, but the angular dependence is improved.

## 5. TGB and Blue phases

The chiral induced liquid crystal systems for compositions with different phase sequences have been subject of extensive experimental investigations in last years. Influence of chirality and pretransitional phenomena on frustrated and incommensurate systems leads to observation exotic structures with unusual properties. Them belongs complex „defect” phases: Blue Phases (BP) and Twist Grain Boundary (TGB) Phases.

BP can occur between cholesteric and isotropic phase. The theory of the structure and symmetry properties of BP was developed within the framework of the Landau phase transition theory and predicted the existence of the intermediate phases [100-105]. Theoretical and experimental results show that cholesteric liquid crystals of short pitch can form up to three distinct blue phases. In order of increasing of temperature they are named BP I, BP II and BP III. BP I and BP II have respectively body centered cubic and simple cubic symmetry. BP III is characterized by a disordered (amorphous) structure. The disordered BP III phase provides the formation of broad Bragg peaks and, therefore, is often called the fog phase.

A wide temperature blue phase and a new- BPS were discovered in induced chiral LC systems [106-108]. Usually in BP I and BP II the peak of selective reflection (Bragg wavelength- $\lambda_B$ ) decreases with increase of temperature or it is temperature independent. Recently the positive temperature dependence of  $\lambda_B$  was observed by. This unusual temperature dependence was also observed in BPS. It was shown that boundary conditions and smectic fluctuations play a decisive role in the formation of BPS.

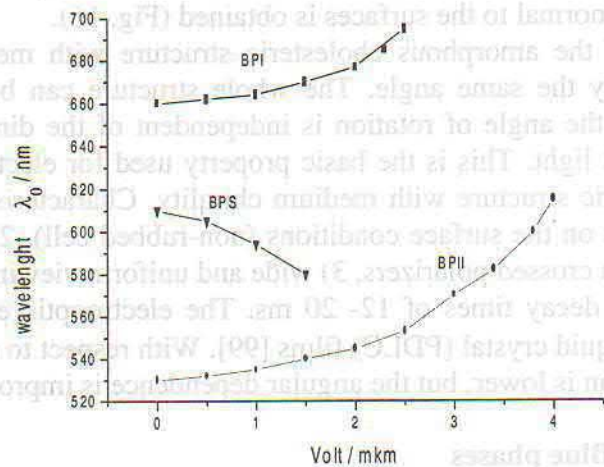
Unusual phase diagram according to order BP phase sequences was observed in induced chiral systems with increasing of concentration of chiral dopant before and after observing BP I phase wide scattering blue phases named by us as a BPA<sub>1</sub> BPA<sub>2</sub> [109-111]. The light scattering spectrum of the phases looks like that observed in BP III.

The influence of several factors (chirality, pretransitional phenomena, boundary conditions, electric field) on characteristics of BP in nemato-chiral mixtures, both cyanobiphenyls, were studied [112,113]. Characteristic features with increasing of chirality are the following: Blue phases from room temperature down to 0°C were detected.. With increasing of concentration of chiral component, together with BP I, BP II, BP III, the supercooled phase BPS and the reentrant BP II, were observed (Fig.17)

It is well-known that the application of of an electric field produces a versatile effect of BP [114-116]. The influence of an electric field on the BPs is mainly connected with the distortions of the cubic lattice and as a result with a shift of the Bragg peaks. Figure 18 shows the dependence of  $\lambda_0$  on the electric field E (V/ $\mu$ m) for BP I, BP II and BP S. Electric field influences more strongly on BP II: a reversible shift of Bragg wavelength up to 80 nm were obtained. Such a shift was also reported in [117], but in our case, the shift was reversible.

“anisotropic” cholesteric structure, is formed [31, 98-99]. The surface, covered by polyamide, orient the molecules parallel to the surface, but without any preferable direction in the surface plane. Thus, a structure with random orientation of liquid crystal molecules and a helical axis oriented normal to the surface is obtained [17].

All parts of the amorphous cholesteric structure can be considered as optically active. In this case, the angle of rotation is independent of the direction of the polarization plane of the incident light. This is the basic property used in the application of this effect in amorphous cholesteric structures with medium cholesteric structure. The low demands on the surface conditions (smooth surface, any position between crossed polarizers, 3) wide and uniform angle, 4) five times less than 10 ms and the heavy times of 12-20 ms. The electro-optic effect was also studied in polymer dispersed liquid crystal (PDLC) [99]. With the effect in non-chiral nematic PDLC films, the transmission is lower, but the angular dependence is improved.



The chiral induced liquid crystal systems for compositions with different phase sequences have been subject of extensive experimental investigations in last years. Influence

**Fig.18.**  $\lambda_0$  versus E for the mixture containing 50 wt. % of CB15 and 50 wt.% of ZhK 807. Notation : ( $\nabla$ ) is BPS at 17.80 °C, ( $\bullet$ ) is BP II at 19.40 °C., ( $\blacksquare$ ) is BP I at 18.80 °C

The detailed studies of BP II showed that the behaviour of  $\lambda_0$  in applied electric field is temperature dependent and rather complicated. The measurements made far from the transition point to BP I showed the red shift (seen from Figs. 12 and 13).

and experimental results show that cholesteric liquid crystals of short pitch can form up to three distinct blue phases. In order of increasing of temperature they are named BP I, BP II and BP III. BP I and BP II have respectively body centred cubic and simple cubic symmetry. BP III

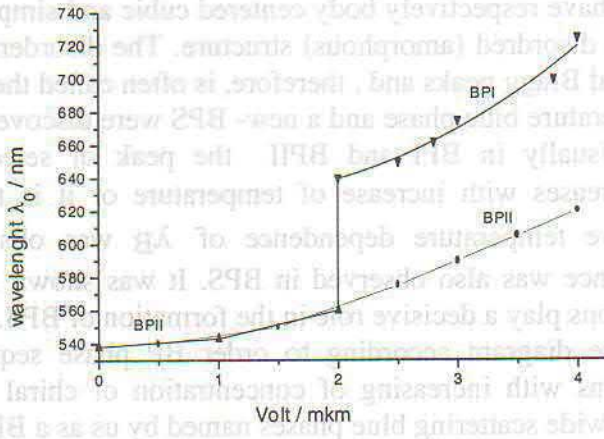


**Fig.19.**  $\lambda_0$  versus E for the mixture containing 49.5 wt. % of CB15 and 50.5 wt.% of ZhK 807. Notation : ( $\bullet$ ) is BP II at 21.10 °C, ( $\blacktriangle$ ) is BP II at 19.85 °C. In the field of the zero-field,  $\lambda_0 = 538$  nm is independent of temperature.

With an approach to the temperature of BP I formation, the reversible BP II→BP I transition is observed at the electric field  $E = 2V/\mu m$  (Figure 19). At  $E > 4V \mu m$ , the reversible BP II→nematic phase transition is observed within the whole temperature range of BP II existence. Thus, the blue phases behave differently in electric fields and some effects are promising in application.

The another possibilities of application is the elaboration and investigation of thermal imaging elements by use of phase transition between two blue phases and thermo-optical properties of this phases [118]. This means the creation of a visualizer with threshold contrast-temperature characteristics, which reduces the requirements to the thermostabilization and

allows regulating the sensitivity of the device. A new BP and wide temperature BP could be used which were discovered in induced chiral LC systems [110,111].

TGB phase is another kind of frustrated phase derived from chiral molecules. In spirit of de Gennes theory, near the phase transition from the cholesteric to smectic A phase, an intermediate phase, called TGB phase, was predicted in [119]. Later this method was extended onto a region of the phase diagram where the cholesteric, smectic A and smectic C\* phases met in the NAC\* point, and existence another phase, TGB C\*, was predicted [120]. Both predicted phases have been discovered experimentally [121,122].

Mixed induced TGB phases were also observed in binary liquid crystalline systems [123,124]. TGB phase was observed also in [125,126,111], when for chiral induced systems nonmesomorphic chiral dopant [38] was used. In this case the pretransitional phase was observed in three component chiral systems, consisted of two nematogenic liquid crystals with different phase sequences (one with smectic A and another with smectic C) and optically active nonmesomorphic dopant. An anomalous selective reflection near the cholesteric-smectic A phase transition was observed. [125]. Calorimetric and X-ray investigations pointed that existence of a TGB phase [126]. The same effect was observed in two component systems [111]. Besides of anomalous selective reflection, the texture, pitch dependence on temperature and behaviour in electric field obtained in [125,126,111] pretransitional phase differed with this one in conventional TGB phase.

In conclusion, observed electrooptic effects in chiral systems are very promising for application, for creation new types of optical devices (filters, UV, Vis. and IR sensors, displays). Chiral liquid crystals are an important material owing to the possibility of changing their unique optical properties easily in external fields. Due to their versatile behavior, new results and applications can be expected in the future.

#### Acknowledgment

The author would like to thank the all co-authors of joint publications, the collaboration with whom was useful and pleasant.

#### REFERENCES

1. P.G. de Gennes and J.Prost, *The Physics of Liquid Crystals*, Clarendon Press, Oxford, (1993)
2. S.Chandrasekhar, *Liquid Crystals*, University Press, Cambridge, (1992).
3. V.A.Beliakov, *Optics of Complex Structured Periodic Media*, Springer, NY, (1992)
4. G.Chilaya, *Physical properties and applications of liquid crystals with induced helicoidal structure*, Metsniereba, Tbilisi, (1985) (in Russian)
5. G.Chilaya, *Rev. Phys.Appliq.* **16**, 193 (1981).
6. G.Solladie and R.G.Zimmermann, *Angew.Chem.* **96**, 335 (1985).
7. Gottarelli, M.Hibert, B.Samori, G.Solladie, G.P.Spada, R.Zimmermann, *J.Am.Chem.Soc.* **105**, 7318, (1983).
8. G.S.Chilaya and L.N.Lisetski, *Sov. Phys. Uspekhi* **24**, 496 (1981).
9. G.S.Chilaya and L.N.Lisetski, *Mol.Cryst.Liq.Cryst.* **140**, 243 (1986).
10. G.S.Chilaya, S.N.Aronishidze, Z.M.Elashvili, M.N.Kushnirenko and M.I.Brodzeli, Abstracts of the 1<sup>st</sup> LC Conference of Socialist Countries, Halle, DDR, (1976), p61
11. G.S.Chilaya, S.N.Aronishidze, Z.M.Elashvili, M.N.Kushnirenko and M.I.Brodzeli, *Soobshch. Akad. Nauk GSSR* **84**, 81 (1976).
12. G.Pelzl, *Z. Chem.* **17**, 264 (1976).
13. S.N.Aronishidze, M.N.Kushnirenko, G.S.Chilaya 5<sup>th</sup> International Liquid Crystal Conference of Socialist Countries, Odessa (USSR), (1983), Abstracts, C-61, V.1, Part 2, P.116.
14. S.N.Aronishidze, M.N.Kushnirenko, S.M.Osadchy, G.S.Chilaya. *Bulletin of the Academy of Sciences of the Georgian SSR*, 114,517, (1984)
15. F.D.Saeva, J.J.Wysocki, *J. Am. Chem. Soc.* **94**, 135 (1971).

17. I.Chabay, Chem. Phys. Lett. **17**, 283 (1972).
18. E.Sackman, J.Voss, Chem. Phys. Lett. **14**, 528 (1972).
19. G.Holzwarth, N.A.W. Holzwarth, J. Opt. Soc. Am. **63**, 324 (1973).
20. H.J.Krabbe, H.Heggemeier, B.Schrader, E.H.Korte, Angew. Chem. **89**, 831 (1977).
21. D.G.Khoshtaria, G.S.Chilaya, A.V.Ivashchenko, V.G.Rumiantsev, 5<sup>th</sup> International Liquid Crystal Conference of Socialist Countries, Odessa (USSR),(1983), Abstracts, C-47,V.1,Part 2, P.94.
22. V.A.Beliakov, V.E.Dmitrienko and V.P.Orlov, Sov. Phys. Uspekhi **22**,63 (1979).
23. V.A.Beliakov, V.E.Dmitrienko, Sov. Phys. Solid State **18**, 1681 (1976).
24. K.A.Suresh, Mol.Cryst.Liquid Cryst. **35**, 267 (1976).
25. S.N.Aronishidze, V.E.Dmitrienko D.G.Khoshtaria and G.S.Chilaya, JETP Lett. **32**,17 (1980)
26. S.M.Osadchy, Sov. Phys. Crystallogr. **29**, 573 (1984).
27. D.G.Khoshtaria, S.M.Osadchy, G.S.Chilaya, Sov. Phys. Crystallogr. **30**, 775 (1985).
28. J.Ferguson, Sci.Am.211, 77, (1964)
29. G.S.Chilaya, Z.M.Elashvili, K.D.Vinokur, Mol.Cryst.Liq.Cryst., 106,67,(1984)
30. G.S.Chilaya and V.G.Chigrinov, Sov.Phys. Crystallogr., 33,154, (1988)
31. K.D.Vinokur; D.G.Sikharulidze, G.S.Chilaya, Z.M.Elashvili, Liquid crystals with helical structure and their applications in displays, Metsniereba, Tbilisi, (1988) (in Russian)
- 32.G.Chilaya G., F.Oestreicher, G.Scherowsky, Mol.Mat.9, 261, (1998).
33. H.Stegemeyer, H.Finkelmann, Naturwissenschaften, 62, 436, (1975)
34. G.S.Chilaya, S.N.Aronishidze, K.D.Vinokur, M.D.Mkhatvrishvili, M.I.Brodzeli, Kristallografiya, 22, 1280, (1977)
35. K.D.Vinokur, S.P.Ivchenko, G.S.Chilaya, Zhurn.Tekhn.Fiz. 49, 1565, (1979); Sov.Phys.Tech.Phys. 24,1870, (1979)
- 36.G.S.Chilaya, Z.M.Elashvili, S.P.Ivchenko, L.N.Lisetski, K.D.Vinokur, Advances in Liquid Crystals, Pergamon Press, Oxford, Budapest, p.1191, (1980)
37. G.S.Chilaya, Z.M.Elashvili, T.S.Piliashvili, K.D.Vinokur, L.N.Lisetski, ibid, p.1185
38. G.S.Chilaya, Z.M.Elashvili, L.N.Lisetski,T.S.Piliashvili,K.D.Vinokur, Mol.Cryst.Liq.Cryst., 74, 261, (1981)
39. P.G. de Gennes,Solid State Commun., 10, 753, (1972)
- 40.G.Chilaya,Z.Elashvili,D.Sikharulidze,S.Tavzarashvili,K.Tevdorashvili,K.Vinokur, Mol.Cryst.Liq.Cryst., 209, 93, (1991).
41. G.S.Chilaya,C.Destrade, Z.M.Elashvili,S.P.Ivchenko,L.N.Lisetski,Nguyen Huu Tihn, K.D.Vinokur,J.Physique Lett. 46, 75, (1985)
- 42.G.S.Chilaya,S.N.Aronishidze,M.N.Kushnirenko, Abstracts of the 4<sup>th</sup> LC Conference of Socialist Countries, Tbilisi, (1981), V.1, P.382
43. S.N.Aronishidze,M.N.Kushnirenko,.G.S.Chilaya, Zh. Tekh. Fiz., 52,157, (1982)
44. G.S.Chilaya, S.N.Aronishidze, M.N.Kushnirenko, Mol.Cryst.Liq.Cryst. (Lett.), 82, 281,(1982)
- 45.K.Hori, Mol.Cryst.Liq.Cryst.(Lett.), 82,13, (1982)
46. K.Hori, Mol.Cryst.Liq.Cryst.(Lett.), 100,75,(1983)
- 47.G.S.Chilaya,A.G.Chanishvili,D.G.Khoshtaria,S.M.Osadchy,Mol.Cryst.Liq.Cryst.,149, 291,(1987)
- 48.G.Chilaya, Nuovo Cimento, 10D,1263, (1988)
49. J. Bömelburg, Ch. Hänsel, G. Heppke, J. Hollid, D. Löttsch, K.-D. Scherf, K. Wuthe and H. Zashke, Mol. Cryst. Liq. Cryst., **192**, 335,(1990).
- 50.G. S. Chilaya and V. G. Chigrinov, Physics-Uspekhi, **36**, 909,(1993).
- 51.G.Petriashvili, G.Chilaya, A, Chanishvili, D.Sikharulidze, G.Heppke, Abstracts of 6<sup>th</sup> International Conference on Ferroelectric Liquid Crystals, Brest, France, (1997), P.342
52. G.Sh.Petriashvili, M.N.Aronishidze, A.A.Khatiashvili, A.G.Chanishvili, G.S.Chilaya,

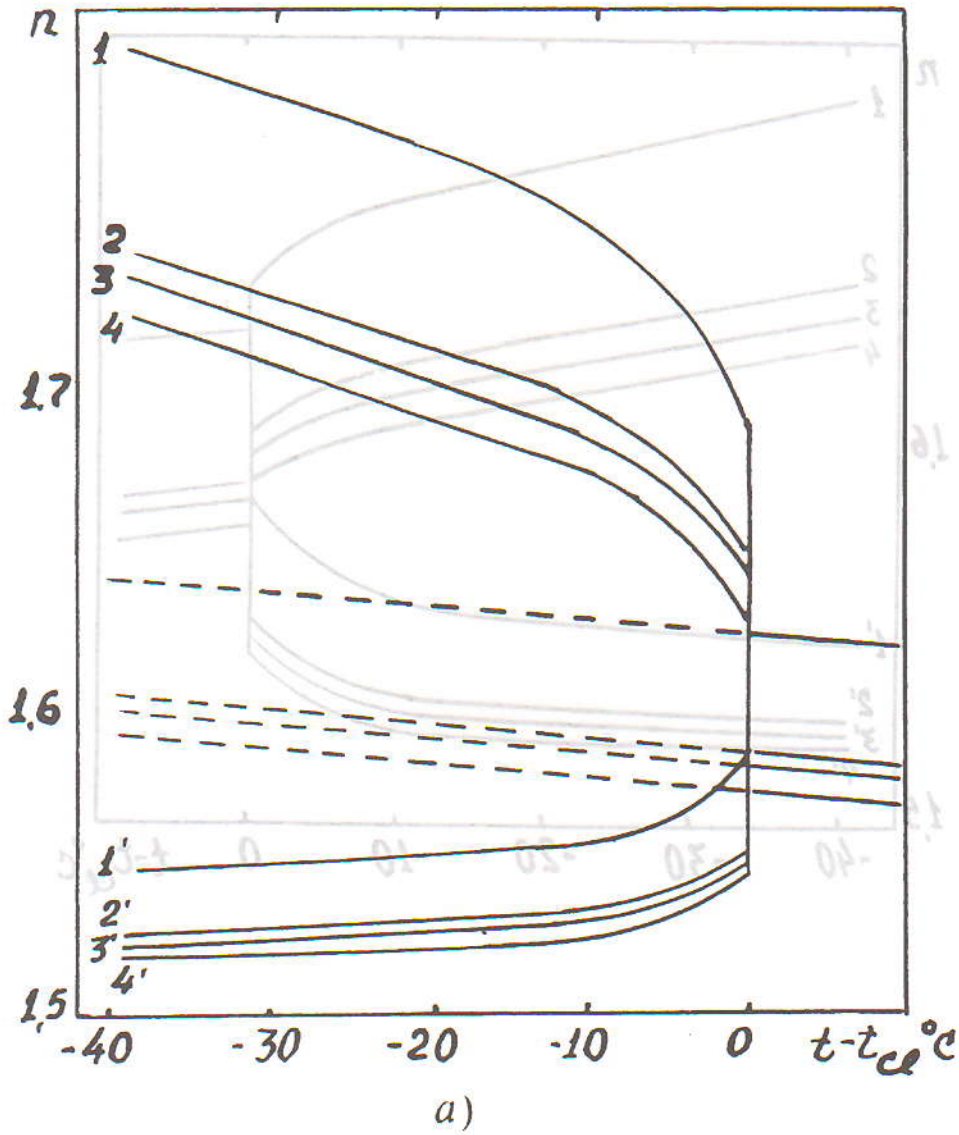
- Crystallography Reports, 42, 499, (1997)
53. J. Fünfschilling and M. Schadt, *Jpn. J. Appl.*, **35**, 84, (1996)
  54. R. Dreher and G. Meier, *Phys. Rev. A*, **8**, 1616, (1973).
  55. A. Sugita, H. Takezoe, Y. Ouchi, A. Fukuda, E. Kuze and N. Goto, *Jpn. J. appl. Phys.* **21**, 1543, (1982).
  56. H. Takezoe, Y. Ouchi, A. Sugita, M. Hara, A. Fukuda and E. Kuze *Jpn. J. appl. Phys.* **21**, 1390, (1982).
  57. H. Takezoe, Y. Ouchi, A. Sugita, M. Hara, A. Fukuda and E. Kuze, *Jpn. J. appl. Phys.*, **22**, 1080, (1983)
  58. E. Miraldi, C. Oldano, P. Taverna Valabrega and L. Trossi, *Mol. Cryst. Liq. Cryst.* **103**, 155, (1983).
  59. E. Miraldi, C. Oldano, P. Taverna Valabrega and L. Trossi, *Jpn. J. appl. Phys.*, **23**, 802, (1984).
  60. C. Oldano, E. Miraldi and P. Taverna Valabrega, *Phys. Rev. A*, **27**, 3291, (1983).
  61. C. Oldano, *Phys. Rev. A*, **31**, 1014, (1985).
  62. G. Heilmeyer, J. Goldmacher, *Proc. IEEE* **57**, 34 (1969).
  63. W. Haas, J. Adams, and G. Dir, *Chem. Phys. Lett.* **14**, 95 (1972).
  64. G. S. Chilaya, V. T. Lazareva, L. M. Blinov, *Kristallografiya* **18**, 203 (1973).
  65. P. G. de Gennes, *Solid State Commun.* **6**, 163 (1968).
  66. R. B. Meyer, *Appl. Phys. Lett.* **12**, 281 (1968).
  67. J. J. Wysocki, J. Adams, and W. Haas, *Phys. Rev. Lett.* **20**, 1024 (1968).
  68. F. J. Kahn, *Phys. Rev. Lett.* **24**, 209 (1970).
  69. W. Harper, "Liquid Crystals", Gordon and Breach, New York, 1967.
  70. N. Oron and M. M. Labes, *Appl. Phys. Lett.* **21**, 243 (1972).
  71. H. Baessler, T. M. Laronge, and M. M. Labes *J. Chem. Phys.* **51**, 3213 (1969).
  72. C. J. Gerritsma and P. van Zanten, *Mol. Cryst. Liq. Cryst.* **15**, 257 (1971).
  73. I. Fedak, R. D. Pringle, and G. H. Curtis, *Mol. Cryst. Liq. Cryst.* **64**, 69 (1980).
  74. G. Chilaya, G. Hauck, H. D. Koswig, G. Petriashvili, and D. Sikharulidze, *Cryst. Res. Tech.* **32**, 25 (1997).
  75. G. Chilaya, G. Hauck, H. D. Koswig and D. Sikharulidze, *Proc. SPIE* **3318**, 351 (1998).
  76. W. Greubel, *Appl. Phys. Lett.* **25**, 5 (1974).
  77. a) G. S. Chilaya, S. N. Aronishidze, K. D. Vinokur, M. I. Brodzeli, *Dep. VINITI*, 1976, # 1874-76;  
b) G. S. Chilaya, S. N. Aronishidze, K. D. Vinokur, S. P. Ivchenko, and M. I. Brodzeli, *Acta Physica Polonica* **A54**, 655 (1978).
  78. M. I. Press, A. S. Arrott, *J. Physique* **37**, 384 (1976).
  79. V. G. Chigrinov, V. V. Beliaev, S. V. Beliaev, and M. F. Grebenkin, *Sov. Phys. JETP* **50**, 994 (1979).
  80. G. Hauck and H. D. Koswig, "Cholesteric-nematic phase change", in: *Selected topics in liquid crystals research*, ed. by H. D. Koswig, Akademie-Verlag, Berlin, 115-139 (1990).
  81. C. G. Lin-Hendel, *Appl. Phys. Lett.* **38**, 615 (1981).
  82. Gerber P. R., *Z. Naturforschung* **36A**, 718 (1981).
  83. Van Sprang H. A., van de Venne, *J. Appl. Phys.* **57**, 175 (1984).
  84. Lee J. C., Allender D. W., Neff V. D., *Mol. Cryst. Liq. Cryst.* **210**, 11 (1992).
  85. Lee J. C., Allender D. W. // *Jpn. J. Appl. Phys.* **33**, 1407 (1994).
  86. Mochizuki A., Kobayashi S., *Mol. Cryst. Liq. Cryst.* **225**, 89 (1993).
  87. Yabe Y., Seo D. -S., *Liq. Crystals* **17**, 847 (1994).
  88. G. S. Chilaya, D. G. Sikharulidze and M. I. Brodzeli, *J. Physique* **C3-40**, C3-274 (1979).
  89. Koike Y., Mochizuki A., Yoshikawa, *Displays* April, p. 93 (1989).
  90. Yabe Y., Saito H., Yoshihara T., Kasahara S., Mochizuki A., Narusava T., *J. SID* **1**, 411 (1993).
  91. G. Chilaya, G. Hauck, H. D. Koswig, and D. Sikharulidze, *J. Appl. Phys.* **80**, 1907 (1996).

- 92.H.S.-Kitzerow, Jpn. J. Appl. Phys., 36, 349-352, 1997
- 93.D.Subacius, S.V.Shiyanowskii, Ph. Bos, O.D.Lavrentovich, Appl.Phys. Lett. 71, 3323,1997
- 94.S.N.Lee, L.C.Chien, S.Sprunt, Appl.Phys.Lett. 72,885,1998
95. H. de Vries, Acta Cryst. 4, 219 (1951).
- 96.A.Chanishvili, G.Chilaya and D.Sikharulidze, Mol.Cryst.Liq.Cryst 207, 53 (1991)
97. A.Chanishvili, G.Chilaya and D.Sikharulidze, Chanishvili A., Chilaya G. and.Sikharulidze D., Appl. Optics 33, 348 (1994).
- 98.a) G.Chilaya, A.Chanishvili, D.Sikharulidze, Proc.SPIE, V.2372, P.96 (1995)
- b) A.Chanishvili, G.Chilaya and D.Sikharulidze, G. Petriashvili, Mol. Mat. 8, 295 (1997).
99. U Behrens., H.-S Kitzerow and G Chilaya, Liq.Cryst. 17, 597 (1994).
- 100.S.A.Brazowski, S.G.Dmirtiev, Sov.Phys.JETP, 42,497,1976
101. S.A.Brazowski, V.M.Filev, Sov.Phys..JETP,48,573,1979
- 102.R.M.Hornreich, S.Shtrikman, Phys.Rev. A, 28,1791,1981
103. R.M.Hornreich, S.Shtrikman, Phys.Rev. A, 30,3264,1984
- 104.V.A, Beliakov, V.E.Dmitrienko, Sov.Phys.Uspekhi, 28,535,1985
105. V.A.Beliakov, V.E.Dmitrienko, Sov.Phys.JETP, 62,1173,1989
- 106.A.G.Chanishvili G.S.Chilaya, Z.M.Elashvili, S.P.Ivchenko, D.G.Khoshtaria, K.D.Vinokur, Mol.Cryst.Liq.Cryst. Letters, 3, 91, 1986
107. G.Petriashvili, G.Chilaya, Sov. Phys. Crystallogr. 36, 752,1991.
- 108.G.Heppke, H.S.Kitzerow, D.Lotzsch and Ch.Papenfuss, Liq.Cryst.8, 408,1990 and
- 109.E.Demikhov, H.Stegemeyer, Liq.Cryst.10, 869,1991
- 110.G.Chilaya and G.Petriashvili, Mol.Mat. 2,195,1993
- 111.G.Chilaya, G.Petriashvili, A.G.Chanishvili, D.G.Sikharulidze, Mol.Mat.8,245,1997
- 112.A.Chanishvili, G.Chilaya, G.Petriashvili, D.Sikharulidze, Abstracts of 17<sup>th</sup> International Liquid Crystal Conference, 1998, P2- 200,
113. G.Petriashvili, D.Sikharulidze, A.Chanishvili, G.Chilaya, Crysatalography Rep., 44,847,1999
- 114.V.E.Dmitrienko, Liq.Cryst.5, 847,1989
- 115.H. -S.Kitzerow, Mol.Cryst.Liq.Cryst.202, 51,1991
- 116.G.Chilaya, G.Petriashvili, Mol.Materials, 2,239,1993):
- 117.G.Heppke, M.Krumrey, F.Oestreicher, Mol.Cryst.Liq.Cryst.99, 99,1983
118. M.Aronishidze, G.Petriashvili, D.Sikharulidze, K.Tevdorashvili, A.Chanishvili, G.Chilaya, Georgian Engineering News,#4,135,1999
- 119.S.R.Renn and T.C.Lubensky, Phys.Rev.A, 38,2132,1988
120. S.R.Renn and T.C.Lubensky, Mol.Cryst.Liq.Cryst.209, 349,1991
- 121.J.W.Goodby, M.A.Waugh, S.M.Stein, E.Chin, R.Pindak, S.Patel, Nature, 337,449,1989
- 122.H.T.Nguyen, A.Bouchta,L.Navallies, P.Barois, N.Isaert, R.J.Tweig,A.Maaroufi, C.Destrade, J. de Physique II,2,1988,1992
- 123.O.D.Lavrentovich, Y.A.Nastishin, V.I.Kulishov, Y.S.Narkevich, A.S.Tolochko, Europhys.Lett., 13,313,1990
- 124.W.Kuczynski, H.Stegemeyer, Mol.Cryst.Liq.Cryst., 209,349,1991
- 125.G.Chilaya,A.Chanishvili,G.Petriashvili,D.Sikharulidze,Mol.Cryst.Liq.Cryst.,261, 3233,1995
- 126.A.Chanishvili,G.Chilaya,M.Neundorf,G.Pelzl,G.Petriashvili,Cryst.Res.Technol.31, 679, 1996

Fig.1b. - Indices of refraction of chiral form (cholesteric LC) : 1-  $n_e$  and 1' -  $n_o$  for 436 nm; 2-  $n_e$  and 2' -  $n_o$  for 546 nm; 3-  $n_e$  and 3' -  $n_o$  for 577 nm; 4-  $n_e$  and 4' -  $n_o$  for 690 nm.

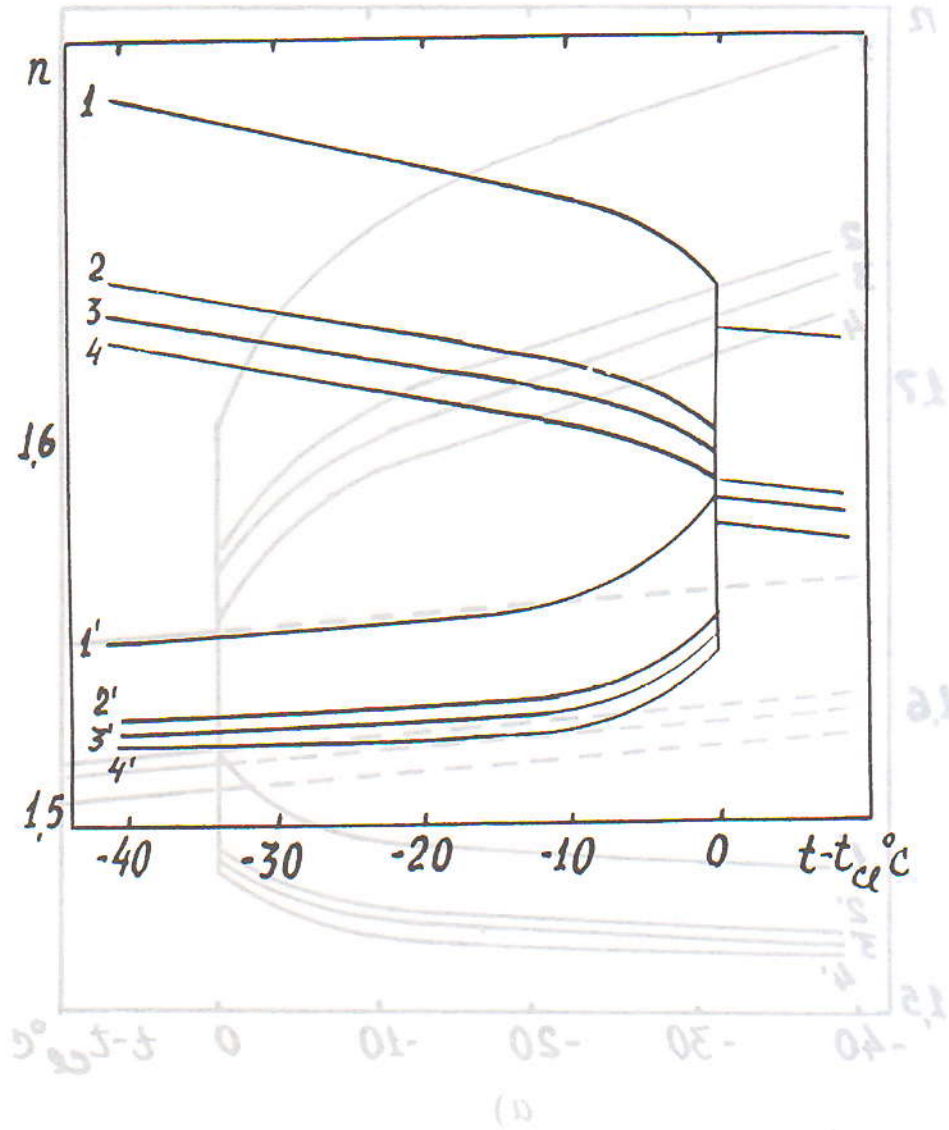
FIGURES

Fig.1a. - Indices of refraction of racemic form (nematic LC) : 1-  $n_e$  and 1' -  $n_o$  for 436 nm; 2-  $n_e$  and 2' -  $n_o$  for 546 nm; 3-  $n_e$  and 3' -  $n_o$  for 577 nm; 4-  $n_e$  and 4' -  $n_o$  for 690 nm.



**Fig.1b.** - Indices of refraction of chiral form (cholesteric LC) : 1-  $n_e$  and 1' -  $n_o$  for 436 nm; 2-  $n_e$  and 2' -  $n_o$  for 546 nm; 3-  $n_e$  and 3' -  $n_o$  for 577 nm; 4-  $n_e$  and 4' -  $n_o$  for 690 nm.

Fig.1a - Indices of refraction of racemic form (nematic LC) : 1-  $n_e$  and 1' -  $n_o$  for 436 nm; 2-  $n_e$  and 2' -  $n_o$  for 546 nm; 3-  $n_e$  and 3' -  $n_o$  for 577 nm; 4-  $n_e$  and 4' -  $n_o$  for 690 nm.



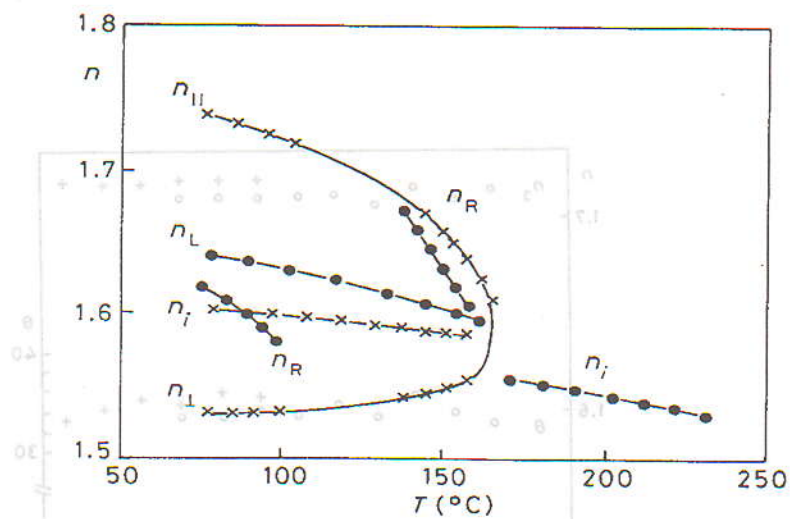


Fig.2. Refractive indices of cholesteric phase of CE-3 for  $\lambda=436\text{nm}$ ;  $\bullet$ - measured values,  $\times$ - calculated values;  $n_i^2 = (2n_{\perp}^2 + n_{\parallel}^2) / 3$ ; The local refractive indices -  $n_{\parallel} \equiv n_e$ ,  $n_{\perp} \equiv n_o$ .

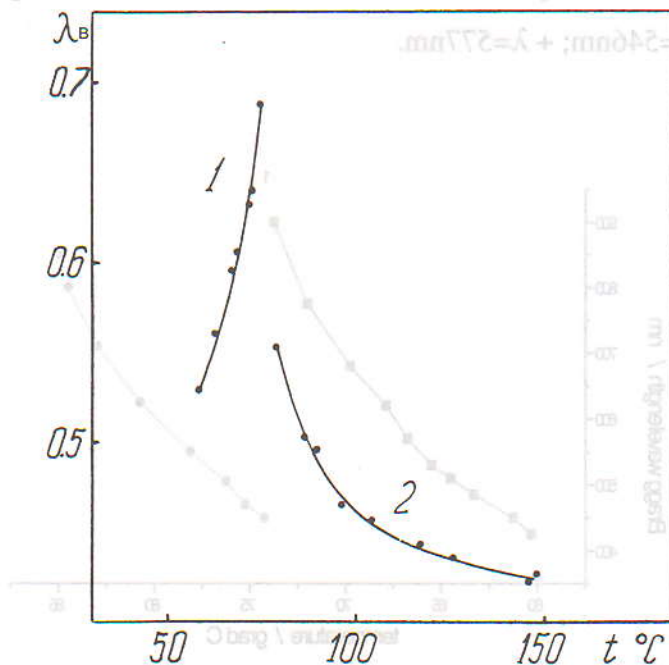


Fig.3. The temperature dependence of the maximum wavelength of Bragg reflection ( $\lambda_B$ ) for CE-3 in smectic C\* (1) and cholesteric phase (2).

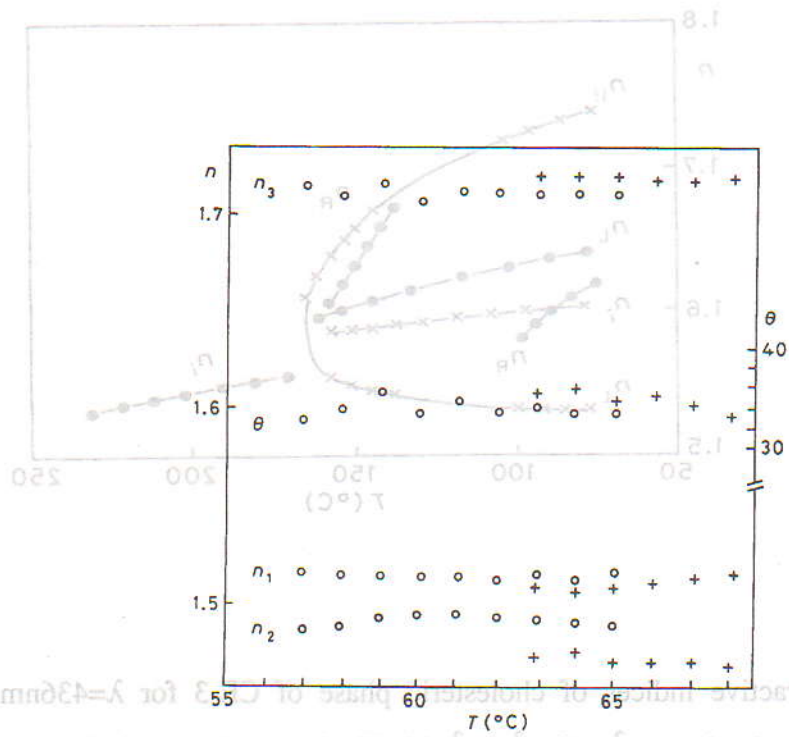


Fig. 4. Temperature dependence of refractive indices and tilt angle of chiral smectic C phase of CE-3;  $\circ$ -  $\lambda=546\text{nm}$ ;  $+$ - measured values,  $\times$ - calculated values;  $n_i^2 = (\Delta n_i^2 + n_o^2) \cos^2 \theta$ ; The local refractive indices -  $n_{\parallel} \equiv n_o$ ,  $n_{\perp} \equiv n_o$ .

Fig. 4. Temperature dependence of refractive indices and tilt angle of chiral smectic C phase of CE-3;  $\circ$ -  $\lambda=546\text{nm}$ ;  $+$ -  $\lambda=577\text{nm}$ .

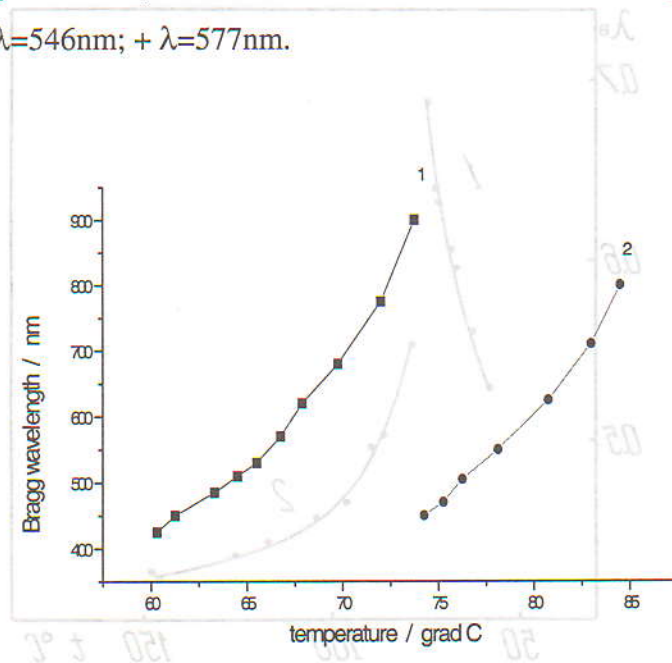


Fig. 5. The temperature dependence of maximum wavelength of Bragg reflection  $\lambda_B$  for CE-3 mixture of 50% OAD in HOAB for inclined angle  $\phi = 20^\circ$  is shown.

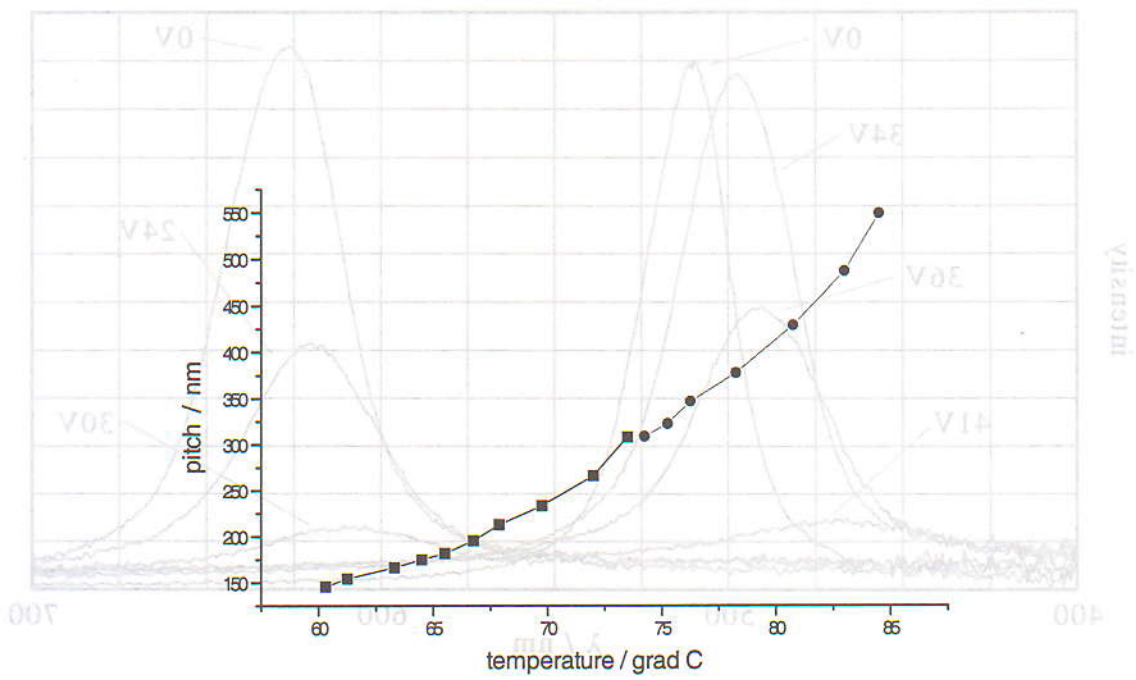


Figure 6. Reflection spectra of N11-602MS (a) in the red (right curves) and in the green (left curves) wavelength region;  $d = 10 \mu\text{m}$ , unipolar impulses of 350 Hz.

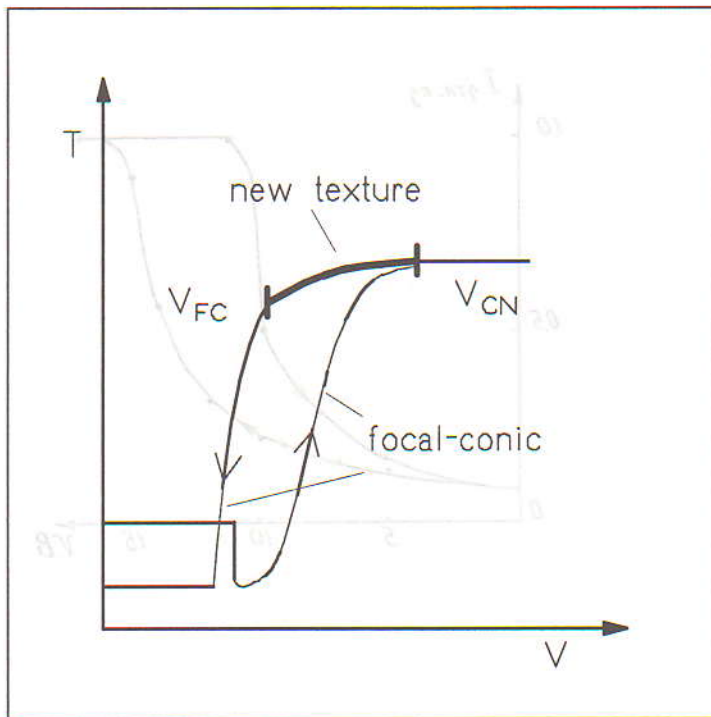
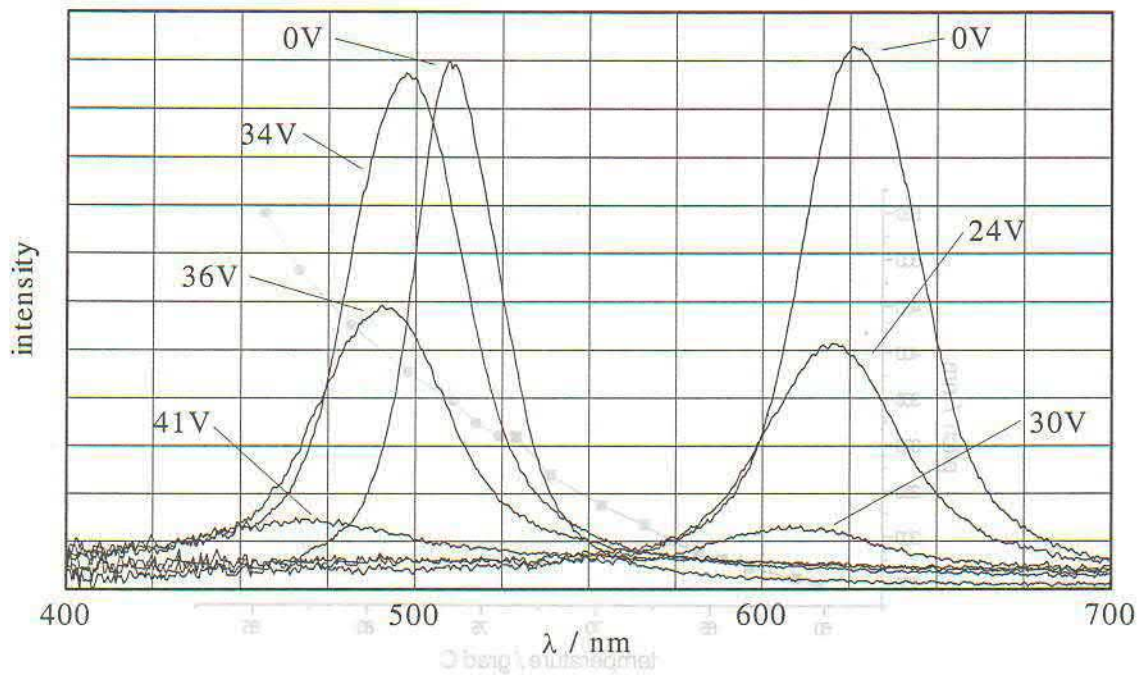
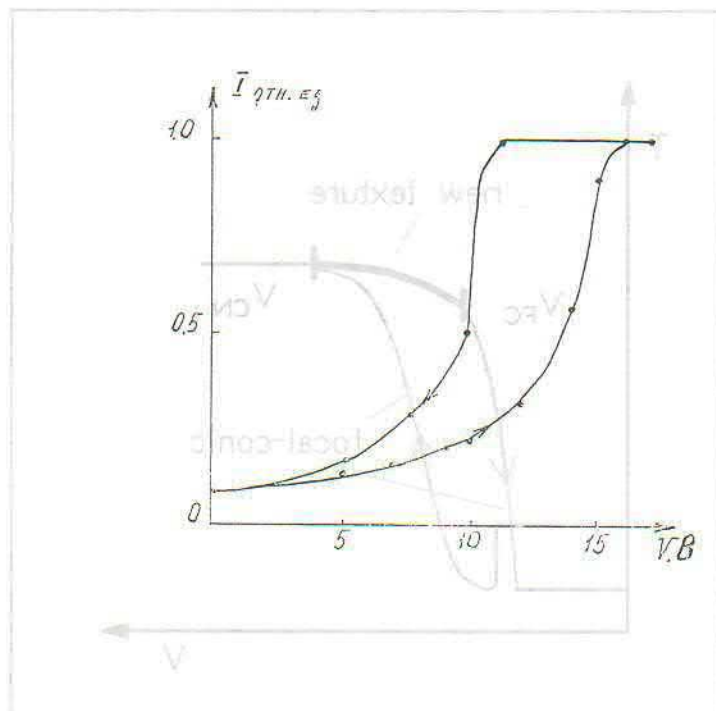


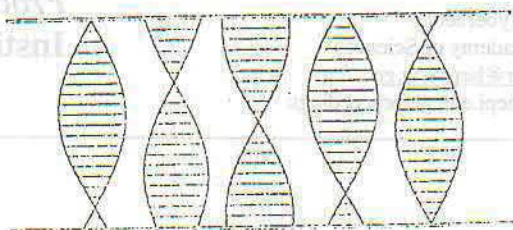
Figure 7. General transmission change of cholesteric cells for increasing and decreasing applied voltage.



**Figure 8.** Reflection spectra of ZLI-6023/S811;  $\lambda_B$  in the red (right curves) and in the green (left curves) wavelength region;  $d = 10 \mu\text{m}$ , unipolar impulses of 350 Hz.



**Fig.11.** The intensity ( $I$ ) dependence of transmitted light on the voltage ( $V$ ) of applied electric field. Mixture : 83.35 % - 4-butyl-4'-methoxyazoxybenzene (BMAOB) + 14.7% - p'-cyanophenyl ester of p-buthylbenzoic acid + 2% - cholesteryl caprate.  $t = 50^\circ \text{C}$ ,  $d = 10 \mu\text{m}$ ,  $P = 9 \mu\text{m}$ ; non-treated cell.



3	λ
2	2

Fig.16. Amorphous cholesteric structure

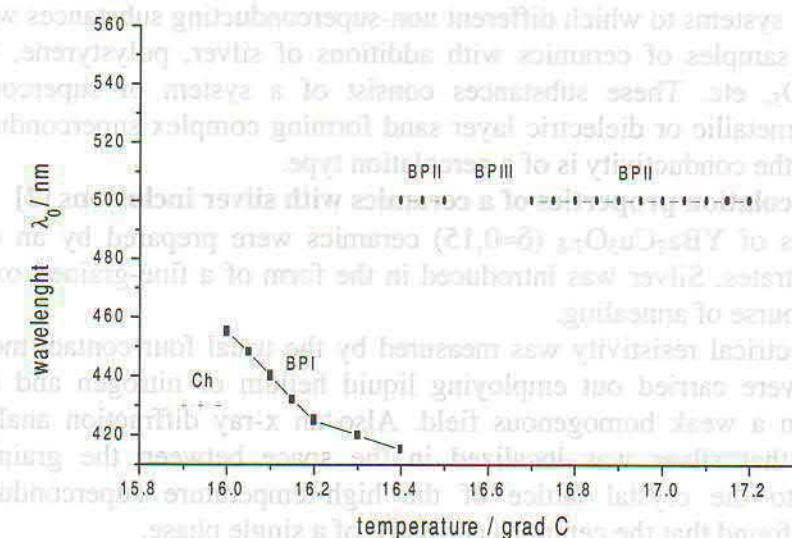
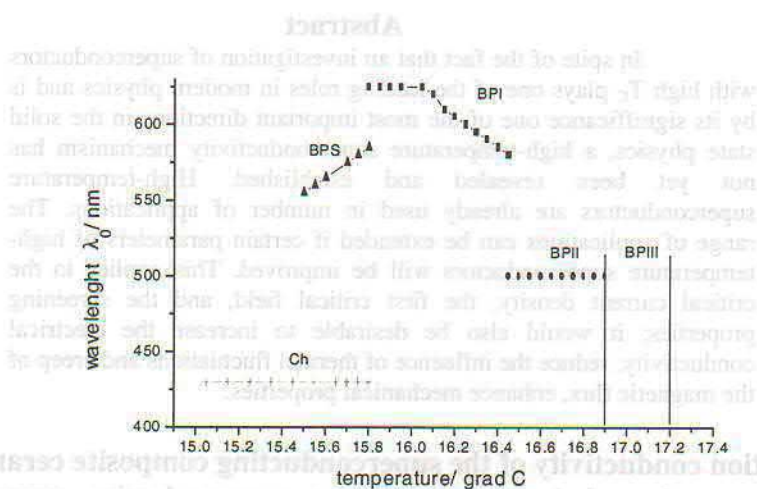
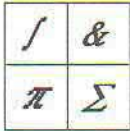


Fig.17. Temperature dependence of  $\lambda_0$  for the mixture containing 53 wt. % of CB15 and 47 wt.% of ZhK 807 during (a) heating and (b) cooling. Notation : (+) is the cholesteric phase, ( $\nabla$ ) is BP S, ( $\bullet$ ) is BP II, ( $\blacksquare$ ) is BP I.



## The Percolation Conductivity, Josephson Effect and Magnetic Properties of the HTSC Systems

J.Sanikidze, S.Odenov, R.Kokhreidze

*Institute of Cybernetics*

### Abstract

In spite of the fact that an investigation of superconductors with high  $T_C$  plays one of the leading roles in modern physics and is by its significance one of the most important directions in the solid state physics, a high-temperature superconductivity mechanism has not yet been revealed and established. High-temperature superconductors are already used in number of applications. The range of applications can be extended if certain parameters of high-temperature superconductors will be improved. This applies to the critical current density, the first critical field, and the screening properties; it would also be desirable to increase the electrical conductivity, reduce the influence of thermal fluctuations and creep of the magnetic flux, enhance mechanical properties.

### 1. Percolation conductivity of the superconducting composite ceramics

Physical properties of the two-component superconducting ceramics have been investigated in number of works [2-4]. The materials were the composites based on yttrium superconducting systems to which different non-superconducting substances were added. Here are studied the samples of ceramics with additions of silver, polystyrene, dielectric green phase  $Y_2BaCuO_5$ , etc. These substances consist of a system of superconducting grains connected with metallic or dielectric layer sand forming complex superconducting networks. In such systems the conductivity is of a percolation type.

#### 1.1 Percolation properties of a ceramics with silver inclusions [2]

Samples of  $YBa_2Cu_3O_{7-\delta}$  ( $\delta \approx 0,15$ ) ceramics were prepared by an original method involving the nitrates. Silver was introduced in the form of a fine-grained oxide, which was reduced in the course of annealing.

The electrical resistivity was measured by the usual four-contact method. Magnetic measurements were carried out employing liquid helium or nitrogen and a vibrating coil magnetometer in a weak homogenous field. Also an x-ray diffraction analysis was made, which showed that silver was localized in the space between the grains and was not incorporated into the crystal lattice of the high-temperature superconducting ceramics, however, it was found that the ceramics consisted of a single phase.

The resistivity measurements yielded the curves corresponding to the onset and completion of the transition. The onset of the transition deduced from the resistivity practically coincided with the onset deduced from the magnetic susceptibility measurements.

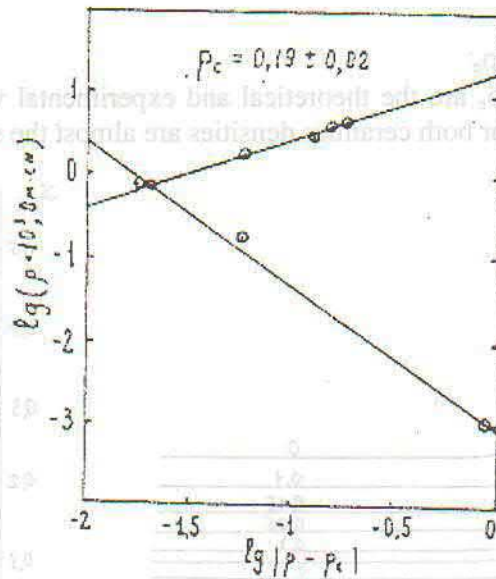


Fig.1.1

The percolation theory applied to conduction between Ag inclusions gives the following expressions for the electrical resistivity:

$$\rho/\rho_0 = (p-p_c)^{-t} \quad \text{for } p > p_c \quad (1.1.1)$$

$$\rho/\rho_0 = (p_c - p)^s \quad \text{for } p < p_c \quad (1.1.2)$$

Here,  $p$  is the volume content of silver,  $p_c$  is the critical value of this content, and  $t$  and  $s$  are the power indexes. In selecting  $p_c$  preference should be given to that value which ensure linear (i.e. power-law) dependences when plotted on a logarithmic scale (fig.1.1); this should be followed by determination of the indexes  $t$  and  $s$ . Selecting the value in that sequence, we obtain  $p_c = 0.19 \pm 0.02$ ,  $t = 1.8 \pm 0.2$ ,  $s = 0.8 \pm 0.1$ . Within the limits of the experimental error these values are identical with these calculated for an fcc lattice [5] or for continual model of percolation [6] and are close to the date obtained for the  $(YBa_2Cu_3O_{7.8})_{1-x}Au_x$  system [7].

## 1.2. Percolation properties of the superconducting composite ceramics $(YBa_2Cu_3O_{7.8})_{1-x}(Y_2BaCuO_5)_x$ [8]

The percolation process, their regularity and influence must be taken into account in many cases of some theoretical and practical interest. Some physical properties of the composite

$(YBa_2Cu_3O_{7.8})_{1-x}(Y_2BaCuO_5)_x$  have been investigated, using  $Y_2BaCuO_5$  ceramics (the green phase) as a dielectric phase. We have studied the behavior of composite superconductors in ac and dc magnetic fields, changing the value of dc field from 0 up to 300 Oe, which was sufficient for our purpose.

As it is known, on the magnetic moment curve  $M_{ZFC}(H)$  (the cooling in zero magnetic field) there is a place, where to the magnetic moment of grains the weak links moment  $M_j(H)$  is added. The latter moment increases with field, reaches the maximum value and gradually decreases to zero. The field, where  $M_j = 0$ , was defined as the critical field  $H_{C2J}$ . A little higher there is a non hysteresis region, where is possible to measure a differential susceptibility  $\chi_d = \chi_d'$  (the imaginary part  $\chi_d''$  here is equal to zero). As it is known, by the use of this value it is possible to measure with a sufficient accuracy the volume part of superconducting phase by the following relation

$$\chi_{SV} = -4\pi\chi_d' = -4\pi\chi_d'^2 \quad (1.2.1)$$

The mass part of superconducting phase can be determined by the relation

$$\chi_{sm} = \chi_{sv} \rho_t / \rho_c \quad (1.2.2)$$

where  $\rho_t$ ,  $\rho_e$  are the theoretical and experimental values of the ceramic density (the theoretical values for both ceramics densities are almost the same).

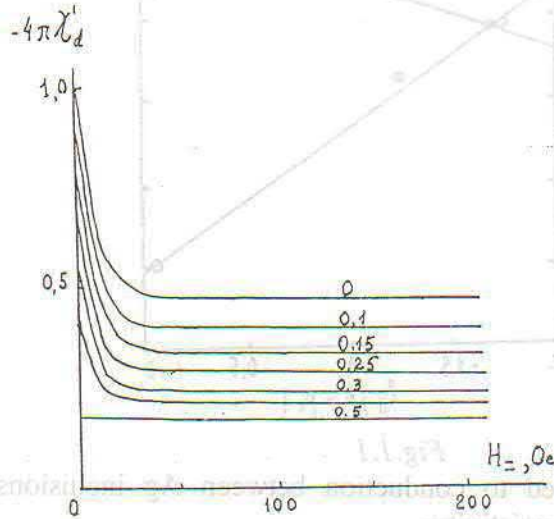


Fig.1.2

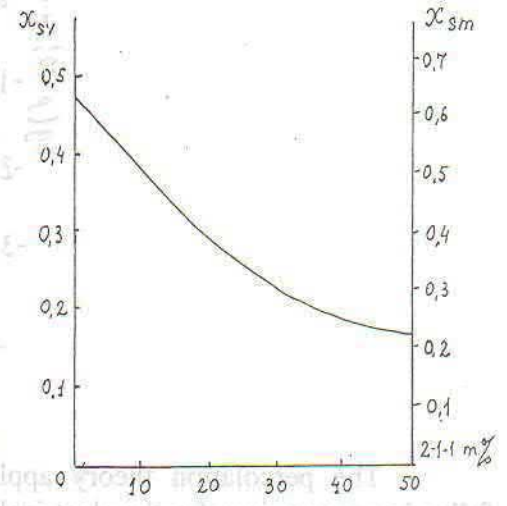


Fig.1.3

The obtained results are given in Fig.1.2. The dependence of the real part of susceptibility on dc magnetic field shows, that for 1 kHz ac field with an amplitude  $\ll O_e$  there is a sharp decrease at the beginning with a gradual transition to a plateau. This can be explained by diamagnetism suppression of the weak links and by the constant diamagnetism of Grains.

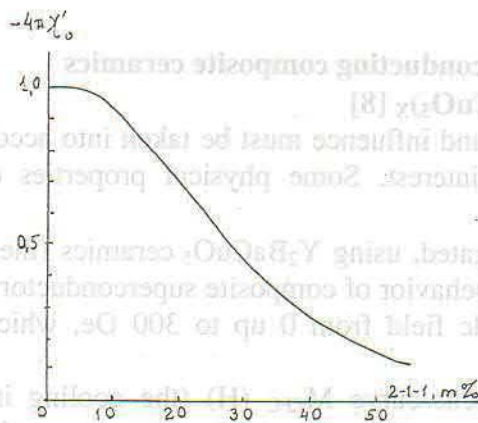


Fig.1.4.

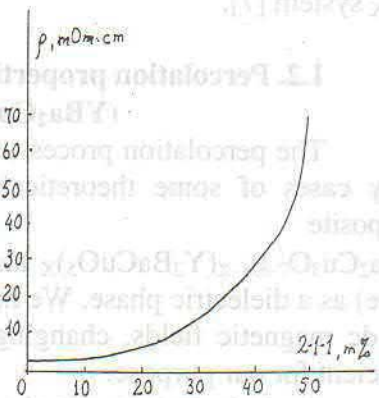


Fig.1.5.

Fig.1.2-1.4 show that for  $H=0$  there is a sharp decrease of  $\chi'(0)$  with the increase of dielectric phase. The possible explanation is the following: the probability of percolation chain forming is sharply decreasing with increase of this phase. The sample resistivity (Fig.1.5) also increases strongly, which qualitatively agree with a theoretical percolation dependence. It is necessary to note, that in reality there exist an additional phase in the initial sample, nearly 33% (Fig.1.3). So, as it can be seen, the content of superconducting phase in the sample is  $(17 \pm 2)\%$ . As the critical current in the sample is very small ( $j_c \sim 10^{-6} j_{c0}$ ), one can consider the

value  $(17 \pm 2)\%$  is a real percolation limit, which is in a good agreement with the expected value [6].

## 2. The Josephson junctions based on the composite high-temperature superconductors [9]

We investigated the percolation processes in HTSC composites. It became evident that such systems may have some Josephson-like properties and for their further improvement it was necessary one of the components of the system to be of high enough electric resistivity. For this purpose the insulator  $Y_2Ba_2CuO_5$  was chosen.

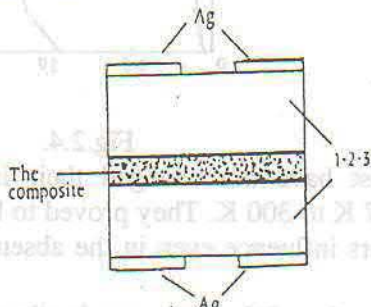


Fig.2.1

The structure of the samples was the following (fig.2.1): between two HTSC region there was a layer, consisting of the composite  $YBa_2Cu_3O_{7-\delta}$  and  $Y_2BaCuO_5$ . The experiments on these samples showed that samples had a clear Josephson effect, when the HTSC concentration in the composite was near the edge of the percolation limit. In fig.2.2 the dependence of the junction voltage on the magnetic flux created by a current in a small coil is shown. The value of the field was of the order of  $10^{-3}$ Gs. The dependence is fully repeating the classical stationary Josephson effect:

$$U \sim \left| \frac{\sin \pi \Phi / \Phi_0}{\pi \Phi / \Phi_0} \right|, \quad (2.1)$$

where  $\Phi$  is the magnetic flux in the junction and  $\Phi_0$  is one quantum of the flux.

The non-stationary effect is given by the relation:

$$2 e U = h \nu \quad (2.2)$$

Here  $2e$  is electron pair charge,  $h$  is Plank constant,  $\nu$  - the frequency of the radiation emitted by the junction, when the voltage is equal to  $U$ . In fig.2.3 the jumps on the characteristics are shown accordingly to relation (2). This demonstrates that in our samples we have seen Josephson effect.

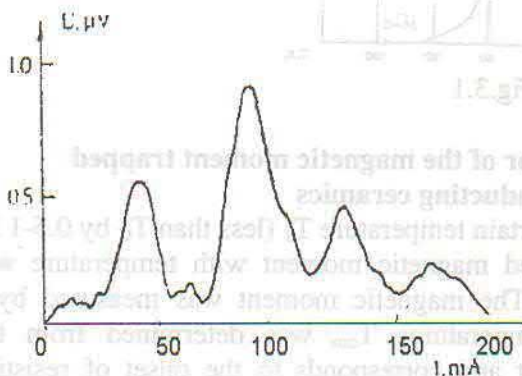


Fig.2.2

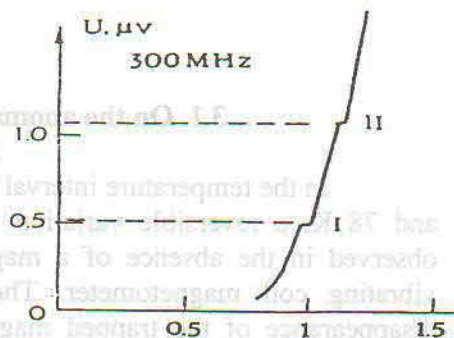


Fig.2.3

The sample characteristics may be in some extent controlled by varying the annealing time. In fig.2.4 it is shown the effect of some annealing on the important parameters – the critical current and differential resistivity of the junctions.

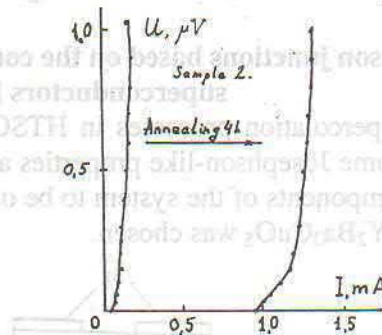


Fig. 2.4.

The samples almost have not changed their initial parameters at a number of temperature cycling from 77 K to 300 K. They proved to be mechanically durable and do not suffer from the water vapours influence even in the absence of additional measures for their protection.

### 3. Magnetic properties of the superconducting ceramics

In the first our works on high-temperature ceramics we investigated the magnetic properties of  $MBa_2Cu_3O_{7.8}$  (M–Y, Yb, Sm, Er) compounds [10,11]. Electric resistivity, high frequency magnetic susceptibility, magnetization and magnetic susceptibility in a weak magnetic field were measured in temperature range from 4,2 to 300 K. A new technology of high-temperature superconductors synthesis of  $MBa_2Cu_3O_{7.8}$  (M – Y, Yb, Sm, Er) compounds is presented which is based on nitric acid salts of rare-earth elements and other components. It is determined that this technology significantly simplifies high-temperature superconductors synthesis and, that the obtained samples by their physical characteristics are identical to those obtained by the known technologies (Fig.3.1).

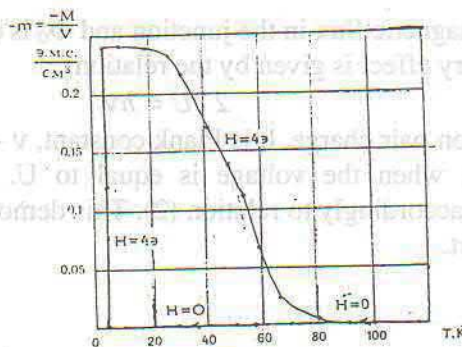


Fig. 3.1

#### 3.1. On the anomalous behavior of the magnetic moment trapped in a superconducting ceramics

In the temperature interval between a certain temperature  $T_1$  (less than  $T_C$  by 0.5-1 K) and 78 K, a reversible variation of the trapped magnetic moment with temperature was observed in the absence of a magnetic field. The magnetic moment was measured by a vibrating coil magnetometer. The critical temperatures  $T_{cm}$  was determined from the disappearance of the trapped magnetic moment and corresponds to the onset of resistive transition. A certain trapped magnetic moment was established after the sample had been heated to  $T_1$ . The sample was then cooled to  $\sim 78$  K, and this was accompanied by a reversible increase of the trapped magnetic moment almost twice its value (the external field was switched off and the terrestrial magnetic field was compensated). A subsequent increase in

temperature to  $T_1$  again led to a decrease of the magnetic moment along the same reversible curve [12].

We can accept the validity of the interpretation results on the basis of the following simplified model. We assume that a ceramic contains microloops with a characteristic mean size less than  $10\mu\text{m}$ , formed by separate crystallites coupled through weak links. Moreover, we assume for the sake of simplicity that the loops are independent of one another and each of them has one weak link.

In this case, integrating over the loop and neglecting the contribution of the current density outside the contact, we obtain the following phase realations:

$$2\pi n = \varphi_j + \frac{2\pi}{\Phi_e} \oint \vec{A} d\vec{l}, \quad \varphi_j = \arcsin I/I_C, \quad (3.1.1)$$

Here,  $\varphi_j$  is the phase difference across a weak link,  $\Phi$  - the magnetic flux,  $\Phi_e$  - a flux quantum, and  $\vec{A}$  - the vector potential. For  $I < I_C$ , we obtain

$$n\Phi_e = \frac{\Phi_0}{2\pi} \frac{I}{I_C} + \Phi \quad (3.1.2)$$

This is the fluxoid equation for a microloop. The temperature dependence of the weak link critical current can be taken in the form  $I_C = I_{C0}(1-t^2)$ , where  $I_{C0} = I_C(t=0)$ ,  $t = T/T_{cm}$ , which describes the experimental results quite well in the required temperature interval considering that  $\Phi = LI/C$  ( $L$  is the inductance of the microloop), and introducing the notation  $\beta = C\Phi_0/2\pi LI_{C0}$ , we obtain

$$\Phi = n\Phi_0[1+\beta/(1-t^2)]^{-1}. \quad (3.1.3)$$

Neglecting the interaction between loops and assuming their geometry to be constant, we can take the same temperature dependence of the magnetic flux and magnetic moment. Hence, normalizing these quantities to their value at temperature  $t_2 = 78 \text{ K}/T_{cm}$ , we obtain

$$M/M(t_2) = \frac{1-t^2}{1-t_2^2} \left( \frac{1+\beta-t_2^2}{1+\beta-t^2} \right). \quad (3.1.4)$$

In order to go over to the magnetic moment of the entire sample, we must add all the elementary magnetic moments. In the simplest case, if we assume that all microloops have identical parameters, the resulting magnetic moment of the sample will be simply described by an expression of the type (3.1.4), which is in a good agreement with the experiment. Normalized magnetic moment as a function of the reduced temperature (see Fig.3.2). The solid lines show the reversible curves obtained on the basis of 3.1.4. The experimental points (1) and (2) correspond to a yttrium ceramic ( $\beta = 0,01$ ) and yttrium ceramic powder ( $\beta = 0,023$ ) and (3) describe the experimental irreversible curve for the magnetic moment, normalized to the same quantity.

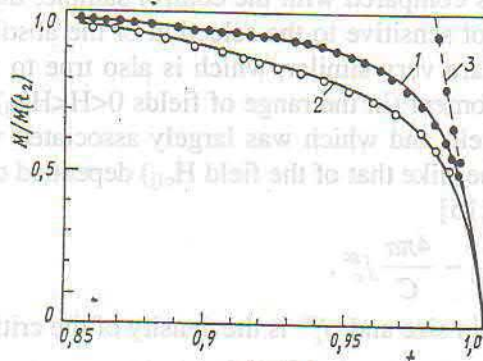


Fig.3.2

It should be noted that a relation similar to (3.1.3) for a thin-film cylinder was first obtained [13] by J.Bardeen. Soon afterwards, this phenomenon was confirmed experimentally

[14], Consequently, the above results can be treated as the analogy of this phenomenon in at HTS ceramics.

### 3.2 Magnetic properties of a ceramic containing silver [2]

A study was made of several characteristics of high-temperature superconducting ceramics with compositions represented by the formula  $(YBa_2Cu_3O_{7.8})_{1-x}Ag_x$ , where  $0 \leq x < 0.4$ , in static magnetic fields. These characteristics included the screening moment, hysteresis, diamagnetic moment. The addition of silver oxide resulted in the appearance of metallic silver in the form of isolated microinclusions when these ceramics were subjected to the heat treatment. Different technologies have been used by different authors and this has resulted in somewhat different dependences of the parameters of ceramics, particularly of the critical current on the concentration of silver.

Figure 3.3 shows the dependence of the screening moment of a ceramic free of silver on the applied static field. When the field was of the order of several Oe a maximum in the dependence  $M(H)$  was observed, the magnetic moment first falls and then rises again; this was accompanied by a gradual destruction of weak links by the field.

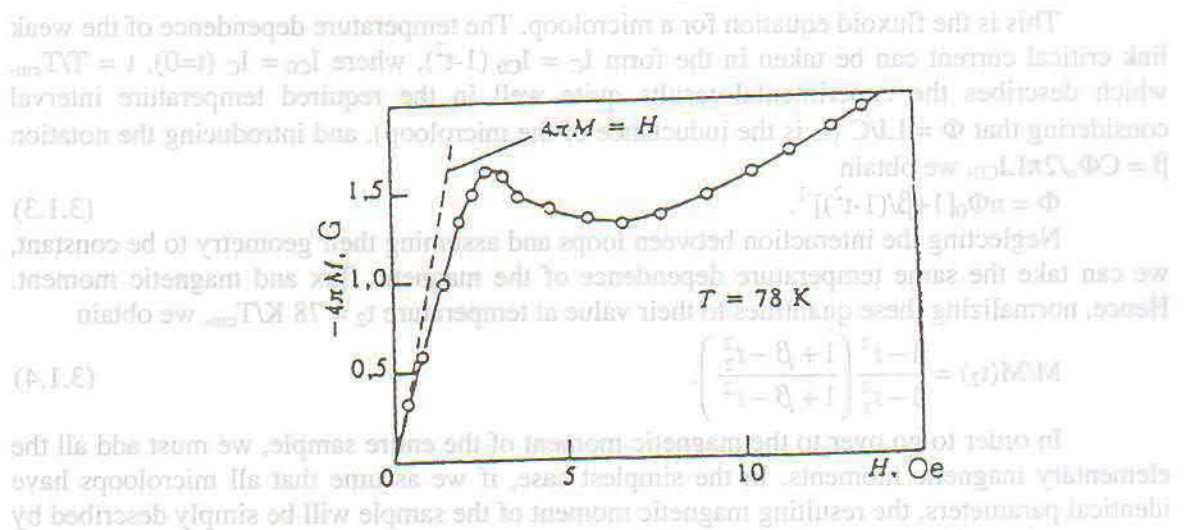


Fig.3.3

It is usual to assume that in a field  $H_{c1j}$  the dependence  $M(H)$  deviates from linearity, i.e. the field begins to penetrate into the sample. However, in reality this field is not exactly  $H_{c1j}$ , i.e. it may be influenced by the demagnetization factor of the sample, by the shape of the grains, etc. We therefore plotted in fig.3.4 the dependences of the normalized quantities  $H_{c1j}/H_{c1j}(0)$  and  $J_c/J_c(0)$  on the silver concentration, which allowed us to determine the influence of silver on these parameters compared with the control sample; these normalized quantities are useful because they are not sensitive to the selection of the absolute values. The dependences  $H_{c1j}/H_{c1j}(0)$  and  $J_c/J_c(0)$  are very similar, which is also true to the  $M_{max}$  curves.  $M_{max}$  is the maximum value of the moment (in the range of fields  $0 < H < H_{c2j}$ ), which screened the internal parts from the external field and which was largely associated with current flowing through weak links so that its value (like that of the field  $H_{c1j}$ ) depended on the critical density. In fact, the value of  $H_{c1j}$  obeyed [15]

$$H_{c1j} \sim \frac{4\pi a}{C} j_c^{gc}, \quad (3.2.1)$$

where  $a$  is the average grain size and  $j_c^{gc}$  is the density of the critical current through the contact between the grains. The density of the critical transport current  $J_c$ , proportional to  $j_c^{gc}$ , can be determined using the model of the critical state in ref.15 the magnetic moment is determined by increasing and reducing the field in the range  $H_{c1j} < H < H_{c2j}$ :

$$j_c = \frac{3c}{R} (M_0 \uparrow - M_0 \downarrow) \quad (3.2.2)$$

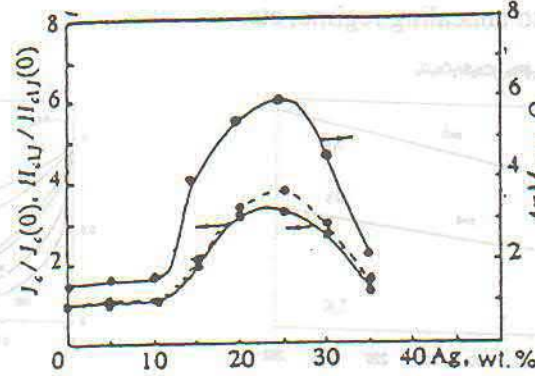


Fig.3.4

However, the quantity on the right-hand side is approximately proportional to  $M_{\max}$ , which accounts for the similarity of the curves. The normalized quantity  $j_c/j_c(0)$ , calculated from Eq(4), is plotted as a dotted curve in in Fig3.4. The value of the magnetic moment due to the currents between the grains can be determined by selecting a small hysteresis loop, which appears in the range of fields that do not exceed the boundaries of the second linear region. The rise of the values of  $H_{c1j}$ ,  $j_c$  and  $M_{\max}$  on increase in the amount of silver can be explained by the supression of creep of the flux due to the presence of silver and improvements in the grain-boundary contacts.

Fig.3.5 shows the hysteresis curves of a control sample (a) and of a sample with 25wt.% Ag(b). In contrast to usual hysteresis curves, Fig.4b has a sharp peak near zero field, correlated with peak near  $H_{c1j}$ . This could be explained by an increase in the contribution of the "small" hysteresis loop, associated with the Josephson current, because of enhancement of these currents against the background of the vortex pinning processes leading to "large" hysteresis loops.

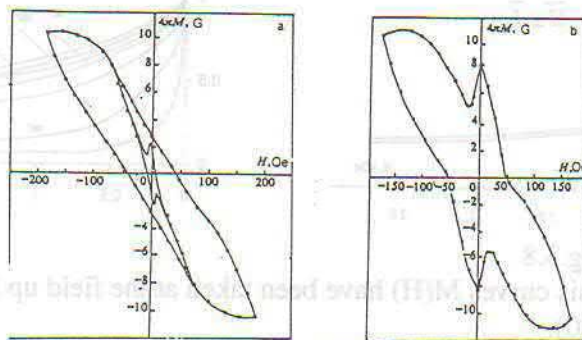


Fig.3.5

Introduction of silver into a ceramic sample improves a number of properties such as the critical current or screening of the Josephson critical field  $H_{c1j}$ , and the best results are obtained when the concentration of silver by weight is between 20 and 30 %.

### 3.3 Magnetic properties of the Bi-containing ceramics [16, 17]

The investigations of the Bi-containing superconducting ceramics are being carried out for long time already. It is known, that such a materials have a number of peculiarities, which makes them rather promising for application in some power appliances, and the textured samples use permits to raise significantly their critical parameters sumultaneously these materials have another peculiarities – a strong flux creep at the nitrogen boiling temperature, sensitivity to annealing regime, etc.

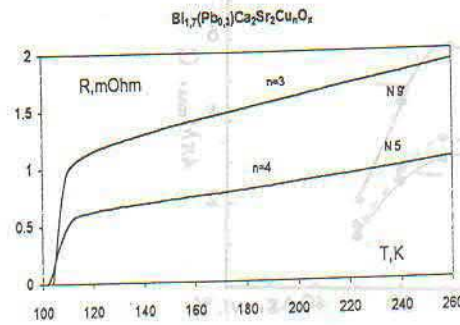


Fig.3.6

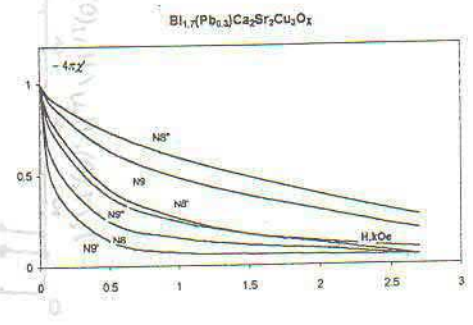


Fig.3.7

We investigated the influence of the processing regime temperature both of the powder and of the pressed samples on the electric and magnetic properties of these samples. For this purpose the reacting mixture in the powder form of the optimal composition  $\text{Bi}_{1.7}(\text{Pb}_{0.3})\text{Sr}_2\text{Ca}_2\text{Cu}_n\text{O}_x$  ( $n=3, n=4$ ) was annealed in the two-stage temperature regime. At the first stage the powder was processed at the synthesis temperature of  $850\text{--}855^\circ\text{C}$  for 30-50 hours, and at the second stage was additional annealing at  $840^\circ\text{C}$ . Then this powder was pressed into the samples (the pressure of  $7 \cdot 10^3$  MPa) and annealed at the temperature  $850^\circ\text{C}$  ( $n=4$ ) and  $855^\circ\text{C}$  ( $n=3$ ) and also at  $840^\circ\text{C}$  for both cases during 4-30 hours. The magnetic properties of the samples were studied by the crossed alternating and direct fields method. For the investigation of current characteristics the samples in the microbridge form with crosssection less them  $1 \text{ mm}^2$  were studied. The results of the investigation are given in fig.3.6-3.9.

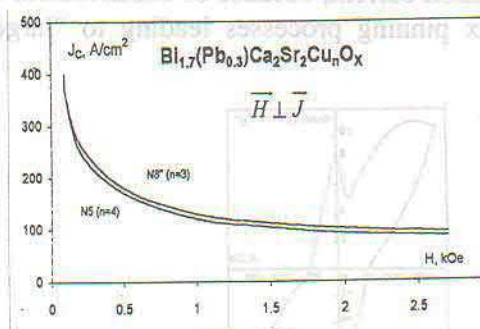


Fig.3.8

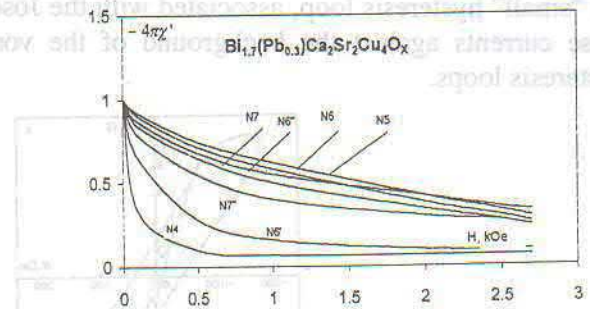


Fig.3.9

The hysteresis curves  $M(H)$  have been taken at the field up to 200 Oe and at different temperatures (Fig.3.10).

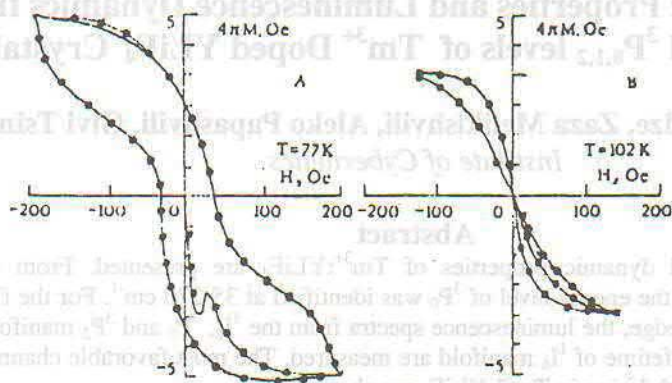


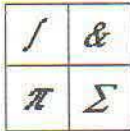
Fig.1

Fig.3.10.

From Fig.3.10 one can see that the curve taken at 102 K is different from the one at 77 K, for the hysteresis loop is desintegrated in two separate ones and at  $H=0$  there is zero magnetic momentum. This interesting fact, as it seems, can be explained by the supposition that the hysteresis of HTSC ceramics is caused partially by weak Josephson-type links, and by Abrikosov flux-linespinning.

#### References

1. Erlier and Recent Aspects of Superconductivity, edited by J.Bednorz, K.Muller, Springer Verlag, 1990
2. J.Sanikidze, S.Odenov, R.Kokhraidze, O.Modebadze, R.Tatulov, N.Birkaya, Superconductivity, v4, N7, p.1218, 1991 (rus)
3. Yu.A.Vidadi, E.Yanmaz, M.Altunbas, H.Karl, Physica C 225,124, 1994
4. P.N.Petrov, D.Balayev et al. Physics of Solid State, 39, N3, 418, 1997 (rus)
5. D.Staufer, Phys. Rep. 54, 1, 1979
6. Б.И.Шкловский, А.Л.Эфрос, Электронные свойства легированных полупроводников, Москва, Наука, 1979
7. G.Xiao, F.Streitz, M.Cieplak et al. Phys. Rev B 38, 776, 1998
8. J.Sanikidze, S.Odenov, R.Kokhraidze, G.Mumladze, I.Mjavanadze, N.Sabashvili, Proceedings of Tbilisi University, 333, Physics 34, 3 2000
9. R.Kokhraidze, S.Odenov, J.Sanikidze, Bulletin of the Georgian Academy of Science 159, N2, 217, 1999
10. Р.Кохреидзе, С.Оденов, Д.Саникидзе, Г.Цинцадзе, М.Чубабрия, Сообщения Академии Наук Грузии, 129, N1, 69,1998
11. Г.Цинцадзе, Д.Саникидзе, О.Модебадзе, С.Оденов, Р.Кохреидзе, М.Коява, Сообщения Академии Наук Грузии, 136, N2, 350,1989
12. R.Kokhraidze, S.Odenov, J.Sanikidze, Sov. J. Low Temp. Phys. 15(4), 248, 1999
13. J.Bardeen, Phys. Rev. Lett. 7, 162, 1961
14. T.Hans, J.Mersereau, Phys. Rev. A 135, N4, 944,1964
15. E.Meilikhov, Sverkhprovodimost (KIAE) 2(9), 5, 1989. Superconductivity 2(9), 7, 1989
16. N.Kekelidze, R.Kokhraidze, G.Mumladze, S.Odenov, J.Sanikidze, G.Tsintsadze, M.Chubabria, Bulletin of theGeorgian Academy of Sciences, 156, N1, 46,1977
17. R.Kokhraidse, A.Mestvirishvili, G.Mumladze, S.Odenov, N.Papunashvili, J.Sanikidze, M.Chubabria, in press.



## Spectroscopic Properties and Luminescence Dynamics from $^1D_2$ , $^1I_6$ and $^3P_{0,1,2}$ levels of $Tm^{3+}$ Doped $YLiF_4$ Crystals

Tamaz Medoidze, Zaza Melikishvili, Aleko Papashvili, Givi Tsintsadze  
*Institute of Cybernetics*

### Abstract

Spectroscopic and dynamic properties of  $Tm^{3+}:YLiF_4$  are presented. From the absorption spectra the energy level of  $^3P_0$  was identified at  $35\,270\text{ cm}^{-1}$ . For the first time to our knowledge, the luminescence spectra from the  $^1I_6$ ,  $^3P_1$  and  $^3P_2$  manifolds and the radiative lifetime of  $^1I_6$  manifold are measured. The most favorable channels for short wavelength lasing in  $Tm^{3+}:YLiF_4$  are observed.

### I. Introduction

Solid-state lasers based on trivalent thulium ( $Tm^{3+}$ ) ions and lasing, substantially, in the infrared and visible spectral ranges has long been recognized [1,2]. For these purposes the ultraviolet spectral range is poorly studied yet. On the other hand, previous investigations [3,4] and our data prompted us to research the high lying energy levels of  $Tm^{3+}$  for the purposes of short wavelength lasing realization.

In this paper we present the study of spectroscopic properties and the luminescence dynamics study for high lying energy levels ( $^1D_2$ ,  $^1I_6$ ,  $^3P_{0,1,2}$ ) of  $Tm^{3+}$  doped  $YLiF_4$  crystals at the room temperature and for two concentration of activator (1 and 2%). We finally report, for the first time to our knowledge, the luminescence lines and radiative lifetimes for several optical transitions in  $Tm^{3+}:YLiF_4$ .

### I. Experimental

The optical absorption spectra of  $Tm^{3+}:YLiF_4$  have been recorded in the visible and ultraviolet spectral regions ( $20\,000 - 40\,000\text{ cm}^{-1}$ ). All the absorption spectra presented in this paper were measured with a Specord M40 (UV-VIS) double-beam spectrophotometer. All emission spectra, in the range  $180 - 1\,100\text{ nm}$ , were taken by single-grating (1200 grooves per mm) double spectrograph/monochromator DFS-452 (top resolution:  $60\,000$  by Rayleigh criterion) and photomultiplier tubes PM-18A (200-600 nm), PM-51 (300-800 nm), PM-62 (400-1200 nm). Excitation was provided by Q-switched (20 ns), frequency-tripled (354.7 nm) and frequency-quartered (266 nm)  $Nd^{3+}:YAG$  laser in a single-pulse and pulse-repetition regimes (up to 100 Hz).

The  $YLiF_4$  (YLF) crystals used in this study has the  $C_{4h}^6$  space-group symmetry with four formula units per unit cell. The lattice-site symmetries of the ions are  $Y^{3+}$  ( $S_4$ ),  $Li^+$  ( $S_4$ ) and  $F^-$  ( $C_1$ ).  $Tm^{3+}$  ions that substitute for  $Y^{3+}$  experience a crystal field of  $S_4$  symmetry [3]. All the samples used were optically high-quality single crystals.

### III. Results and Discussion

#### 1. Absorption spectra

All the measured absorption spectra presented in this paper correspond to optical transitions from the ground state manifold ( $^3H_6$ ) at 300K.  $YLiF_4$  has an effective phonon energy  $490\text{ cm}^{-1}$  [5] and consequently one can suppose, that at 300 K all Stark levels ( $\Gamma_i$ ) of the  $^3H_6$  manifold are involved in an absorption process. The absorption spectra from  $^3H_6$  manifold to the energy levels of the  $^1I_6$  and  $^3P_{0,1,2}$  are presented in Fig.1 (2% sample) and for the  $^1D_2$  in the Fig. 2 (1 and 2% samples).

In the absorption spectra one can clearly observe five groups of spectral lines. These groups are identified as absorption to the  $^1D_2$ ,  $^1I_6$ ,  $^3P_0$ ,  $^3P_1$ ,  $^3P_2$  manifolds. Absorption in the range  $37\ 000 - 38\ 800\ \text{cm}^{-1}$  corresponds to the  $^3H_6 \rightarrow ^3P_2$  transition. Due to selection rules for  $S_4$  symmetry, this spectral band must involve 29 transition lines. Observed profile of the spectral band points that the peaks at  $37730$ ,  $37760$ ,  $38020$ ,  $38240$  and  $38300\ \text{cm}^{-1}$  caused by these transitions ( $\Gamma_i \rightarrow \Gamma_j$  ( $i \neq j$ )). Here  $\Gamma_i$  is the crystalline quantum number labeling Stark levels ( $i = 1, 2, 3, 4$  in our case).

Absorption in the range  $36\ 100 - 36\ 700\ \text{cm}^{-1}$  corresponds to the  $^3H_6 \rightarrow ^3P_1$  transition. Due to the selection rules 17 transitions between Stark levels are allowed. These transitions are observed as three groups. The analysis of the peak at  $36\ 540\ \text{cm}^{-1}$  shows, that it can be identified as  $^3H_6$  ( $0\ \text{cm}^{-1}; \Gamma_2$ )  $\rightarrow$   $^3P_1$  ( $36540\ \text{cm}^{-1}; \Gamma_{3,4}$ ) transition. The analysis of peak at  $36\ 480\ \text{cm}^{-1}$  shows that this peak is consists of two transitions  $^3H_6$  ( $0,30\ \text{cm}^{-1}; \Gamma_2, \Gamma_{3,4}$ )  $\rightarrow$   $^3P_1$  ( $36480\ \text{cm}^{-1}; \Gamma_1$ ) and the third wide band with peak at  $36\ 190\ \text{cm}^{-1}$  are the transitions from the higher Stark levels of  $^3H_6$  to the Stark levels of  $^3P_1$  (hot bands).

When identifying  $^3P_0$  some difficulties occur. At present there is no consent about its energy value. Following calculations [3] corresponding energy value of  $^3P_0$  is  $35\ 830\ \text{cm}^{-1}$  whereas the calculations and experimental data of [4] pointed to  $35\ 540\ \text{cm}^{-1}$ . However the significant discrepancies between results of [3,4] and our data takes place. In absorption spectra (see Fig.1), in the energy range  $35500 - 35900\ \text{cm}^{-1}$  (for the both concentration of activator) it is impossible to eliminate any peak. On the other hand, at  $35\ 270\ \text{cm}^{-1}$  the sharp peak is observed, in addition it well fitted to Lorentzian. Consequently one can identify this peak caused by  $^3H_6$  ( $0, \Gamma_2$ )  $\rightarrow$   $^3P_0$  ( $35\ 270, \Gamma_1$ ) transition. Granting this, one can suppose, that the energy of  $^3P_0$  is  $35\ 270\ \text{cm}^{-1}$  and the broad peak at the low energy side in the spectrum are the hot bands.

Absorption in the range  $34\ 300 - 34\ 900\ \text{cm}^{-1}$  corresponds to the  $^3H_6 \rightarrow ^1I_6$  transition. These transitions are observed as two groups with peaks at  $34\ 490$  and  $34\ 770\ \text{cm}^{-1}$ . Due to the selection rules 75 transitions between Stark levels are allowed. Because of small energy gaps between Stark levels and availability of such amount of transitions, it is impossible to segregate correctly each transition at the room temperature.

Absorption in the range  $27\ 500 - 28\ 400\ \text{cm}^{-1}$  corresponds to the  $^3H_6 \rightarrow ^1D_2$  transition (Fig.2). Due to the selection rules 29 transitions between Stark levels are allowed. For the 2% sample three well-separated peaks and the shoulder (at the high-energy side) are observed. For the 1% sample the observed peaks are five. Obviously, for both samples, certain group of transitions forms each peak. The peaks at  $27\ 630$  and  $27\ 930\ \text{cm}^{-1}$  are the same for both samples. The peaks at  $27\ 990$  and  $28\ 030\ \text{cm}^{-1}$ , observed only for 1% sample, due to concentration broadening overlap and generate the peak at their center of gravity ( $28\ 010\ \text{cm}^{-1}$ ). The shoulder in the range of  $28\ 200\ \text{cm}^{-1}$  does not accord within transitions between Stark levels adjusted from [3].

On the basis of absorption spectra we give the diagram of  $\text{Tm}^{3+}:\text{YLiF}_4$  energy levels (Fig.3)

## 2. The Luminescence spectra

The luminescence from the  $^1D_2$  manifold was observed by excitation with the radiation of the frequency-tripled ( $354.7\ \text{nm}$ ) YAG:Nd $^{3+}$  laser. The diagram of excitation and observed luminescence transitions ( $180 \leq \lambda \leq 1100\ \text{nm}$ ) from  $^1D_2$  manifold is presented in Fig.3b. (Observed transient luminescence transitions is not applied). Also, in the Fig. 4, the whole, normalized luminescence spectra from  $^1D_2$  manifold is presented. It should be noted that the most intensive are the transitions  $^1D_2 \rightarrow ^3F_4$ ,  $^3H_6$ .

The diagram of excitation and observed luminescence transitions from  $^1I_6$  and  $^3P_{0,1,2}$  manifolds is presented in Fig.3a. At the first time, by the radiation of the frequency-quartered

(266 nm) YAG:Nd<sup>3+</sup> laser the <sup>3</sup>P<sub>2</sub> level was excited. The 3 and 2 effective phonons required to bridge the energy gap between <sup>3</sup>P<sub>2</sub> - <sup>3</sup>P<sub>1</sub> - <sup>3</sup>P<sub>0</sub>, <sup>1</sup>I<sub>6</sub> manifolds. Consequently, due to nonradiative transitions, from <sup>3</sup>P<sub>2</sub> the effective population of <sup>1</sup>I<sub>6</sub> occurs via the <sup>3</sup>P<sub>1</sub> manifold. Since this transitions have the multiphonon nature then relaxation process pass slowly, and this allow for registration the luminescence from <sup>3</sup>P<sub>2</sub> and <sup>3</sup>P<sub>1</sub> under the nanosecond excitation. In the Fig. 5, the luminescence spectra from these manifolds to the <sup>3</sup>F<sub>4</sub> are presented.

In the Fig. 6 the normalized spectra of luminescence from the <sup>1</sup>I<sub>6</sub> manifold, in the 280 – 480 nm range, is presented. It should be noted that the most intensive are the transitions <sup>1</sup>I<sub>2</sub> → <sup>3</sup>F<sub>4</sub>, <sup>3</sup>H<sub>4</sub>.

### 3. The luminescence dynamics

The decay of <sup>1</sup>D<sub>2</sub> and <sup>1</sup>I<sub>6</sub> manifolds measured at the room temperature is presented in Fig. 7 and Fig. 8. The luminescence decay curves from <sup>1</sup>D<sub>2</sub> manifold is well fitted to the exponential decay. The 1% and 2% samples have the significantly different values of luminescence lifetimes: 57.5 μs for 1% sample and 34.5 μs for 2% one. Such significant difference, of course, is specified by the concentration of activator. The luminescence decay curve from <sup>1</sup>I<sub>6</sub> manifold (2%) does not fitted well to the exponential decay. One can suppose, that the <sup>1</sup>I<sub>6</sub> manifold is populated via the <sup>3</sup>P<sub>2</sub> - <sup>3</sup>P<sub>1</sub> - <sup>3</sup>P<sub>0</sub> - <sup>1</sup>I<sub>6</sub> relaxation channel and transient population may cause such derivation. The 1% and 2% samples also have the significantly different values of luminescence lifetimes: 88.2 μs for 1% sample and 66.3 μs for 2% sample. As well it should be noted that the luminescence lifetimes of <sup>1</sup>I<sub>6</sub> manifold is exceed the luminescence lifetimes of <sup>1</sup>D<sub>2</sub> manifold.

## IV. Conclusions

- At the room temperature the absorption spectra of Tm<sup>3+</sup>:YLiF<sub>4</sub> mainly formed by the hot bands.
- In the absorption spectra the energy level of <sup>3</sup>P<sub>0</sub> is identified at 35 270 cm<sup>-1</sup>
- The effective excitation channel of <sup>1</sup>I<sub>6</sub> via the <sup>3</sup>P<sub>2</sub> manifold is observed.
- The luminescence spectra from <sup>1</sup>D<sub>2</sub>, and for the first time to our knowledge, from the <sup>1</sup>I<sub>6</sub>, <sup>3</sup>P<sub>1</sub> and <sup>3</sup>P<sub>2</sub> manifolds in Tm<sup>3+</sup>:YLiF<sub>4</sub> are observed.
- The most intensive luminescence channel for each high energy level is transition to the <sup>3</sup>F<sub>4</sub> manifold. These channels are the most favorable for short wavelength lasing.
- The radiative lifetimes of <sup>1</sup>D<sub>2</sub> manifold in Tm<sup>3+</sup>:YLiF<sub>4</sub> were measured for the 1% (57.5 μs) and 2% (34.5 μs) concentrations of activator.
- For the first time to our knowledge, the radiative lifetimes of <sup>1</sup>I<sub>6</sub> manifold in Tm<sup>3+</sup>:YLiF<sub>4</sub> were measured for the 1% (88.2 μs) and 2% (66.3 μs) concentrations of activator.

## References

- [1]. A.A. Kaminskii. Phys. Stat. Sol. (a) **148**, 9 (1995)
- [2]. V. Sudesh, E.M. Goldys. J. Opt. Soc. Am. **B 17**, 1068 (2000)
- [3]. H.P. Jenssen, A. Linz, R.P. Leavitt, C.A. Morrison and D.E. Wortman. Phys. Rev. **B11**, (1975)
- [4]. M. Dulick, G.E. Faulkner, N.J. Cockroft and D.C. Nguyen. Journal of Luminescence **48&49**, 517 (1991)
- [5]. E.B. Sveshnikova, A.A. Stroganov and N.T. Timofeev, Opt. Spektrosk. **64**,73 (1988)

# Figures

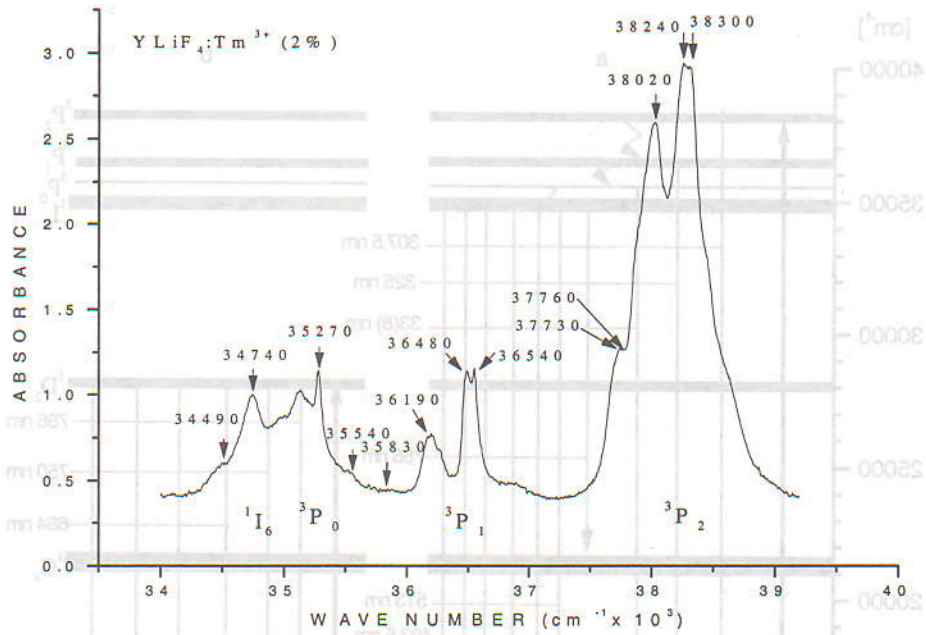


Fig.1. Absorption spectra of <sup>1</sup>I<sub>6</sub>, <sup>3</sup>P<sub>0,1,2</sub> manifolds at T = 300 K.

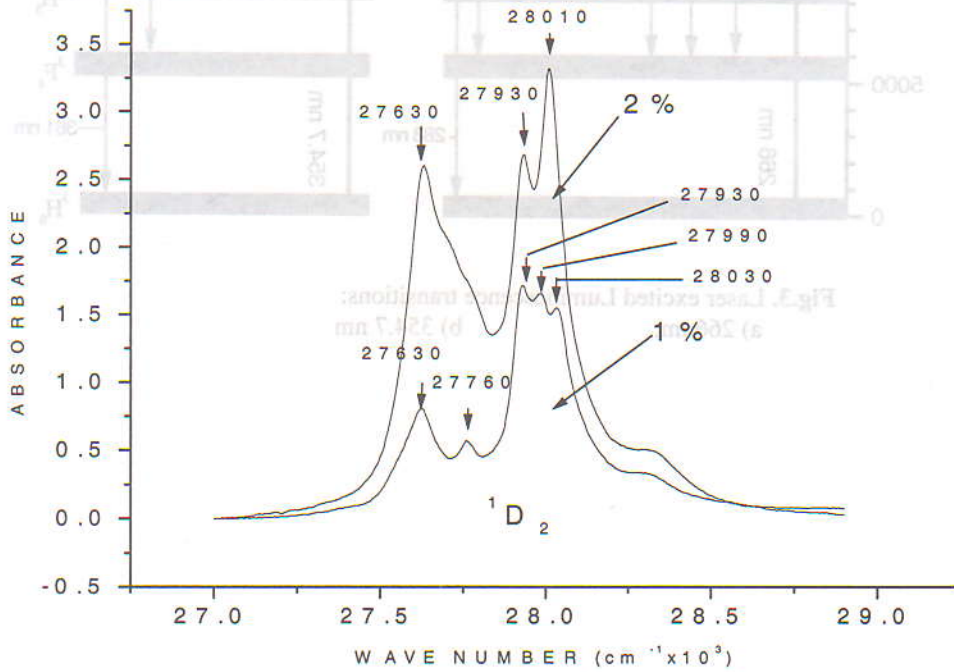


Fig.2. Absorption spectra of <sup>1</sup>D<sub>2</sub> manifold for 1% and 2% samples at T=300 K.

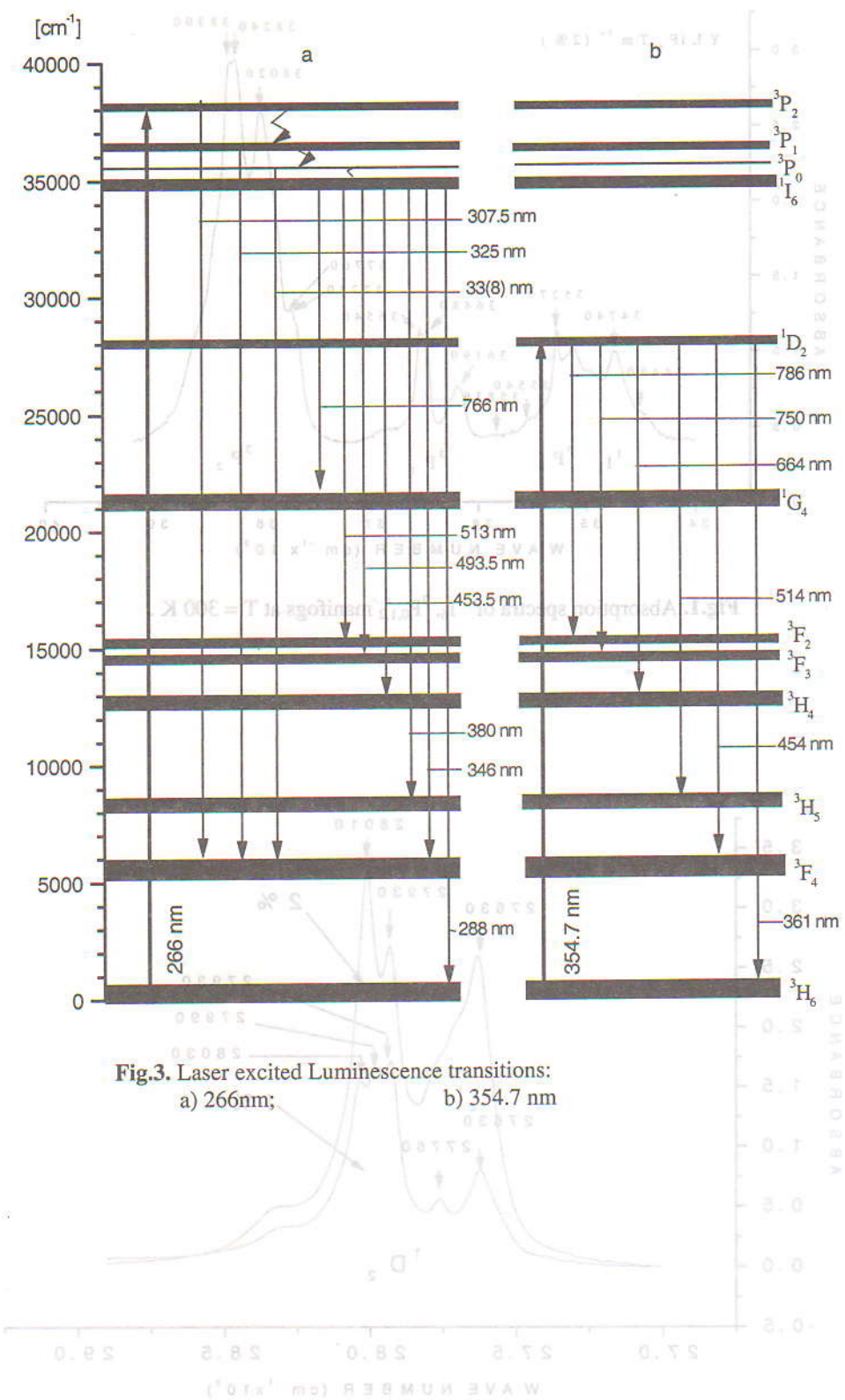


Fig.3. Laser excited Luminescence transitions:  
 a) 266nm; b) 354.7 nm

Fig.2. Absorption spectra of  $^1D_2$  manifold for 1% and 5% samples at T=300 K.

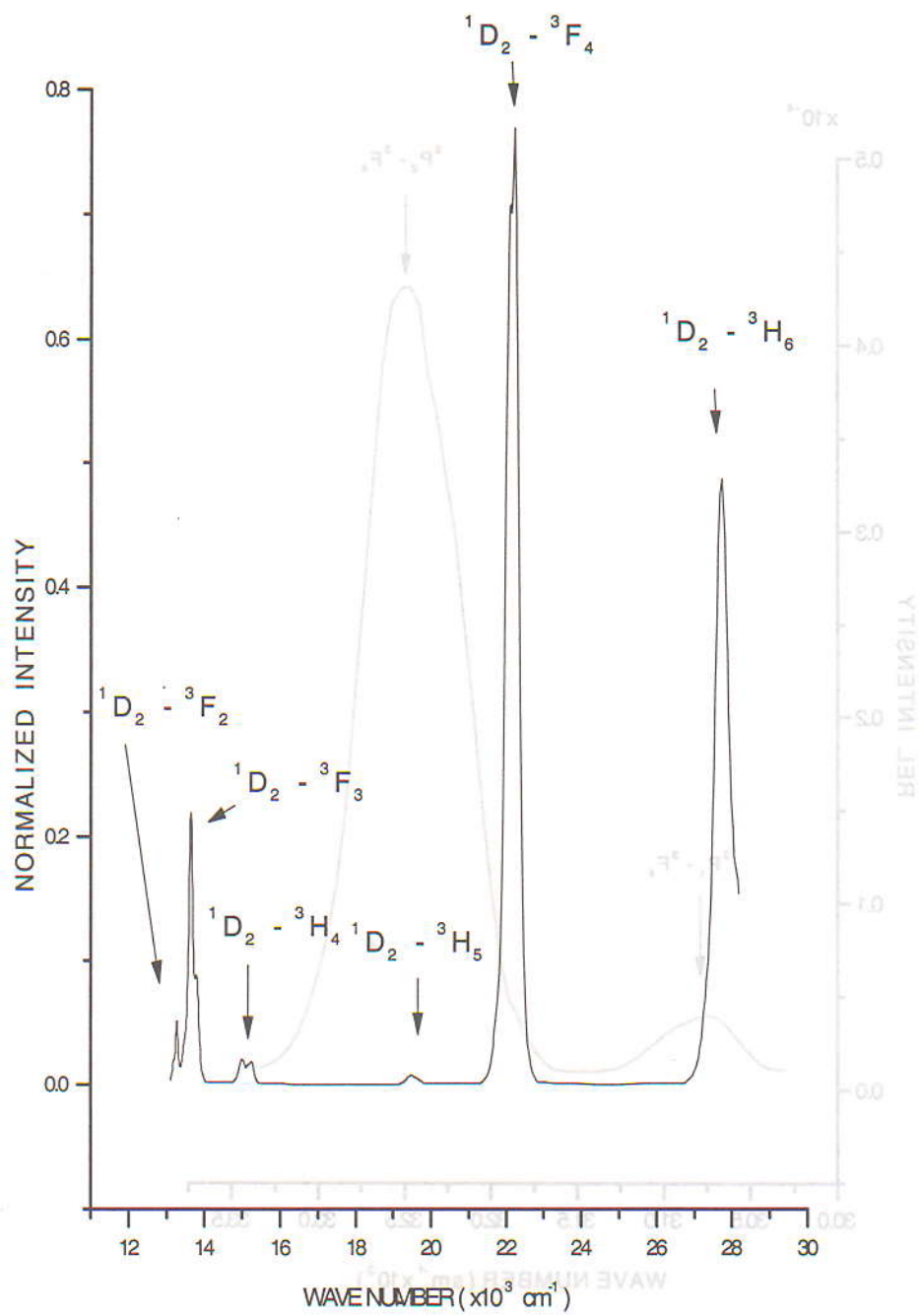


Fig.4. Luminescence spectra from  $^1D_2$  manifold.

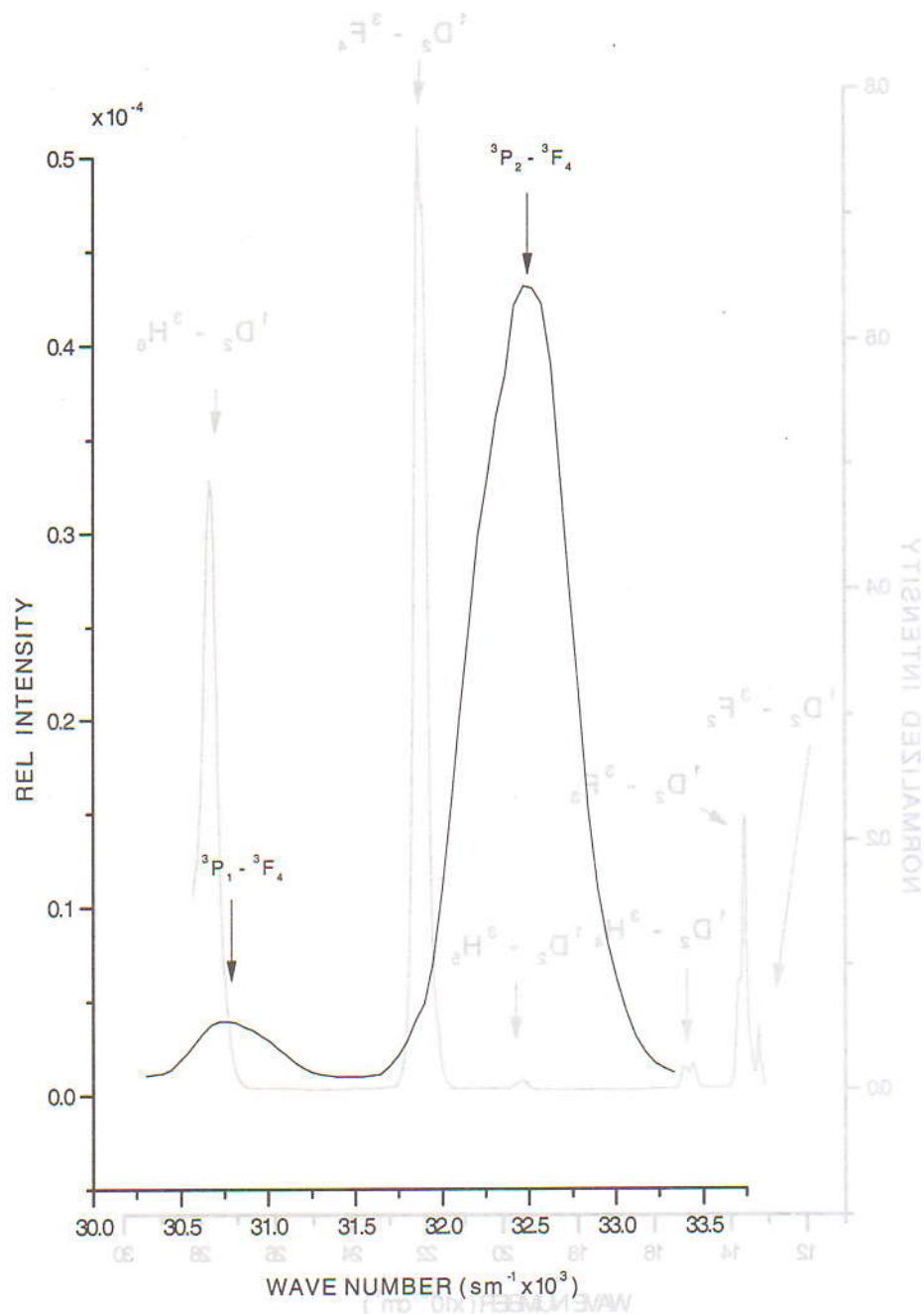


Fig. 5. Luminescence spectra from  ${}^3P_2$  and  ${}^3P_1$  manifolds.

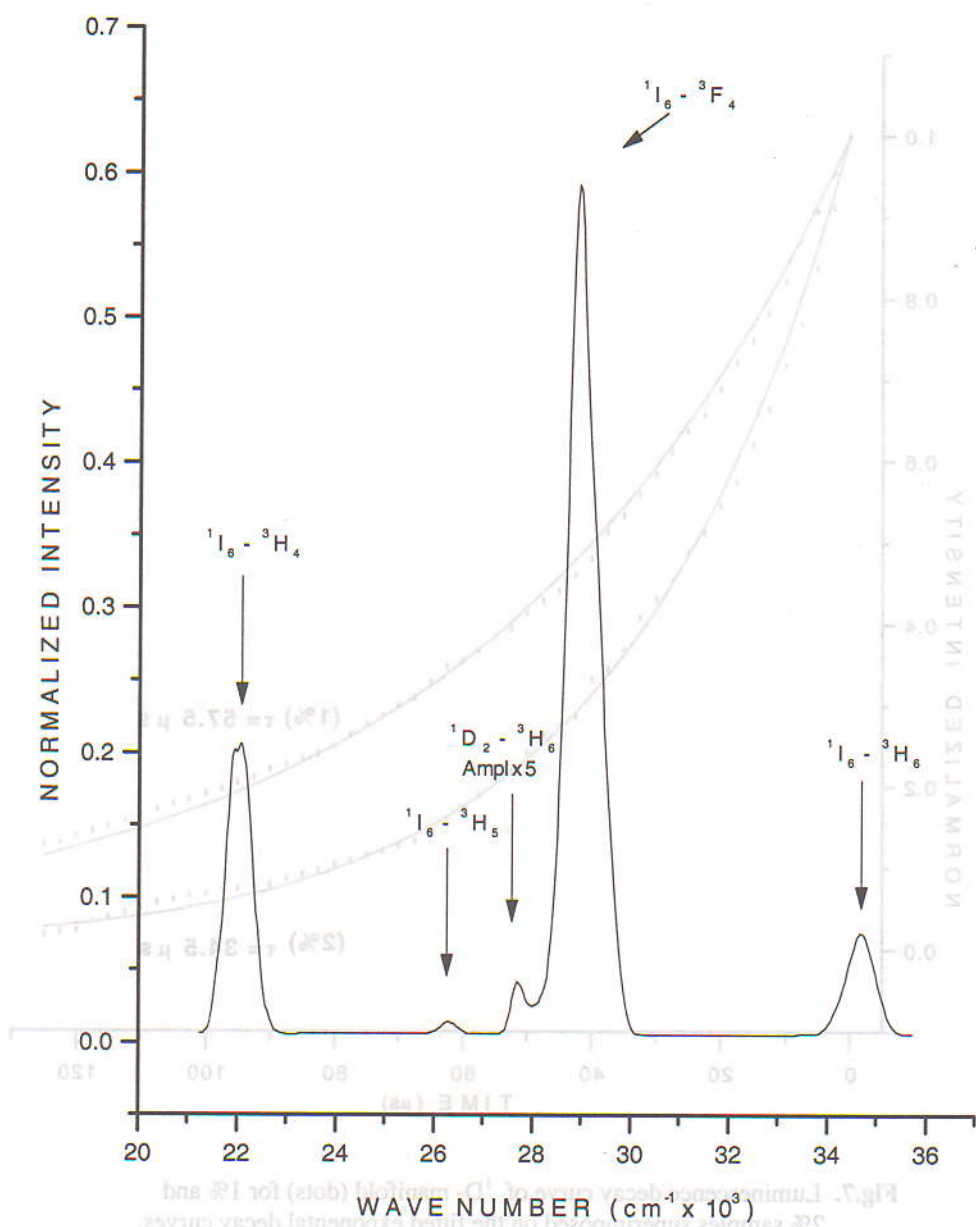


Fig.6. Luminescence spectra from  ${}^1I_6$  manifold.

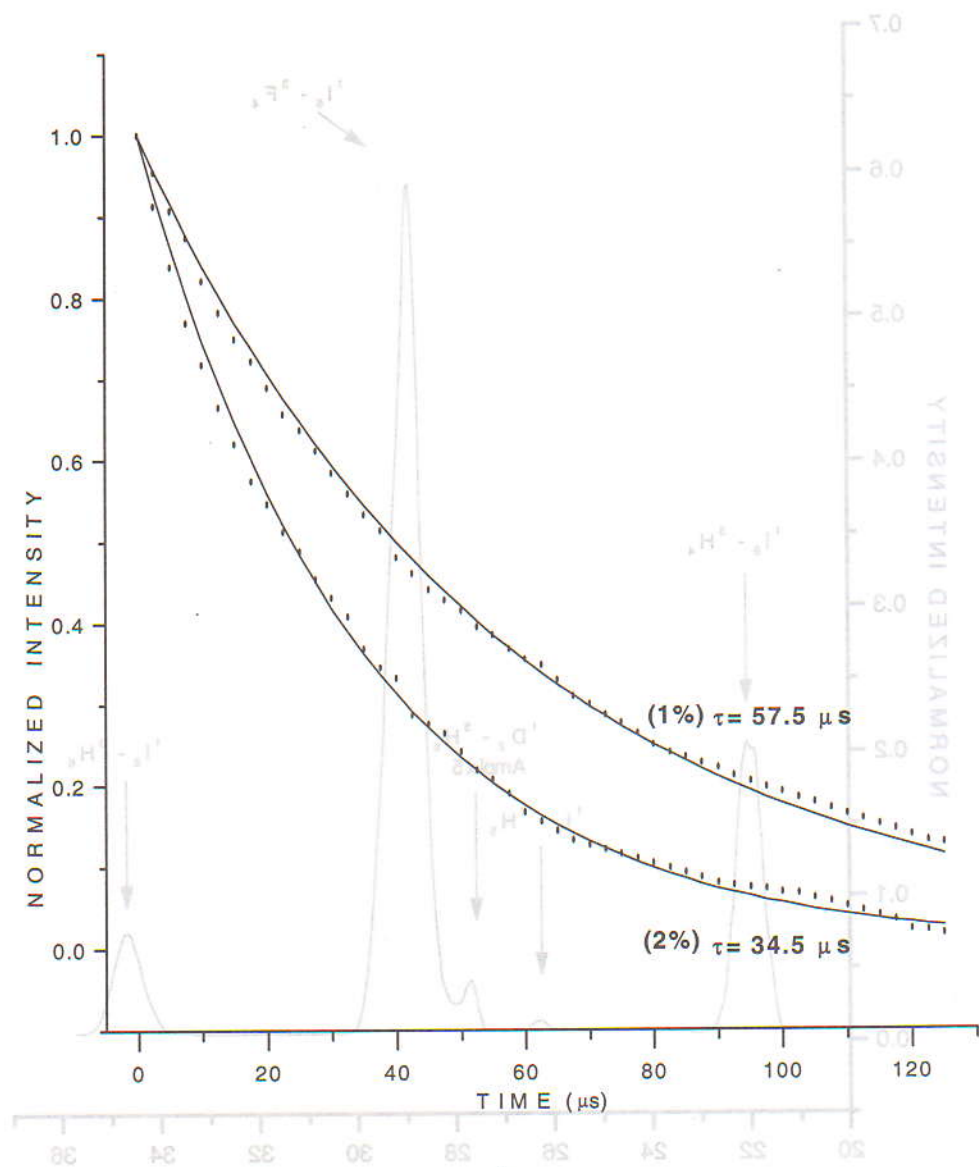


Fig.7. Luminescence decay curve of  $^1D_2$  manifold (dots) for 1% and 2% samples superimposed on the fitted exponential decay curves.

Fig.6. Luminescence spectra from  $^1D_2$  manifold.

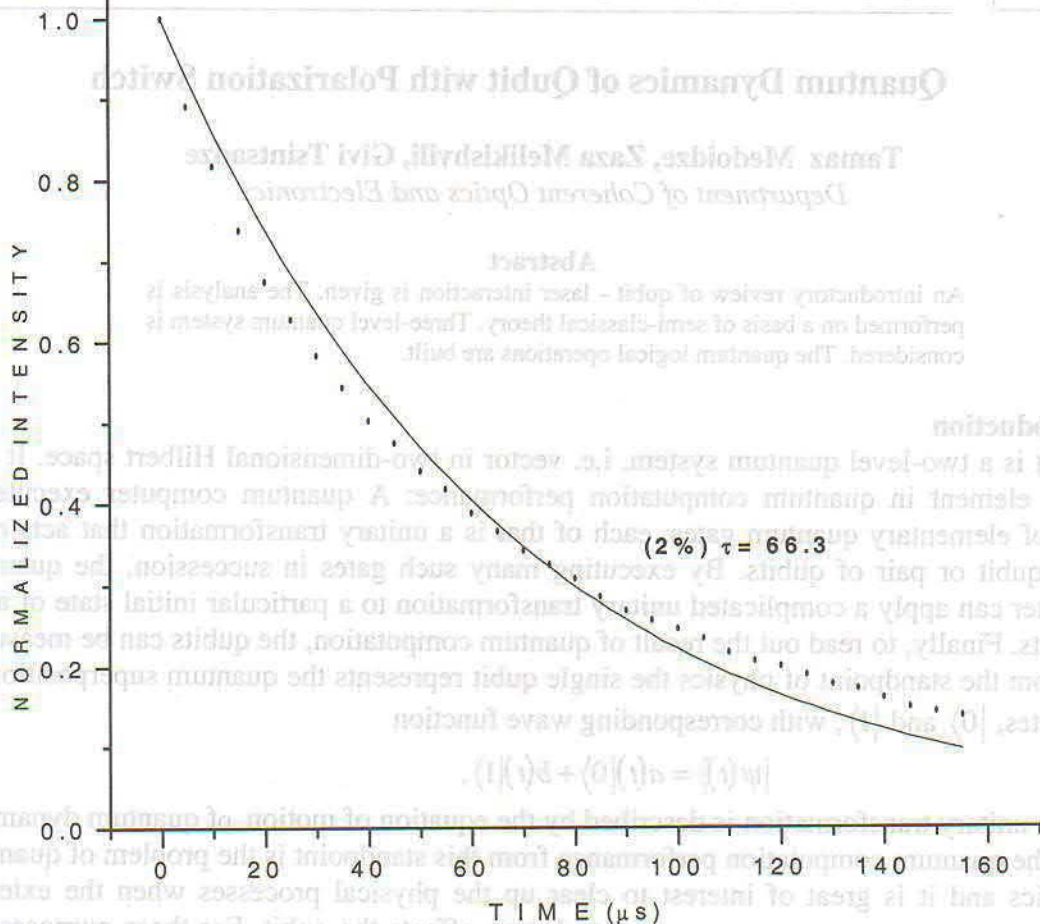
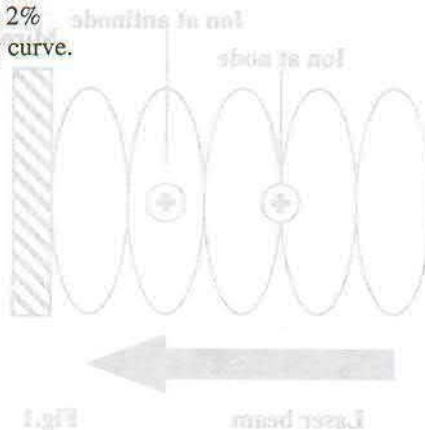


Fig. 8. Luminescence decay curve (dots) of  $^1I_6$  manifold for 2% sample superimposed on the fitted exponential decay curve.



Further study of interaction between the laser and ion manifold [2].  
 One can build using a semi-classical approach in which the laser field is described classically and the ion quantum-mechanically. For the coherent light source, such as laser, the validity of the semi-classical approach turns to the following condition imposed on the electric field strength of radiation [4]:

$$E \gg \sqrt{\hbar c \Delta \lambda} \lambda$$

where  $\lambda$  is the wavelength of radiation, and  $\Delta \lambda$  is

the linewidth in the emission spectrum. For the typical values of laser radiation ( $\lambda = 500 \text{ nm}$  and  $\Delta \lambda = 0.01 \text{ nm}$ ,  $E \gg 1 \text{ V/cm}$ ) and one can say that this condition is fulfilled in the laser-stop (ion) interaction experiments.

## II. Laser-dipole interaction

Let us introduce the wave function of three-level quantum particle in the standard form:

$$|\Psi(t)\rangle = a(t)|0\rangle \exp(-iE_0 t/\hbar) + b(t)|1\rangle \exp(-iE_1 t/\hbar) + c(t)|2\rangle \exp(-iE_2 t/\hbar) \quad (1)$$



## Quantum Dynamics of Qubit with Polarization Switch

**Tamaz Medoidze, Zaza Melikishvili, Givi Tsintsadze**  
*Department of Coherent Optics and Electronics*

### Abstract

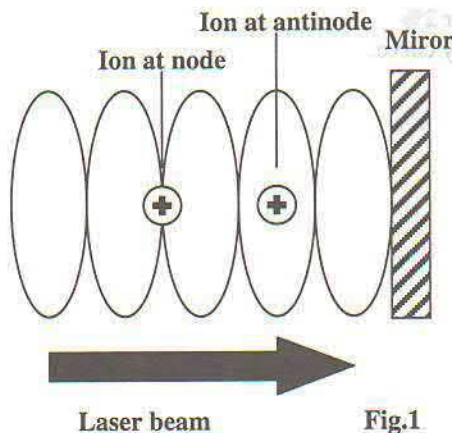
An introductory review of qubit - laser interaction is given. The analysis is performed on a basis of semi-classical theory. Three-level quantum system is considered. The quantum logical operations are built.

### I. Introduction

A qubit is a two-level quantum system, i.e. vector in two-dimensional Hilbert space. It is a central element in quantum computation performance: A quantum computer executes a series of elementary quantum gates, each of that is a unitary transformation that acts on a single qubit or pair of qubits. By executing many such gates in succession, the quantum computer can apply a complicated unitary transformation to a particular initial state of a set of qubits. Finally, to read out the result of quantum computation, the qubits can be measured [1]. From the standpoint of physics the single qubit represents the quantum superposition of two states,  $|0\rangle$  and  $|1\rangle$ , with corresponding wave function

$$|\psi(t)\rangle = a(t)|0\rangle + b(t)|1\rangle,$$

and the unitary transformation is described by the equation of motion of quantum dynamics. Thus, the quantum computation performance from this standpoint is the problem of quantum dynamics and it is great of interest to clear up the physical processes when the external



perturbation affects the qubit. For these purposes, let us now consider in detail the model of performing the laser operations on the qubits formed from two-level ions [2].

Further study of interaction between the laser and ion one can build using a semi-classical approach, in which the laser field is described classically and the ion quantum-mechanically. For the coherent light source, such as laser, the validity of the semi-classical approach turns to the following condition imposed on the electric field strength of radiation [4]:

$$E \gg \sqrt{\hbar c \Delta\lambda / \lambda^5},$$

where  $\lambda$  is the wavelength of radiation, and  $\Delta\lambda$  is the linewidth in the emission spectrum. For the typical values of laser radiation ( $\lambda = 500\text{nm}$  and  $\Delta\lambda \sim 0.01\text{nm}$ ),  $E \gg 1\text{V/cm}$  and one can say that this condition is fulfilled in the laser-atom (ion) interaction experiments.

### II. Laser-qubit interaction

Let us introduce the wave function of three-level quantum particle in the standard form:

$$|\Psi(t)\rangle = a(t)|0\rangle \exp(-i E_0 t / \hbar) + b(t)|1\rangle \exp(-i E_1 t / \hbar) + c(t)|2\rangle \exp(-i E_2 t / \hbar). \quad (1)$$

Assume that  $|0\rangle$  interacts with  $|1\rangle$  and  $|2\rangle$ , and  $|2\rangle$  does not interact at all with  $|1\rangle$ . Under these conditions general expressions for the three-level quantum particle are

$$\begin{aligned} i\hbar \frac{da(t)}{dt} &= V_{01}b(t)\exp(-i\omega_{10}t) + V_{02}c(t)\exp(-i\omega_{20}t), \\ i\hbar \frac{db(t)}{dt} &= V_{01}^*a(t)\exp(i\omega_{10}t), \\ i\hbar \frac{dc(t)}{dt} &= V_{02}^*a(t)\exp(i\omega_{20}t), \end{aligned} \quad (2)$$

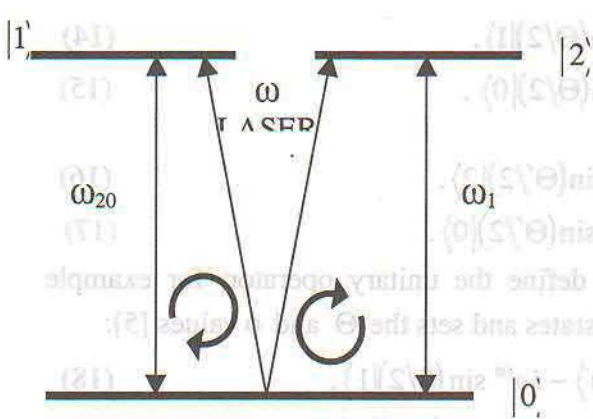
where  $\omega_{mn} = \omega_m - \omega_n$ ;  $V_{mn} = \langle m|\hat{V}_i|n\rangle = V_{nm}^*$  and  $V_{21} = 0$ .

Now, let us consider the laser beam, with polarization switch, in a standing wave configuration (see Fig.1, 2), propagating along the resonator axis ( $z$ )

$$\mathbf{E} = 2(\boldsymbol{\varepsilon}_r \text{ or } \boldsymbol{\varepsilon}_l)E_0 \cos(\omega t)\cos(kz), \quad (3)$$

and interacting with quantum particle located at  $z_0$ . In (3)  $\boldsymbol{\varepsilon}_i$  is the polarization vector,  $E_0$  is the amplitude of the electric field,  $\omega$  is the laser frequency and  $k = \omega/c$  is the wavenumber.

We assume that the laser beam with  $\boldsymbol{\varepsilon}_r$  couples only  $|0\rangle$  and  $|1\rangle$ , and with  $\boldsymbol{\varepsilon}_l$  couples only



$|0\rangle$  and  $|2\rangle$  but not vice-versa. As well the laser frequency to be  $\omega \approx \omega_{mn}$ . Substituting (3) in (2) one can immediately obtain two pairs of equations

$$\begin{cases} i \frac{da(t)}{dt} = b(t)\Omega_1 \exp(i\Delta_1 t) \\ i \frac{db(t)}{dt} = a(t)\Omega_1^* \exp(-i\Delta_1 t) \end{cases}, \quad (4)$$

for  $\boldsymbol{\varepsilon}_r$  switch

Fig. 2. Three-level quantum particle in the field of laser radiation with polarization switch.

$$\begin{cases} i \frac{da(t')}{dt} = c(t')\Omega_2 \exp(i\Delta_2 t') \\ i \frac{dc(t')}{dt} = a(t')\Omega_2^* \exp(-i\Delta_2 t') \end{cases} \text{ for } \boldsymbol{\varepsilon}_l \text{ switch.} \quad (5)$$

where the detunings

$$\Delta_1 = \omega - \omega_{10}, \quad (6)$$

$$\Delta_2 = \omega - \omega_{20} \quad (7)$$

and the Rabi frequencies are given by

$$\Omega_1 = \frac{eE_0}{\hbar} \langle 0|\hat{r}|1\rangle \boldsymbol{\varepsilon}_r \cos(kz), \quad (8)$$

$$\Omega_2 = \frac{eE_0}{\hbar} \langle 0|\hat{r}|2\rangle \boldsymbol{\varepsilon}_l \cos(kz). \quad (9)$$

One can represent these frequencies as

$$\Omega_1 = \frac{|\Omega_1|}{2} \exp(i\phi), \quad (10)$$

$$\Omega_2 = \frac{|\Omega_2|}{2} \exp(i\phi'). \quad (11)$$

If we assume that the detunings in equations (4) and (5) are zero (for example, if  $|1\rangle$  and  $|2\rangle$  are magnetic sublevels), then these equations have the following solutions:

$$\begin{pmatrix} a(t) \\ b(t) \end{pmatrix} = \begin{pmatrix} \cos(\Theta/2) & ie^{i\phi} \sin(\Theta/2) \\ ie^{-i\phi} \sin(\Theta/2) & \cos(\Theta/2) \end{pmatrix} \begin{pmatrix} a(0) \\ b(0) \end{pmatrix}, \quad (12)$$

$$\begin{pmatrix} a(t') \\ c(t') \end{pmatrix} = \begin{pmatrix} \cos(\Theta'/2) & ie^{i\phi'} \sin(\Theta'/2) \\ ie^{-i\phi'} \sin(\Theta'/2) & \cos(\Theta'/2) \end{pmatrix} \begin{pmatrix} a(0) \\ b(0) \end{pmatrix}, \quad (13)$$

where  $\Theta = |\Omega_1|t$  and  $\Theta' = |\Omega_2|t'$ .

### III. Quantum logical operations

Writing down the wave function for the single qubits one immediately finds the following dressed states:

$$|0(t)\rangle = \cos(\Theta/2)|0\rangle - ie^{i\phi} \sin(\Theta/2)|1\rangle, \quad (14)$$

$$|1(t)\rangle = \cos(\Theta/2)|1\rangle - ie^{-i\phi} \sin(\Theta/2)|0\rangle, \quad (15)$$

and

$$|0(t')\rangle = \cos(\Theta'/2)|0\rangle - ie^{i\phi'} \sin(\Theta'/2)|2\rangle, \quad (16)$$

$$|2(t')\rangle = \cos(\Theta'/2)|2\rangle - ie^{-i\phi'} \sin(\Theta'/2)|0\rangle. \quad (17)$$

Under appropriate polarization switch one can define the unitary operator, for example  $\hat{V}(\Theta, \phi)$ , which affects the qubit  $|0(t)\rangle$  and  $|1(t)\rangle$  states and sets the  $\Theta$  and  $\phi$  values [5]:

$$\hat{V}(\theta \Rightarrow \Theta, \phi \Rightarrow \phi)|0(t)\rangle = \cos(\theta/2)|0\rangle - ie^{i\phi} \sin(\theta/2)|1\rangle, \quad (18)$$

$$\hat{V}(\theta \Rightarrow \Theta, \phi \Rightarrow \phi)|1(t)\rangle = \cos(\theta/2)|1\rangle - ie^{-i\phi} \sin(\theta/2)|0\rangle. \quad (19)$$

or

$$\hat{V}(\theta, \phi) = \begin{pmatrix} \cos(\theta/2) & ie^{i\phi} \sin(\theta/2) \\ ie^{-i\phi} \sin(\theta/2) & \cos(\theta/2) \end{pmatrix}. \quad (20)$$

All this operations for single qubit has the form of rotation, whereas quantum logical operations are required that have the form of a reflection [5,6]. To perform this operation the third level (in this case  $|2\rangle$ ) is necessary. For example, if  $\hat{V}(\pi, \pi/2)$  is applied ( $\pi$ -pulse) to single qubit, one can obtain that this operator changes  $|0\rangle$  into  $|1\rangle$  and vice-versa (with a  $\pi$  phase shift):

$$\hat{V}(\pi, \pi/2): \begin{cases} |0\rangle \rightarrow |1\rangle \\ |1\rangle \rightarrow -|0\rangle \end{cases}.$$

After the polarization switch and affecting with  $\hat{V}'(2\pi, \pi/2)$ , the  $2\pi$ -pulse changes a sign of the basic states  $|0\rangle$  and  $|2\rangle$ :

$$\hat{V}'(2\pi, \pi/2): \begin{cases} |0\rangle \rightarrow -|0\rangle \\ |2\rangle \rightarrow -|2\rangle \end{cases}.$$

It is easily seen, that using the operator  $\hat{V}(\pi, \pi/2)$  in conjunction with  $\hat{V}'(2\pi, \pi/2)$ , one can perform the *NOT* operation:

$$\hat{V}(\pi, \pi/2): \begin{matrix} |0\rangle \rightarrow |1\rangle \\ |1\rangle \rightarrow -|0\rangle \end{matrix} \Rightarrow \hat{V}'(2\pi, \pi/2): \begin{matrix} |0\rangle \rightarrow -|0\rangle \\ |2\rangle \rightarrow -|2\rangle \end{matrix} \Rightarrow \begin{matrix} |0\rangle \rightarrow |0\rangle \\ |1\rangle \rightarrow |1\rangle \end{matrix} \equiv \text{NOT}$$

0	1
1	0

Similarly, the single-bit Hadamard operation  $\hat{R}$  can be performed with  $\hat{V}(3\pi/2, \pi/2)$  and  $\hat{V}'(2\pi, \pi/2)$  operators:

$$\hat{V}(3\pi/2, \pi/2): \begin{matrix} |0\rangle \rightarrow -\frac{1}{\sqrt{2}}|0\rangle + \frac{1}{\sqrt{2}}|1\rangle \\ |1\rangle \rightarrow -\frac{1}{\sqrt{2}}|0\rangle - \frac{1}{\sqrt{2}}|1\rangle \end{matrix} \Rightarrow \hat{V}'(2\pi, \pi/2): \begin{matrix} |0\rangle \rightarrow -|0\rangle \\ |2\rangle \rightarrow -|2\rangle \end{matrix} \Rightarrow$$

$$\begin{matrix} |0\rangle \rightarrow \frac{1}{\sqrt{2}}|0\rangle + \frac{1}{\sqrt{2}}|1\rangle \\ |1\rangle \rightarrow \frac{1}{\sqrt{2}}|0\rangle - \frac{1}{\sqrt{2}}|1\rangle \end{matrix} \equiv \hat{R}$$

### References

- [1]. J. Preskill. *Physics Today*, V. **52**, 24-30, (1999)
- [2]. D.F.V. James. *Appl. Phys. B* **66**, 181-190 (1998)
- [3]. H.S. Freedhoff. 1) *J. Chem. Phys.* **54**, 1618 (1971); 2) *J. Phys. B* **22**, 435 (1989)
- [4]. N.B. Delone, V.P. Krainov. *Atom in Strong Light Field* (Springer-Verlag, Berlin, Heidelberg, 1985)
- [5]. R.G. Huges, D.F.V. James, J.J. Gomez, M.S. Gully, Holzcheiter, P.G. Kwiat, S.K. Lomereaux, C.G. Peterson, V.D. Sandberg, M.M. Schauer, C.M. Simmons, C.E. Thorburn, D. Tupa, P.Z. Wang, A.G. White. Preprint (1997) quant-ph/ 9708050
- [6]. G. Giorgadze. *The Gauge Quantum Computation*. Proc. Inst. Cyber. Vol.1, N 1 (2000).

$\int$	$\&$
$\pi$	$\Sigma$

Institute of Cybernetics  
Georgian Academy of Sciences  
E-mail: cyber@hepi.edu.ge  
http://cyber.hepi.edu.ge/proceedings

*Proceedings*  
**Institute of Cybernetics**  
Vol.1, N 2, 2000

## **Properties of CuI nanocrystallites embedded in a glass matrix: from quantum confinement to bulk band parameters**

**O.Gogolin , G.Mshvelidze and E.Tsitsishvili**

*Institute of Cybernetics Georgian Academy of Sciences*

**M.Schmidt , A. Hepting, and C.Klingshirn**

*Institut fur Angewandte Physik, Universitat Karlsruhe, Germany*

**A.Kamilli, W.Send and D.Gerthsen**

*Labor fur Elektronenmikroskopie, Universitat Karlsruhe, Germany*

### **Abstract**

We report the linear absorption spectra of relatively large copper iodide nanocrystals embedded in an aluminaborosilicate host network structure. The spectra reveal pronounced exciton lines of both the zincblende and the layered hexagonal structures. In the approximation of the weak confinement regime, the translational masses for the  $Z_{12}$  - and  $Z_3$  - excitons, as well as the anisotropy of the  $Z_{12}$  - exciton band, i.e. the exciton Luttinger parameters, are deduced from the spectral positions of the exciton lines.

The Copper Halide compounds are model semiconductors for the investigation of exciton, biexciton- and polariton properties [1]. Great scientific efforts have been made to study the basic properties of bulk crystals and of nanocrystallites (NC) of such compounds as CuCl and CuBr [2]. The information about the compound CuI (both for bulk and NCs) is rather poor [3]. One of the reasons for this lack of data is the polymorphic structure of CuI and difficulties to obtain monophase samples. At normal pressure and room temperature samples of bulk CuI films exhibit three coexisting modifications : zincblende type, wurtzite type and a layered hexagonal structure [4],[5]. The volume fractions of the different crystal phases strongly depend on the way of the sample preparation, i.e. on the substrate temperature, on the thickness of the films and on the annealing time and temperature. The optical spectra for CuI films reflect the structural peculiarities above. Thus, the absorption spectra consist of several pronounced excitonic lines, which are usually labeled as  $Z_{12}$  and  $Z_3$  for cubic,  $H_1$  and  $H_2$  for layered hexagonal, and  $W_1$  and  $W_2$  for wurtzite modifications [5]. Only a few papers, to our knowledge, are devoted to the study of CuI NCs embedded in a glass matrix [6],[7],[8]. It was found, that the optical spectra in this case are similar to those in CuI films, indicating that NCs of different crystal structure occur in the samples.

In the present paper the absorption spectra of CuI NCs embedded in a glass matrix are studied. The experimental results are used to determine some band parameters of bulk CuI crystals. The glasses with CuI NCs were prepared from high purity  $SiO_2$  - 51.54%,  $B_2O_3$  - 25.8%,  $Al_2O_3$  - 7.2%,  $Sb_2O_3$  - 0.31%,  $K_2O$  - 1.03%, and  $Na_2O_3$  - 13.4 wt%, and CuI - 0.72 wt%, as described elsewhere [6]. Pieces of the glass were subject to annealing processes of varying temperature and duration. The transmission electron microscopy (TEM) and high resolution TEM (HRTEM) was carried out with a Philips CM200 FEG/ST electron microscope at an electron energy of 200 keV. The instrument is characterized by a Scherzer resolution of 0.24 nm and an information limit of 0.15 nm. The samples were prepared by mechanical grinding, dimpling and  $Ag^+$ -ion milling. The TEM investigations show that the size distribution of the particles is significantly inhomogeneous and, usually, exhibits two well

resolved maxima. This situation differs from the case of the other monophase Cooper Halide NCs such as CuCl and CuBr [2]. We assume that CuI NCs with different crystal structures are simultaneously present in the samples and that they can have different average sizes. Thus, the observed size distribution is an intrinsic feature of the samples and results from the sum of the distributions of each kind of NCs. As it will be seen below, the optical spectra confirm this conclusion. Note, however, that the TEM investigations show only the cubic particles. In Fig.1, as an illustration, the HRTEM image of a single crystalline particle with radius about 4.8nm is shown. This image is typical for the  $\langle 110 \rangle$ -zone axis of the zincblende structure. The non-cubic particles are neither found in HRTEM, nor by the TEM diffraction pattern technique. This fact can be related with the considerably high processing temperature for the TEM investigations. It is known, for example, that in order to obtain homogeneous thin CuI films with only cubic structure, they have to be additionally annealed [9]. Therefore we assume, that the NC with hexagonal structure undergo a phase transition to the cubic one during the sample processing for TEM investigations.

The main purpose of this paper is to evaluate the hole masses for cubic bulk CuI crystals from NC data. The reason is, that the corresponding information is not rich [3]. For cubic CuI crystals two different values for the hole mass are reported,  $m_v = 1.4m_0$  and  $m_v = 2.3m_0$ . There is no information about the Luttinger parameters for the exciton bands. Only the warping parameter for the  $Z_{12}$  - exciton band is reported in [10]. The average sizes of NCs will be also deduced from the optical spectra and compared with TEM data. In our case the TEM investigation shows essentially inhomogeneous size distribution of CuI NCs and therefore it seems is not a good tool to determine the average radii with high accuracy.

The experimental study of quantum size effects is one of the possible ways to obtain some information about the band parameters in bulk crystals, as well as on the average sizes of the NCs. Usually, the quantum size effects in semiconductor NCs are classified into three categories, depending on the ratio between the average radius of the NCs  $\bar{R}$  and the exciton Bohr radius  $a_{ex}$  in bulk crystals [11]. The case of small NCs ( $\bar{R} < a_{ex}$ ) corresponds to the strong confinement, when the electrons and the holes are individually confined and the electron-hole interaction can be regarded as a perturbation. The region of an intermediate confinement occurs when the NCs radius  $\bar{R} \cong a_{ex}$ . In this case the size effects in NCs with large hole masses are governed mostly by the quantization of the electron motion, in particular in I - VII semiconductor compounds. Therefore, the confinement energies of the excitons arising from different valence bands, as e.g. the  $Z_{12}$  - and  $Z_3$  - excitons, are almost the same in the intermediate regime [12]. The weak confinement regime corresponds to large NCs, with  $\bar{R} > a_{ex}$ , and the confinement energies are relative small, of the order or less than the exciton binding energy  $E_{ex}$ . In this limit the excitons are confined as a whole and, hence, the confinement energies are determined by their translational masses. Thus, some information about exciton masses and their anisotropy can be obtained in the conditions of weak confinement. The Cooper Halides have small exciton Bohr radii and large exciton binding energies [3], and hence are good materials of the weak confinement regime.

To reach the weak confinement regime the CuI - doped glass samples were annealed at relatively high temperatures of  $620^{\circ}\text{C}$ - $630^{\circ}\text{C}$  during long times up to 80 hours. The absorption spectra of nine different samples were investigated. A typical one is depicted in Fig.2. The spectrum in Fig.2 refers to the sample with annealing time 40 hours at  $630^{\circ}\text{C}$  and is similar to those in bulk films of CuI. Indeed, it consists of four excitonic lines from which one pair, the  $Z_{12}$  - and  $Z_3$ - lines, is related with the cubic phase and the other pair, the  $H_1$ - and  $H_2$ - lines, is due to the hexagonal layered structure. Note, that in all prepared samples the peaks due to the wurtzite structure are not observable. They are expected close to the  $Z_{12}$ - and  $Z_3$  - lines

[5] and, probably, are not resolved. In what follows we consider mainly the features of the  $Z_{12}$ - and  $Z_3$ - lines.

The blue shifts of the  $Z_{12}$ - and  $Z_3$ - lines in Fig.2 are  $\Delta E_{z_{12}} = 20meV$  and  $\Delta E_{z_3} = 13meV$ , i.e. they are smaller than the exciton binding energy  $E_{ex} = 58meV$  [3]. It is noticeable, that these shifts are significantly different for the two excitons. This feature is typical for all other investigated samples, too. However, the ratio  $\Delta E_{z_{12}}/\Delta E_{z_3}$  is almost unchanged and differs only slightly from one sample to the other. This is illustrated in Fig.3, where the ratio  $\Delta E_{z_{12}}/\Delta E_{z_3}$  for all the examined samples is shown in dependence on the annealing time. The mean value of the ratio is equal 1.55 and is significantly larger than one. These peculiarities, as well as the fact that the observed blue shifts are smaller than or of the order of the exciton binding energy, is specific to the weak confinement regime. Thus, one can state that in the examined samples the weak confinement regime is realized.

The theory of the quantum size effects in the weak confinement limit has been described in Ref.[13]. In this paper the phenomena of the exciton quantization in cubic NCs is investigated taking into account the anisotropy of the valence band  $\Gamma_8$  and its interaction with the valence band  $\Gamma_7$ . In the case of CuI crystals the binding energy  $E_{ex}$  is much less than the spin-orbit splitting  $\Delta_{so} = 630meV$  [3]. Therefore, we use below the approximate expressions from Ref.[13], which are valid in the limit of noninteracting valence subbands. Then, the spectral positions of the  $Z_{12}$ - and  $Z_3$ -exciton lines are given simply by

$$\hbar\omega_{z_{12}} = E_g - E_{ex} + \Delta E_{z_{12}}, \quad \hbar\omega_{z_3} = E_g + \Delta_{so} - E_{ex} + \Delta E_{z_3}. \quad (1)$$

The confinement energies in Eq.(1) are equal to

$$\Delta E_{z_3} = 0.67\pi^2 \frac{\hbar^2}{2M_{z_3}\bar{R}^2}, \quad \Delta E_{z_{12}} = 0.67 \frac{\hbar^2}{2M_h\bar{R}^2} \left( \phi^{3/2} \right)^2, \quad (2)$$

where  $M_{z_3}$  is the  $Z_3$ - exciton translational mass,  $M_h$  is the translational mass of the "heavy" exciton and  $\phi$  is a root of the transcendental equation cited in Ref.[13]. The root value depends on the ratio of the "light" exciton mass  $M_l$  to the "heavy" exciton mass  $M_h$ . The numerical factor results from the averaging over the distribution function of the particle sizes. In spherical approximation the translational exciton masses are defined by the Luttinger parameters  $\tilde{\gamma}_1$  and  $\tilde{\gamma}_2$  for the exciton bands [14]:

$$M_{z_3} = \frac{m_0}{\tilde{\gamma}_1}, \quad M_l = \frac{m_0}{\tilde{\gamma}_1 + 2\tilde{\gamma}_2}, \quad M_h = \frac{m_0}{\tilde{\gamma}_1 - 2\tilde{\gamma}_2}, \quad (3)$$

As noted above, the band parameters  $\tilde{\gamma}_1$  and  $\tilde{\gamma}_2$  for CuI crystals have not been reported so far, but only two different values for the hole masses [3]. It seems reasonable to consider the smallest mass  $m_v = 1.4m_0$  as corresponding to the average hole mass for the valence band  $\Gamma_8$ . Since the electron mass is  $m_e = 0.33m_0$  [3], the average translational mass for the  $Z_{12}$ - exciton can be assumed to be  $\bar{M}_{z_{12}} \cong (M_h + M_l)/2 = 1.7m_0$ . Then, using Eqs.(2) and (3) one can determine the exciton Luttinger parameters  $\tilde{\gamma}_1$  and  $\tilde{\gamma}_2$  as well as the average radius  $\bar{R}$  of the NCs.

As follows from Eqs.(2), the ratio between the blue shifts of the  $Z_{12}$ - and  $Z_3$ - lines is independent of the NC's size and is governed only by the parameter  $\tilde{\gamma}_1/\tilde{\gamma}_2$ . This ratio is given by

$$\frac{\Delta E_{z_{12}}}{\Delta E_{z_3}} = \frac{\tilde{\gamma}_1 - 2\tilde{\gamma}_2}{\tilde{\gamma}_2} \left( \frac{\phi^{3/2}}{\pi} \right)^2. \quad (4)$$

A theoretical plot of the dependence of the ratio  $\Delta E_{z_{12}} / \Delta E_{z_3}$  Eq.(4) on the parameter  $\tilde{\gamma}_2 / \tilde{\gamma}_1$  is given in Ref. [13] and is repeated in Fig.3.

As one can see in Fig.3, the mean value  $\Delta E_{z_{12}} / \Delta E_{z_3} = 1.55$  corresponds to the ratio of the band parameters  $\tilde{\gamma}_2 / \tilde{\gamma}_1 \cong 0.21 \pm 0.03$ . Using the average translational mass  $\bar{M}_{z_{12}} = 1.7m_0$  and the ratio  $\tilde{\gamma}_2 / \tilde{\gamma}_1$  above one can deduce the band parameters  $\tilde{\gamma}_1$  and  $\tilde{\gamma}_2$ , as well as the excitonic masses  $M_{z_3}$ ,  $M_h$  and  $M_l$ . Thus, one obtains that the Luttinger parameters are  $\tilde{\gamma}_1 \cong 0.72 \pm 0.04$  and  $\tilde{\gamma}_2 \cong 0.15 \pm 0.03$ , while the translational masses are  $M_{z_3} = (1.4 \pm 0.1)m_0$ ,  $M_h = (2.4 \pm 0.1)m_0$  and  $M_l = (1 \pm 0.1)m_0$ .

In Ref. [15] on the magneto - optical studies of the  $Z_{12}$  exciton - polariton in CuI crystals a set of the exciton parameters, in particular the Luttinger parameter  $\tilde{\gamma}_2$ , have been used. The value  $\tilde{\gamma}_2 \cong 0.2$  has been chosen, which is close to our value of  $\tilde{\gamma}_2 \cong 0.15 \pm 0.05$ . However, the authors of Ref. [15] note, that their set of the parameters is not unique.

Now we estimate the average sizes  $\bar{R}$  of the NCs for the examined samples. Using the upper Eq.(2a) for  $Z_3$ -exciton, we find that the average radius of the cubic NCs for the sample in Fig.2 is  $\bar{R} \cong 3.8nm$ . The obtained size is significantly larger than the exciton Bohr radius in bulk CuI crystals  $a_{ex} = 1.5nm$  [16], justifying again the approximation of the weak confinement regime. The average radii of cubic NCs in the other investigated samples are obtained as above and are ranging from  $\bar{R} \cong 2.2nm$  to  $\bar{R} \cong 4.3nm$ . The TEM investigations for the same samples show that the average radii of NCs are ranging from  $\bar{R} \cong 2nm$  to  $\bar{R} \cong 5.2nm$ . The inset in Fig.3 shows the experimental shifts of the  $Z_{12}$  - and  $Z_3$  - lines in dependence of the average radii obtained by TEM for several samples. The two solid lines represent the size dependence of the energy shifts given by Eq.(2). The theoretical curves are calculated for the exciton masses  $M_{z_{12}} = 1.4m_0$ ,  $M_h = 2.4m_0$  and the Luttinger parameter  $\tilde{\gamma}_2 / \tilde{\gamma}_1 = 0.21$ . One can see that the sizes obtained from optical spectra are compatible with TEM data within experimental error. Note, that it has to be kept in mind that the volume probed by TEM ( $\approx 2\mu m^3$ ) and thus the number of NCs is much smaller than in the case of optical spectroscopy ( $\approx 10^7 \mu m^3$ ).

In the case of hexagonal CuI crystals, the  $Z_{12}$ - exciton band is split into two anisotropic  $H_1$  and  $H_2$  - bands, defined by the transversal and longitudinal masses [14]. In the limit of weak confinement the quantization energies for the  $H_1$  - and  $H_2$  - excitons can be approximately described by Eqs.(2a) with replacing the mass  $M_{z_3}$  by the average mass  $M_{H_1}$  or  $M_{H_2}$ . Average translational masses of the  $H_1$  - and  $H_2$  - excitons  $M_{H_1} = 3.7m_0$  and  $M_{H_2} = 2.3m_0$  have been reported in Ref. [6], where, however, the averaging over the size distribution was not taken into account. If we take the corresponding numerical factor equal to 0.67 into account, we find that the masses are  $M_{H_1} = 2.5m_0$  and  $M_{H_2} = 1.5m_0$ . Using these values of the masses and the experimental blue shifts of the  $H_1$  - and  $H_2$  - lines in Fig.2 ( $\Delta E_{H_1} = 29meV$ ,  $\Delta E_{H_2} = 49meV$ ) one obtains that the average size of the hexagonal NCs is  $\bar{R} \cong 2nm$ . This value is close to the excitonic Bohr radius and thus can be regarded as an estimation *only*. Nevertheless, one can conclude that in the studied samples with relatively large crystallites the average sizes of the cubic and of hexagonal NCs are noticeably different

and that the latter are smaller in agreement with the bimodal size distribution observed in TEM mentioned above.

It is known, that some special conditions are required in order to prepare monophase CuI films which are selected in an empirical way [5],[9]. We have observed that in the case of CuI NCs in a glass matrix the empirical choices of the glass composition and of the growth parameters also allow to obtain almost monophase NCs. As an example, the absorption spectra of two such samples are given in Fig.4. The arrows in Fig.4 show again the positions of the bulk exciton lines. The spectrum a) in Fig.4 consists of the two pronounced peaks,  $H_1$  and  $H_2$ , due to hexagonal NCs and only a weak broad line which can be attributed to cubic ones. Thus the sample contains mainly the hexagonal NCs. Inversely, the spectrum b) shows clearly the dominating presence of the cubic NCs. The observed cubic NCs are in this case relatively small, in contrast to the previous case shown in Fig.2. As one can see from Fig.4, the blue shift of the  $Z_{12}$  line  $\Delta E_{z_{12}} \cong 130meV$  is more than twice larger than the exciton binding energy.

In summary, the linear absorption spectra of copper iodide nanocrystals embedded in an aluminaborosilicate glass matrix are measured. The typical spectra show the simultaneous presence of NCs with different crystal structures. The average sizes of the cubic and hexagonal NCs are noticeably different. The translational masses for the  $Z_{12}$  - and  $Z_3$  - excitons and the Luttinger parameters for the  $Z_{12}$  - exciton band have been deduced.

#### ACKNOWLEDGEMENTS

This work has supported by the VW Stiftung.

#### REFERENCES

- [1] B. Honerlage, R. Levy, J.B. Grun, C. Klingshirn, and K. Bohnert, *Physics Reports* **124**, 161 (1985).
- [2] U. Woggon, *Optical Properties of Semiconductor Quantum Dots*, Springer, **136**, (1996).
- [3] Landolt - Bornstein, New Series, Group III, Vol.17b, Springer - Verlag, Berlin (1982) and *ibid.* Vol.41b (2000).
- [4] R.N. Kurdyumova, and R.V. Baranova, *Sov. Phys. Cryst.* **6**, 318 (1961).
- [5] M. Cardona, *Phys. Rev.* **152**, 269 (1963).
- [6] O. Gogolin, Yu. Berozashvili, G. Mshvelidze, E. Tsitsishvili, S. Oktjabrski, H. Giessen, and C. Klingshirn, *Sem. Sc. Technol.* **6**, 401, (1991).
- [7] Y. Masumoto, T. Kawazoe, *J. Lum.* **66-67**, 142 (1995).
- [8] Y. Masumoto, K. Kawabato, and T. Kawazoe, *Phys. Rev. B* **52**, 7834 (1995).
- [9] L. Bedikyan, V. Miloslavskii, and L. Ageev, *Optika i Spectroskopia*, **47**, 225 (1979).
- [10] J.L. Deiss, A. Daunois, A. Chouiyakh, and O. Gogolin, *Sol. St. Comm.* **53**, 79 (1985).
- [11] A.I. Efros, and A.L. Efros, *Sov. Phys. - Semicond.* **16**, } 772 (1982).
- [12] A.I. Ekimov, A.I. Efros, M.G. Ivanov, A.A. Onushchenko, and S. K. Shumilov, *Sol. St. Commun.* **69**, 565 (1989).
- [13] A.I. Ekimov, A.A. Onushchenko, A.G. Plyuchin, and A.I. Efros, *Zh. Eksp. Teor. Fiz.* **88**, 1490, (1985).
- [14] G.L. Bir and G.E. Pikus, *Symmetry and Strain - Induced Effects in Semiconductors*, Keter, Jerusalem (1974).
- [15] S. Suga, K. Cho, Y. Niji, J.C. Merle, and T. Sauder, *Phys. Rev. B* **22**, 4931 (1980).
- [16] T. Itoh, Y. Iwabuchi, and T. Kirihara, *Phys.Stat.Sol. B* **146**, 531 (1988).

FIGURES

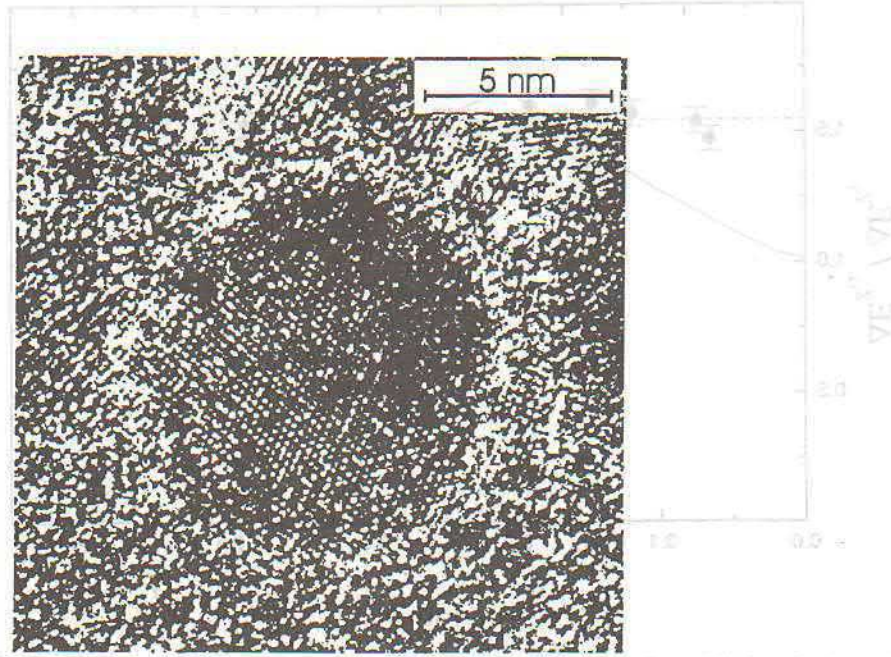


FIG. 1. HRTEM image of a single crystalline particle with radius about 4.8nm.

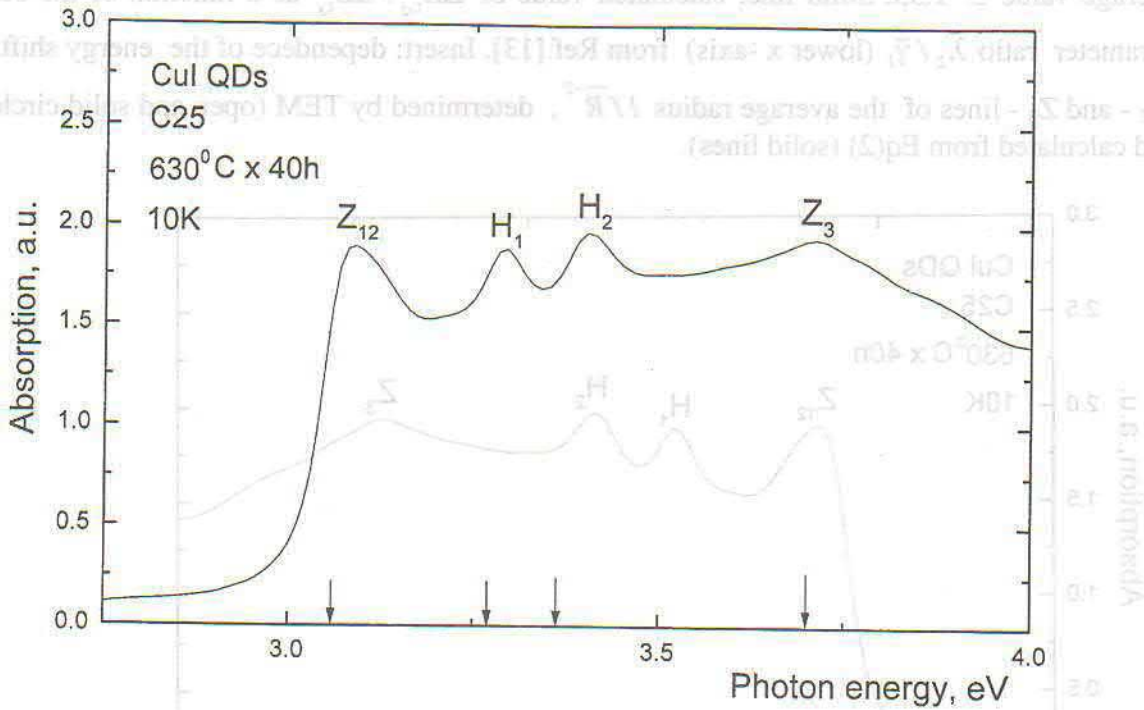


FIG. 2. Linear absorption spectrum for a CuI-doped glass sample, annealed during 40 hours at 630°C. The spectral positions of cubic and hexagonal excitons in bulk crystals are shown by arrows.

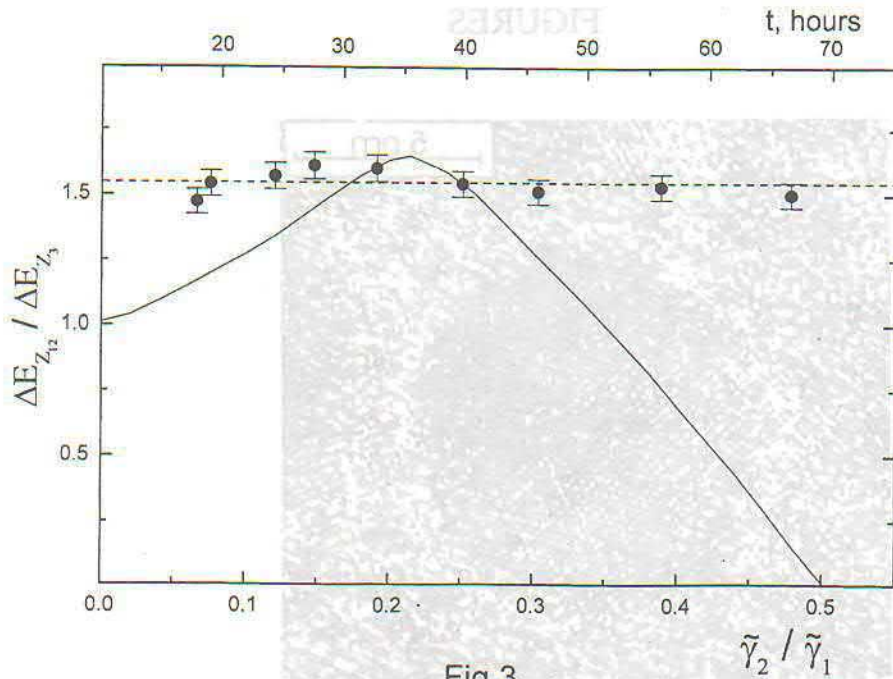


Fig.3

The ratio of the shifts of the  $Z_{12}$  - and  $Z_3$  - lines  $\Delta E_{z_{12}} / \Delta E_{z_3}$ . Full circles: experimental points for samples subjected to different annealing times (upper x - axis). Dashed line: average value  $\cong 1.55$ . Solid line: calculated value of  $\Delta E_{z_{12}} / \Delta E_{z_3}$  as a function of the band parameter ratio  $\tilde{\lambda}_2 / \tilde{\lambda}_1$  (lower x -axis) from Ref.[13]. Insert: dependence of the energy shift of  $Z_{12}$  - and  $Z_3$  - lines of the average radius  $1/\bar{R}^{-2}$ , determined by TEM (open and solid circles) and calculated from Eq(2).

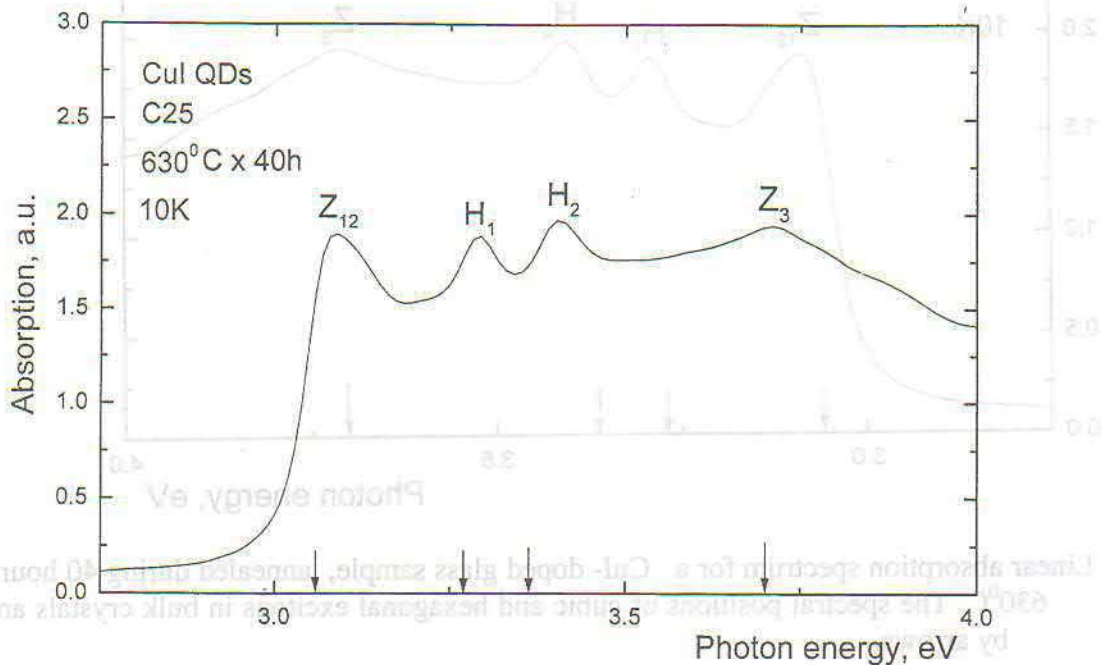


FIG. 4 Linear absorption spectra for CuI - doped glasses with nearly monophasic NCs: hexagonal NCs, b) - cubic NCs. The bulk positions of the exciton lines are shown by arrows. The spectra are displaced vertically for clarity.



## Fine structure of exciton levels in strained quantum dots

E. Tsitsishvili

*Institute of Cybernetics Georgian Academy of Science*

*Institut für Angewandte Physik, Universität Karlsruhe, Germany*

### Abstract

The excitonic ground state in a single quantum dot (QD) with a structural anisotropy is studied in dependence on the magnitude of the electron-hole exchange interaction. Structural anisotropy is described phenomenologically by lattice deformation. A fine structure of the exciton levels is due to an interplay of the deformations and exchange interaction and is the more pronounced the smaller are the quantum dots. The lattice deformations are the reason for an optical anisotropy in a strained quantum dot. The exchange interaction, however, suppresses the polarization effects which are much more significant in large QDs. An additional decrease of the optical anisotropy arises from a coexistence of structural and epitaxial deformation.

### I. Introduction

The optical investigations of self-assembled quantum dots (SAD) show a significant polarization dependence of the photoluminescence (PL) spectra. Such optical anisotropy effects in (Ga)InAs SADs have been reported, for example, in Refs. [1], [2], [3]. The anisotropy was attributed to the nonspherical shape of the SAD's. Recently a strong polarization dependence of the linear PL spectra was observed in InP SADs embedded in a  $\text{Ga}_{0.5}\text{In}_{0.5}\text{P}$  matrix which showed ordering in a lateral superlattice [4],[5]. Luminescence from a single quantum dot (QD) is studied by the micro-PL technique and a doublet fine structure of the exciton levels is found. The observed fine structure and optical anisotropy was attributed to an interplay of the electron-hole exchange interaction and the asymmetrical crystal structure of the InP/ $\text{Ga}_{0.5}\text{In}_{0.5}\text{P}$  system. Similar results have been reported for GaAs/AlGaAs quantum wells and were attributed to the effect of long-range exchange interaction on the fine structure of the localized excitons [6],[7]. Theoretical consideration of the fine structure of the excitonic levels refers mostly, to our knowledge, to nanocrystallites (see, for instance, [8]) and excitons localized on laterally-anisotropic islands in quantum wells [9].

In this paper the internal structure of the ground exciton state in a single QD with an anisotropic lattice structure is studied. The purpose is to investigate how the ground exciton state in QDs is influenced by an interplay of a structural anisotropy and short-range electron-hole exchange interaction. Such interplay can be essentially important in small QDs where the exchange interaction can be enhanced very much over the bulk value. Structural anisotropy of a single QD is described phenomenologically by lattice deformations. Lattice mismatch effects between the QD and its matrix are also considered.

The paper contains two Sections. In the first one the formulation of the problem is described. In the next Section the fine structure splitting of the exciton levels and the optical transition probabilities in a single strained QD are calculated and their dependence on the magnitude of the exchange energy is discussed. The results are obtained for the  $[\bar{1}\bar{1}\bar{1}]$ - and  $[111]$ -strained QDs and the  $[001]$ - epitaxial strain is also taken into account.

## II. Formulation of the problem

Simultaneous influence of deformations and exchange interaction on the ground state of the exciton in bulk cubic crystals has been studied in Ref.[10] by means of the invariant method. This phenomenological method is based on the group theory and is well suited to model the scenario of strained QD's. The Hamiltonian of the problem  $H = H_{exc} + H(\varepsilon)$  contains two parts due to the short-range exchange interaction and the deformations, respectively. The Hamiltonian  $H_{exc}$  is assumed to be independent of deformations and for cubic crystals contains three constants[10]. One of them determines a trivial shift of the exciton state as a whole, the two other describe the symmetrical and the nonspherical parts of the exchange interaction, respectively. As usual, the latter is small and in what follows we take this constant equal to zero. Then, the ground state of the exciton is splitted by the symmetrical exchange interaction into two states with a different total momentum  $F$  ( $\vec{F} = \vec{J} + \vec{\sigma}$ , where  $\vec{J}$  is the hole momentum,  $J = \frac{3}{2}$ , and  $\vec{\sigma}$  is the electron momentum,  $\sigma = \frac{1}{2}$ ). One of them, five-fold degenerate state corresponds to the momentum  $F=2$ . These states are optically forbidden (in dipole approximation) and the basis wave functions are transformed under  $E+F_1$  representation of the  $T_d$  group (in the notations from [10]). The other, three-fold degenerate state, corresponds to the momentum  $F=1$  and is optically active. The basis wave functions are transformed as  $x$ ,  $y$  and  $z$  ( $F_2$  representation). The probabilities to excite these states are equal. Thus, in nondeformed cubic crystals, as is well known, there is no optical anisotropy.

In the presence of deformations the crystal symmetry is reduced and the terms  $E+F_1$  and  $F_2$  are splitted. Because of the mixing of the states with different momentum  $F$ , some of the forbidden states become allowed, depending on the deformation direction. For relatively small deformations, when the exciton binding energy is larger than the deformation energy, the Hamiltonian  $H(\varepsilon)$  is the same as for the valence band  $\Gamma_{8v}$  with replacing the band constants by the exciton ones. Then, the nontrivial part of the total Hamiltonian  $H$  is given by [10]:

$$H = \left( a + \frac{5}{4}b \right) \varepsilon - b \sum_i J_i^2 \varepsilon_{ii} - \frac{d}{\sqrt{3}} \sum_{ij} [J_i J_j] \varepsilon_{ij} + \Delta_{exc} (\vec{J}\vec{\sigma}). \quad (1)$$

In Eq. (1) the constants  $a$ ,  $b$  and  $d$  are the exciton deformation potentials,  $\Delta_{exc}$  is the exchange constant,  $\varepsilon_{ij}$  is the deformation tensor, and  $\varepsilon = \sum_i \varepsilon_{ii}$ . The ground state of the exciton is described by the basis wave function  $\Psi_{n\mu} = \varphi_n \psi_\mu$ , where  $\varphi_n$  is the spin wave function and  $\psi_\mu$  is transformed as the eigenfunctions  $|\vec{J}, j_z\rangle$  of the momentum  $\vec{J}$  and its projections  $j_z = \pm 3/2, \pm 1/2$ .

When the quantization axis  $z$  is chosen to be parallel to the strain, the Hamiltonian (1) reduces to two different blocks which can be diagonalized analytically [10]. In general, all the eight terms are splitted due to an interplay of the deformations and exchange interaction. Two of the terms which refer to the momentum projections  $F_z = \pm 2$  are totally forbidden. The other six states are polarized along the main axes of the deformation tensor  $\varepsilon_{ij}$ . For the specific directions of the deformations, some of these states can be degenerate.

As noted above, the reviewed results for the bulk crystals can be apply to the case of the QDs. The QDs are assumed to be influenced by some internal strain presented in the system. It can be, for example, the chemical strain due to the formation of composition modulation planes in the matrix, as is supposed in Ref.[4],[5]. Because of a strong enhancement of the exchange interaction in the small QDs, the properties of the fine structure of the exciton levels in dependence on the exchange energy are of interest. Usually, the bulk exchange constant  $\Delta_{exc}$  is

small, of the order of a few tens  $\mu eV$ , but can be enhanced in small QDs by a hundred times [8]. The deformation splitting in the CuPt-ordered crystals, for example, is of the order of a few tens meV [11]. Thus, if for strained bulk crystals or very large QDs the deformations are much more important than the exchange interaction, in small QDs the both factors can be similarly significant.

In the next Section some examples of the differently oriented deformations are considered. The structure of the ground exciton state, as well as the probabilities of the excitonic transitions are discussed in dependence on the magnitude of the exchange energy. The case when light propagates along the growth direction of the structure is mostly of interest.

### III. Fine structure of the exciton levels in a single strained QD

Consider a single QD with a cubic lattice structure which is affected by deformations along some cubic direction. The QDs are assumed to be spherical and relatively large to use an effective-mass approximation. The lattice mismatch between the matrix and the QDs leads to an additional epitaxial deformation  $\varepsilon_{ij}^{ep}$ , which depends on the matrix composition and the growth direction. In what follows we consider the system grown in the [001] direction.

#### A. Quantum Dots Strained in the $\{110\}$ - and $\{111\}$ -directions

Let us first assume that lattice deformations are oriented along the  $[\bar{1}10]$ -cubic axis. Such structural anisotropy has been reported for GaInAs systems which show the formation of composition modulation planes along the  $[\bar{1}10]$ -direction [1],[2],[3]. The main axes of the deformation tensor  $\varepsilon_{ij}$  in this case are the  $[\bar{1}10]$ -,  $[110]$ -, and  $[001]$ -directions. One can check that the eigenenergies of the Hamiltonian (1) which refer to the optically active states, are given by

$$E_{\pi\sigma_1\sigma_2}^{\pm} = -\frac{\Delta_{exc}}{2} \pm \delta_{\pi\sigma_1\sigma_2}, \quad (2)$$

where

$$\begin{aligned} \delta_{\pi} &= \sqrt{\Delta_{110}^2 + 4\Delta_{exc}^2 + 4\Delta_{exc}\Delta_{\varepsilon}(1 + 3a/4)}, \\ \delta_{\sigma_1} &= \sqrt{\Delta_{110}^2 + 4\Delta_{exc}^2 - 2\Delta_{exc}\Delta_{\varepsilon}(1 + 3a/2)}, \\ \delta_{\sigma_2} &= \sqrt{\Delta_{110}^2 + 4\Delta_{exc}^2 - 2\Delta_{exc}\Delta_{\varepsilon}}, \end{aligned} \quad (3)$$

and the anisotropic factor

$$\alpha = \frac{d}{2\sqrt{3b}} \frac{S_{44}}{S_{11} - S_{12}} - 1. \quad (4)$$

In Eqs. (2) and (3) the deformation energy  $\Delta_{110} = \Delta_{\varepsilon}(1 + 3\alpha/2 + 3\alpha^2/4)^{1/2}$ ,  $\Delta_{\varepsilon} = bP(S_{11} - S_{12})$ , and  $S_{11}, S_{12}$  are the elastic compliance constants. At given deformation potential  $b$  and constants  $S_{11}$  and  $S_{12}$ , the sign of the deformation energy is determined by the kind of the strain  $P$ , namely tension or compression, respectively. In the former case the strain is positive,  $P \geq 0$ , and in the latter case it is negative,  $P \leq 0$ . The notations  $\pi, \sigma_1$  and  $\sigma_2$  indicate the terms polarized parallel ( $\pi$ -term) and perpendicular (along the  $[110]$  axis -  $\sigma_1$ -term and along the  $[001]$  axis -  $\sigma_2$ -term) to the strain, respectively.

The probabilities of the excitonic optical transitions are proportional to the following quantities:

$$W_{\pi}^{\pm} = 1 \mp \frac{2\Delta_{exc} + \Delta_{\varepsilon}\left(1 + \frac{3}{4}\alpha\right)}{\delta_{\pi}},$$

$$W_{\sigma_1}^{\pm} = I \mp \frac{2\Delta_{exc} - \frac{I}{2}\Delta_e \left(1 + \frac{3}{2}\alpha\right)}{\delta\sigma_1},$$

$$W_{\sigma_2}^{\pm} = I \mp \frac{2\Delta_{exc} - \frac{I}{2}\Delta_e}{\delta\sigma_2}. \quad (5)$$

The exciton energies (2) and the transition probabilities (5) depend on the relative contribution of the exchange interaction and deformations, as well as on the anisotropic factor  $\alpha$ . From Eqs. (2) and (3) follows that in the absence of the exchange interaction, i.e. for  $\Delta_{exc} = 0$ , the six terms Eq. (2) are splitted by the deformations into two three-fold degenerate levels. The energy separation between upper and down sets is determined by the deformation energy  $2|\Delta_{l10}|$ . At finite  $|\Delta_{exc}|$  each degenerate term, the upper set, as well as the down one, is fully splitted into a triplet due to an interplay of the deformations and exchange interaction. A splitting of the  $\sigma$ -terms disappears when the anisotropic factor  $\alpha = 0$ . Usually, the constant  $\alpha$  is small and the splitting between the  $\sigma$ -terms is negligible. For instance, in the InP crystals the anisotropic factor is  $\alpha \cong -0.1, -0.3$  [11].

The energy separations between the  $\pi$  and  $\sigma$ -terms,  $\Delta E^+ = E_{\pi}^+ - E_{\sigma_1}^+$  (for the upper level set) and  $\Delta E^- = E_{\pi}^- - E_{\sigma_1}^-$  (for the down set), differ from each other only by a sign,  $|\Delta E^+| = |\Delta E^-| \equiv \Delta E$ . As follows from expressions (2) and (3), for a small exchange energy  $|\Delta_{exc}| \ll |\Delta_e|$  the splitting  $\Delta E$  linearly increases with increasing  $|\Delta_{exc}|$ , while for a large  $|\Delta_{exc}| \gg |\Delta_e|$  it is almost independent of the exchange interaction and is determined by the deformation energy  $|\Delta_e|$ . In Fig.1 the energy separation  $\Delta E$  is shown in dependence on the exchange energy by curve 1. All energies are given in units of the deformation energy  $|\Delta_e|$ . The exchange energy is assumed to be negative,  $\Delta_{exc} < 0$  [14]. The constant  $\alpha$  is taken to be small,  $\alpha = -0.1$ , and a splitting of the  $\sigma$ -terms is negligible. Fig.1(a) is calculated for a negative deformation energy  $\Delta_e < 0$ . The opposite case when  $\Delta_e > 0$  is presented in Fig.1(b). One can see in Fig.1 that in both cases the splitting  $\Delta E$  increases linearly when  $|\Delta_{exc}|$  is small with respect to the deformation energy  $|\Delta_e|$ . When  $|\Delta_{exc}|$  is large,  $\Delta E$  limits to a constant value  $\Delta E \cong 1.5|\Delta_e|$ . For the intermediate value of  $|\Delta_{exc}| \cong |\Delta_e|$  the splitting  $\Delta E$  behaves a little different depending on the kind of strain. When the deformation energy is negative, it changes smoothly with  $|\Delta_{exc}|$ , as is seen in Fig.1(a). When  $\Delta_e > 0$ , a weak nonmonotonic dependence occurs. As one can see in Fig.1(b),  $\Delta E$  reaches its maximal value equal to  $\Delta E \cong |\Delta_{exc}|$  at  $|\Delta_{exc}| \cong 0.5|\Delta_e|$ , then decrease a little and at large  $|\Delta_{exc}|$  limits to a constant.

From Eq. (5) follows that the probabilities to excite the  $\pi$ -terms are independent of the exchange energy  $|\Delta_{exc}|$  when the deformation energy is negative,  $\Delta_e < 0$ , and the constant  $\alpha$  is small. For the upper  $\pi$ -term the probability  $W_{\pi}^+ = 2$  and for the down  $\pi$ -term  $W_{\pi}^- = 0$ . In the other cases the transition probabilities change with  $|\Delta_{exc}|$ , as is shown in Fig.2. Fig.2 is calculated using the same parameters as Fig.1, namely, the exchange energy is negative,  $\Delta_{exc} < 0$ , the anisotropic constant is  $\alpha = -0.1$ . Figs.2(a) and 2(b) refer to the cases when the deformation energy  $\Delta_e < 0$  and  $\Delta_e > 0$ , respectively. As one can see in Fig.2, at a small  $|\Delta_{exc}|$  some down terms are allowed and the upper terms are forbidden, depending on a sign of

$\Delta_e$ . Note, however, that for large exchange energy only the upper exciton states are optically active. It is easy to check that the energy distance between the allowed and forbidden states in this case is close to the exchange splitting  $4|\Delta_{exc}|$ , as in the absence of the deformations. Thus, when the exchange interaction is dominant, the QDs behave as unstrained ones, as can be expected.

Assuming that a structure is grown along the [001]-axis and light propagates in the same direction. Then the only states which are polarized in the (001) plane are optically allowed. When the strain is also oriented in this plane, differently polarized states are excited, the  $\pi$ - and  $\sigma$  terms. Because of the different transition probabilities, an optical anisotropy occurs in this case.

The anisotropy can be determined by the degree of linear polarization:  $P^\pm = (W_\pi^\pm - W_{\sigma_i}^\pm) / (W_\pi^\pm + W_{\sigma_i}^\pm)$ . The polarization effects are due to the deformations, while the exchange interaction itself is not a reason of any anisotropy. In the absence of the deformations the probabilities to excite the exciton states are equal, as follows from Eq. (5). It is evident, therefore, that an interplay of the deformations and exchange interaction reduces the anisotropic effects. In order to illustrate this fact, the polarization degree  $P^+$  for the upper states in dependence on the exchange energy is shown in Fig.3 by curves 1. One can see that the polarization degree  $P^+$  has its maximum when the exchange energy is equal to zero,  $\Delta_{exc} = 0$ . At finite  $\Delta_{exc}$  the quantity  $P^+$  decreases. It changes, however, differently for different deformations, tension or compression. When the deformation energy is negative the quantity  $P^+$  smoothly decreases with increasing  $\Delta_{exc}$  from its maximal value  $P^+ \cong 0.6$  and approaches zero for large exchange energies, see Fig.3(a). When the deformation energy is positive  $\Delta_e > 0$ , the term  $E_\pi^+$  is forbidden for small exchange energies and therefore the polarization degree is  $P^+ = -1$ . Then the quantity  $P^+$  sharply decreases and limits to zero, as for the previous case.

Thus, for the case when a structural anisotropy of a single QD is described by the  $[\bar{1}10]$  strain, the main results are the following. An optical anisotropy in the (001) plane is present. The polarization effect is significant in the large QDs when a structural anisotropy is dominant over the exchange interaction. In the small QDs for which the exchange interaction is much enhanced and the deformations are of small value, an optical anisotropy is negligible. Two exciton terms which have close but different energies can be excited when light is polarized in the (001) plane. The constituents of a doublet are fully polarized in this plane, along the  $[\bar{1}10]$ - and  $[110]$ -axes. The energy distance between these terms increases with  $\Delta_{exc}$  and, thus, is larger in small QDs than in the large ones.

As was noted above, a doublet structure of the exciton levels in (Ga)InAs SADs, as well as an optical anisotropy has been reported in Refs. [4],[5]. An exact *quantitative* comparison between the experimental data from [4],[5] and theoretical results above is not possible, because of a nonspherical shape of the QDs investigated in experiment. An asymmetrical shape of QDs, as is mentioned above, can be also a reason for an optical anisotropy and a fine structure splitting. This has been shown in Refs. [4],[5] for unstrained InP QDs which have a polarization degree of the order of 10%. But, there is still a nice *qualitative* agreement between theoretical results and experimental observations for the case of strained QDs. In particular, it is found in experiment that each constituent of a doublet is fully polarized, one along the  $[\bar{1}10]$ - and other along the  $[110]$ - cubic axes. It is also found that large size QDs show stronger optical anisotropy than small ones, as is obtained theoretically.

Consider now the case when the deformations are oriented along the  $[111]$ - axis. Such type of structural anisotropy is presented in III-IV ternary and quaternary compounds which exhibit CuPt-type long-range ordering along one of the  $\{111\}$  cubic diagonals [13],[14]. When

a structural anisotropy of a single QD is described by the strain along the [111]- axes, the eigenenergies and transition probabilities are given by expressions similar to Eqs.(2), (3) and (5) with  $\alpha = 0$ , as follows from Eq. (1). In addition, the deformation energy has to be replaced by  $\Delta_\epsilon \rightarrow d\epsilon \perp S_{44} / \sqrt{3}$ , where  $S_{44}$  is the elastic compliance constant. Thus, the main results obtained for the  $[\bar{1}\bar{1}0]$  strain are still valid. Especially the dependence of the quantities of interest, such as the energy splitting  $\Delta E$ , probabilities of the optical transitions  $W$  etc., on the exchange energy  $\Delta_{exc}$  given by figures above. Notice, however, that the deformation tensor  $\epsilon_{ij}$  has now the other main axes, which coincide with the [111]-,  $[\bar{1}\bar{1}\bar{2}]$ - and  $-\bar{1}\bar{1}0$  directions. Therefore, assuming that light is polarized in the (001) plane, one obtains different results. Namely, both terms excited in this plane, the  $\pi$ - term and the two-fold degenerate  $\sigma$ - term, are only partially polarized.

## B. Lattice Mismatch Effect

In real systems SADs are usually strained due to the lattice mismatch between the QDs and the matrix. When the structure is grown in the [001] direction, the epitaxial strain itself is not a reason of an optical anisotropy in the (001) plane. Indeed, from Eq.(1) follows that for the [001]-strain only the  $\sigma$ - terms are excited with the equal probabilities and there is no anisotropy in the (001) plane. However, if the matrix also affects the QDs in some direction other than the [001] axis, then the exciton levels suffer both perturbations due to the lattice mismatch and asymmetrical crystal structure. Below we consider the effect of a coexistence of structural and epitaxial deformations.

When the systems are grown in the [001] direction, the epitaxial strain is defined by the relative deformation  $\epsilon_{001} = \epsilon_{xx}^{ep} - \epsilon_{zz}^{ep}$ , where the coordinate axis  $x||[100], y||[010], z||[001]$ , and the strain  $\epsilon_{zz}^{ep}$  and  $\epsilon_{xx}^{ep}$  are parallel and perpendicular to the [001] direction, respectively. According to the continuous elasticity theory, the strain  $\epsilon_{zz}^{ep}$  and  $\epsilon_{xx}^{ep}$  are related as follows [14]:

$$\epsilon_{zz}^{ep} = -\frac{2C_{12}}{C_{11}} \epsilon_{xx}^{ep} \quad (6)$$

where  $C_{11}$  and  $C_{12}$  are the elastic constant,  $\epsilon_{xx}^{ep} = (a_m - a_d)/a_d$ , and  $a_m$  and  $a_d$  are the lattice constants in the matrix and the QDs, respectively. The relative epitaxial deformation follows from Eq.(6):

$$\epsilon_{001} = \epsilon_{xx}^{ep} - \epsilon_{zz}^{ep} = \frac{C_{11} + 2C_{12}}{C_{11}} \frac{a_m - a_d}{a_d} \quad (7)$$

Epitaxial effects are, evidently, more important when the lattice mismatch is relatively large and the contribution of the epitaxial strain can be compare with the structural deformations. One of the typical example of the structures with a large lattice mismatch is InP/Ga<sub>0.5</sub>In<sub>0.5</sub>P system. The relative difference of the lattice constants in InP/Ga<sub>0.5</sub>In<sub>0.5</sub>P structure is  $|a_m - a_d|/a_d \sim 10^{-2}$  [12].

In the presence of double deformation, the [001] epitaxial strain and the  $[\bar{1}\bar{1}0]$  structural anisotropy, the exciton energies are given by

$$E_{\pi\sigma, \sigma_2}^\pm = -\frac{\Delta_{exc}}{2} \pm \delta_{\pi, \sigma_1, \sigma_2}^{(ep)}, \quad (8)$$

where

$$\sigma_\pi^{(ep)} = \sqrt{\Delta_{110}^2 + 4\Delta_{exc}^2 + \Delta_{ep}^2 + 4\Delta_{exc}\Delta_\epsilon(I + 3a/4) - \Delta_{ep}(2\Delta_{exc} + \Delta_\epsilon)},$$

$$\sigma_\pi^{(ep)} = \sqrt{\Delta_{110}^2 + 4\Delta_{exc}^2 + \Delta_{ep}^2 - 2\Delta_{exc}\Delta_\epsilon(I + 3a/2) - \Delta_{ep}(2\Delta_{exc} + \Delta_\epsilon)},$$

$$\sigma_{\sigma_2}^{(ep)} = \sqrt{\Delta_{110}^2 + 4\Delta_{exc}^2 + \Delta_{ep}^2 - 2\Delta_{exc}\Delta_{\epsilon} + \Delta_{ep}(4\Delta_{exc} + \Delta_{\epsilon})}, \quad (9)$$

In expression (9) the epitaxial energy  $\Delta_{ep} = b\epsilon_{001}$  and the relative deformation are given by Eq.(7). The notations  $\pi, \sigma_1$ , and  $\sigma_2$  refer to the  $[\bar{1}\bar{1}0]$ -,  $[110]$ -, and  $[001]$ -polarizations, respectively. From Eqs.(8) and (9) follows that the epitaxial strain leads to an additional splitting of the  $\sigma$ - terms. The lattice mismatch changes also the energy separation  $\Delta E$  between the  $\pi$ - and  $\sigma_1$ - terms and affects the transition probabilities. In the presence of the epitaxial strain the probabilities are given by

$$W_{\pi}^{\pm} = I \mp \frac{2\Delta_{exc} + \Delta_{\epsilon} \left(1 + \frac{3}{4}\alpha\right) - \frac{1}{2}\Delta_{ep}}{\sigma_{\pi}^{(ep)}},$$

$$W_{\sigma_1}^{\pm} = I \mp \frac{2\Delta_{exc} - \frac{1}{2}\Delta_{\epsilon} \left(1 + \frac{3}{2}\alpha\right) - \frac{1}{2}\Delta_{ep}}{\delta_{\sigma_1}^{(ep)}},$$

$$W_{\sigma_2}^{\pm} = I \mp \frac{2\Delta_{exc} - \frac{1}{2}\Delta_{\epsilon} + \Delta_{ep}}{\delta_{\sigma_2}^{(ep)}}. \quad (10)$$

As noted above, the lattice mismatch effects are essential when the epitaxial and structural deformations are comparable. As an illustration, the energy spacing  $\Delta E$  and the degree of polarization  $P^+$  for such case are shown by curves 2 in Fig.1 and Fig.3, respectively. The epitaxial strain is assumed to be negative and equal to  $\Delta_{ep} = -0.5|\Delta_{\epsilon}|$ . One can see in Fig.1 that the main changes of the splitting  $\Delta E$  take place when all the three factors, a structural anisotropy, the lattice mismatch and the exchange interaction, are equally important. At small and large  $|\Delta_{exc}|$  the epitaxial effect is of small value. From Fig.3 follows that in the presence of the epitaxial deformations the maximal value of the polarization degree is smaller. Thus, the epitaxial effect induces a reduction of the optical anisotropy in the (001) plane due to the  $[\bar{1}\bar{1}0]$  deformations. In addition, the polarization degree shows a more smooth decrease with  $|\Delta_{exc}|$  particularly, when the deformation energy is positive, see Fig.3(b).

In summary, the ground state of exciton in a single QD with a structural anisotropy is studied in dependence on the magnitude of the electron-hole exchange interaction. Since a magnitude of the short-range exchange energy in a small QD is determined by its size, the obtained results describe implicitly a change of the structure of the exciton state with the QDs sizes. Structural anisotropy is described phenomenologically by the deformations. The case when the structure is grown in the  $[001]$  direction and light is polarized in the (001) plane is mostly of interest. The main results are the following. A doublet structure of the exciton levels is the more pronounced the smaller are the QDs, since this is an effect of a coexistence of the deformations and exchange interaction. The polarization effects, on the contrary, are essential in the large QDs, because they are due to the structural deformations. When the QDs sizes decrease, an optical anisotropy reduces. An interplay of a structural anisotropy and the lattice mismatch leads to an additional suppression of the polarization effects. When the exchange interaction is very enhanced and a structural anisotropy is of small value, then the splitting of the exciton terms becomes almost independent of the QDs sizes and is determined by the deformation energy. An optical anisotropy in this case is negligible. The theoretical results are in a qualitative agreement with the experimental observations.

### Acknowledgments

This work was supported by DFG. We are grateful to H. Kalt for a fruitful discussion.

### References

- [1]. H. Saito, K. Nishi, S. Sugou, and Y. Sujimoto, Appl. Phys. Lett. 71, 590 (1997).
- [2]. Y. Nabetani, T. Ishikawa, S. Noda, and A. Sasaki, J. Appl. Phys. 76, 347 (1994).
- [3]. M. Henini, S. Sanguinetti, S.C. Fortuna, E. Grilli, M. Gruzzi, G. Panzarini, L.C. Andreani, M.D. Upward, P. Moriarty, P.H. Beton, and L. Eaves, Phys. Rev. B 57, 6815 (1999).
- [4]. M. Sugisaki, H-W. Ren, S.V. Nair, K. Nishi, S. Sugou, T. Okuno, and Y. Masumoto, Phys. Rev. B 59, R5300 (1998) and references therein.
- [5]. H-W. Ren, M. Sugisaki, S. Sugou, K. Nishi, A. Gromy, and Y. Masumoto, Jpn. J. Appl. Phys.38, 2438 (1999).
- [6]. D. Gammon, E.S. Snow, B.V. Shanabrook, D.S. Katzer, and D. Park, Phys. Rev. Lett. 76, 3005 (1996).
- [7]. E. Blackwood, M.J. Snelling, R.T. Harley, S.R. Andrews, and C.B.T. Foxon Phys. Rev. B 50, 14246 (1994).
- [8]. U. Woggon, Optical Properties of Semiconductor Quantum Dots (Springer-Verlag, Berlin, 1996) and references therein.
- [9]. S.V. Goupalov, E.L. Ivchenko and A.V. Kavokin, Proc. Int. Symp., Nanostructures: Physics and Technology, St. Petersburg, 322 (1996).
- [10]. G.L. Bir, G.E. Pikus Symmetry and Strain-Induced Effects in Semiconductors (Wiley, New York, 1974).
- [11]. S-H. Wei and A. Zunger, Phys. Rev. B 57, 8983 (1998) and references therein.
- [12]. Landolt-B ddotorstein, Numerical Data and Functional Relationships in Science and Technology ,New Series, Group III, Vol. 22a, Pt. Springer-Verlag, Berlin, 1987.
- [13]. D.M. Follstaedt, R.P. Schneider, Jr., and E.D. Jones, J. Appl. Phys. 77, 3077 (1995) and references therein.
- [14]. S-H. Wei and A. Zunger, Phys. Rev. B 49, 14 337 (1994)

Figures

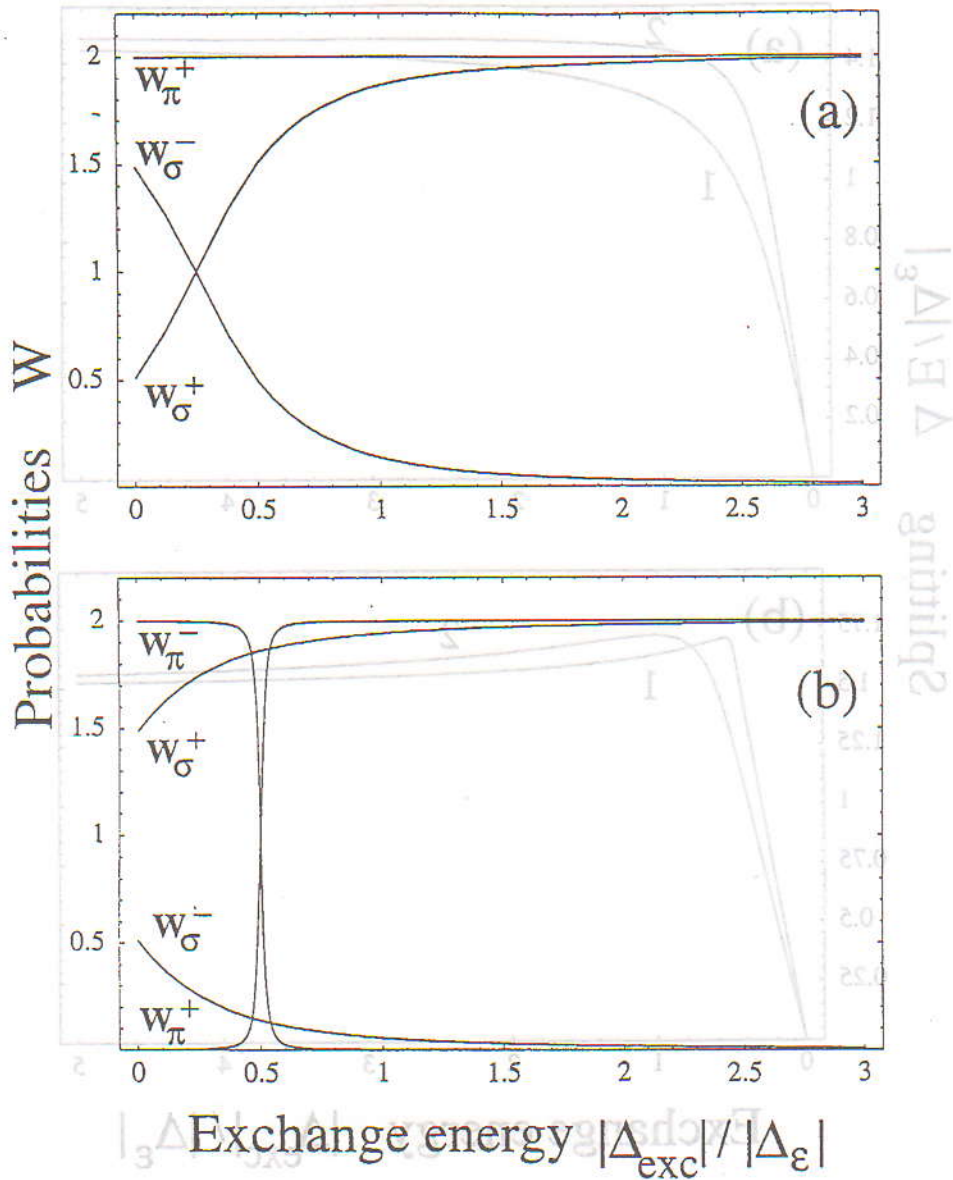


Fig. 1. Transition probabilities versus exchange energy: for the negative (a) and positive (b) deformation energy  $\Delta_{\epsilon}$ . Exchange energy is in units of the deformation energy  $|\Delta_{\epsilon}|$ . Doublet splitting versus exchange energy: for the negative (a) and positive (b) deformation energy  $\Delta_{\epsilon}$ ; curves 1 - no lattice mismatch, curves 2 - coexistence with the epitaxial strain. The epitaxial energy  $\Delta_{ep} = -0.5|\Delta_{\epsilon}|$ . All energies are given in units of the deformation energy  $|\Delta_{\epsilon}|$ .

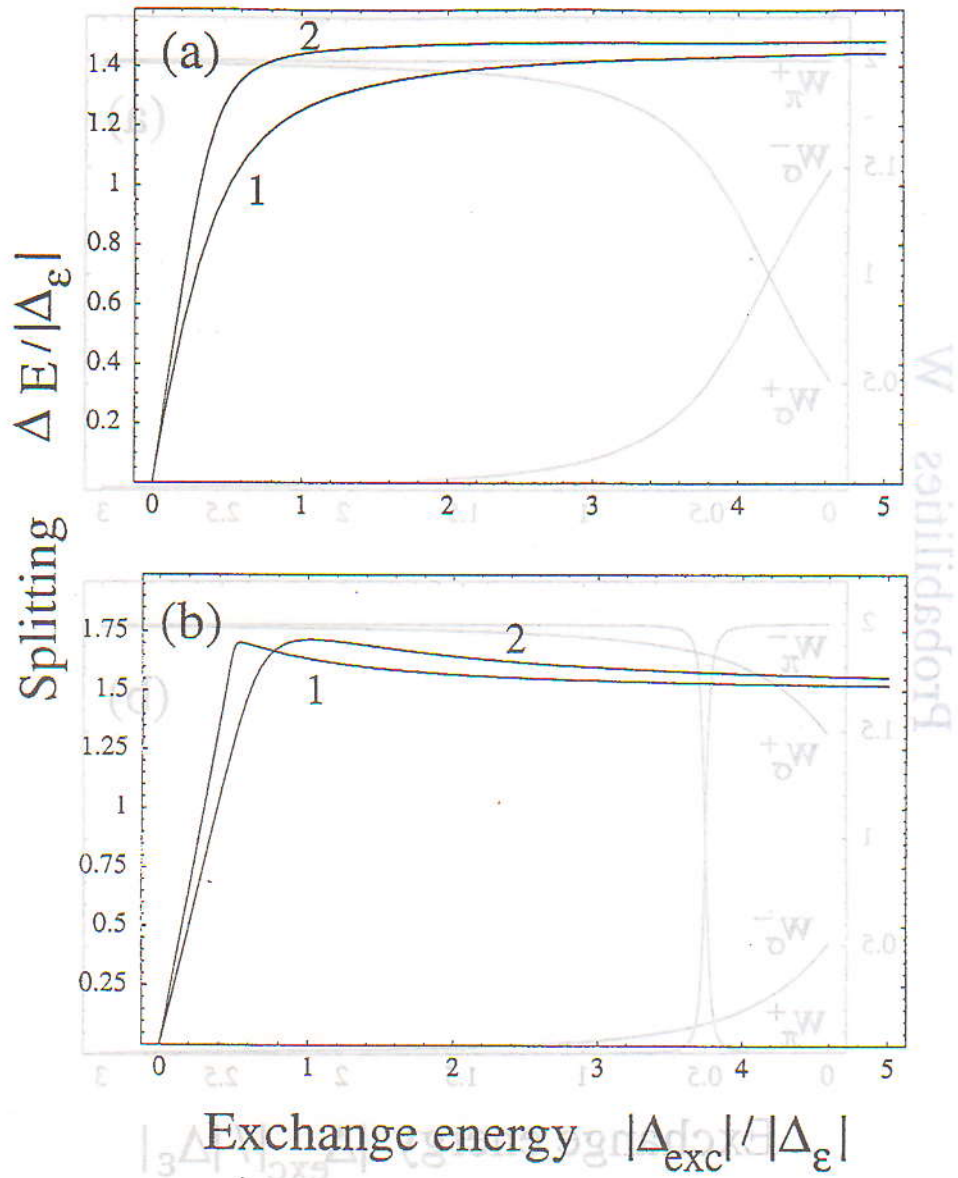
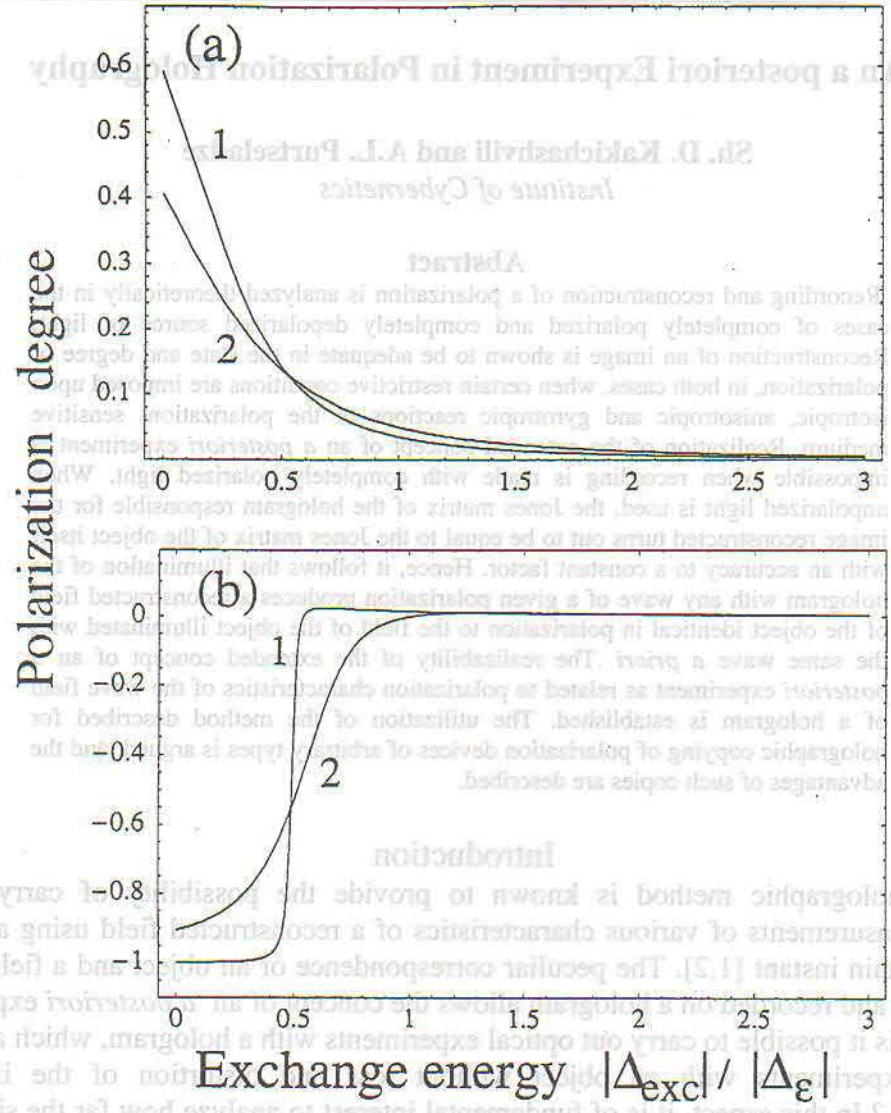


Fig.2.

Transition probabilities versus exchange energy: for the negative (a) and positive (b) deformation energy  $\Delta_\epsilon$ . Exchange energy is given in units of the deformation energy  $|\Delta_\epsilon|$ .

Doublet splitting versus exchange energy: for the negative (a) and positive (b) deformation energy  $\Delta_\epsilon$ ; curves 1 - no lattice mismatch, curves 2 - coexistence with the epitaxial strain. The epitaxial energy  $\Delta_\epsilon = -0.2|\Delta_\epsilon|$ . All energies are given in units of the deformation energy  $|\Delta_\epsilon|$ .



Exchange energy  $|\Delta_{exc}| / |\Delta_{\epsilon}|$

Fig. 3.

Polarization degree versus exchange energy: for the negative (a) and positive (b) deformation energy  $\Delta_{\epsilon}$ ; the epitaxial energy  $\Delta_{ep} = -0.5|\Delta_{\epsilon}|$ . Exchange energy is given in units of the deformation energy  $\Delta_{\epsilon}$ .

The extended concept of an a posteriori experiment turned out to be realizable with respect to polarization characteristics of the wave field of an object and its polarization hologram. It was shown theoretically and experimentally in [4] that polarization holographic recording with the use of a completely unpolarized light source makes it possible in the subsequent reconstruction by a wave of arbitrary polarization to reconstruct a field identical to the field of the object illuminated with the same wave. The situation is illustrated in the figure. The reason for such a substantial completeness of the holographic experiment turns out to be in the



## An a posteriori Experiment in Polarization Holography

Sh. D. Kakichashvili and A.L. Purtseladze  
*Institute of Cybernetics*

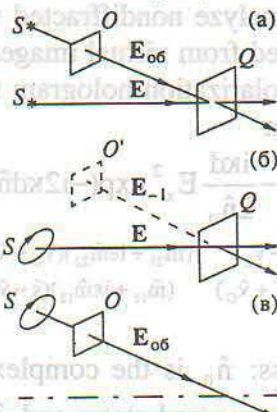
### Abstract

Recording and reconstruction of a polarization is analyzed theoretically in the cases of completely polarized and completely depolarized source of light. Reconstruction of an image is shown to be adequate in the state and degree of polarization, in both cases, when certain restrictive conditions are imposed upon isotropic, anisotropic and gyrotropic reactions of the polarization-sensitive medium. Realization of the extended concept of an *a posteriori* experiment is impossible when recording is made with completely polarized light. When unpolarized light is used, the Jones matrix of the hologram responsible for the image reconstructed turns out to be equal to the Jones matrix of the object itself with an accuracy to a constant factor. Hence, it follows that illumination of the hologram with any wave of a given polarization produces a reconstructed field of the object identical in polarization to the field of the object illuminated with the same wave *a priori*. The realizability of the extended concept of an *a posteriori* experiment as related to polarization characteristics of the wave field of a hologram is established. The utilization of the method described for holographic copying of polarization devices of arbitrary types is argued, and the advantages of such copies are described.

### Introduction

The holographic method is known to provide the possibility of carrying out *a posteriori* measurements of various characteristics of a reconstructed field using a hologram fixed at a certain instant [1,2]. The peculiar correspondence of an object and a field scattered by this object and recorded on a hologram allows the concept of an *a posteriori* experiment to be extended: is it possible to carry out optical experiments with a hologram, which are directly similar to experiments with an object without loss and distortion of the information reconstructed? In this aspect, it is of fundamental interest to analyze how far the similarity in information between the fields of an object and its hologram extends. Apparently, variations in the illumination geometry and the wavelength in the process of reconstruction significantly transform the image and prohibit the realization of the concept of an extended *a posteriori* experiment. Nevertheless, holographic copies of lenses and mirrors satisfy the extended concept to a considerable extent, because they focus and transform arbitrary beams incident on a hologram just as originals of these lenses and mirrors do. Multicolored Denisyuk reflecting holograms also furnish such a possibility when the color of the reconstructing wave is varied. In this case, the hologram forms a field that is colorimetrically identical to the object itself [3]. In scalar holography, the possibilities of realizing the concept of an extended *a posteriori* experiment are likely to be exhausted by these particular cases. The extended concept of an *a posteriori* experiment turned out to be realizable with respect to polarization characteristics of the wave field of an object and its polarization hologram. It was shown theoretically and experimentally in [4] that polarization holographic recording with the use of a completely unpolarized light source makes it possible in the subsequent reconstruction by a wave of arbitrary polarization to reconstruct a field identical to the field of the object illuminated with the same wave. The situation is illustrated in the figure. The reason for such a substantial completeness of the holographic experiment turns out to be in the

physically limiting redundancy of the polarization hologram obtained in unpolarized light, containing, according to current concepts, all kinds of polarization states of a source illuminating the object in the form of wave trains rapidly following each other.



On the extended concept of an *a posteriori* experiment in polarization holography: (*S*) light source, (*O*) object, (*O'*) reconstructed image of the object, and (*Q*) polarization hologram. (a) Recording of a polarization hologram in completely unpolarized light; (b) reconstruction of a holographic image by a wave of a given polarization; and (c) illumination of the object by a wave of a given polarization.

It is believed that material copies of various objects can be produced on this basis in the distant future (from private conversations with Yu. N. Denisyuk). Despite a good fraction of fantasy, such a possibility is by no means forbidden by laws of nature (conversion of a gamma quantum into an electron-positron pair, etc.). The unique relation between spatial frequency spectra of an object and its three-dimensional hologram, demonstrated in [5], is an argument in favor of this.

In the present work, polarization holographic recording and reconstruction is considered theoretically, in the general case of an arbitrary object and the most general isotropic-anisotropic-gyrotropic reaction of a polarization-sensitive medium. Unpolarized light is represented in the form of an arbitrary elliptically polarized basis of two mutually incoherent components.

### Results and discussion

First, we consider briefly polarization holographic recording with completely polarized light of a coherent source [6].

Let a wave of arbitrary elliptic polarization be used as a source

$$\mathbf{E} = E_x \exp[i(\omega t + \varphi)] \begin{pmatrix} 1 \\ i\varepsilon \end{pmatrix}, \quad (1)$$

where  $\varepsilon = E_y / E_x, 0 \leq \varepsilon \leq 1$ .

Upon passing through an object, the transmitted field is represented in the form

$$\mathbf{E}_{ob} = M_{ob} \mathbf{E} = E_x \exp[i(\omega t + \varphi + \delta)] M_{ob} \begin{pmatrix} 1 \\ i\varepsilon \end{pmatrix}, \quad (2)$$

Where  $M_{ab} = \begin{pmatrix} \hat{m}_{11} & \hat{m}_{12} \\ \hat{m}_{21} & \hat{m}_{22} \end{pmatrix}$  is the complex Jones matrix [7] of an arbitrary vector object, and  $[\delta]$  is the phase term determined by the angle of intersection with the reference wave. In this case, the total field takes the form

$$\mathbf{E}_\Sigma = \mathbf{E} + \mathbf{E}_{ob} = E_x \exp[i(\omega t + \varphi)] (1 + \exp(i\delta) M_{ob}) \begin{pmatrix} 1 \\ i\varepsilon \end{pmatrix}. \quad (3)$$

The total field is mapped in a polarization-sensitive medium in the form of light-induced anisotropy and gyrotropy and converts each elementary portion of it into a kind of a gyrotropic crystal [8,9].

In this work, we do not analyze nondiffracted waves, real images, and convolutions, because they are spatially separated from virtual images and do not introduce interference. In this case, the Jones matrix of a polarization hologram responsible for the reconstruction of a virtual image is written in the form

$$M_{-1} \approx -\frac{ikd}{2\hat{n}_0} E_x^2 \exp(-i2kd\hat{n}_0) \exp(i\delta) \times \begin{pmatrix} (\hat{m}_{11} + i\epsilon\hat{m}_{12})(\hat{s} + \hat{v}_L) - i\epsilon(\hat{m}_{21} + i\epsilon\hat{m}_{22})(\hat{s} - \hat{v}_L) & (\hat{m}_{21} + i\epsilon\hat{m}_{22})(\hat{v}_L + \hat{v}_G) - i\epsilon(\hat{m}_{11} + i\epsilon\hat{m}_{12})(\hat{v}_L - \hat{v}_G) \\ (\hat{m}_{21} + i\epsilon\hat{m}_{22})(\hat{v}_L + \hat{v}_G) - i\epsilon(\hat{m}_{11} + i\epsilon\hat{m}_{12})(\hat{v}_L - \hat{v}_G) & (\hat{m}_{11} + i\epsilon\hat{m}_{12})(\hat{s} - \hat{v}_L) - i\epsilon(\hat{m}_{21} + i\epsilon\hat{m}_{22})(\hat{s} + \hat{v}_L) \end{pmatrix} \quad (4)$$

Here,  $d$  is the hologram thickness;  $\hat{n}_0$  is the complex refractive index of the polarization-sensitive medium in the initial unexposed state; and  $\hat{s}, \hat{v}_L, \hat{v}_G$  are the isotropic, anisotropic and gyrotropic reactions of the polarization-sensitive medium, respectively [10].

Once the hologram is illuminated with the initial reference wave, the reconstructed field is written in the form

$$E_{-1} \approx E_x \exp[i(\omega t + \varphi)] M_{-1} \begin{pmatrix} 1 \\ i\epsilon \end{pmatrix} \quad (5)$$

Simple analysis of (5) shows that the reconstructed field adequate to the field of the initial object is formed only if the conditions

$$\begin{aligned} (\hat{s} + \hat{v}_L) &\neq 0, \\ (\hat{s} - \hat{v}_L) = (\hat{v}_L + \hat{v}_G) &= 0, \\ (\hat{v}_L - \hat{v}_G) &\neq 0 \end{aligned} \quad (6)$$

are satisfied. This, we have  $\hat{s} = \hat{v}_L$ , and  $\hat{v}_G = -\hat{v}_L$ . These conditions are satisfied by a wide class of polarization-sensitive media, studied in detail in [10].

Using the conditions presented, from (5), we get

$$E_{-1} \approx -\frac{ikd}{\hat{n}_0} \hat{v}_L (E_x^2 + E_y^2) \times \exp(-i2kd\hat{n}_0) \exp[i(\omega t + \varphi + \delta)] M_{ob} \begin{pmatrix} 1 \\ i\epsilon \end{pmatrix} \quad (5')$$

This expression is equal to the object field within a constant factor [compare with (2)]. However, if we illuminate a polarization hologram with a reconstructing wave whose characteristics are different from those of the reference wave ( $\epsilon' \neq \epsilon, \varphi' \neq \varphi$ ), we detect irreversible transformation of the image polarization with respect to the field of the object illuminated with the same wave,

$$E_{-1}' \approx -\frac{ikd}{\hat{n}_0} \hat{v}_L E_x^2 (1 + \epsilon\epsilon') \times \exp(-i2kd\hat{n}_0) \exp[i(\omega t + \varphi' + \delta)] M_{ob} \begin{pmatrix} 1 \\ i\epsilon \end{pmatrix} \quad (5'')$$

Hence, it follows that it is impossible to carry out an *a posteriori* experiment in accordance with the extended concept. This restriction proves to be fundamental and follows from the principle of operation of a polarization hologram in the case of completely polarized of a coherent source.

If a polarization hologram is produced with a completely unpolarized coherent source, the situation is radically different. Such sources are widespread in laboratory practice and are technically realized by coupling an isotropic working medium of a laser to an isotropic cavity, for example, with the help of vacuumtight bellows for gas lasers.

Let us first we consider the field of the total wave  $E_{\Sigma,*}$  in the combination of the reference wave  $E_*$  and the object wave  $E_{ob,*}$  with the completely unpolarized light from a coherent source

$$\begin{aligned} E_{\Sigma,*} &= E_* + E_{ob,*}, \\ E_* &= E_x \exp i\alpha \begin{pmatrix} \cos \theta \\ \sin \theta \end{pmatrix} \oplus E_x \exp i\beta \begin{pmatrix} \sin \theta \\ -\cos \theta \end{pmatrix}, \\ E_{ob,*} &= ME_* \exp -i\delta = \exp -i\delta \begin{pmatrix} A_x \exp i\varphi_x \\ A_y \exp i\varphi_y \end{pmatrix} \oplus \exp -i\delta \begin{pmatrix} B_x \exp i\psi_x \\ B_y \exp i\psi_y \end{pmatrix}. \end{aligned} \quad (7)$$

Here for simplisity (and without loss of generality) the illuminating wave of the source  $S$  will be assumed in the subsequent calculations to be represented as an orthogonal basis of linear polarization with the polarization vector oriented at an angle  $\theta$ . The reference wave propagates along the  $z$  axis. The propagation of the object wave is at a small angle to the  $z$  axis, and is described by the corresponding phase shift  $\delta$  in the recording plane  $Q$  of the hologram. The matrix  $M$  is the Jones matrix of an arbitrary anisotropic-gyrotropic object. The incoherent components of the object wave, written in explicit form, describe completely the radiation transmitted through the object. This sign  $\oplus$  means the incoherent summation of the amplitudes [11,14]. The real part of  $E_{\Sigma,*}$  describes the electric field vector

$$\begin{aligned} \text{Re}(E_{\Sigma,*}) &= p \cos \omega t + q \sin \omega t, \\ p &= \begin{pmatrix} E_x \cos \theta \cos \alpha + A_x \cos(\varphi_x - \delta) \oplus [E_x \sin \theta \cos \beta + B_x \cos(\psi_x - \delta)] \\ E_x \sin \theta \cos \alpha + A_y \cos(\varphi_y - \delta) \oplus [-E_x \cos \theta \sin \beta + B_y \cos(\psi_y - \delta)] \end{pmatrix}, \\ q &= \begin{pmatrix} E_x \cos \theta \sin \alpha + A_x \sin(\varphi_x - \delta) \oplus [E_x \sin \theta \sin \beta + B_x \sin(\psi_x - \delta)] \\ E_x \sin \theta \sin \alpha + A_y \sin(\varphi_y - \delta) \oplus [-E_x \sin \theta \sin \beta + B_y \sin(\psi_y - \delta)] \end{pmatrix}. \end{aligned} \quad (8)$$

We assume that the polarization-sensitive medium of the hologram material reacts to the actinic radiation in the most general way, reflecting all three Stokes parameters of the combined radiation. This is equivalent to  $\hat{s} \neq 0, \hat{v}_L \neq 0, \hat{v}_G \neq 0$ , where these symbols are the coefficients of the photosensitive medium that describe its isotropic, anisotropic and gyrotropic response to the action of elliptically polarized light [12].

The Jones matrix of this medium has been derived in the linear approximation in [13] and has the form

$$M_{L,G} \approx \exp -ikdn_0(1 - \tau_0) \times \left[ 1 - \frac{ikd}{2} \hat{\mu} \hat{s} (p_x^2 + q_x^2 + p_y^2 + q_y^2) \right] \begin{pmatrix} m_{11} & m_{12} \\ m_{21} & m_{22} \end{pmatrix},$$

where  $\hat{\mu} = (1 + i\tau_0)/n_0(1 + \tau_0^2)$ ,  $n_0$  and  $\tau_0$  are the initial refractive index and extinction of the holographic medium, and

$$\begin{aligned} m_{11} &= 1 - \frac{ikd}{2} \hat{\mu} \hat{v}_L [p_x^2 + q_x^2 - (p_y^2 + q_y^2)], \\ m_{12} &= -\frac{ikd}{2} \hat{\mu} [\hat{v}_L 2(p_x p_y + q_x q_y) - i\hat{v}_G 2(p_x q_y - p_y q_x)], \\ m_{21} &= -\frac{ikd}{2} \hat{\mu} [\hat{v}_L 2(p_x p_y + q_x q_y) + i\hat{v}_G 2(p_x q_y - p_y q_x)], \\ m_{22} &= 1 + \frac{ikd}{2} \hat{\mu} \hat{v}_L [p_x^2 + q_x^2 - (p_y^2 + q_y^2)]. \end{aligned} \quad (9)$$

From the matrix we use only those components that are responsible for forming the reconstructed field, and we substitute into them the values of  $\mathbf{p}$  and  $\mathbf{q}$  from Eqs.(6) and impose the conditions  $\hat{\mathbf{s}} = \hat{\mathbf{v}}_L = -\hat{\mathbf{v}}_G$ , which ensure that the state of polarization is restored without any distortions. For these conditions we have

$$\mathbf{M}_{-1,*} = k \exp -i\delta (\exp -i\alpha A + \exp -i\beta B), \quad (10)$$

where

$$k = -ikd\hat{\mu}\hat{\mathbf{v}}_L E_x \exp -ikdn_0(1-\tau_0),$$

$$\mathbf{A} = \begin{pmatrix} A_x \exp i\varphi_x & 0 \\ 0 & A_y \exp i\varphi_y \end{pmatrix} \begin{pmatrix} \cos \theta & \sin \theta \\ \cos \theta & \sin \theta \end{pmatrix},$$

$$\mathbf{B} = \begin{pmatrix} B_x \exp i\psi_x & 0 \\ 0 & B_y \exp i\psi_y \end{pmatrix} \begin{pmatrix} \sin \theta & -\cos \theta \\ \sin \theta & -\cos \theta \end{pmatrix}.$$

It is easy to see that illumination of the hologram (10) by the light of the initial reference wave gives the reconstructed field of the object up to a multiplicative factor

$$\mathbf{E}_{-1,**} = \mathbf{M}_{-1,*} \mathbf{E}_* = k \mathbf{E}_{ob,**} \quad (11)$$

write (1)-(4) when, unpolarized light is represented in the form of an arbitrary elliptically polarized basis of two mutually incoherent components:

$$\mathbf{E}_{**} = E_x \exp[i(\omega t + \varphi)] \begin{pmatrix} 1 \\ i\varepsilon \end{pmatrix} \oplus E_x \exp\left[i\left(\omega t + \psi - \frac{\pi}{2}\right)\right] \begin{pmatrix} i\varepsilon \\ 1 \end{pmatrix} \quad (1')$$

where  $\varphi$  and  $\psi$  are the initial phases of two mutually incoherent components of completely unpolarized light, respectively.

The field of the object illuminated with wave (1') is written in the form

$$\mathbf{E}_{ob,**} = E_x \exp[i(\omega t + \varphi + \delta)] \mathbf{M}_{ob} \begin{pmatrix} 1 \\ i\varepsilon \end{pmatrix} \oplus E_x \exp\left[i\left(\omega t + \psi - \frac{\pi}{2}\right)\right] \mathbf{M}_{ob} \begin{pmatrix} i\varepsilon \\ 1 \end{pmatrix} \quad (2')$$

In this case, the field of the total wave takes the form

$$\begin{aligned} \mathbf{E}_{\Sigma,**} &= \mathbf{E}_{**} + \mathbf{E}_{ob,**} \\ &= E_x \exp[i(\omega t + \varphi)] (1 + \exp(i\delta) \mathbf{M}_{ob}) \begin{pmatrix} 1 \\ i\varepsilon \end{pmatrix} \oplus \\ &\oplus E_x \exp\left[i\left(\omega t + \psi - \frac{\pi}{2}\right)\right] (1 + \exp(i\delta) \mathbf{M}_{ob}) \begin{pmatrix} i\varepsilon \\ 1 \end{pmatrix}. \end{aligned} \quad (3')$$

After cumbersome transformations with conditions (6) taken into account, the Jones matrix of the hologram thus obtained turns out to be

$$\mathbf{M}_{-1,**} \approx -\frac{ikd}{\hat{n}_0} \hat{\mathbf{v}}_L \exp(-i2kd\hat{n}_0) \exp(i\delta) \mathbf{M}_{ob}. \quad (4')$$

It follows from (4') that the Jones matrix responsible for the formation of the virtual image is identical within a factor to the Jones matrix of the object itself. Hence, it follows that illumination of the hologram with any wave of a given polarization produces the reconstructed field of the object identical in the state and the degree of polarization to the field the object illuminated with the same wave *a priori*. Thus, any ellipsometric experiments can be carried out the hologram, the same as with the object itself.

The situation appears paradoxical to a considerable degree. Thus, a polarization hologram obtained with an unpolarized source of light turns out to be more informative

compared to the case of a completely polarized source of light and allows an *a posteriori* experiment to be performed in accordance with the extended concept. The paradox manifest itself in the fact that the entropy of unpolarized light is higher (the thermodynamic temperature is lower) than that of completely polarized light (correspondingly, the thermodynamic temperature is higher) for equal energies [15,16]. Nevertheless, an unpolarized coherent source of light appears to be more informative in holography. Such a situation may generate a need in the reformulation of notions of the nature of unpolarized light in comparison with the existing ones. In [4], possible mechanisms for the explanation of this phenomenon on the basis of a photon echo and other [17] were proposed. However, the theoretical analysis carried out in this work does not require any special mechanisms for the operation of a polarization-sensitive medium compared to familiar ones. We believe that the most natural explanation is in a higher (maybe, physically limiting) redundancy of a polarization hologram produced in unpolarized light in comparison with the case of completely polarized light.

It should also be noted that the series of experiments carried out earlier confirmed the preliminary theoretical consideration in full [4]. Experiments on copying a number of polarizing devices (linear polarizers, quarter-wave and half-wave phase plates, etc.) by the method described above were also carried out. In complete agreement with the theory developed, the operation properties of polarization holographic copies produced at a single wavelength turned out to be almost constant over the entire range of operating wavelengths in the transparent region of the holographic material.

## References

- [1]. Gabor D., *Proc. Roy. Soc.*, 1949, vol. 197, pp.454-487.
- [2]. Denisyuk. Yu. N., *Dokl. Akad. Nauk SSSR*, 1962, vol. 144, no. 6, p. 1275.
- [3]. Denisyuk, Yu. N., *Opt. Spektrosk.*, 1963, vol. 15, no.4, pp. 552-532.
- [4]. Kakichashvili, Sh.D. *Pis'ma Zh. Tekh. Fiz.*, 1993, vol.19, no. 14, pp. 5-8.
- [5]. Sukhanov, V.I. and Denisyuk, Yu. N., *Opt. Spektrosk.*, 1970, vol. 28, no.1, pp. 126-131.
- [6]. Kakichashvili, Sh.D., *Pis'ma Zh. Tekh. Fiz.*, 1980, vol. 6, no. 1, pp. 6-9.
- [7]. Jones, R.C., *J. Opt. Soc. Am.*, 1941, vol.31, pp. 488-493.
- [8]. Weigert, F., *Ann. Phys. (Paris)*, 1920, vol. 63, pp. 682-725.
- [9]. Zocher, H. and Coper, K., *Z. Phys. Chem. (Leipzig)*, 1928, vol. 132, pp. 313-319.
- [10]. Kakichashvili, Sh.D., *Polyarizatsionnaya golografiya (Polarization Holography)*, Leningrad, 1989.
- [11]. Kakichashvili, Sh.D., *Zh. Tekh. Fiz.*, 1989, vol. 59, no.2, pp. 26-34.
- [12]. Kakichashvili, Sh.D., *Opt. Spektrosk.* 1987 vol. 63, no.4, pp. 911-917.
- [13]. Kakichashvili, Sh.D., *Kvantovaya Elektron. (Moscow)* 1983 vol.10, no.10, pp.1976-1981.
- [14]. Kakichashvili, Sh.D., *Zh. Tekh. Fiz.*, 1995, vol. 65, no. 7, pp. 200-204.
- [15]. Planck, M., *Theorie der Warmestrahlung*, Leipzig, 1932.
- [16]. Born, M., *Optik*, Berlin: Springer, 1933. Translated under the title *Optika*, Krakov, 1937.
- [17]. Rebane. A.K., Kaarli, R.K., and Saari, P.M., *Pis'ma Zh. Eksp. Teor. Fiz.*, 1983, vol. 38, pp. 320-324.



## Synthesis of Polarized Hologram by Micro Half-wave Phase Plates

Tariel Ebralidze  
*Institute of Cybernetics*

### Introduction

The work describes synthesis of polarized hologram by micro phase plates. There is considered the case of obtaining hologram by linearly polarized plane waves [1,2].

In [1,2] works discrete form of hologram was studied obtained by linearly polarized plane waves. The sampling points on the hologram were chosen points, where interference of object and reference waves give linearly polarized light. Was shown, that if amplitudes of reference and object waves are equal, then for synthesis of polarized hologram, distribution the identical micro phase plates in the sampling points of the hologram is sufficient.

It is necessary, only, that the phase plates' optical axes coincided to the polarization vector of summary wave in those points.

It is clear, that such way of coding is not normal for the case, when the amplitudes of reference and object waves are not equal to each other. In common, at sampling points, with coding of polarization vector's direction will be necessary coding the module of the same vector.

This work offers the method of coding the module of polarization vector with anisotropical grains. By that method in sampling points, in unit area circle random location of micro half-wave phase plates took place. Their concentration is proportional to light intensity and optical axes are coinciding to the light vector in sampling points.

There was shown that the hologram obtained by such way of coding is polarized.

This work has interest not only for computer-aided synthesis of polarized hologram, but also for optical holography, as for some cases it could be foundation of anisotropic grains photoinducing in anisotropy photoinducing layers [3,4].

### 2. Coding of optical information by anisotropic grains

As we noticed, in recording wave points having linear polarization, we bring to the conformity in circle having unit area to the anisotropic grains scattered randomly. Concentration of grains is proportional to the light intensity, but their optical axes are collinear to the light vector.

*Fig.1* depicts schematically the circle having unit area and the grains located in it. The arrows show the axes of grains.

Suppose that grains represent half-wave phase plates. Then acting of grains on the polarization vector of illuminating light will be described by following Jones's matrix [5]:

$$\begin{bmatrix} \cos 2\psi & \sin 2\psi \\ \sin 2\psi & -\cos 2\psi \end{bmatrix},$$

where  $\psi$  is an angle constructed by optical axis of phase plate to *OX* axis of *XOY* coordinate system. From here follows that, in sampling points for Jones's matrix of grain collection, we can write

$$A^2 \begin{bmatrix} \cos 2\psi & \sin 2\psi \\ \sin 2\psi & -\cos 2\psi \end{bmatrix} \quad (2.1)$$

where  $A^2$  is a module of polarization vector in sampling points.

So, according to the offered rule of coding in sampling points a hologram influence on the polarization of the illuminating light is described by (2.1) matrix.

### 3. Discrete representation of the interference pattern of linearly polarized plane waves

We examine superposition of linearly polarized plane coherent waves according to specially selected scheme [1,2]. Reference wave was incident the  $XOY$  plane normally and the object wave was incident inclined (see Fig. 2). The wave vector of object wave constructs angle to the  $XOY$  plane's normal, but its polarization vector is situated in the  $XOY$  plane and constructs angle to the axis  $OX$ .

It is clear, that reference and object waves light vectors in the plane of waves superposition is described suitable to the formulae:

$$\vec{E}_0 = \vec{e} a_0 \cos \omega t, \quad \vec{E}_1 = \vec{\sigma} a_1 \cos(\omega t - ky \sin \theta). \quad (3.1)$$

Here  $\vec{e}$  is unit vector directed across the polarized vector of reference wave;  $\vec{\sigma}$  is unit vector directed across the axis  $OX$ ;  $a_0$  and  $a_1$  are properly amplitudes of reference and object waves;  $\omega$  is cyclic frequency;  $k = \frac{2\pi}{\lambda}$  is wave number;  $\lambda$  is length of wave;  $t$  is time variable;  $y$  - coordinate of observation point.

Following from the expression (3.1) projections of summary waves' light vector will be on the coordinate axis:

$$E_x = a_0 \sin \alpha \cos \omega t, \quad E_y = (a_0 \cos \alpha + a_1 \cos(ky \sin \theta)) \cos \omega t + a_1 \sin(ky \sin \theta) \sin \omega t. \quad (3.2)$$

As it is known [6], polarized light is completely characterized by Stokes four parameters. To examine that for (3.2) wave, Stokes all four parameters will be harmonic function of coordinate  $y$  with the period  $\frac{\lambda}{\sin \theta}$  is not difficult. As according to the sampling theorem for discrete representation of harmonic function [7] is sufficient to take two samples on each period. That is why for discrete representation of wave (3.2) taking samples with interval  $\frac{\lambda}{2 \sin \theta}$  will be sufficient.

We select points of sampling where wave (3.2) is linearly polarized. It is clear [6] that the coordinates of those points are defined from the condition  $\sin(ky \sin \theta) = 0$  - and is equal to

$$y_m = \frac{\lambda}{2 \sin \theta} m, \quad (3.3)$$

where  $m = 0, \pm 1, \dots$ . So, those sampling points are satisfying requests of the sampling theorem.

At the sampling points (3.2) obtains following form:

$$E_x = a_0 \sin \alpha \cos \omega t, \quad E_y = (a_0 \cos \alpha + (-1)^m a_1) \cos \omega t$$

That is why state of polarization for even  $m$  in summary wave defines:

$$\sin \psi_1 = \frac{a_0 \sin \alpha}{A_1}, \quad \cos \psi_1 = \frac{a_0 \cos \alpha + a_1}{A_1}, \quad A_1 = \sqrt{a_0^2 - a_1^2 + 2a_0 a_1 \cos \alpha}$$

But for odd  $m$  it defines:

$$\sin \psi_2 = \frac{a_0 \sin \alpha}{A_2}, \quad \cos \psi_2 = \frac{a_0 \cos \alpha - a_1}{A_2}, \quad A_2 = \sqrt{a_0^2 + a_1^2 - 2a_0 a_1 \cos \alpha}. \quad (3.4)$$

where  $\psi_{1,2}$  is an angle constructing by polarization vector to the axis  $OX$ , and  $A_{1,2}$  are amplitudes in the summary wave.

So light polarization parameters in sampling points are defined by formulae (3.4).

#### 4. Construction of discrete hologram and pattern reconstruction from it

Now suppose, at the sampling points on the hologram are distributed half-wave phase plates by the said rules of coding. Then we shall have one-dimensional grating, for the nodes of even numbers of which according to the formulae (3.4) and (2.1) the Jones matrix will have following form:

$$\begin{bmatrix} (a_0 \cos \alpha + a_1)^2 - a_0^2 \sin^2 \alpha & 2(a_0 \cos \alpha + a_1)a_0 \sin \alpha \\ 2(a_0 \cos \alpha + a_1)a_0 \sin \alpha & -(a_0 \cos \alpha + a_1)^2 + a_0^2 \sin^2 \alpha \end{bmatrix}, \quad (4.1)$$

and for odd number nodes

$$\begin{bmatrix} (a_0 \cos \alpha - a_1)^2 - a_0^2 \sin^2 \alpha & 2(a_0 \cos \alpha - a_1)a_0 \sin \alpha \\ 2(a_0 \cos \alpha - a_1)a_0 \sin \alpha & -(a_0 \cos \alpha - a_1)^2 + a_0^2 \sin^2 \alpha \end{bmatrix}. \quad (4.2)$$

Suppose, that constructed discrete hologram is illuminated by reference wave, polarization vector of which constructs generally angle to the axis  $OX$ . Maxwell's vector of such wave is given in [5]:

$$\begin{bmatrix} \cos \beta \\ \sin \beta \end{bmatrix}. \quad (4.3)$$

Suppose that light in hologram is transmitted only through the anisotropic grains. Then, if (4.1) and (4.2) matrices multiply on the vector (4.3), we obtain Maxwell vector of wave reconstructed from the hologram. It will be suitable for even and odd sampling points on the hologram:

$$\begin{bmatrix} ((a_0 \cos \alpha + a_1)^2 - a_0^2 \sin^2 \alpha) \cos \beta + 2(a_0 \cos \alpha + a_1)a_0 \sin \alpha \sin \beta \\ 2(a_0 \cos \alpha + a_1)a_0 \sin \alpha \cos \beta + (-(a_0 \cos \alpha + a_1)^2 + a_0^2 \sin^2 \alpha) \sin \beta \end{bmatrix}, \quad (4.4)$$

$$\begin{bmatrix} ((a_0 \cos \alpha - a_1)^2 - a_0^2 \sin^2 \alpha) \cos \beta + 2(a_0 \cos \alpha - a_1)a_0 \sin \alpha \sin \beta \\ 2(a_0 \cos \alpha - a_1)a_0 \sin \alpha \cos \beta + (-(a_0 \cos \alpha - a_1)^2 + a_0^2 \sin^2 \alpha) \sin \beta \end{bmatrix}. \quad (4.5)$$

So, in the reconstructed wave in even points of sampling the light will have polarization determined by (4.4), and for odd numbers will have another polarization determined by (4.5). Both of them are linear.

Points determined by even numbers make one grating and odd numbers another grating. The period of both gratings is the same. But grating constructed by points of even numbers is shifted by the half of period then grating constructed by odd numbers. That is why it is clear that both gratings will make similar diffraction orders, but in given order they will propagate waves generally in different phase [7]. In even number diffraction orders (4.4) and (4.5) vectors will be summarized and in odd number diffraction orders they will be subtracted.

As it is known from reference [7] pattern reconstruction from hologram takes place in an order with odd numbers. That is why we are interested in subtraction of (4.4) and (4.5) vectors, which has following form:

$$4a_0a_1 \begin{bmatrix} \cos(\alpha - \beta) \\ \sin(\alpha - \beta) \end{bmatrix}. \quad (4.6)$$

We see, that from hologram synthesized from half-wave phase plates, during illumination with reference wave takes place reconstruction of object wave (the reconstructed

wave is linearly polarized and its Maxwell vector is proportional to the amplitude of object wave). When reconstructing reference wave is exact copy of recording wave ( $\beta = \alpha$ ), according to the (4.5) object wave will be reconstructed from hologram with its own polarization:

$$4a_0a_1 \begin{bmatrix} 1 \\ 0 \end{bmatrix},$$

i.e. Maxwell's vector has direction of axis OX in reconstructed wave.

### 5. Conclusion

So, we have shown that synthesis of polarized hologram is possible by half-wave micro phase plates. If we locate the half-wave micro plates in linearly polarization's points of linearly polarized plane waves hologram so that their effective area is proportional to the intensity of light and optical axes are parallel to the vector of polarization in this points, it is possible to record and reconstruction of polarization vector of subject wave.

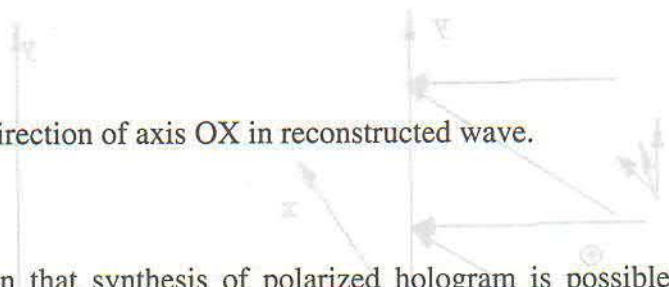


Fig. 2

### Figures



Fig. 1

Schematic of grain clusters within the unit circle; the arrowed lines indicate the directions of grain optic axes.

### References

- [1] T. D. Ebnalidze "On a Model of Anisotropic Diffraction Grating" Opt. Spectrosc., 23, 944 (1982);
- [2] T. D. Ebnalidze, M. A. Ebnalidze, Appl. Opt., 31, 4720 (1992);
- [3] Tanel D. Ebnalidze and Alexander N. Muminidze, Appl. Opt., 44, 448 (2005);
- [4] Tanel D. Ebnalidze, Nadeia A. Ebnalidze, and Alexander N. Muminidze, Appl. Opt., 37, 6161 (1998);
- [5] A. Gerard, J. M. Burch, Introduction to Matrix Methods in Optics, (London, New York, Sydney, Toronto, 1972);
- [6] M. Born and E. Wolf, Principles of Optics, (Pergamon Press, New York, 1967);
- [7] Robert J. Collier, Christoph B. Burckhardt, Lawrence J. Savransky, Optical Holography, (Academic Press, New York and London, 1971).

wave is linearly polarized and its Maxwell vector is proportional to the amplitude of object wave). When reconstructing reference wave is exact copy of recording wave ( $\vec{E} = \vec{E}_0$ ), according to the (4.2) object wave will be reconstructed from hologram with its own polarization.

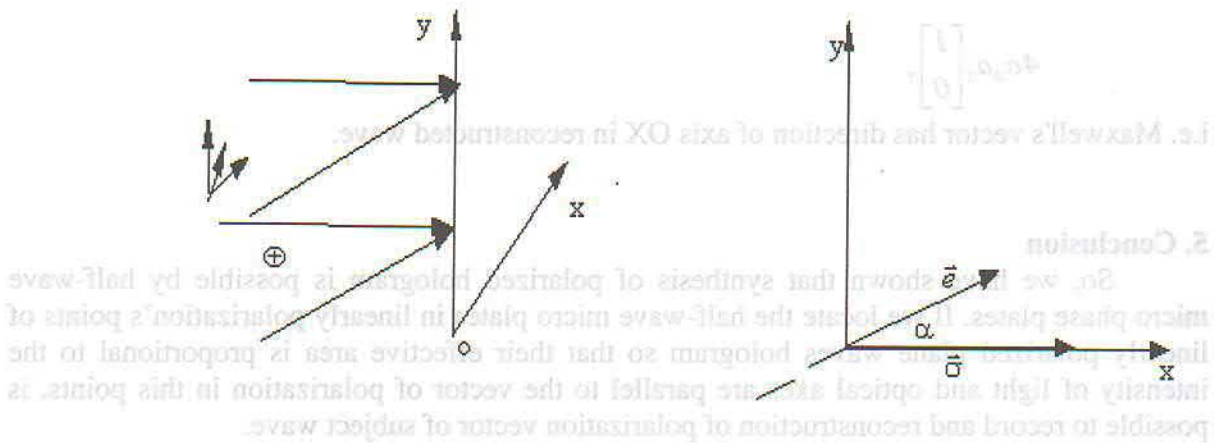


Fig. 2.

### References

- [1]. T. D. Ebralidze, "On a Model of Anisotropic Diffraction Grating", *Opt. Spectrosk.*, **53**, 944, (1982);
- [2]. T. D. Ebralidze, N. A. Ebralidze, *Appl. Opt.*, **31**, 4720 (1992);
- [3]. Tariel D. Ebralidze and Alexandre N. Mumladze, *Appl. Opt.*, **29**, 446 (1990);
- [4]. Tariel D. Ebralidze, Nadia A. Ebralidze, and Alexandre N. Mumladze, *Appl. Opt.*, **37**, 6161, (1998);
- [5]. A. Gerrard, J. M. Burch, *Introduction to Matrix Methods in Optics*, (London. New York. Sydney. Toronto. 1975);
- [6]. M. Born and E. Wolf, *Principles of Optics*, (Pergamon, New York, 1964);
- [7]. Robert J. Collier, Christoph B. Burckhardt, Lawrence H. Lin, *Optical Holography*, (Academic Press, New York and London, 1971).



## **Bioferromagnetic Liquid (BFML) as a Tool for Investigation of Biophysico-chemical Activity of Cell**

**M. G. Akhalaya, V. P. Beria**

*Institute of Cybernetics*

The chemical method of obtaining ferromagnetic suspension and its modification (1) considerably increased the number of works investigating the physic-chemical characteristics of magnetic liquids (ML) (2). This gave possibility to solve fundamental problems as well as applied tasks on the bases of application of the unique properties of ML - colloidal suspensions of ferro- and ferrymagnetic materials in the nonmagnetic liquid medium.

The first investigations were mainly connected with the use of the ML in technique, later ML were applied in biology and medicine. We investigated the toxic effects of ML and its ingredients on the culture of cells and on mice, rats and dogs. We showed that oleic acid is toxic and it has lethal influence in dose 400 mg/kg, at the same time the particles of magnetite (PM) have not such effect (3). So it was impossible to use ML directly in biology and medicine, despite of quite high magnetizing of saturation. There are some data about the use of PM for controllable contrastization of hollow organ (4), making depot of medical preparation (5,6), local increasing of temperature (7). But the liquid magnetic mixtures used in these works are not steady in the biological objects. It results in their sticking together, aggregation and loss of their magnetic property.

All this raised the problem of creating a new class of BFML, the physic-chemical characteristics of which are compatible with the vital processes. Such BFML must not have toxic effects on all the levels of a living organism, must be steady in a biological medium with high magnetization which will allow to use their magnetic, reologic, hydrodynamic, mechanical and the other properties for medical and biological purposes.

The method of obtaining BFML consisted of obtaining PM, cleaning it thoroughly from the ions of soluble salts, addition of stabilizer, hypersound dispersion, heating and the consequent centrifugation. In some cases the methodology varies insignificantly. The biological objects were: stray dogs, male rats of Wistar weighing 180-200 g, laboratory white mice and the culture of the spleen cells, culture of Goldish staphylococcus, and culture of *Escherichia coli*.

The magnetite concentration in the experiments were determined by the level of signal of ferromagnetic resonance on the radiospectrometer RS-1301 (USSR). Hypersound dispersion was carried out on the device URS-7N (USSR). The photos were obtained by the electronic microscope JEM-100 (Japan). Reductive-Oxidative potentials (Red/Ox pot) were obtained by potentiometer LP-60 (USSR). Concentration of oxygen was investigated on the radiometer ABC-1 (Denmark). The constant magnetic field was created by samari-cobalt magnet with induction of magnetic field 5kA/m. Steadiness at gravity field was defined on the centrifuge VAC-601(DDR), separate factor was 6000g during 15 minutes. Steadiness of

BFML in biological medium was studied for identical pH with appearance of PM of size more than 1000 nm by the optical microscope BIOLAM (USSR). Magnetization of saturation was measured with a ballistic method on the device made especially for this purpose.

BFML synthesized by us are PM the size of which is 100-150 Å. They are stabilized in water solution with biologically active compounds such as sodium salt of ATP, ascorbic acid (vita C), pyridoxine (vita B6), twin-80, fibrinogen, human serum albumen,  $\gamma$ -aminocaproic acid, citric acid, pepsin, cholesterol, lecithin etc. The properties of the synthesized BFML were characterized by the following indices – the size and the density of PM, magnetization of saturation, steadiness in the field of gravity, pH and steadiness in the range of pH, the concentration of ferromagnetic phase, steadiness in a biological medium (8-17). The size of the obtained materials gives possibility to study the processes of action particles on the cells. It was established that even during the first minutes of injection PM into the vessels of the



**Figure 1** Liver tissue (x 30000) after 7 day following the injection of PM.

experimental animal PM penetrate into the cells of kidney, spleen and lungs. This occurs without any visual injuries of the outer membrane of the cell, probably with the transport canals (Fig 1). The terminal target of the PM are the cells of reticulo-endothelial systems of liver, megacariocytes and polymorphonuclear leukocytes of the brain bones and so the macrophages

of lungs. This allows to conclude that PM taken out of bloody system and then from the organism have an ability to penetrate through the walls of capillaries are typical.

The balance of quantum of magnetite injected and taken out of the organism shows, that about 7-15% of dispersional phase reserves in cells of reticule-endothelial systems. 30% of this quantity dissolved, forming metal-albumen complex. The speed of taking out the magnetite from the organism is determined by interacting of particles with the membranes of endothelial cells and macrophages in the system of microcirculation and it happens by changing the physic-chemical properties of the outer environment of cell. It may be connected with decreasing of binding and surface density of membrane, changes of pH, Ox/Red pot and  $pO_2$  activities of the water over the region of contacts of the PM with membrane.

It is found potentiometrically, that injection of BFML through the circulatory system makes deep decreasing of  $pO_2$  of biological environment. For this time there is change of pH to the alkaline side and Ox/Red pot in the region of accumulation of reduced forms.

Changes of energetic metabolism in case of permeation of the PM into intercellular medium induce changes of biological activity of cells. The lipid layer of the membrane and the sizes of particles have the same order and higher affinity between each other, which makes the transportation process easier. But the electrostatic barrier prevents approaching of the PM and membrane of cell and despite of intensive thermal movement characteristic for the small particles, the PM do not permeate into separate cell structures (18).

The results of the investigation carried out for studying the interaction of the PM with bacterial cells are of great interest. Goldish staphylococcus and Echerichia coli were used as the objects. The culture containing  $10^7$ - $10^9$  cells per ml was added to the magnetite suspension, the final concentration of which in the solution was  $2,5 \times 10^{14}$  PM/  $sm^3$  and pH was 8,5-9. The solution was mixed by samari cobalt magnet during 1 min. and then put on the magnet till its full division into layers. Time of incubation lasted from 1 min. till 4 hours. It was established that for the correlation of particles  $10^4$ - $10^6$  per 1 microbe cell is noted full sterility. The electronic microphotos of bacterium, the time of exposition of which with PM was correspondingly 5 minutes and 3 hours are presented in fig. 2 and 3. It is shown, that if during the first minutes of the experiment, on the walls of microbe cell there are no injures, then after 3 hours the cell is deformed and filled with PM.

As the volume concentration of dispersion phase and microbe cells is below 1% it may be considered that casual accumulation of particles around the cells is hardly probable.



Figure 2 Staphylococcus (x 120000) 5 min after incubation with PM.

The quantity of particles around the microbe cells does not depended on pH in the range of 3-8, that testifies absence of the influence effect of the size of dzeta potential on that process.

On the bases of the literature and the results of the experiments carried out there was predicted the availability of long active magnitophoretic powers, generated by cells and representing themselves coherent oscillation of frequency  $10^{10}$ - $10^{12}$ hz. The magnetophoretic powers generated at this time are more than electrophoretic ones. That may be the reason of directed motion of PM on the surface of cell (19).

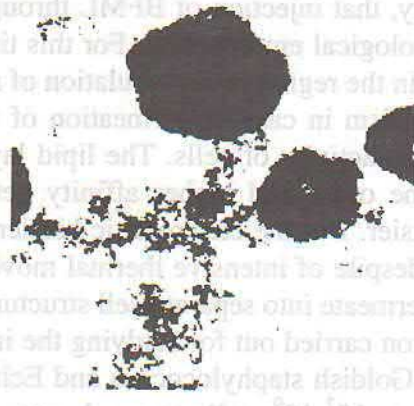


Figure 3 Staphylococcus ( x 120000 ) 3 hours after incubation with PM.

Destroying of walls and membranes of microorganisms following it may be connected with magnetostrictional or thermal heating. So there exists a possibility of energetic destruction of biological membrane and as the result of it, permeation of the PM into the cell.

#### Summary

The magnetic particles measured by EPR radiospectrometer and determined in cells by the method of electronic microscopy may serve as an instrument for investigation of biophysico-chemical mechanism of activity of cell.

#### References

- [1]. W.C.Elmore, Phys. Rev., 54 (1938) 309, 1092.
- [2]. E.E.Bibik, O.V.Buzunov, Achievements in the field of obtaining and applying the ferromagnetic liquids. Rev. in El. Tech., Ser. 6, Materials, Iss. 7 (660). ICSR, Electronics, Moscow, 1979, 60. (In Russian).
- [3]. M.G.Akhalaya, M.S.Kakiashvili, V.P.Beria, Perspective of applying the magnetic liquids in biology and medicine. B. Phys. properties of magnetic liquids. Sverdlovsk, SCUr, 1983, 115-121. (In Russian).
- [4]. E.H.Frei et al, J. Appl. Phys., 1968, 39, 999-1001.
- [5]. K.Sugibayashi, et al, Biomater., 1982, 3, 181-185.
- [6]. K.Y.Widder et al, Eur. J. Cancer and Clin Oncol. 1983, 19, 141-145.
- [7]. Y.N.Weinstein, et al, Science, 1979, 204, N2, 188-191.
- [8]. M.G.Akhalaya, M.S.Kakiashvili, Method of obtaining the ferroliquid. B.I., 1981, N43, A.S. 882938. (In Russian).
- [9]. M.G.Akhalaya, M.S.Kakiashvili, V.P.Beria, Method of obtaining the ferroliquid. B.I. 1982, N35, A.S. 960126. (In Russian).
- [10]. M.G.Akhalaya, M.S.Kakiashvili, V.P.Beria, Method of obtaining the ferroliquid. B.I. 1983, A.S. 981232. (In Russian).
- [11]. M.G.Akhalaya, M.S.Kakiashvili, V.P.Beria, Method of obtaining the coll. sol. magnetite. B.I. 1983, N26, A.S. 1028602. (In Russian).
- [12]. M.G.Akhalaya, M.S.Kakiashvili, Method of obtaining the ferroliquid. A.S. 1050220. (In Russian).

- [13]. M.G.Akhalaya, K.A.Zakaraya, M.S.Kakiashvili, Method of obtaining the magnet. liquid, for biolog. invest., A.S. 1107490. (In Russian).
- [14]. M.G.Akhalaya, M.S.Kakiashvili, Method of obtaining the ferroliquid. A.S. 1141695. (In Russian).
- [15]. M.G.Akhalaya, et al, Method of obtaining the magnet.liquid, for biolog. invest., A.S. 1185804. (In Russian).
- [16]. M.G.Akhalaya, M.S.Kakiashvili, Method of obtaining the ferroliquid. A.S. 1363552. (In Russian).
- [17]. M.G.Akhalaya, et al, Method of defining the level of activity of phagocytos of leucocytes A. S. 1403796. (In Russian).
- [18]. M.G.Akhalaya, M.S.Kakiashvili, E.R.Volter, Experimental invest. and modell. of magnet. liquids dyn. in organism, B. Biocybernet. and Bioph. Tb. Mecniereba. 1988 7-28. (In Georgian).
- [19]. M.G.Akhalaya, et al, Phys. Lett., 1984, 101A, 7, 367-370.

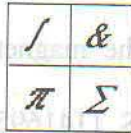
Consider a system of two mirror layers situated above the optical axis on which an object is located at a distance  $-z$  [Fig.1]. We employ below the rule of signs - a standard procedure in geometric optics-for the segments and focal lengths [3]. Given the height  $y_0$  and length  $d_0$  of the initial layer closest to the axis, we construct an image by the system of rays emanating from a point of the object and undergoing only one reflection on each layer. In the general case, some rays pass through without being reflected and others undergo multiple reflections. It is obvious that for each position of the object and given characteristics of the setup  $y_0$  and  $d_0$  can always be chosen so that there would be no multiple reflection. Under these conditions an image of a point is formed at a distance  $z'$  in the form of a scattering spot of definite dimensions. A simple calculation shows that the dimension of the scattering spot in a plane perpendicular to the axis is

$$(1) \quad y' = \frac{2d_0 y_0}{|z| + d_0}$$

where  $y_0$  is the height of the zone of the nth layer. The collection of mirror layers in Fig.1a clearly functions as a cylindrical lens in the meridional section. If this setup is crossed with a second, identical setup then an image is also formed for the sagittal section. Ultimately, it is possible to form a system of rectangular elements with mirror layers which will operate in both sections simultaneously (Fig.1b). It is easy to see from the drawing that the system described above forms a pseudoscopic image with unit magnification. Thus an object closest to the system is focused closer to the system than a more distant object. Moreover, it is obvious that if a converging pencil of rays is incident on the system, then a diverging pencil emanates from the system. In the latter case, the virtual image formed is also pseudoscopic. This provides a rationale for naming the device described above a "pseudoforn" (from the Greek pseudos-false + the Latin fornare - to form). Although rays which have passed through without reflection are spatially separated from the useful image, in many cases it may be necessary to eliminate them completely. Then a separate calculation must be made for each position and angular size of the object. This reduces somewhat the generality of the operation of the pseudoforn.

A geometric-optics calculation of the length and height of the zone of the nth layer gives

$$(2) \quad h_n = \frac{b}{1 + \frac{bn}{a}}, \quad z_n = \frac{z_0}{1 + \frac{bn}{a}}, \quad D_n = z_n - y_n$$



## Pseudoform-an Optical Element Forming a Pseudoscopic Image

**Sh. D. Kakichashvili**  
*Institute of Cybernetics*

In microwave antenna engineering it has been known for a long time that a collection of plane-parallel metal plates has a directing effect on radiation [1,2]. However, the fact that devices of this type also focus optical radiation and that this effect is easily described in terms of geometric optics has been neglected. In contrast to ordinary lenses and mirrors, this device forms a pseudoscopic image, and the fact that this is the only alternative to an orthoscopic image gives promise of definite applications.

Consider a system of that mirror layers situated above the optical axis, on which an object is located at a distance  $-s$  [Fig.1a]. We employ below the rule of signs – a standard procedure in geometric optics-for the segments and focal lengths [3]. Given the height  $y_0$  and length  $d_0$  of the initial layer closest to the axis, we construct an image by the system of rays emanating from a point of the object and undergoing only one reflection on each layer. In the general case, some rays pass through without being reflected and others undergo multiple reflections. In is obvious that for each position of the object and given characteristics of the setup  $y_0$  and  $d_0$  can always be chosen so that there would be no multiple reflection. Under these conditions an image of a point is formed at a distance  $s'$  in the form of a scattering spot of definite dimensions. A simple calculation shows that the dimension of the scattering spot in a plane perpendicular to the axis is

$$\rho = \frac{2d_0 y_n}{|s| + d_0}, \quad (1)$$

where  $y_n$  is the height of the zone of the  $n$ th layer.

The collections of mirror layers in Fig.1a clearly functions as a cylindrical lens in the meridional sections. If this setup is crossed with a second, identical setup then an image is also formed for the sagittal section. Ultimately, it is possible to form a system of rectangular elements with mirror layers which will operate in both sections simultaneously(Fig.1b).It is easy to see from the drawing that the system described above forms a pseudoscopic image with unit magnification. Thus an object closest to the system is focused closer to the system than a more distant object. Moreover, it is obvious that if a converging pencil of rays is incident on the system, then a diverging pencil emanates from the system. In the latter case, the virtual image formed is also pseudoscopic. This provides a rationale for naming the device described above a “pseudoform” (from the Greek pseudos-false +the Latin formare –to form). Although rays which have passed through without reflection are spatially separated from the useful image, in many cases it may be necessary to eliminate them completely. Then a separate calculation must be made for each position and angular size of the object. This reduces somewhat the generality of the operation of the pseudoform.

A geometric-optics calculation of the length and height of the zone of the  $n$ th layer gives

$$d_n = \frac{d_0}{1 + \frac{nd_0}{s}}, \quad y_n = \frac{y_0}{1 + \frac{nd_0}{s}}, \quad D = y_n - y_0, \quad (2)$$

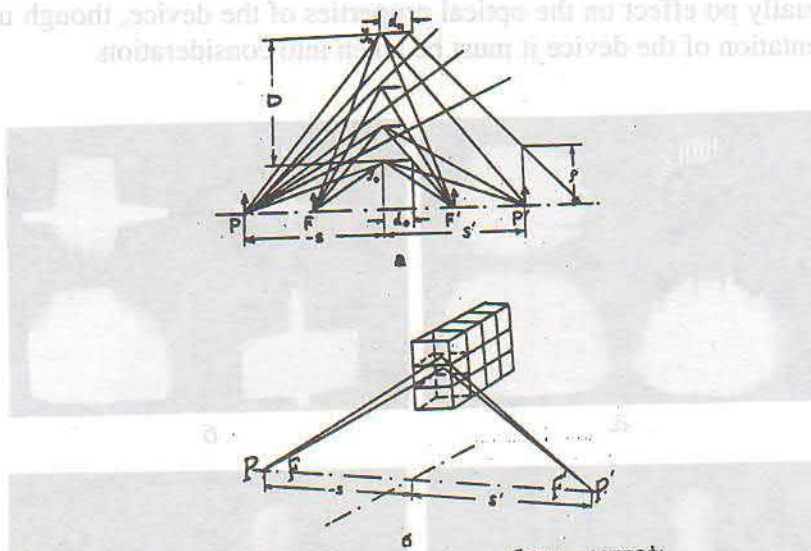


Fig. 1 a) Geometric scheme of the operation of the pseudoform: b) operation of a rectangular pseudoform.

where  $D$  is the linear aperture of the pseudoform.

As an example, we give the following dimensions:  $n = 100$ ,  $d_0 = 0.2$  mm,  $y_0 = 200$  mm,  $s = -100$  mm,  $d_n = 0.25$  mm,  $y_n = 250$  mm,  $D = 50$  mm. In this example the length of the mirror layers from the zeroth to the last zone changes insignificantly  $d_n - d_0 = 0.05$  mm. The distance between the layers also varies insignificantly:  $y_n - y_{n-1} = 0.4008$  mm;  $y_1 - y_0 = 0.6234$  mm. The size of the scattering spot is  $p = 0.998$  mm. The characteristic of the pseudoform for virtually any given resolution and aperture ratio can be calculated with the help of Eqs. (1) and (2).

We now consider the operation of a pseudoform in combination with standard lenses. Because of the asymmetric arrangement of the pseudoform with respect to the optical axis the off-axis fragments of these lenses must be considered. From the relation between conjugate segments of the pseudoform  $s' = -s$  it follows that the two positions of the pseudoform relative to the lens are substantially nonequivalent. This has no analog in Gaussian optics of ordinary optical systems. If the pseudoform is placed in front of a lens, then the position of the conjugate segment where the image of the object is formed can be represented in the form

$$\frac{1}{s''} = \frac{1}{f'} - \frac{1}{s+d}, \quad (3)$$

where  $d$  is the distance between the pseudoform and the lens and  $f'$  is the focal length of the lens. When the pseudoform is placed behind a lens, the conjugate section is represented in a form different from Eq. (3):

$$\frac{1}{s''} = \frac{(s+f')}{(s+f')d - f's}. \quad (4)$$

An entire series of unusual designs can be obtained for well-known optical systems on the basis of the difference between Eq. (3)-(4).

In order to verify the above discussion, a pseudoform was constructed consisting of a collection of aluminum-coated glass plates in the technically simplest variant. The entire collection of plates was optically glued together and cut in the transverse direction. Then the entrance and exit surfaces were optically worked. Ultimately, two such plane-parallel plates were optically glued together in a position crossed with respect to the layers. Each aluminum-coated plate was 1.2 mm thick. The pseudoform of 10×10 mm. The presence of the glass

medium had virtually no effect on the optical properties of the device, though undoubtedly in a future implementation of the device it must be taken into consideration.

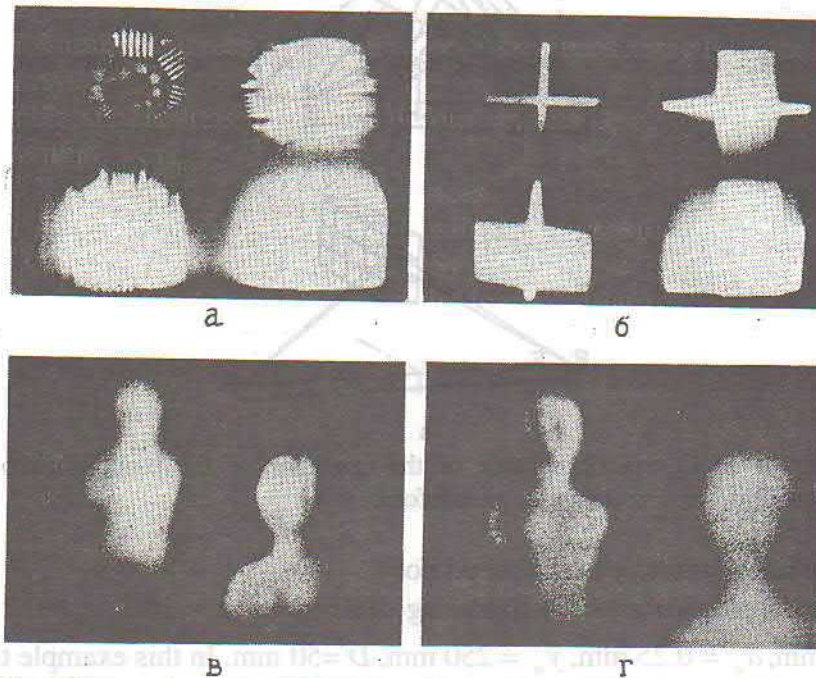


Fig. 2 Images formed by the experimental pseudoform: a) Ashcheulov optical test pattern (reduced by a factor of two), b) image of a luminescent cross (reduced by a factor of two); c) three-dimensional scene focused on a nearby object (full scale); d) three-dimensional scene focused on a distant object (full scale).

Figure 2a displays an image obtained of an Ashcheulov optical test pattern by means of the pseudoform described above. The spots to the right of and below the image were formed as a result of reflection of rays only from the horizontally or the vertically oriented elements of the composite pseudoform. The spot at bottom right was formed by light passing through without reflection. It is evident from the photograph that they are spatially separated from the useful image and, as indicated above, they result from the mismatch of the characteristics of the device and the position of the object. As an illustration of what was said about the secondary rays, we present an image obtained of a cross using the same pseudoform (Fig. 2b). Figures 2c, d display photographs of a three-dimensional scene in the form of two identical sculptures with focusing on a nearby object ( $s = -100 \text{ mm}$ ) and a distant object ( $s = -200 \text{ mm}$ ) object. The experiment confirmed unequivocally the pseudoscopic character of the three-dimensional scene focused by the pseudoform. The device resolution calculated from Eq.(1) to be 1.7 lines/mm agrees with the value measured directly from the optical test pattern: 1.6 lines/mm.

The possible applications of the pseudoform and its holographic implementation will be discussed in a future work.

#### References

- [1]. A.Z. Fradin. *Antenna Feeder Systems* [in Russian], Svyaz, Moscow (1977).
- [2]. S.Kornblit. *Microwave Optics* [in Russian], Svyaz, Moscow (1980).
- [3]. G.G.Slusarev. *Geometric Optics* [in Russian], Moscow (1946).



## **Polarization Holographic Memory of Superhigh Capacity**

**Kakichashvili Sh., Kilosanidze B.**

*Institute of Cybernetics*

### **Abstract**

The model of polarization holography memory in the cylindrical block of polarization sensitive media with use of 90° scheme of adding of operating beams has been described. It is shown experimentally the possibility of obtaining the big volume of recorded and readed information with ultimately low noises and high selectivity of reading. The preliminary estimations show the possibility of receiving the superhigh (up to 1 Terabit) volume of data storage by means of described system.

In 1963 Van Heerden discovered the ability of three-dimensional holograms to perform integral operations similar to associative accesses in memory systems [1]. Some of the estimations of holographic memory systems by Yu.Denisyuk [2] are dedicated to the similar problems.

The above-mentioned applications of holography for the creation of optical memory systems are based on the scalar theory of electromagnetic waves. In this case it is assumed, that it is possible to record and reproduce holographically three wave field characteristics: amplitude, relative phase and wavelength. As it is known, this possibility is given by the recording of the distribution of intensity of the summary wave throughout the surface and volume of a hologram [3,4]. However in scalar theory of holography an important initial characteristic of an object wave field – its polarization state – is not reflected on a hologram and is not reproduced during reconstruction. The schematic solution of the polarization reflection in scalar methods of holographic recording and reconstruction didn't succeed because of the principally unavoidable distortions.

The experimental attempts of creation the holographic memory systems in the framework of scalar method ended in failure because the mutual influence of recorded pictures, the sharp drop of the contrast of restored images and rapid saturation of recording medium.

With the appearance of the polarization holographic method, that assumes the recording of holograms in polarization sensitive media possessing the so-called Veigert-effect [5], essential more rich perspectives appear also for holographic memory [6]. This is due to the appearance of the possibility of adequate reflection in each point of recording medium additionally three more independent characteristics of a wave field: ellipticity, orientation and rotation direction of a summary light ellipse. In this case the polarization hologram turns out similar to a gyrotropic crystal with spatially variable characteristics according to the volume of hologram [7]. Such principally limiting ample quantity of the initial data recorded on the material carrier enables ultimately complete information to be recorded and in principle should allow the information of ultimately big capacity to be read too.

The model of holographic memory with the use of polarization scheme of recording and reconstruction at the 90° angle of meeting of operation beams was experimentally investigated by us. The recording was made in a cylindrical block of the polarization holographic medium. The linear polarized object and reference beams for which the direction of oscillation of electrical vectors in the whole volume of recording medium was orthogonal, were used during recording (Fig. 1a). Such geometry of the scheme allows to exclude the

influence of the scalar reaction of recording medium and the necessity of its agreement with the vector reaction of the same medium [7]. The light-sensitive block had the possibility of rotation around the axis of a cylinder holding the arbitrary position from  $0^\circ$  to  $360^\circ$  relative to an object beam (Fig. 1b). The reference beam passed the block volume from the side of generatrix of the cylinder. For the exclusion of the disturbance of the parallelity of a reference beam inside the block it immersed in the immersion with a refraction coefficient which is close to the material of the block (it is not shown in Fig 1). The object beam passed through the whole volume of recording material, holographically recording in it while meeting the reference beam. So the scheme allows each direction of a reference beam to check an independent object beam. In this model the memory system is the additional summation of many polarization holograms that were obtained by successive exposition one and the same volume of a medium at various orientations relative to operating beams. The polarization of a reference wave and an object wave remains constant during recording. The isotropic amplitude transparencies were used as objects. In the process of reading a recorded picture is taken out of memory without disturbance from other pictures in the direction of a reference beam corresponding to this picture or during the rotation of the holographic block (Fig. 1c). Two types of polarization sensitive materials were used in the experiment: alumina-borosilicate photochromic glasses and polymer with azodye "Mordant pure yellow" introduced into the matrix [7]. The materials with optically polished surfaces were given in the form of a cylinder (diameter 10 mm, height 2 mm). The recording was done with polarized radiation of He-Ne laser ( $\lambda = 632.8\text{nm}$ ) and He-Cd laser ( $\lambda=441.7\text{nm}$ ) which is actinic for the used materials.

As the experiment served only to get estimation conclusions we confined ourselves to about 50 sequential holographic recordings in each of the media. Angular selectivity of reading the neighbouring images experimentally defined amounted to 1 angular minute. In the process of restoration independently recorded pictures practically did not influence each other. The diffuse noise according to visual estimation did not exceed the scattering of both the recording media before recording. For polymer sample there also was carried out an experiment of nondestructive reading by means of nonactinic radiation of He-Ne laser. In this case the change of the direction of the angle of reading in meridional section of the scheme enabled the image with diffraction efficiency of the order of 10% to be restored. This fact is especially important from the point of view of preserving the memory system while reading and in conditions of room temperature.

The received preliminary experimental results give reason to make estimation calculations of storage capacity of the described system. We can conclude that the system in principle can record about  $10^4$  pictures by the number of the addressed directions of a reference wave. In case of the supposed volume of one picture of about  $10^5$  bit the capacity of the system is  $10^9$  bit with the density of storage of about  $10^7$  bit/mm<sup>3</sup>. The increase of the size of a cylinder block of recording evidently increases this density.

It will be noted that the capacity of the memory system evidently can be increased still twice replacing the entrance face of a cylindrical element by the exit one. Besides there is still one more real possibility of increasing the capacity of memory up to the volume in terabit ( $10^{12}$  bit). It follows from Fig. 2 that by changing in meridional section of the upper half-space so that the polarization vector of a reference wave is perpendicular to the picture plane, we can succeed in preserving the main features and merits of the proposed scheme with the essential increase of the volume up to the meanings given above. In this case the consecutive positions of the reference wave in the meridional section are taken also with step in 1 angular minute.

The proposed model allows memory element to be copied. Two light sensitive blocks: the original on which the whole information has already been recorded and the copy on which it is supposed to rewrite the information, - join each other and have the possibility to turn around like the whole. The system of re-recording is lighted by the common reconstructing (reference) wave. In this case the wave reconstructed by the original adds in the copy-block

REFERENCES

with the reference wave and is recorded in it. It is also possible to imagine the scheme of recording when both the blocks are simultaneously lighted on all sides like a circular hologram and the process of re-recording of all the picture is done at one go.

In conclusion we shall note that the described device can also solve problems of identifying optical images [8]. Each hologram in this case plays the part of a polarization holographic spatial filter. When presenting the identifiable object to the device, when the correlative signal appears in one of the directions from the cylindrical block of the hologram we can judge about the presence of the image of the given image among the collection of many images initially recorded in the block of memory.

The authors thank Prof. V.Sukhanov for giving one of the media to record polarization holograms used in this work, and also D.Kahkichashvili for useful discussions.

FIGURES

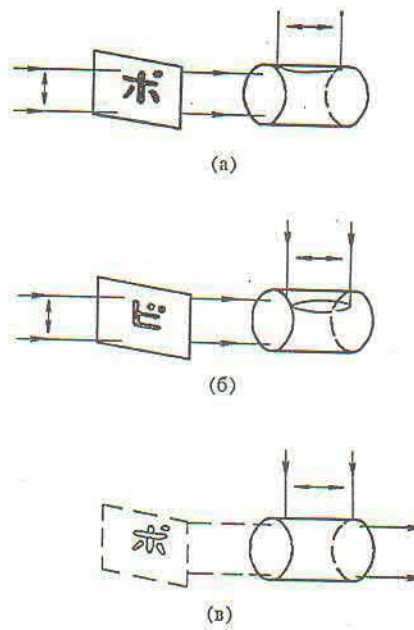


Fig.1. The scheme of recording in the block of memory:  
 a) of one picture; b) of another picture while rotating the block at some angle; c) the scheme of reconstruction

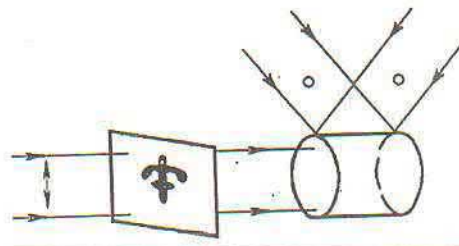


Fig.2. The scheme of recording while changing the direction of propagation of a reference beam.

## REFERENCES

1. Van Heerden P.J. // Appl. Opt. 1963. Vol.2. No.4. P. 393-400.
2. Denisyuk Yu.N. // In: Optical Holography. Moscow, 1982. Vol.2. P. 691-729.
3. Gabor D. // Nature. 1948. Vol.161. P. 777-778.
4. Denisyuk Yu.N. // The Reports of the Academy of Sciences of the USSR, 1962. Vol. 144. No.6. P. 1275-1278.
5. Weigert F. // Verhandl. Deutschen Physik. Ges. 1919. Bd. 21. S. 479-483.
6. Kakichashvili Sh.D. // Optics and Spectroscopy. 1972. Vol. 33. No.2. P. 324-327.
7. Kakichashvili Sh.D. // Polarization Holography. Leningrad, 1989. - 142 p.
8. Vander Lugt A. // IEEE Trans. 1964. Vol. IT-10. N0.2. P. 139-145.

The authors thank Prof. V. Sukhanov for giving one of the media to record polarization holograms used in this work, and also D. Kakichashvili for useful discussions.

## FIGURES

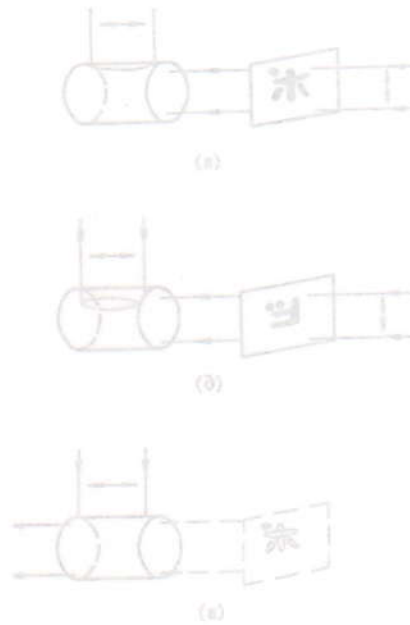


Fig. 1. The scheme of recording in the block of memory: a) of one picture; b) of another picture while rotating the block at some angle; c) the scheme of reconstruction

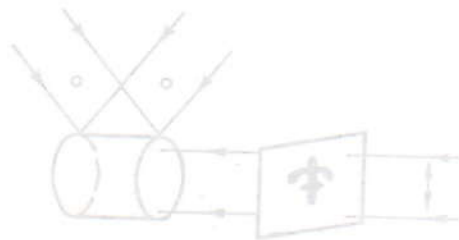


Fig. 2. The scheme of recording while changing the direction of propagation of a reference beam.



## Dispersion of the Rotation of the Axis of Photoinduced Anisotropy in Polarization-Sensitive Media

Sh. D. Kakichashvili and S.S. Petrova  
*Institute of Cybernetics*

The rotation of the axis of photoinduced anisotropy was first described in [1]. In an initially isotropic medium illuminated by polarized light the axis of the photoinduced anisotropy is found to rotate relative to the direction of polarization of the radiation that induced it. In more recent publications, no attention was paid to measurements of the orientation of the axis of the photoinduced anisotropy, since it was assumed a priori that the axis of the induced anisotropy coincided identically with the direction of polarization of the light [2,3].

Recently, studies in our laboratory have revealed that rotation of the axis occurs for a very broad class of polarization sensitive media prepared by various means.

In the present letter we present illustrative data on the dependence of the angle of rotation on the wavelength of the analyzing light for the azo dye mordant pure yellow [4] introduced into a gelatin matrix, and a silver-halide finely dispersed photographic emulsion VR-P [5], developed in an aqueous solution of paraphenyldiamide. This study is intended to draw the attention of investigators to the rotation effect, which we believe contains important information on the photo-induced processes at the elementary level and on the structure of the absorbing oscillators.

For the measurements we used a modified SF-18 spectrophotometer with a polaroid placed in the measuring channel parallel to the plane of polarization of the illuminating beam. The samples were fastened in a holder with a precise graduated circle that could be placed in the measuring channel in front of the polaroid.

The holder with the sample was fastened in the illumination system and the plane of polarization of the activating light was marked precisely.

With this sensing system for the measurements of the light-induced anisotropy, the rotation of the axis of anisotropy when the modified spectrophotometer is used is calculated by the formula [6]:

$$\alpha = \frac{1}{2} \arctan \frac{I_{45} - I_{-45}}{I_{90} - I_0}$$

where  $I$  is the measured intensity at the corresponding angles

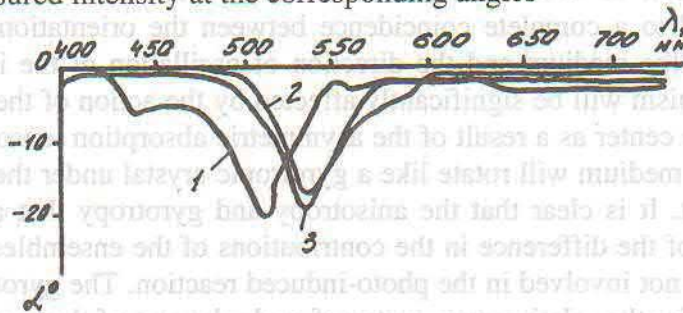


FIG.1

of orientation of the sample relative to the system of the measuring polarizer.

In Fig.1 shows the calculated curves of the angle of rotation as functions of the wavelength of the analyzing radiation. These curves are for the mordant pure yellow azo dye in a gelatin matrix. The illumination was at the wavelength  $\lambda = 488.0$  nm from an argon laser. Curves 1,2, and 3 correspond to an energy density of 22,90, and  $300 \text{ J/cm}^2$ , respectively. Similar curves were obtained for illumination at the wavelengths 441.6, 457.0, and 514.5 nm.

In Fig.2 shows the dependence of the angle of rotation on the wavelength of the analyzing light for the commercial photographic film VR-P, developed in a 0.1% aqueous solution of paraphenyldiamide. A He-He laser operating at the wavelength  $\lambda = 632.8$  nm was used for the illumination. Curves 1,2, and 3 correspond to energy densities of 0.2, 0.8, and  $3 \text{ J/cm}^2$ .

An analysis of the curves of Figs.1 and 2 indicate that completely different mechanisms are involved in the rotation the anisotropic photo-induced process with distinctly different behavior in the dispersion curves.

The sensitometric measurements in the samples rotated relative to the measuring beam show that sign of the rotation does not change. This is unambiguous evidence for the gyrotropic nature of the rotation of the axis of photoinduced anisotropy.

At the present time we cannot advance any complete explanation for the cause or the mechanisms of the effect or for its sign or the behavior or the dispersion curve. It is possible to state with some certainty that the internal structure of the light sensitive centers plays the major role in the effect, while the role of the matrix is less important.

For example, the sample with the azo dyes introduced into polyvinyl alcohol produce a rotation effect that qualitatively differs little from samples of the same dye in the gelatin matrix. In a medium that initially is macroscopically isotropic and nongyrotropic, all possible spatial orientations of the light-sensitive centers are equally probable. Under these conditions the

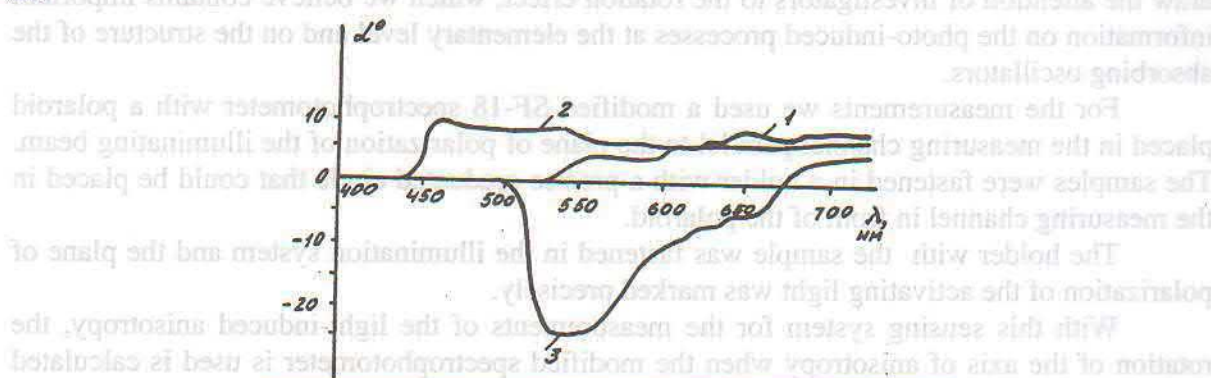


FIG.2

probability of occurrence of an anisotropic photo-induced process is proportional to  $\cos^2 \theta$ , where  $\theta$  is the angle between the direction of the absorption transition of the light-sensitive center and the direction of oscillation of the electric vector of the actinic light. Such a mechanism must lead to a complete coincidence between the orientation the light-induced axis of anisotropy of the medium and the direction of oscillation of the inducing radiation. However, this mechanism will be significantly affected by the action of the gyrotropy arising at each photosensitive center as a result of the asymmetric absorption tensor of this center. In the final analysis, the medium will rotate like a gyrotropic crystal under the action of linearly polarized actinic light. It is clear that the anisotropy and gyrotropy that are induced in the crystal are the result of the difference in the contributions of the ensembles of light-sensitive centers that are or are not involved in the photo-induced reaction. The gyrotropy that arises in this way is evidence for the relative asymmetry of each element of these ensembles. We can also suppose that the molecular gyrotropy is an inherent property, at least in center that is transformed by the light.

In conclusion we note that the rotation of the axis of the photo-induced anisotropy and the behavior of its dispersion curve may carry important information on the photophysical and photochemical properties of the photo-induced processes.

### References

- [1]. Sh. D. Kakichashvili, *Opt. Spektrosk.* 56, 977 (1984) [*Opt.spektrosk.(USSR)* 56, 599 (1984)].
- [2]. S.V. Cherdyntsev, *Zh. Eksp. Teor.Fiz.* 18, 352,1948.
- [3]. P.P.Feofilov, *Dokl. Akad. Nauk SSSR* 98, 949,1954.
- [4]. B.I.Stepanov, *Introduction to the Chemistry and Technology of Organic Dyes* [in Russian], Khimiya, Moscow (1977).
- [5]. Sh. D. Kakichashvili and V.G. Shaverdova, *Pis' ma Zh.Tekh.Fiz.*5, 266 (1979) [*Sov. Tech.phys. Lett.* 5, 107 (1979)].
- [6]. Sh. D. Kakichashvili, *Polarization Holography* [in Russian], Nauka, Moscow (1989).



## **Electrochemically Deposited Schottky Barrier Height**

**T. Laperashvili, I. Imerlishvili.**

*Institute of Cybernetics*

The metal/semiconductor (M/S) interface is an important subject in electronic technology because every semiconductor device needs the interface to communicate with outside circuits. The mechanism of Schottky barrier (SB) formation remains a leading question in the physics of semiconductor interfaces. But despite of several decades of intense study there exist no quantitative theory of SB heights. One of the reasons is difficulty of obtaining reproducible MS Schottky contacts with ideal volt-current characteristics, that is necessary to comparison experimental results with theory.

Although they were reported that fabrication M-S contacts with reproducible ideal I-V characteristics may be achieved by electrolyses [1,2] and by electrochemical deposition of different metals on the semiconductors [3-5]. There are a large number of reports about fabrication M-S contacts mainly, by vacuum evaporation of metals on semiconductor.

We were fabricated Schottky contacts by the chemical deposition of metals (Ni, Au, Cu, Pt, Pd) and by the electrochemical deposition of metals (Ni, Cu, Pt, Pd, In, Ga, Al, Sb, Bi) from aqueous solution its salts on the III-V semiconductors (GaP, GaAs, InP). At first we were investigated electrochemically deposited In/GaP, Ga/GaP, Sb/GaP, Bi/GaP, Pd/GaP SB height [5-7] and was obtained the sufficiently disadvantage from Bardeens theory [8] of formation Schottky contact on the III-Vs semiconductors. Latter Charada et al. [9] reported very surprising results of investigation metal /GaP SB height. MS interfaces they were obtained by ultra high vacuum evaporation of In, Al, Cu, Ge and Au onto cleaned GaP surfaces and they have been studied that by photoemission with synchrotron radiation [9]. They found Schottky limit behavior of SB heights from metal work function

In this paper is described the electrochemically method of fabrication ideality Schottky diodes metal/GaP. The electrical and photoelectric characteristics have been studied and they, were analyzed in the usual way [10] to calculate the ideality factor ( $n$ ) and barrier height ( $\phi$ ). The values of coefficient  $n$  and SB height are presented in Tab. I. The barrier heights are compared with the metal work function.

Samples used for the fabrication of M-S diodes were growing by Chochralski method especially undoped n-type GaP into (111) oriented wafers. The thickness and carrier concentration was 200-250  $\mu\text{m}$  and  $(2-4) \cdot 10^{17} \text{ atom/cm}^3$  respectively. At first ohmic contact to the one side of wafer was formed by alloying of indium at the temperature  $600^\circ\text{C}$  during 5 min in hydrogen. Then the sample with ohmic contact and wire for proceeding the power was coated with chemical stable polystyrene solution except the area where the metal will be deposited. The wafers were then etched chemically, rinsed in distilled water and were transferred immediately into electrolyte.

Deposition of metal was done by the usual electrochemical method. Electrolyte was poured into quartz glass. The semiconductors wafer was used as the one electrode and as another electrode was used aluminum, nickel or platinum wafer respectively. for deposition Ni, Al or other metals. The aqueous solution of chlorides have been used as an electrolyte which consisted also NaOCl. At first, semiconductor's wafer was used as the anode and cleaning of semiconductors surface was done. Then the potential was immediately changed in opposite direction and deposition of metal on freshly cleaned surface was done in the same solution in a united technological process. After the process of metalisation the samples were washed in distilled water. The polystyrene film was removed mechanically and boiling

in acetone. Then samples were cut into pieces of area 1-3 mm<sup>2</sup>, and were measured electric and photo electric characteristics.

The forward bias current-voltage (IV) characteristic of obtained diodes plotting in coordinates (V, lnI) was straight line for a wide range of current (10<sup>-11</sup>-10<sup>-2</sup>)A. So that it is possible to analyze in terms termoionic emission theory of Bette. according with the (IV) characteristics of a Schottky diode at V>3kT/q may be expressed as

$$J=J_s \exp(qV/nkT) \quad (1)$$

Where n=q/kT dV/d(lnJ) is ideality factor, V is the applied forward bias, J - the measured current at a given value of V, q-the electron charge, k-Boltzmanns constant, T-the temperature, J<sub>s</sub>-the extrapolated zero bias saturation current, n is the diode quality factor. The n value is near unity in an ideal diode. Both the J<sub>s</sub> and n may be deduced from the intercept and slope of the J vs. V plot, respectively. The Shottky barrier height have been evaluated via the expression

$$\phi(I-V)=kT/q \ln(SA^*T^2/J_s) \quad (2)$$

where S is the diode area, A\* effective Richardsons constant. Value for A\* of 150,8 A/cm<sup>2</sup>/K<sup>2</sup> was obtained from work of G.P.Schwarz and Gualteri [11].

Junction capacitance was measured at a frequency of 1 MHz as a function of applied reverse voltage by using automatic capacitance bridge model L2-28. Digitized 1/C<sup>2</sup> vs. reverse bias plots were evaluated by using linear regression obtained the intercept V<sub>0</sub>, which determines V<sub>D</sub>-kT/q. V<sub>D</sub> is known as the diffusion potential. The 1/C<sup>2</sup> curves were linear in the bias range utilized (0-3V). The CV measured barrier height was obtained from the expression

$$\phi(C-V)=V_0 + E_F + kT/q \quad (3)$$

Where E<sub>F</sub> is the fermi level. The quantity of E<sub>F</sub> + kT/q = 0.1ev for our samples.

SB heights were obtained also by applying the Fauler theory [10,p.60]. Photo response measurements were carried out by using a tungsten lamp KUM end a monochromatic DMR-4. The short circuit photo current was detected synchronously by using a look-in amplifier.

Table I. Schottky barrier heights on GaP.

	Metal													
Φ <sub>B</sub> eV	Au	Cu	Ag	Pt	Mg	Al	Mi	Mo	Cr	In	Ga	Bi	Sb	Pd
n	5.1	4.65	4.26	5.43	3.61	4.78	5.15	4.21	4.5	4.12	4.0		4.55	5.12
A.M.Coulai et.ol [12]														
CV	1.34	1.34	-	1.52	1.09	1.14								
I <sub>φ</sub> hv	1.28	1.20				1.05								
N														
Tan E. Lei et. Ol														
CV	1.30	1.30	1.14	1.45	-	1.16	1.27	1.13	1.18					
IV	1.30	1.32	1.14	1.5	-	-	1.30	-	1.2					
n														
G.P.Schwartz et. Ol [10]														
CV			1.25			1.21								
IV			1.17			1.11								
I <sub>φ</sub> hv			1.25			1.21								
n														
P. Charada et. Ol [9]														
I <sub>φ</sub> hv	1.3		1.16		1.17				0.3					
n														
Present study														
CV	1.3	1.3		1.5		1.1			0.77	0.78	1.3	1.1	1.12	
IV	1.27	1.26		1.5		1.04			0.80	0.77			1.2	
I <sub>φ</sub> hv	1.28	1.25		1.4		1.11			0.74	0.80				

n	1.04	1.1		1.05	1.03		1.02	1.02		
---	------	-----	--	------	------	--	------	------	--	--

Photo excitation over the barrier ( $\phi < h\nu < E_g$ ) was measured and Fowler plots of photo current spectrum show liner regions extrapolate of which gives the barrier height  $\phi_B(I, h\nu)$ .

The values of coefficient n and SB heights  $\Phi_B$  are presented in the Table I. For comparison the barrier height have been presented in table I, together with the results of [9,11-13]. Good agreement is found between the results of our studies for metals, suggesting that if the interfaces are fabricated by using electrochemically cleaning of the surface of the semiconductors and electrochemical deposition metals the SB is reproducible so well as by using ultra height vacuum evaporation of metals on the clean cleaned interface of semiconductor.

For determination mechanism of formation SB on GaP have been fabricated In/GaP, Ga/GaP and  $In_xGa_{1-x}$  ( $0 < X < 1$ ) and was investigated behavior SB height from the orientation and from doping materials. We used by Chochralsky method obtained 110 oriented, with Te and S doped GaP. Concentration was  $6.10^{17}$ - $2.10^{18}$   $cm^{-3}$ . Ideality factor observed samples  $n < 1.08$  and barrier height was changed sufficiently:  $0.53 < \Phi_B\{In/GaP\} < 0.9eV$  and  $0.64 < \Phi_B\{Ga/GaP\} < 1.05eV$ . Have been studied also SB heights In/GaP, Ga/GaP and  $In_xGa_{1-x}$  structures fabricated the same sample and was found that  $\Phi_B\{In_xGa_{1-x}/GaP\} < \Phi_B\{In/GaP\}$  and  $\Phi_B\{In_xGa_{1-x}/GaP\} < \Phi_B\{Ga/GaP\}$ . This experimental results is difficult to understand via Bardeens or Shottkys theory. They may be described by using modified defect model [15].

In conclusion the possibility using electrochemical method of fabrication ideality SB was illustrated.

SB heights was compared with of SB heights fabricated by ultra heigh vacuum evaporation and was found a good agreement with results for metals: Au, Cu, Pt, Al. Bisaisd it was found that SB height is more sensitive from kind of dopping impurity and from the orientation of samples for In/GaP, Ga/GaP ( $\nabla\Phi_B = 0.4eV$ ) then for others metals ( $\nabla\Phi_B = 0.1eV$ ).

Comparisons have also been made the SB heights  $\Phi_B\{In/GaP\}$ ,  $\Phi_B\{Ga/GaP\}$  with  $\Phi_B\{In_xGa_{1-x}/GaP\}$  ( $0 < X < 1$ ) fabricated on the same sample and was found that  $\Phi_B\{In_xGa_{1-x}/GaP\} < \Phi_B\{In/GaP\}$  and  $\Phi_B\{In_xGa_{1-x}/GaP\} < \Phi_B\{Ga/GaP\}$ .

The SB height have been compared with the metal work function. The observed nonlinearity behavior suggests that Mechanism of formation SB on n-GaP may be described by no Bardeens model, what is igniring the rol of metal  $\partial\Phi_B/\partial\Phi_M = 0$  and not Sottky model, according vith  $\partial\Phi_B/\partial\Phi_M = 1$ . The Shottky limit have been obtained on GaP and have been reported as very surprising result in [9].

We Think, that observed results of our study may be described using modification defect model of Tersoff according with the final position of Fermi level may be governed by more then one mechanism. [15].

### References

- [1]. Y.A.Goldberg, D.N.Nasledov, B.V.Tsarenkov. (in Russian). PTE N3 p.207-209.1971
- [2]. Y.A.Goldberg, T.A.Laperaschvili, G.A.Hakaschidze, B.V.Tsarenkov (in Russian). The letters to J. Tech. Phys. v.14. p.886-889. 1982
- [3]. G.S.Korotchenkov, I.P.Molodian. (in Russian). Physics and Technical of Semiconductors v.12. N2. p.245-247. 1978
- [4]. P.H.Mito, Roy Sbchoshk, A.NH.Dow Solid St. El. v.22. p.793-795. 1987
- [5]. M.B.Baxtadze, T.A.Laperaschvili, I.N.Saginaschvili. (in Russian). Proceedings of Tbilisi university v.224. Physics. P.120-129. 1983
- [6]. T.A.Laperaschvili, G.A.Nakaschidze (in Russian). The J. Tech. Phys. v.55. N4. P.732-735. 1985
- [7]. T.A.Laperaschvili. (in Georgian). Proceedings of Tbilisi university v.306. Physics.32. p.185-202. 1991
- [8]. J.Bardeen Phys. Rev. v.71. N10. P.717-727. 1947

[9]. P.Charada, L.J.Brilson, M.Slade and R.E.Vituro, D.Kelday, N.Tache, M.Kelly, and G.Margaritondo. Unpinned Shottki Barrier Formation at Metal-GaP Interfaces; A Representative III-V Compound Interface. J. Vac. Sci. Technol. B v5. N4. P.1075-1079

[10]. E.X.Roderic Metal-Semiconductor Contacts. Oxford, 1978 p.208.  
 [11]. H.B,Michaelsin, J.Appl.phys,v,48.p.4729, 1977,  
 [12]. G.P.Schwartz and G.J.Cualteri. Schottky barrier height variation on the polar (111) faces of n-GaP. J.Appl. Phys. v.58. N12. p.4621-4625. 1985.  
 [13]. A.M.Cowley and S.M.Ze. Surface States and Barrier Height of Metal-Semiconductor Systems. J.Appl. Phys. v.36. N10. p.3212-3219. 1965  
 [14]. Tan F.Lei, Chung L.Lee and Chun Y Chang. Metal/n-GaP Schottky Barrier Heights. Solid St. El. v.22. p.1035-1037. 1979  
 [15]. J.Tersoff, Phys.Rev. Lett. v. 52, p.465, 1984.

It is shown the possibility to measure simultaneously the optical constants and magneto-optical parameter of the ferromagnetic using the geometry of the external Kerr effect. The obtained results can be apply to the thin magnetic films also.  
 Key words: Magneto-optic Ellipsometry, Ferromagnetic Thin Films

The ellipsometrical method of measurements of the ferromagnetic parameters is considered in Ref.[1]. All linear magneto-optical effects are defined by the optical constants, such as the refraction coefficient  $N = n - ik$  and the magneto-optical parameter  $Q = Q_1 - iQ_2$  which is proportional to the magnetization. As usual, the optical constants and magneto-optical parameter are measured separately. This leads to the essentially different results. Therefore, the simultaneous measurements of these quantities are of interest.

Since the magneto-optical parameter  $Q$  is very small,  $|Q| \ll 1$ , basic ellipsometrical ratios can be written as follows:

$$(1) \quad \frac{\tan \psi + \delta \psi}{\tan \psi - \delta \psi} = \frac{1 + iQ \sin 2\psi}{1 - iQ \sin 2\psi}$$

In this expression  $\psi$  and  $\Delta$  are the ellipsometrical angles and  $\delta$ ,  $\epsilon$  are the Fresnel amplitude coefficients, as well as  $\delta\psi$ ,  $\delta\Delta$ ,  $\delta\epsilon$ , and  $\delta\epsilon'$  are the small contributions due to the magnetization. The ellipsometrical angles on the left hand side of expression (1) are measured by experiment. The Fresnel coefficients on the right hand side of expression (1) contain the optical constant  $N$  and the magneto-optical parameter  $Q$ , which have to be defined in the general case of an arbitrary magnetization  $\hat{Q}$  and  $\hat{Q}'$  have a complicated form and the separation of the right hand side of expression (1) into the pure optical and magneto-optical part is very difficult. It is convenient to choose the geometry of the external Kerr effect when the magnetization is perpendicular to the plane of incidence of light. In this case the contribution  $\delta\epsilon = 0$  and expression (1) is more simple. Assuming also that the angles  $\psi$  and  $\Delta$  are small, one can approximately write the left hand side of expression (1) as follows:

$$(2) \quad \frac{\tan \psi + \delta \psi}{\tan \psi - \delta \psi} = \left( 1 + \frac{2 \sin 2\psi}{\sin 2\psi} iQ \right) = \frac{1 + iQ \sin 2\psi}{1 - iQ \sin 2\psi}$$

One can see from equality (2) that the optical and magneto-optical part are separated. The measurement methods of the optical constants are well known [2]. In expression (2) the term  $\delta\psi$  due to the magnetization is related with the magneto-optical parameter  $Q$  by the following way [2,4]:

$$(3) \quad \delta \psi = -iQ \frac{\sin 2\psi}{(N \cos \psi + \cos \psi)}$$

$\int$	$\&$
$\pi$	$\Sigma$

Institute of Cybernetics  
Georgian Academy of Sciences  
E-mail: cyber@hepi.edu.ge  
http://cyber.hepi.edu.ge/proceedings

Proceedings  
Institute of Cybernetics  
Vol.1, N 2, 2000

## Ellipsometrical Methods of the Measurements of the Magneto-Optical Parameter

O.I. Bakradze

Institute of Cybernetics

### Abstract

It is shown the possibility to measure simultaneously the optical constants and magneto-optical parameter of the ferromagnetic using the geometry of the equatorial Kerr effect. The obtained results can be apply to the thin magnetic films also.

**Key words:** Magneto-optic, Ellipsometry, Ferromagnetic, Thin Films

The ellipsometrical method of measurements of the ferromagnetic parameters is considered in Ref.[1]. All linear magneto-optical effects are defined by the optical constants, such as the refraction coefficient  $N=n-ik$  and the magneto-optical parameter  $Q=Q_1-iQ_2$ , which is proportional to the magnetization. As usual, the optical constants and magneto-optical parameter are measured separately. This leads to the essentially different results. Therefore, the simultaneous measurements of these quantities are of interest.

Since the magneto-optical parameter  $Q$  is very small,  $|Q| \ll 1$ , basic ellipsometrical ratio can be written as follows:

$$\operatorname{tg}(\psi + \delta\psi)e^{i(\Delta+\delta\Delta)} = \frac{r_p + \delta r_p}{r_s + \delta r_s} \quad (1)$$

In this expression  $\psi$  and  $\Delta$  are the ellipsometrical angles and  $r_p$ ,  $r_s$  are the Fresnel amplitude coefficients, as well as  $\delta\psi$ ,  $\delta\Delta$ ,  $\delta r_p$  and  $\delta r_s$  are the small contributions due to the magnetization. The ellipsometrical angles on the left hand side of expression (1) are measured by experiment. The Fresnel coefficients on the right hand side of expression(1) contain the optical constant  $N$  and the magneto-optical parameter  $Q$ , which have to be defined. In the general case of an arbitrary magnetization  $\delta r_p$  and  $\delta r_s$  have a complicated form and the separation of the right hand side of expression (1) into the pure optical and magneto-optical part is very difficult. It is convenient to choose the geometry of the equatorial Kerr effect when the magnetization is perpendicular to the plane of incidence of light. In this case the contribution  $\delta r_s=0$  and expression (1) is more simple. Assuming also that the angles  $\delta\psi$  and  $\delta\Delta$  are small, one can approximately write the left hand side of expression (1) as follows:

$$\operatorname{tg}\psi e^{i\Delta} \left( 1 + \delta\psi \frac{2}{\sin 2\psi} + i\delta\Delta \right) = \frac{r_p + \delta r_p}{r_s} \quad (2)$$

One can see from equality (2) that the optical and magneto-optical part are separated. The measurement methods of the optical constants are well known [2]. In expression (2) the term  $\delta r_p$  due to the magnetization is related with the magneto-optical parameter  $Q$  by the following way [3,4]:

$$\delta r_p = -iQ \frac{\sin 2\varphi}{(N \cos \varphi + \cos \varphi')^2}, \quad (3)$$

where  $\varphi$  and  $\varphi'$  are the angles of incidence and reflection of light. Using the Snellius law  $\cos \varphi' = \sqrt{1 - \sin^2 \varphi / N^2}$  and the Maxwell formula  $\varepsilon = N^2$ , one obtains from expression (2) that

$$\delta\psi \frac{2}{\sin 2\psi} + i\delta\Delta = -iQ \sin 2\varphi \frac{\varepsilon}{\varepsilon^2 \cos^2 \varphi - \varepsilon + \sin^2 \varphi}. \quad (4)$$

Let us set the real and imaginary parts of the left hand side of expression (4) to the right hand side ones. Then, one have finally

$$\begin{aligned} Q_1 \sin 2\varphi &= \frac{2A}{\sin 2\psi} \delta\psi - B\delta\Delta, \\ Q_2 \sin 2\varphi &= -A\delta\Delta - \frac{2B}{\sin 2\psi} \delta\psi, \end{aligned} \quad (5)$$

where

$$A = \varepsilon_2 \cos^2 \varphi - \frac{\varepsilon_2 \sin^2 \varphi}{\varepsilon_1^2 + \varepsilon_2^2}, \quad B = \varepsilon_1 \cos^2 \varphi - I + \frac{\varepsilon_1 \sin^2 \varphi}{\varepsilon_1^2 + \varepsilon_2^2}, \quad (6)$$

$$\varepsilon_1 = n^2 - k^2, \quad \varepsilon_2 = 2nk.$$

It is easy to check that the expression obtained above leads to the known formula for the equatorial Kerr effect [3]:

$$\delta R_p / R_p = 2 \sin 2\varphi \frac{Q_1 A - Q_2 B}{A^2 + B^2}. \quad (7)$$

The parameters of the thin magnetic films  $N$  and  $Q$  can be significantly different from ones in bulk materials. Consider now a single magnetic film. One can use the Airy formulae which take into account the multibeam interference. Noticable, that for the equatorial geometry the phase angle  $\beta = \frac{2\pi d}{\lambda} (N^2 - \sin^2 \varphi)^{1/2}$  ( $d$  is the physical width of the film) is not influenced by the magnetization [4]. Then one obtains the expression similar to equation (4), where at the right hand side appears the interference factor:  $[\exp(i2\beta) + r_p^2] / [\exp(i2\beta) - r_p^2]$ .

Measurements can be performed using the usual ellipsometer. The sample have to be alternating magnetized and the optical and magneto-optical signals are analyzed at each wave length of light. The magneto-optical signal  $S(\Omega)$  is proportional to the alternating magnetization function  $I(H)$ , where  $\Omega$  is the alternating magnetization frequency. It is important to achieve that the signal  $S(\Omega)$  has no longitudinal contributions. One can use, as an example, a simple the polarizer-subject-analyzer scheme ellipsometer (PSA) [1,2]. The polarizer azimuth is  $P = +\pi/4$  and the analyzer azimuths are  $A = +\pi/4, 0, -\pi/4$ . Let us the measured optical signals are  $J^+, J^0$  and  $J^-$ , the magneto-optical signals are  $\delta J^+, \delta J^0$  and  $\delta J^-$ , and their ratios are  $S^+ = \delta J^+ / J^+, S^0 = \delta J^0 / J^0$  and  $S^- = \delta J^- / J^-$ . Take first zero azimuth, what corresponds to the equatorial Kerr effect. Then, the ratio  $S^0 = \delta J^0 / J^0$ , as was expected. At fixed incidence angle of light  $\varphi$  one can deduce the function  $S(\Omega)$ , but not the both parameters  $Q_1$  and  $Q_2$ . For the nonzero azimuth one obtains

$$\begin{aligned} \delta\psi &= \frac{I}{4\text{tg}\psi} \left[ (S^+ + S^-) + (S^+ - S^-) \sin 2\psi \cos \Delta \right], \\ \delta\Delta &= (S^+ + S^-) \frac{\cos 2\psi \text{ctg} \Delta}{4 \sin^2 \psi} + (S^+ - S^-) \frac{I}{2 \sin \Delta} \left( \frac{\cos^2 \Delta}{\text{tg}\psi} - \frac{I}{\sin 2\psi} \right). \end{aligned} \quad (8)$$

Analyzing expression (8), one can see that the factors at the sum  $(S^+ + S^-)$  and the difference  $(S^+ - S^-)$  depend strongly on the angle of incidence  $\varphi$ . In polarization-modulation

ellipsometer [2] the light polarization is modulated with the frequency  $\omega$ . The optical signals are modulated with the same frequency  $\omega$  and a double frequency  $2\omega$ , while the magneto-optical signals are additionally modulated with a frequency  $\Omega$ . Therefore, performing the Fourier analyze and combining the signal ratios, one can to deduce the desired parameters  $Q_1$  and  $Q_2$ .

### Reference.

- [1] O.I. Bakradze, J. Opt. Technology, 66,5,p.73(1999)
- [2] R.M.A. Azzam, N.M. Bashara, Ellipsometry and Polarized Light, Nort-Holl. Publ. Comp.,N.Y.(1977)
- [3] G.S. Krinchik, Physics of the Magnetic Phenomena, Moscow Univ. Publ., Moscow (1976)
- [4] A.V. Sokolov, Optical Properties of Metals, GIMFL, Moscow (1961)

/	&
π	Σ

## Relationship of Porous Media Tortuosity on Porosity Coefficient

Tamaz Karchava  
 Institute of Cybernetics

Learning of fluid filled porous media acoustic features is important for determining physical measures of porous media and functional relations between them. Biot's works are of particular importance among the works dedicated to this issue [1]. He received motion equations of the system's porous media-fluid in LaGrange's formality where fluid, solid component and induce mass density are reduced. Acknowledged interpretation of induce mass density does not satisfy number of experimental results, raising necessity for introducing additional conditions [2]. Below we can see that the formality used by Biot contains such interpretation of these equations which do not need introduction of the aforementioned additional conditions. Simultaneously here comes the possibility of finding relationship between porous media tortuosity and porosity coefficient.

Let us consider the sample where porous media with fluid is seen as common  $p_m$  density and  $v_m$  velocity of solid particles and fluid mixture and we can have the following image:

$$p_m = \phi p_f + (1 - \phi) p_{st} \quad (1)$$

Where  $\phi$  is porosity coefficient and  $p_f$  and  $p_{st}$ , correspondingly, are density of fluid and solid particles.

During sound spreading fluid acquires  $v_f$  velocity and solid component -  $v_{st}$  velocity, and mixture volume unit impulse equals to:

$$p_m v_m = \phi p_f v_f + (1 - \phi) p_{st} v_{st} \quad (2)$$

Taking into consideration (2), mixture motion equation has the following image:

$$\phi p_f \partial v_f / \partial t + (1 - \phi) p_{st} \partial v_{st} / \partial t = F \quad (3)$$

Where  $F$  is a force acting on mixture volume unit.

Generally, during sound spreading  $M$  mass body is not fully over-flown by fluid. Because of this we have the following equation [3]:

$$p_{st} \partial v_{st} / \partial t = p_f \partial v_f / \partial t - \Delta p \partial (v_{st} - v_f) / \partial t \quad (4)$$

Where  $\Delta p$  is an induce mass [3] falling on moving solid body unit volume. Relying on (4) equation, solid component motion equation for a unit volume mixture can be registered as following:

$$(1 - \phi) p_{st} \partial v_{st} / \partial t + \Delta p (1 - \phi) (\partial v_{st} / \partial t - \partial v_f / \partial t) = (1 - \phi) p_f \partial v_f / \partial t + F_1 \quad (5)$$

Where  $(1 - \beta) p_f \partial v_f / \partial t + F_1$  is a force acting on solid component. In non condensed sample  $F_1$  is equal to zero, and  $F = -\nabla p$ ; Taking this into consideration we get the following images from (3) and (5):

$$p_{11} \partial^2 U_{st} / \partial t^2 + p_{12} \partial^2 U_f / \partial t^2 = -(1 - \phi) \nabla p \quad (6)$$

$$p_{22} \partial^2 U_f / \partial t^2 + p_{12} \partial^2 U_{st} / \partial t^2 = -\phi \nabla p \quad (7)$$

Where  $U_{sl}$  and  $U_f$  are, correspondingly, solid component and fluid displacements vectors in mixture volume unit;  $v_{sl} = \partial U_{sl} / \partial t$ ;  $v_f = \partial U_f / \partial t$ . And

$$p_{11} = (1 - \phi)p_{sl} - p_{12} \quad (8)$$

$$p_{22} = \phi p_f - p_{12} \quad (9)$$

$$p_{12} = -\phi(1 - \phi)\Delta p \quad (10)$$

It should be also mentioned herein that [1] basic similarity of Biot's theory is automatically fulfilled.

$$p_{11} + 2p_{12} + p_{22} = \phi p_f + (1 - \phi)p_{sl} \quad (11)$$

Which means that (6) and (7) represent Biot's simplified equations [1].  $p_{11}$  and  $p_{22}$ , correspondingly, represent reduced density of solid component and fluid. News of the revised sample are the image of  $p_{12}$ , which are given in formula (10) and represent reduced induce mass to rivers mark mixture unit volume and not the induce mass as it used to be understood till present.

Now let us show that we can generally receive Boit's equations. For this purpose let us present  $F$  and  $F_f$  forces in the following way:

$$F = A\nabla(\nabla U_{sl}) + B\nabla(\nabla U_f) + C\nabla \times \nabla \times U_{sl} \quad (12)$$

$$F_f = P_1\nabla(\nabla U_{sl}) + Q_1\nabla(\nabla U_f) - N_1\nabla \times \nabla \times U_{sl} - F_{fr} \quad (13)$$

Where  $A, B, C, P_1, Q_1, N_1$  represent indefinite coefficients;  $F_{fr}$  is a friction force acting on fluid. After small restructuring (3) and (5) equations, taking into consideration (12) and (13) image, are reduced to Biot's motion equation:

$$p_{11}\partial^2 U_{sl} / \partial t^2 + p_{12}\partial^2 U_f / \partial t^2 = P\nabla(\nabla U_{sl}) + Q\nabla(\nabla U_f) - N\nabla \times \nabla \times U_{sl} - \phi F_{fr} \quad (14)$$

$$p_{22}\partial^2 U_f / \partial t^2 + p_{12}\partial^2 U_{sl} / \partial t^2 = Q\nabla(\nabla U_{sl}) + R\nabla(\nabla U_f) + \phi F_{fr} \quad (15)$$

Where  $P, Q, N$  and  $R$  are coefficients of elasticity introduced by Biot and  $A = P + Q$ ;  $B = Q + R$ ;  $N = N_1 = -C$ ;  $P_1 = P - (1 - \phi)Q / \phi$  and  $Q_1 = Q - (1 - \phi)R / \phi$ .  $\phi F_{fr}$  represents reduced friction force and corresponds to  $b(v_{sl} - v_f)$  member in Biot's equations [1], where

$$b = \eta\phi^2 / K \quad (16)$$

$\eta$  is fluid viscosity coefficient, and  $K$  is permeability of porous media. It should be noted that Biot's equations are reduced to (6) and (7) equations in case their image is  $Q = 0$  and  $N = 0$  and we receive image (10) for  $p_{12}$ .

Forthcoming from (9) and (10) images

$$p_{22} = \phi p_f \alpha \quad (17)$$

Which is brought in as an additional condition in Berryman's work [2].  $\alpha$  is tortuosity of porous media, and in our case it equals to:

$$\alpha = 1 + (1 - \phi)\Delta p / p_f = 1 + (1 - \phi)r \quad (18)$$

Forthcoming from (10) and (18)

$$p_{12} = -\phi(\alpha - 1)p_f \quad (19)$$

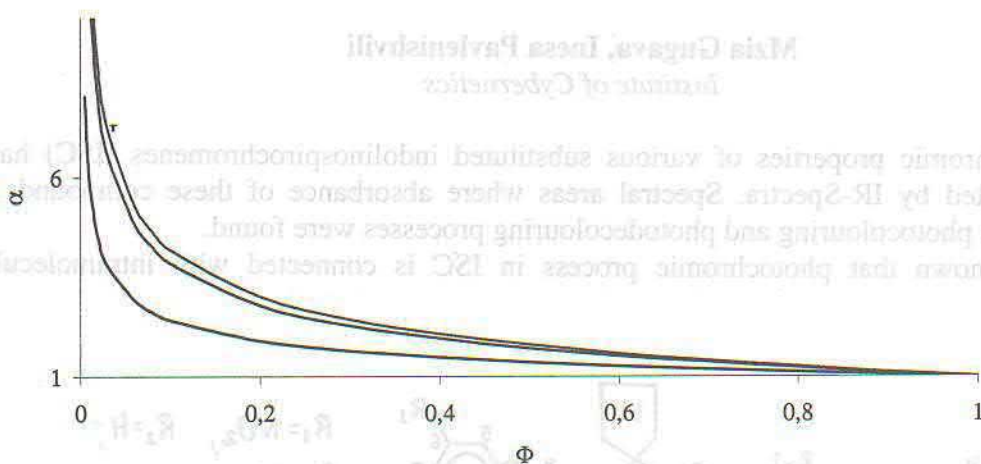
Which also coincides with work [2] result, but with diverse  $\alpha$  image. We receive the following image for solid component reduced density:

$$p_{11} = (1 - \phi)(p_{sl} + \phi r p_f) \quad (20)$$

Dependency of  $\alpha$  tortuosity on porosity coefficient is partially defined by formula (18). The thing is that ratio  $\Delta p / p_f = r$  does not depend on fluid density, but on the surface form [2] created by solid component. This shows that this ratio should contribute to this issue. Let us

consider limit  $\phi \rightarrow 1$  for this purpose. Reduced density of solid component in this limit equals to zero and only fluid equation remains; induce mass density ( $\rho_{12} = 0$ ) and  $\alpha = 1$  also become equal to zero which is guaranteed by the multiplier  $1 - \phi$ . As to the  $\Delta p / p_f = r$  multiplier it is an ultimate number for small  $(1 - \phi)$  [3] and we can register:

$$\lim \Delta p / p_f = \Gamma, \text{ when } \phi \rightarrow 1.$$



In limit  $\phi \rightarrow 0$  only equation (14) and  $\rho_{12} \rightarrow 0$  should remain. Simultaneously, according to the experimental results  $\alpha$  strives to infinity in this limit. We can satisfy both conditions if  $\Delta p / p_f \sim \phi^{-k}$ , where we receive the following image for  $0 < k < 1$  and for tortuosity:

$$\alpha = 1 + (1 - \phi)\phi^{-k}\Gamma \quad (22)$$

Graphics of this relationship are presented on the picture for  $k = 0,5$  and three meanings of  $\Gamma : 0,5; 1$  and  $1,2$ . Graphics are built from bottom to top according to the increase of  $\Gamma$  meaning.

### References

- [1]. M.A. Biot, J. Acoust. Soc. Am. 28, 168, (1956); J. Acoust. Soc. Am. 34, 1254, (1962); J. Appl. Phys. 33, 1482 (1962); M.A. Biot and D.G. Willis, J. Appl. Mech. 24, 594 (1957)
- [2]. J.G. Berryman, Appl. Phys. Lett., 37, 382 (1980)
- [3]. Л. Д. Ландау Е. М. Лифшиц, "Гидродинамика", Москва, Наука (1988)

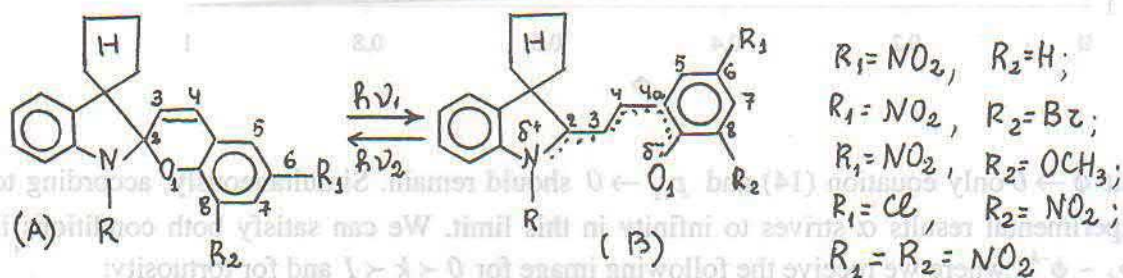
$\int$	$\&$
$\pi$	$\Sigma$

## IR – Spectra and Electrone Structure of IndolinSpirochromenes

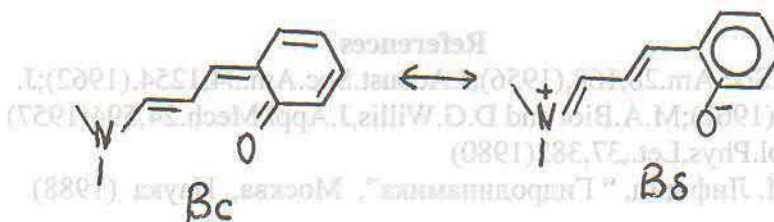
Mzia Gugava, Inesa Pavlenishvili  
 Institute of Cybernetics

Photochromic properties of various substituted indolinSpirochromenes (ISC) have been investigated by IR-Spectra. Spectral areas where absorbance of these compounds is observed at the photocoloring and photodecoloring processes were found.

It is known that photochromic process in ISC is connected with intramolecular redistribution.



The coloured form of ISC is known to represent a resonance form of chinoidal ( $B_c$ ) and bipolar ( $B_b$ ) structures:



We tried to define the influence of the substituents nature in the chromen part of ISC on the contribution of these structures.

It has been found that the electron-acceptor nature of the substituent causes equilibrium shift to the coloured form and stabilizes it. Such, if the  $NO_2$  group is substituted in the 6 position of ISC, the  $C_3 - C_4$  bond is characterized by band in IR –spectra near  $1605 - 1620 \text{ cm}^{-1}$ , and when this group is in 8-position, this band is shifted to  $1575 \text{ cm}^{-1}$ . Band characterizing C -N bond is shifted by  $10 - 25 \text{ cm}^{-1}$  (from  $1420 - 1440 \text{ cm}^{-1}$  to  $1410 - 1415 \text{ cm}^{-1}$ ).

Increasing the  $C_3 - C_4$  and  $C_2 - N$  bond order with amplification of electron-acceptor properties of substituents ( $6 - NO_2, 8 - OCH_3; 6 - NO_2; 6, 8 - NO_2$ ) allows to conclude, that bipolar structure contribution in the open form of the ISC increases. In the case of  $6 - Cl, 8 - NO_2$  substituted ISC  $C_3 - N$  bond order is decreased perhaps as a result of predominance of chinoid structure contribution in the coloured form.

For qualitative interpretation of contribution IR-spectral data the quantum-chemical calculation of idealised structure of the closed (A) and open (B) form has been done by the MINDO/3 method [1]. Distribution of charges on the ISC atoms has been calculated (table)

**Distribution of charges on atoms and dipole moments for uncoloured (A) and coloured (B) forms of ISC**

Structures		Q <sub>ind</sub> *	Q <sub>Chrom</sub> *	q(C <sub>2</sub> )	q(O <sub>1</sub> )	Dipole moment
R <sub>1</sub> =H, A		-0,120	-0,414	0,537	-0,482	1,53
R <sub>2</sub> =H; B		0.120	-0.308	0.186	-0.572	5,97
R <sub>1</sub> =NO <sub>2</sub> , A		-0,093	-0,445	0,534	-0,486	5,91
R <sub>2</sub> =H; B		0.242	-0.475	0.226	-0.598	14,44
6,8 A		-0,037	-0,497	0,533	-0,464	7,78
NO <sub>2</sub> B		0.315	-0.552	0.240	-0.571	19,52

If the charge on the spiro-C-atom leaves out of account, two orthogonal cycles (indoline and chromen) in noncoloured form has negative charges, and chromen has the larger one. For unsubstituted and metoxysubstituted ISC it is the same. In the closed form EA substituents decrease the electron density in the indoline part and increase in the chromen one. It is possible to say charge transfer from indoline to the chromen part and as a result making easier opening of the C<sub>spiro</sub>-O bond.

Substituents also influence the dipole moment of the molecule: a EA properties of substituents are amplified, the dipole moment of ISC molecules in both forms increases as well, and equilibrium is shifted between the formation heat of A and B forms.

Theoretical calculations are in agreement with the experimental thermodynamic and kinetic parameters of ISC. [2-3]

**References**

- [1]. Shembelov G.A., Ustiniuk U.A., Mamaev V.M, Quantum-chemical methods of estimation of molecules; M. Chemistry, 1980, p.254
- [2]. Japaridze K.G., Spirochromenes, Tbilisi, Mecniereba, 1979, p. 110
- [3]. Gugava M.T., Japaridze K.G., Pavlenishvili I. Ya. Izvestia, Academy of Sciences of Georgia, Serie – Chemistry., 1989 v. 15, No 2, pp 144-150.



### High-Temperature superconductivity in the Lu-Ca-Ba-Cu-O system

N. Margiani, V. Jgamadze, L. Mzhavanadze,  
 N. Sabashvili, G. Shurgaia, G. Tsintsadze

*Institute of Cybernetics*

The discovery of high- $T_c$  perovskite-structured cuprate superconductors [1] has generated a worldwide research effort within the field of superconductivity. In the past 10 years, a group at the Institute of Cybernetics have contributed substantially in understanding the fundamental physical properties of superconducting materials as well as in development of fabrication techniques for superconducting operational elements (e.g., wires, planar spirals and electromagnetic solenoids) which are candidates for a wide array of potential applications including electric power storage and transmission [2-5].

Investigation of the empirical physico-chemical and structural factors necessary for high- $T_c$  superconductivity to occur plays significant role in understanding the mechanism of superconductivity, finding new superconductors and possible technological uses for these materials. The presently known high- $T_c$  cuprate superconductors have common structural features and may be represented by ideal formula  $A_mE_2R_{n-1}Cu_nO_{2n+m+2}$  with a stacking sequence of  $m$  layers of (AO) inserted between two layers of (EO) on top of  $n$  layers of  $(CuO_2)$  interleaved by  $(n-1)$  layers of  $R$ , where  $A$  and  $E$  are various cations [6]. The  $CuO_2$  layers can occur singly or in groups. The important feature of the high- $T_c$  superconductors is that within a group, the individual  $CuO_2$  layers are separated exclusively by  $R=Ca, Y$  or  $Ln$  (lanthanides) cations. For example, unit cell of  $YBa_2Cu_3O_7$  superconductor contains two  $CuO_2$  layers ( $n=2$ ), separated by  $Y$ . These double  $CuO_2$  planes are intercalated by  $BaO$  and  $CuO$  layers (i.e.,  $A=Cu, m=1, E=Ba$ ). Layers in the cuprate superconductors can be grouped into two, namely the active (superconducting) block of  $R_{n-1}(CuO_2)_n$  and the charge-reservoir block of  $(EO)(AO)...(EO)$  which provides carriers for the active block necessary for superconductivity.

Properties and crystal structures of the high- $T_c$  superconductors can be altered by substitutional or additive doping including the modification of the charge reservoir and active blocks. In particular, from previous investigations of several groups [7] and based upon our analysis of  $T_c$ 's dependence on the parameter, which represents the ratio of anion (i.e., oxygen) atomic index to the sum of the indices of cations entered the structure, it can be concluded, that partial or total heterovalent substitution of non-copper cations by other cations with smaller valences and appropriate modification of active block by inserting of additional couple of  $(Ca)(CuO_2)$  layers is the promising route to design new perovskite-structured superconducting materials and to raise of  $T_c$ -values of presently known superconductors ( this problem will be discussed in detail in a forthcoming paper).

As example of above approach we report in this paper the preliminary results of search for high- $T_c$  superconductivity in the Lu-Ba-Cu-O system, additionally and substitutionally doped by calcium.

The samples were prepared by using the ordinary solid state reaction method. Depending upon the desired starting composition, powders of  $\text{Lu}_2\text{O}_3$ ,  $\text{CaCO}_3$ ,  $\text{BaO}_2$  and  $\text{CuO}$  were mixed in appropriate proportions and sintered for 35 h in air with intermediate grindings. The samples were then thoroughly reground and pressed into disk-shape pellets under a pressure of 6,4 Gpa. These pellets were sintered for 6 h in air and then cooled to room temperature in a furnace. Starting compositions and sintering temperatures of the powdered and pelletized samples are listed in Table 1.

According to the experimental data [8], the lower limit of Ln ionic radius tolerated in  $\text{LnBa}_2\text{Cu}_3\text{O}_7$  is  $r=0,985\text{\AA}$  (8-coordination).  $\text{Lu}^{3+}$  has a smaller ionic radius ( $0,97\text{\AA}$ ) than the lower limit value and hence  $\text{LuBa}_2\text{Cu}_3\text{O}_7$  could not be synthesized [8]. Samples No.1 and No.2 were prepared in order to confirm the data of [8]. To investigate the effect of heterovalent substitution of smaller  $\text{Lu}^{3+}$  ( $r=0,97\text{\AA}$ ) by larger  $\text{Ca}^{2+}$  cations ( $r=1,12\text{\AA}$ ) on the conductivity behaviour, the Ca-substituted sample No.3 (with about 7% excess Cu) was prepared. In the sample No.4 about 15% of  $\text{Ba}^{2+}$  cations are replaced by  $\text{Ca}^{2+}$  cations. Starting compositions denoted as No.5 (with a little excess of Cu) and No.6 correspond to the general formula of high- $T_c$  cuprate superconductors  $A_mE_2R_{n-1}\text{Cu}_n\text{O}_{2n+m+2}$ , where  $m=0$ ,  $E=\text{Ba}$ ,  $R=[\text{Lu}_{1-x}\text{Ca}_x]$ ,  $n=3$  and 4, respectively. It should be noted that one must take in account the possibility of either  $\text{Lu}^{3+}$  or  $\text{Ba}^{2+}$  substitution by  $\text{Ca}^{2+}$ .

Table1. Starting compositions and sintering temperatures of the investigated samples

Sample No.	Starting composition	Sintering temp,K (powder)	Sintering temp.,K (pellet)
1	$\text{LuBa}_2\text{Cu}_3\text{O}_y$	1175	1175
2	$\text{LuBa}_2\text{Cu}_{3,2}\text{O}_y$	1175	1175
3	$[\text{Lu}_{0,7}\text{Ca}_{0,3}]\text{Ba}_2\text{Cu}_{3,2}\text{O}_y$	1195	1203
4	$\text{Lu}[\text{Ba}_{1,7}\text{Ca}_{0,3}]\text{Cu}_3\text{O}_y$	1175	1175
5	$[\text{Lu}_{0,35}\text{Ca}_{0,65}]_2\text{Ba}_2\text{Cu}_{3,2}\text{O}_y$	1195	1195
6	$[\text{Lu}_{0,5}\text{Ca}_{0,5}]_3\text{Ba}_2\text{Cu}_4\text{O}_y$	1195	1203

For the characterization of superconducting properties, the resistivity-temperature measurements were carried out by the standard four-probe method and diamagnetism was checked inductively.

Temperature dependence of resistivity of Ca-substituted and Ca-added ceramic samples are presented in Fig.1.

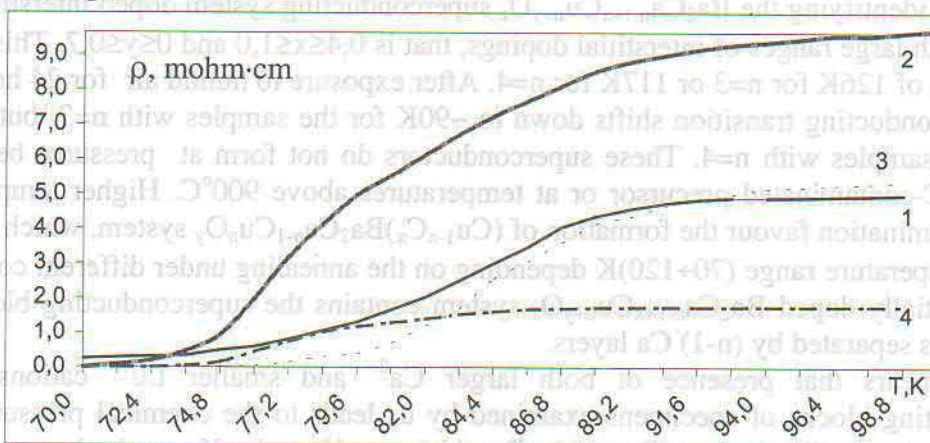


Fig.1. Temperature dependence of resistivities of the samples investigated

1.  $[\text{Lu}_{0,7}\text{Ca}_{0,3}]\text{Ba}_2\text{Cu}_{3,2}\text{O}_y$
2.  $\text{Lu}[\text{Ba}_{1,7}\text{Ca}_{0,3}]\text{Cu}_3\text{O}_y$
3.  $[\text{Lu}_{0,35}\text{Ca}_{0,65}]_2\text{Ba}_2\text{Cu}_{3,2}\text{O}_y$
4.  $[\text{Lu}_{0,5}\text{Ca}_{0,5}]_3\text{Ba}_2\text{Cu}_4\text{O}_y$

Room temperature resistivities  $\rho(300\text{K})$ , onset of superconducting transition  $T_c(\text{on})$  and end point  $T_c(\text{zero})$  are listed in Table 2.

Table 2. Room temperature resistivities and superconducting transition temperatures in the Lu-Ca-Ba-Cu-O system

Sample No.	Starting composition	$\rho(300\text{K})$ , mohm·cm	$T_c(\text{on})$ , K	$T_c(\text{zero})$ , K
1	$\text{LuBa}_2\text{Cu}_3\text{O}_y$	$\sim 4 \cdot 10^6$	-	-
2	$\text{LuBa}_2\text{Cu}_{3,2}\text{O}_y$	$\sim 4 \cdot 10^6$	-	-
3	$[\text{Lu}_{0,7}\text{Ca}_{0,3}]\text{Ba}_2\text{Cu}_{3,2}\text{O}_y$	3,2	92	<68
4	$\text{Lu}[\text{Ba}_{1,7}\text{Ca}_{0,3}]\text{Cu}_3\text{O}_y$	14	91	68
5	$[\text{Lu}_{0,35}\text{Ca}_{0,65}]_2\text{Ba}_2\text{Cu}_{3,2}\text{O}_y$	6	95	76
6	$[\text{Lu}_{0,5}\text{Ca}_{0,5}]_3\text{Ba}_2\text{Cu}_4\text{O}_y$	2,7	86	73

The ceramic samples with starting compositions of  $\text{LuBa}_2\text{Cu}_3\text{O}_y$  and  $\text{LuBa}_2\text{Cu}_{3,2}\text{O}_y$  show semiconducting behaviour in the temperature range (77÷300)K:

$\rho(77\text{K}) \cong 1 \text{ Mohm}\cdot\text{cm}$  and  $\rho(300\text{K}) \cong 4 \text{ Kohm}\cdot\text{cm}$ . Therefore, our results are in good agreement with the literature data of [8]. When Lu is partially substituted by Ca the resistivity curve begin to have metallic-like component below about 170K. Incorporation of Ca in Lu-Ba-Cu-O system creates a superconducting state: as it can be seen from Fig.1, onset of the wide superconducting transition occurs at 92K although resistivity versus temperature curve does not exhibits  $T_c(\text{zero})$  at temperatures above 70K. Temperature dependences of  $\rho$  for other Ca-doped specimens are metallic-like above  $T_c(\text{on})$  and zero resistances achieved near the liquid nitrogen boiling point (see Fig.1 and Table 2). Magnetic measurements have confirmed the presence of superconductivity in the all Ca-doped samples.

The reasons for the broad superconducting transitions and differences in  $\rho$  are not clear but they may be associated with differences in calcium content and grain structure as well as with intergrain contacts and impurity phases. This tentative explanation imply that Ca plays an important role in normal state transport properties and superconductivity of the Lu-Ca-Ba-Cu-O system.

It is interesting to note that C.W.Chu et al.[6] succeeded in synthesizing under high pressure and identifying the  $\text{Ba}_2\text{Ca}_{n-1+x}\text{Cu}_{n+y}\text{O}_z$  superconducting system doped interstitially by (Ca, Cu), with large ranges of interstitial dopings, that is  $0,4 \leq x \leq 1,0$  and  $0 \leq y \leq 0,7$ . This system displays a  $T_c$  of 126K for  $n=3$  or 117K for  $n=4$ . After exposure to humid air for 24 hours, the sharp superconducting transition shifts down to  $\sim 90\text{K}$  for the samples with  $n=3$ , but only to  $\sim 116\text{K}$  for samples with  $n=4$ . These superconductors do not form at pressures below 3,5 GPa, from C-contaminated precursor or at temperatures above  $900^\circ\text{C}$ . Higher temperatures and C-contamination favour the formation of  $(\text{Cu}_{1-x}\text{C}_x)\text{Ba}_2\text{Ca}_{n-1}\text{Cu}_n\text{O}_y$  system, which exhibits  $T_c$  in the temperature range (70÷120)K depending on the annealing under different conditions [6]. Interstitially doped  $\text{Ba}_2\text{Ca}_{n-1+x}\text{Cu}_{n+y}\text{O}_z$  system contains the superconducting block of n ( $\text{CaO}_2$ ) layers separated by (n-1) Ca layers.

It appears that presence of both larger  $\text{Ca}^{2+}$  and smaller  $\text{Lu}^{3+}$  cations in the superconducting blocks of specimens examined by us leads to the chemical pressure effect arising from the smaller ionic radius of  $\text{Lu}^{3+}$ , which manifests itself as a lattice contraction

when compared with the superconducting system synthesized under high pressure by C.W.Chu et al. We believe that a contraction of the lattice favours the preparation of superconducting samples in the Lu-Ca-Ba-Cu-O system under ambient pressure. Undoubtedly, the range of Ca content in the Lu-Ca-Ba-Cu-O system (synthesized under ambient pressure) for which the superconductivity exists is a question that merits further research. Structural studies of Lu-Ca-Ba-Cu-O superconducting system would also be of value.

It is well known that isovalent substitution of  $\text{Ln}^{3+}$  ions for  $\text{Y}^{3+}$  in  $\text{YBa}_2\text{Cu}_3\text{O}_7$  has a profound effect on the magnetic order but does not change substantially superconducting properties of this system [7-8]. The heterovalent substitution of non-magnetic Ca for magnetic and non-magnetic R cations ( $\text{R}=\text{Y},\text{Ln}$ ) in the R-Ba-Cu-O system and modification of superconducting block by incorporation (i.e., addition) of Ca should be used as a fruitful route for studying the effects of local magnetic moments, charge carrier concentration ( $\text{Ca}^{2+}$  acts as a dopant of holes) and R ionic radius (i.e., chemical pressure) on the electric and magnetic properties of R-Ca-Ba-Cu-O system and remain a subject of current research.

In summary, several compositions in the Lu-Ca-Ba-Cu-O system were synthesized under ambient pressure by usual ceramic method and measured resistively and magnetically. After substitution or addition of Ca in the starting composition of  $\text{LuBa}_2\text{Cu}_3\text{O}_7$  the samples become superconductors. Resistivity measurements show that the charge transport properties in the normal state and superconducting transitions are significantly affected by the calcium-doping. It seems that with improved starting compositions and material processing conditions it will be possible to obtain superconducting ceramics in the Lu-Ca-Ba-Cu-O system with higher critical temperatures.

#### References

1. J.G.Bednorz and K.A.Müller. *Z.Phys.B* **64**,189(1986)
2. S.N.Lukin, O.P.Teslia and G.A.Tsintsadze(in Russian). *Low Temp.Phys.***17**, 656 (1990)
3. N.Kekelidze, R.Kokhreidze, G.Mumladze, S.Odenov, J.Sanikidze, G.Tsintsadze and M.Chubabria (in Georgian). *Proceed. Georg. Acad. Sci.* **156**, 46 (1997)
4. N.Margiani, T.Medoidze, J.Nakaidze, T.Nakaidze, G.Nakashidze and G.Tsintsadze. *Bull. Georg. Acad. Sci.* **160**, 241 (1999)
5. N.Margiani, V.Jgamadze, N.Sabashvili, B.Tabidze, G.Shurgaia and G.Tsintsadze. *Bull. Georg. Acad. Sci.* **161**, 46 (2000)
- 6.C.W.Chu, Y.Y.Xue, Z.L.Du, Y.Y.Sun, L.Gao, N.L.Wu, Y.CaO, I.Rusakova and K.Ross. *Science.* **277**, 1081 (1997)
7. *Physical properties of high- $T_c$  superconductors* (ed. by D.M.Ginzberg). Mir, Moscow, 1990
8. A.M.Umarji. *Ind.J.Techn.* **28**, 320 (1990)



## Fiber Optics in Optoelectronics

**Khanzerifa Gaprindashvili**  
*Institute of Cybernetics*

Investigations in the field of fiber optics were one of the main directions of the Institute of cybernetics. Works in this field were being carried in two directions: fundamental investigation in the field of development of materials and elements for fiber optics operating in different frequency range for creation the physico-technical principles for optical processing of information and development of optoelectronic elements and equipments in which fiber elements perform the functional loading.

After assimilation of existing methods for obtaining spinneret and rod optical fiber in the section there were development a new multispinneret method and a number of the new technologies for obtaining of special fiber suitable for making the active and passive lightquider of any length with packing in row. For this, it had become necessary to develop the novel technological equipment and apparatus furnaces, fiber drawing systems and devices for hightemperature compacting in order to obtain the rigid fiberoptical elements [1,2].

A broad frequency range of electromagnetic modes used in optoelektronic and neds for optical features required development the glasses transparent in visible, ultraviolet and infrared frequency range, photoluminescence, photochromic glass as elements of active medium, semiconductive glasses as well as glasses in which it is possible to amplify optical signals on the base of laser effect for consrtuction of active functional elements [4,5].

For the first time in the section wee obtained optical glass and fiber with laser effects doped with neodymium (4-6%) generating at the wavelength of 1,06 nm and performing at room temperature in pulsed operation.

In laser fibers it determined the transition effect of radiation from one fiber to the other that was used for suppression of radiation in fiber lasers. It is determined, that suppression coefficient depends on radiation energy of suppressing laser and increases with its increasing. This phenomenon allowed making synchronic fiber-laser emitters and logic elements [8].

It is obtained storage element with signal carrier in a form of ring in which the memory signal is supplied to the ring laser through seal of fiber laser. Investigations are carried out for obtaining the active (laser) fibers doped with erbium, helium, europium and terbium. There were determined the structure of obtained fibers as well as optical features thereof [11,18].

Together with TSU it is developed "multielement neodymium spokelike laser.

Luminescence fiber broadens the sphere of application of fiber optics both in optoelectronics and in devices for displaying, monitoring and controlling. It is syntesired luminescence glass suitable for obtaining the luminescenel optical fiber. In order to obtain rigid elements, fibers were being packed in cassettes and vibrated until undistorted image was obtained. At special temperature conditions fibers and faceplates had been sintesed. Absorption spectrum is between 0;27-0,34 nm with quantum output 49,3%, persistence time is 15-25 nit. The developed luminescencing fiberglass faceplates were used as arget in cathode-ray tubes. The obtained tubes persistence time was 0,2 sec. With high resolution – to 200l/nm [3].

In 1962 it was raised a question to obtain photochromic glass and fiber.

For measuring the optical and relaxation characters of synthesized by us photochromic glass, there were developed a method and a experimental device.

Optical glass with cladding of photochromic glass allowed obtaining new kind of lightcontrolling optical fibers with slow (8-10h) and fast reversibility processes. All glass samplers synthesized by us the maximum lightemission have in the range of 0,6-0,75 nm before irradiation. On the base of photochromic optical fiber is made adaptive optical element allowing increasing uniformity of the image illuminance with significant brightness drop in image texture. Darkening level of faceplate obtained from photochromic glass is more higher than that of initial glass and maximum additional optical density is about  $\Delta D_x=0,11.$ , for glasses  $\Delta D_x= 0,10$  ; in faceplates it is reached more faster, in 20 sec. And in glass in 300 sec [12,15].

Khalcogenide and oxide semiconductive glasses have a great disadvantage for use in optoelectronics because of absence of transparence in visible range and so, to obtain optical semiconductive glasses being transparent in visible range is of great interest for optoelectronics. For the first time there were studied systems of  $WO_3 - P_2O_5 - PbO$  and  $WO_3 - P_2O_5 - R_2O - TiO_2 - CdO$  for the purpose of obtaining the transparent glasses. For all synthesized glasses it was studied the temperature dependence of electroconduction in the interval 293-473<sup>0</sup> K and it was determined activation of thermal energy. The obtained glasses are high transparent (75-90%) in infrared and visible ranges, chemically stable in atmospheric conditions and have enough high electroconduction of  $10^{-7} - 10^{-8,5} \text{ ohm}^{-1} \text{ cm}^{-1}$  at room temperature. These glasses may be used in electronics and optoelectronics [10,11].

For the purpose of making the stable switches and elements of memory we have synthesized semiconductive glasses in the system of  $WO_3 - P_2O_5 - CeO_2$ . The glasses have low levels of electrical resistance, activation energy and relatively high softening temperature 650-850<sup>0</sup> C. Devices made of films of such composition, with thickness 20, with graphite electrodes, have S – like volt-ampere feature and switching intensity is about  $10^{-5}/\text{cm}$ .

Fiber –glass faceplate with current – conducting fiber solved the task of making image-converter and increased contrast range and resolving power of the converter. The said device converts radiation  $\lambda_1= 0,72$  to  $\lambda_2=0,51$ . On the 1 cm and of converter there was placed 100 separate cells.

For recognition the visual images it was necessary to develop and realize special recognizing automatic machines functioning in real –time and having some functional features of biological visual analyses. Principle of operation of such bionical devices is based on use of studied structural-functional mechanism of visual system of humans and animals.

Investigation made in this direction together with colleagues from Ukraine showed that a number of new solutions of this problem will allow to use the principles of element base of optics and optoelectronics. There were developed fiber components intended for transformation of light flux at the input and inner layers of image analasers as well as the device for making input transformers with a great number of parallel channels.

Model of neurons are made with specific features include absence of galvano-reducing in circuits of synaptic inputs and axone outputs [7,9].

There are made models of processor – the model of first layers of retina and the analysis model of the images form containing correlats of neuron analysing circuits type of receptive field in form of optoelectronic analogies; neuron – like elements with direct and inverse transformations of light energy to electric energy by horisontal summation.

There is made experimental model-fiber analogue of receptive fields, which is a mosaic of 400 elements modulating the excitation and braking. Such models may be used in making of artificial retina.

On the base of photochromic optical fiber thereis developed an adaptive optical element allowing increasing uniformity of image illumination with significant brightness drop in image texture.

On the base of multiskanel fiber there is developed the model of multichannel analyzer of image, which contains compact input matrix of regular placed fibers on the wall surface of which there are two photodetectors.

Development of the cathoderay tubes and different optoelectronic devices and equipment with fiber-optic elements requires constructive solution of the sealing problem of fiber element with other elements of equipment for which the fire welding acceptable electro-vacuum techniques is appeared to be unsuitable. Therefore, there are developed the new materials giving vacuum-tight weld and having high roscopicity for sealing of fiber elements, for example, glassceramic cements with different coefficient of thermal expansion. The developed technology for obtaining the glassceramic cements was introduced in enterprises of electro-vacuums industry [3].

Also, it was developed mica-crystallina materials.

Broadening of the spectral range aside near area of infrared spectrum required development of new glasses. On the base of oxygen glass, transparent to 5; there were fiber-optic elements.

Focons of infrared fiber with diameter relation of 3:0.2mm were being used for increasing angle of view ( $15^0$ ) of semiconductive photodetectors. Investigations had been carried out in SSI, p/b A-3726 (Moscow).

Unique features of fiber radiation both passive and active provided their use in medicine. Existed endoscopes had enough large diameters (17-18mm.) and were illuminated by electrical lamp of size 2-3 mm, which when used for a long time may be cause a burn of mucons membrane. Taking into consideration the fiber radiation, there were developed endoskopos on the base of optical fiber of diameter 7-8 mm allowing to prolonged examination of patient without burn of mucons membrane. The developed endoskopos were used in the Institute of surgery (Georgia) for examination of architectonics of mitral valve, moreover this process was being photographed through the endoscope on the photofilm]. Endoscopes of different configuration had been used by Institutes of medicine, Gynecology, Urology.

Especially must be noted the developed and manufactured ophthalmological instrument intended for diagnostics of intraocular pressure, for removal of foreign body and tumors from eyes and also for local illumination of almost inaccessible parts of eyes during the operation.

There were developed also operation scalpel with "cold" light, claw of tweezers, diaphonoscope both straight and beaded. All these instrument were tested in the Institute of Helmohoth, by prof. Gundareva. Materials of investigation in this direction are published in 18 works (local and foreign magazines).

The section of fiber optics did co-works both with Academy Institutes and department enterprises. Especially, with Institute of semiconductors AS Ukraine (the head of Institute Ac. Svechnikov). During co-working there were developed: options for translation and determination high voltage stress and for galvanic isolation of controllable and controlling circuits; optoelectronic speed-responding relay device for measuring velocity and linear sizes of the object and reading out an information from punch card; input device for searching tracking systems. For automatic control of zero-indicators and etc; there is developed model of insect eye, which consists of sintered set of focons, which in image input plane generates spherical surface corresponding to the shape of the insect facet eye providing angle of view  $180^0$ .

For reduction a portion of skew rays percolating through fiber, there was developed optical fiber light quid cladding of which has greater refractive index than that of core thereby allowing increase considerable a noise immunity of optoelectronic elements.

On the base of low-dimension focons there is developed converter providing transmission of the printed text image preliminary diminished 15-20 times with anamorphism index 5-6. There is developed a system of multifunctional optoelectronic logical -temporally

converters of optical range through use of which it became possible measure spatial – temporary distribution light flux intensity in dynamics [6,13].

For the first time there were developed fiber elements for transmission the soft x-radiation on curvilinear path.

Results of This investigation were published in scientific magazines, in USA, Yugoslavia and Poland, in all 21 publications. On this work it was defended thesis for a Doctor's degree.

Investigations were made on synthesis of physico-chemical and electric features of lead-silicate, alkaline-silicate and nonalkaline-borate glasses containing oxides of polyvalency elements as well as lead-borate halogen-containing and lead-cadmiumborate glasses. Influence of rare earth elements on the electric features of these glasses was thoroughly investigated. For the first was carried out investigation of transporting processes in the synthesized lead-silicate glasses. On this work there were defended 5 theses [14,16,18].

To determination the kind of liquid there are developed and made devices – refractometers on the base of fiber optics. Priority is confirmed and invention is patented and published [9].

The fiber-optics section works on synthesis and investigation of electroconductive and photoactive polymere system (1999-2001). The work “Electroconducting polymere composition” is patented.

The fiber – optics section works on obtaining and investigation of the new type of active glasses. Investigations are being carried out on optical and photoelectric indices in hard organic and inorganic media.

By collaborators of the section are published 2 monographs, more than 130 scientific works, obtained more than 160 certificates, some of them are patented: in England, Germany, Sweden, Italy, France, Austria, Finland. By collaborators are defended 3 Doctor's and 12 candidate theses. Some of works are marked off diploma and deeds.

### References

- [1]. В. Веинберг, Д. Саттаров. „Оптика световодов „. Из-во „Машиностроение“. 1969г.
- [2]. Х.И. Гаприндашвили, Г.П. Митагвария. „Стеклокристаллический материал с пьезоэлектрическими свойствами“. Сообш. АН ГССР, №1, т.43. 1966 г.
- [3]. Х.И. Гаприндашвили, Л.Т. Хелая. „Люмин. оптич. волокно для экранов ЭЛТ“. Сообш. АН ГССР, №3, т.63. 1966 г.
- [4]. Х.И. Гаприндашвили, Ш.Ш. Гватуа и др. „Вынужд. излучение активных волоконных нитей“. Радиоэлектр. и электроника т.13.11. 1968.
- [5]. Х.И. Гаприндашвили, Р.П. Джангобеков и др. „Применение фокона в оптик“. Сообш. АН ГССР, т.55. 1969 г.
- [6]. Х.И. Гаприндашвили, Р.П. Джангобеков „Волоконный фильтр“. Спец. радиоэлектроника, вып.7, 1972.
- [7]. Х.И. Гаприндашвили, Ю.Л. Чибалашвили „Координатор цели бионич“. Спец. радиоэлектроника, вып.2, 1972.
- [8]. Х.И. Гаприндашвили, Ш.Ш. Гватуа, В.В. Чавчанидзе и др. „Пороговые врем. и спектр. характеристики волоконного лазера,,. Сбор. „Квантовая электроник,,. №3(14), 1973.
- [9]. Х.И. Гаприндашвили „Перспектива использования оптоэлектронного принципа преобразования при моделировании нейронов сетчатки“. Спец. радиоэлектроника, вып.1, 1976.
- [10]. Х.И. Гаприндашвили. „Радиационные свойства волокон ИК диапазона“. Труды ИК АН ГССР, т.3. 1977.
- [11]. Х.И. Гаприндашвили, Р.П. Джангобеков, Д.И. Накаидзе. Книга, из-во „Мецниереба“ 1984.

- [12]. В. Гомелаури, Н. Папунашвили, Н. Сихарулидзе. „Фотохромное ст-ло для сердцевины оптического волокна”. Известия АН ГССР. 1987, т-13, № -2, серия химич. с. 148-153.
- [13]. Х.И. Гаприндашвили., Р.П. Джангобеков „Дискретизатор сплошного оптического поля”. „Оптоэлектроника”. 1989. с. 136.
- [14]. „Оптические преобразователи физических величин”. „Оптоэлектроника”, 1989. с 111 Координационное совещание соц. стран по проблеме ОР.
- [15]. Х. Гаприндашвили., Н. Папунашвили., В. Рябцева и др. „Исследование синтеза фотохромных стекол для сердцевины оптического волокна”. „Физика и химия стекла” т.17, №14, 1991, с. 616-622.
- [16]. R. Jangobekov, Kh. Gaprindashvili, Materials and Technology of Guides Modelling, Stimulation and Control. A. Amse Ress, vol. 35, № 1, 1991, pp. 35-41.
- [17]. Г. Чантурия, Ю. Благидзе, Ш. Гватуа и др. „Перенос энергии возбуждения между редкоземельными ионами ( $P^{3+}$ - $Nd^{3+}$ ) в силикатном стекле”. „Квантовая электроника” №1, 2000г.
- [18]. Чантурия Г. Гватуа Ш. Татарашвили Р. Салуквадзе Н. Кикодзе Н. Гомелаури В. Гаприндашвили Х. „перенос энергии возбуждения между редкоземельными ионами ( $P^{3+}$ -  $Nd^{3+}$ ) в боратном стекле. Georgian Engeneering News. 1999, №4
- [19]. Гаприндашвили Х. Каракозов К. „Волоконно-оптический рефрактометр”. Georgian Engeneering News. 2000г.

#### References

- [1] В. Бенндорф, Д. Саттаров „Оптика световодов”, №-80 „Машиностроение”, 1987г.
- [2] Х.И. Гаприндашвили, Р.П. Джангобеков „Стеклофизические свойства материалов”, Сб. АН ГССР, №1, т.43, 1986 г.
- [3] Х.И. Гаприндашвили, Ш.И. Гватуа и др. „Ионно-оптич. волокно для сердцев. ЭПТ”, Сб. АН ГССР, №3, т.63, 1986 г.
- [4] Х.И. Гаприндашвили, Ш.И. Гватуа и др. „Внутр. излучение в активном волокнистом инд. резонаторе”, Рязанский в.естник, т.13, №1, 1988.
- [5] Х.И. Гаприндашвили, Р.П. Джангобеков и др. „Применение фибры в оптике”, Сб. АН ГССР, т.23, 1989 г.
- [6] Х.И. Гаприндашвили, Р.П. Джангобеков „Волоконный фибр. Спектр. анализ”, Сб. АН ГССР, т.23, 1989 г.
- [7] Х.И. Гаприндашвили, Ю.Б. Благидзе „Коррелятор излучения”, Сб. АН ГССР, т.23, 1989 г.
- [8] Х.И. Гаприндашвили, Ш.И. Гватуа, В.В. Рябцева и др. „Пороговые эффекты в спектре кератического волновода”, Сб. „Квантовая электроника”, №14, 1973.
- [9] Х.И. Гаприндашвили „Перспективы использования оптоэлектронного принципа преобразования при моделировании нейронных сетей”, Сб. Рязанский в.естник, т.13, №1, 1988.
- [10] Х.И. Гаприндашвили „Резонансные свойства волокон НК дназон”, Труды НК АН ГССР, т.3, 1977.
- [11] Х.И. Гаприндашвили, Р.П. Джангобеков, Д.Н. Никитас, К.И. Куня, №-80 „Машиностроение”, 1984.

ISBN 99928-846-1-4



9 789992 884614